SYNTHESIS, CHARACTERIZATION AND EVALUATION OF SOME NOVEL NON STEROIDAL MOLECULES FOR THE TREATMENT OF PROSTATE CANCER

Thesis Submitted for the Award of the Degree of

DOCTOR OF PHILOSOPHY

in

Pharmaceutical Chemistry

By

Shubham Kumar

Registration Number: 42000292

Supervised By

Dr. Pankaj Wadhwa (23400)

Department of Pharmaceutical Chemistry (Associate Professor)

School of Pharmaceutical Sciences

LOVELY PROFESSIONAL UNIVERSITY, PUNJAB

2024

DECLARATION

I, hereby declared that the presented work in the thesis entitled "**Synthesis, Characterization And Evaluation Of Some Novel Non Steroidal Molecules For The Treatment Of Prostate Cancer**" in fulfillment of degree of **Doctor of Philosophy (Ph. D.)** is outcome of research work carried out by me under the supervision of Dr. Pankaj Wadhwa working as Associate Professor, in the School of Pharmaceutical Sciences of Lovely Professional University, Punjab, India. In keeping with general practice of reporting scientific observations, due acknowledgments have been made whenever work described here has been based on findings of other investigator. This work has not been submitted in part or full to any other University or Institute for the award of any degree.

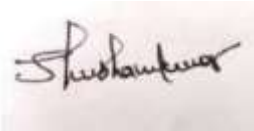

(Signature of Scholar)

Name of the scholar: Shubham Kumar

Registration No.: 42000292

Department/school: School of Pharmaceutical Sciences

Lovely Professional University,

Punjab, India

CERTIFICATE

This is to certify that the work reported in the Ph. D. thesis entitled "**Synthesis, Characterization And Evaluation Of Some Novel Non Steroidal Molecules For The Treatment Of Prostate Cancer**" submitted in fulfillment of the requirement for the award of the degree of **Doctor of Philosophy (Ph.D.)** in the School of Pharmaceutical Sciences, is a research work carried out by Shubham Kumar, 42000292, is bonafide record of his/her original work carried out under my supervision and that no part of thesis has been submitted for any other degree, diploma or equivalent course.

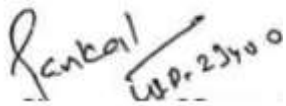

(Signature of Supervisor)

Name of supervisor: Dr. Pankaj Wadhwa

Designation: Associate Professor

Department/school: School of Pharmaceutical Sciences

University: Lovely Professional University

ABSTRACT

Prostate cancer is a prevalent and second leading cause of cancer-related deaths in males worldwide. The World Health Organization (WHO) reports approximately 1.4 million males suffering from prostate cancer, with an estimated 376,000 deaths attributed to the disease. Earlier reported drugs usually target androgen receptors which are crucial in prostate cancer treatment and also can be categorized into steroidal and non-steroidal classes. Prostate cancer remains a significant global health concern, necessitating the continual exploration of novel therapeutic approaches. This abstract encapsulates the comprehensive research endeavor focused on the design, synthesis, and evaluation of non-steroidal molecules as potential anti-prostate agents. The investigation seeks to address the limitations of current treatment modalities and introduce pure antagonists of the androgen receptor compounds that could enhance efficacy while minimizing adverse effects. The design phase of this study involves the meticulous exploration of molecular structures with a focus on non-steroidal frameworks. The study began with an extensive literature review, which identified oxadiazole-based molecules as promising candidates. In the first series, a rational drug design approach aligned with a pharmacophore-based design approach was employed to develop molecules with specific structural features known to inhibit prostate cancer growth. Based on above, the first series (**MS01-MS15**) comprised 15 molecules based on 3,5-disubstituted oxadiazoles with various electron-donating and electron-withdrawing group substitutions was designed. These compounds were successfully synthesized through a robust synthetic route, ensuring high purity and reproducibility. The structural elucidation of each compound was accomplished using advanced spectroscopic techniques, including NMR and mass spectrometry. *In vitro* analyses, starting with the MTT assay using PC-3 cell lines, revealed that **MS14** exhibited high potency compared to bicalutamide, with **MS14** as the most promising compound. Subsequent ROS and androgen receptor inhibition assays demonstrated that **MS14** increased ROS production and reduced androgen receptor expression in a dose-dependent manner, indicating its effectiveness in inhibiting prostate cancer growth. A molecular docking study provided insights into the interaction patterns of these compounds with the androgen receptor. ADMET analyses revealed favourable

physicochemical properties and manageable toxicity profiles for several compounds, including **MS14**.

Our research aimed to discover pure antagonists of the androgen receptor for more effective and safer prostate cancer treatment. The structural optimization of these molecules was carried out based on previous series results which revealed that compounds with electron-withdrawing groups (EWGs) were found to exhibit superior anti-prostate cancer activity compared to those with electron-donating groups (EDGs). Based on the above, the second series (**SP01-SP25**) was designed with EWGs on both rings and a vinyl group between the phenyl and oxadiazole rings to enhance hydrophobic interactions. All 25 compounds in this series were successfully synthesized, and their structures were confirmed through comprehensive spectroscopic analyses. To evaluate the anti-prostate activity of the synthesized compounds, *in vitro* assays were conducted. The MTT assay results showed that compound **SP04** was found most potent compound against PC-3 cells. Subsequent ROS production and androgen receptor inhibition assays further validated **SP04**'s efficacy in inducing ROS production and reducing androgen receptor expression. A docking study provided insights into the interaction patterns of these compounds with the androgen receptor, and ADMET analyses indicated favorable physicochemical properties and manageable toxicity profiles.

The results of the study revealed compound **MS14** with fluoro substitution had shown good activity, yielding an IC_{50} value of 370.37 nM. Compound **MS14** emerged as the most potent compound in the series (**MS01-MS15**), displaying an increased binding affinity of -9.0 kcal/mol and engaging in two hydrogen bond interactions with Arg752 and Gln711, respectively. In series **SP01-SP25**, compound **SP04**, substituted with a fluoro group, demonstrated the highest activity with an IC_{50} value of 238.13 nM. It formed three hydrogen bonding interactions with amino acid residues Arg752, Gln711, and Lys808, boasting a binding affinity of -9.5 kcal/mol. Moreover, the pharmacokinetic analyses highlighted the favorable bioavailability and distribution profiles of these compounds, emphasizing their potential for further development. Structure-activity relationship studies provided valuable insights into the crucial molecular features influencing the anti-prostate activity of the synthesized molecules.

In conclusion, this research is a promising effort to identify pure antagonists of the androgen receptor for prostate cancer treatment. Compounds like **MS14** and **SP04** show significant potential in inhibiting prostate cancer growth and may offer safer alternatives to current treatments. Further *in vivo* studies using compound **SP04** could provide valuable insights into its potential as a novel therapeutic option, potentially improving the prognosis and treatment options for prostate cancer patients.

Keywords: Prostate Cancer, Androgen Receptor, Oxadiazoles, PC-3, ROS, Molecular Docking, ADMET.

ACKNOWLEDGEMENT

It is a moment of gratification and pride to look back with a sense of contentment at the long-travelled path, to be able to recapture some of the fine moments, to be able to think of the infinite number of people, some who were with me from the beginning, some who joined me at some stage during the journey, whose kindness, love and blessings has brought me to this day. I wish to thank each one of them from the bottom of my heart First and foremost, I would like to thanks the "**almighty**" for showering blessings of life and wisdom over me and for never forsaking me, even when I have forgotten, at too many occasions, to pray and thank him for all the blessings that he bestows on me. I express my thanks to the Chancellor sir, **Dr. Ashok Mittal** and Pro-Chancellor Mam **Dr. Rashmi Mittal** for providing us supportive and friendly atmosphere, excellent research facilities in and around the region, exposure to the scientific word and platform to rise. I would like to acknowledge my indebtedness and render my warmest thanks to my supervisor, **Dr. Pankaj Wadhwa** who made this work possible. Their friendly guidance and expert advice have been invaluable throughout all stages of the work. I appreciate all his contributions of time, ideas, and efforts to make my Ph.D experience productive and stimulating and imbibed the strength in me to work hard through this endeavour. Indeed, the words at my command are inadequate to express my gratifications to my esteemed teacher and guide who helped me in struggling this path of research. A journey is easier when you travel together. I would like to thank **Dr. Paranjeet Kaur** for her guidance in the initial tenure of my Ph.D. I would like to show my greatest appreciation to **Dr. Poonam Piplani** for their valuable suggestions and approval of my research work and exemplary recognition. I would also like to thanks Ph.D. scholars and my friends **Ms. Pooja Gauri Naik**, **Ms. Pooja** and **Ms. Anuradha** for their time to time help, support, guidance. I feel highly obliged and have immense pleasure in expressing my heartfelt thanks to Dean **Prof. Monica Gulati** as well as HOD **Dr. Sachin Kumar Singh**, and other senior faculty members like **Dr. Gurinder Singh**, **Dr. Rajesh Kumar**, **Dr. Sanjeev Kumar Sahu**, **Dr. Iqubal Singh**, **Dr. Sumant Saini**, **Dr. Charanjeet Kaur**, **Dr. Bhupinder Kapoor**, **Dr. Vikas Sharma**, **Dr. Gurdeep Singh**, **Dr. Mukta Gupta**, **Mr. Sharfuddin Mohammad**, **Dr. Ankit Yadav**, **Dr.**

Dileep Singh Bhagel and **Dr. Amritansh Bhanot**. I extend my sincere greetings and gratitude to **Dr. Amit Mittal**, whose invaluable guidance has been instrumental in bringing me to this point. Thank you very much, sir, for nurturing my future. I express my sincere thanks to my lovable friends **Mr. Praveen Giri**, **Mr. Aman Jhanjotar**, **Mr. Love Chawla**, **Ms. Seema Yadav**, **Mr. Shubham Kumar**, **Mr. Rakesh Kumar**, **Mr. Vinay Kar Pathak**, **Mr. Abhishek Birla**, This work would not have been possible without their, support and encouragement. I am also thankful to my seniors and most humble person I ever met **Dr. Hardeep Singh**, **Ms. Shivani Sharma** and **Ms. Priyanka**. I acknowledge the help given by my juniors **Shrawan Hudda**, **Muskan Magan**, **Shareef Shaik**, **Shivam**, **Manish** and **Amir** and all other who always support and helped me during the course. I personally express my thanks to my laboratory attendants **Mr. Manoj Kumar** and **Vaibhav** and all other non-teaching staff for their help and invaluable assistance. Last but not the least, this thesis would not have been possible without the confidence, endurance and support of my family. My family has always been a source of inspiration and encouragement. I wish to thanks my father Sh. **Adesh Kumar**, mother **Smt. Mithlesh Devi**. I would not be able to come to this position without the sacrifices made by my parents. A lot of support was provided by my elder sister **Kiran**, brother in law **Sunny** and my lovable nephew **Ansh**. They believed in me, before I believe in myself. Thank you for always being with me. Last but the most important person who has always guided me during my Ph.D, supported me in my tough times, and always cared for me in every situation, **Ms. Pinky Arora**, and this work would not be possible without your encouragement, love, kind support and believe. Thank you, my dear love, for always being on my side and helped me in every situation. Above all I thank **Lord Shiva** and My parents for showering their infinite bounties, clemencies and graces upon me and for being my constants companions, the strongest source of motivation, inspiration and my ultimate Guardians; to them I owe a lifelong indebtedness.

Shubham Kumar

Dedicated to

My Family

TABLE OF CONTENTS

1.	**Introduction**			**1-14**
	1.1.	Anatomy of Prostate Gland		**1-2**
	1.2.	Causes of Prostate Cancer		**3**
		1.2.1.	*Inherited Gene Mutation*	**3-4**
		1.2.2.	*Acquired Gene Mutation*	**4-5**
	1.3.	Diagnosis of Cancer		**5-7**
		1.3.1.	*Prostate Specific Antigen (PSA)*	**5**
		1.3.2.	*Digital Rectal Examination*	**5**
		1.3.3.	*Magnetic Radio Imaging (MRI) Scan*	**6**
		1.3.4.	*Biopsy*	**6**
		1.3.5.	*Staging of Cancer*	**6-7**
	1.4	Treatment Available against Prostate Cancer		**7-12**
		1.4.1.	*Active Monitoring*	**8**
		1.4.2.	*Cryotherapy*	**8**
		1.4.3.	*Radiation*	**8-9**
		1.4.4.	*Brachytherapy*	**9**
		1.4.5.	*External Beam Radiation Therapy*	**9**
		1.4.6.	*Radical Prostatectomy*	**9**
		1.4.7.	*Hormonal Therapy*	**9**
		1.4.8.	*Immunotherapy*	**10**
		1.4.9.	*Chemotherapy*	**10-12**
	1.5	Role of Androgen Receptors		**13-14**
2.	**Review of Literature**			**15-30**
	2.1	Arylpiperazine based derivatives		**15-17**
	2.2.	Bicalutamide based derivatives		**17-18**
	2.3.	Flavonoid-based derivatives		**18-20**
	2.4.	Benzamide based derivatives		**20-21**
	2.5.	Triazole based derivatives		**21-22**
	2.6.	Furanocumarin/ Curcumin/piperazine based derivatives		**22-23**
	2.7.	Oxadiazole based derivatives		**23-28**
	2.8.	Miscellaneous Agents		**28-30**
3.	**Rationale, Aim and Objective**			**31-33**

	3.1.	Rationale		**31-33**
	3.2.	Aim		**33**
	3.3.	Objectives		**33**
4.	**Materials and Methods**			**34-38**
	4.1	Procedure of *in vitro* study upon PC-3		**34-36**
		4.1.1.	*Cell Viability Assay*	**33**
		4.1.2.	*ROS Measurement*	**35**
		4.1.3.	*Androgen Receptor Inhibition Assay*	**35**
		4.1.4.	*Immunofluorescence study for AR inhibition*	**35-36**
	4.2.	Computational Studies		**36-38**
		4.2.1	*Protein Selection and Preparation*	**36**
		4.2.2.	*Validation of Protein for Docking*	**37**
		4.2.3.	*Molecular Docking Program*	**37-38**
	4.3	*Absorption, Distribution, Metabolism and Excretion (ADME) Analysis*		**38**
	4.4	Toxicity Analysis		**38**
5.	**Design, Synthesis, Characterization and Biological Evaluation of 3,5-Diphenyl-1,2,4-Oxadiazoles (MS01-MS15)**			**39-64**
	5.1.	Designing of 3,5-Diphenyl-1,2,4-Oxadiazoles (MS01-MS15)		**39**
	5.2.	Chemistry		**40-43**
		5.2.1.	General Synthesis of 3,5-Diphenyl-1,2,4-Oxadiazoles (MS01-MS15)	**40**
		5.2.2.	*Procedure for Synthesis of N'-Hydroxybenzimidamide (2)*	**40-41**
		5.2.3.	*Procedure for Synthesis of N'-(Benzoyloxy)Benzimidamide (4a-4o)*	**41-42**
		5.2.4.	*Procedure for Synthesis of Substituted 3,5-Diphenyl-1,2,4-Oxadiazoles (MS01-MS15)*	**42-43**
	5.3	Spectral Characterization of The Compounds (MS01-MS15)		**43-47**
	5.4.	Results		**47-52**
		5.4.1.	*Cell Viability Assay*	**47-49**
		5.4.2.	*Molecular Docking Analysis*	**49-52**
	5.5	Discussion		**53-57**
	5.6	ROS Production Assay in PC3 Cell Lines		**57-58**
	5.7	Androgen Receptor Inhibition Assay		**59-61**
	5.8	Absorption, Distribution, Metabolism, and Excretion (ADME)		**61-62**

		Analysis of Synthesized Compounds (MS01-MS15) And Bicalutamide		
	5.9	Toxicity Analysis of (MS01-MS15) Compounds and Bicalutamide		**63-64**
6.	**Design, Synthesis, Characterization and Biological Evaluation Of 3-Phenyl-5-Styryl-1,2,4-Oxadiazoles SP01-SP25**			**65-97**
	6.1.	Designing of 3-Phenyl-5-Styryl-1,2,4-Oxadiazoles (SP01-SP25)		**65-66**
	6.2.	Chemistry		**66-70**
		6.2.1.	*General Synthesis of 3-Phenyl-5-Styryl-1,2,4-Oxadiazoles (SP01-SP25)*	**66**
		6.2.2.	*Procedure for Synthesis of N'-hydroxybenzimidamide (2a-2e)*	**67**
		6.2.3.	*Procedure for Synthesis of Substituted N'-(cinnamoyloxy)benzimidamide (4a-4y)*	**67-68**
		6.2.4.	*Procedure for Synthesis of Substituted 3-Phenyl-5-Styryl-1,2,4-Oxadiazoles (SP01-SP25)*	**69-70**
	6.3.	Spectral Characterization of the compounds (SP01-SP25)		**70-78**
	6.4.	Results		**78-84**
		6.4.1.	*Cell Viability Assay*	**78-80**
		6.4.2.	*Molecular Docking Analysis*	**80-84**
	6.5.	Discussion		**85-89**
	6.6.	ROS Production Assay in PC3 Cell Lines		**89-90**
	6.7.	Androgen Receptor Inhibition Assay		**90-92**
	6.8.	Absorption, Distribution, Metabolism, and Excretion (ADME) Analysis of SP01-SP25 And Bicalutamide		**92-94**
	6.9	Toxicity Analysis of SP01-SP25 and bicalutamide		**95-97**
7.	**Conclusion**			**98-100**
8.	**References**			**101-115**

LIST OF FIGURES

Figure Number	Title	Page Number
1	Showing anatomy of prostate gland	**2**
2	Role of androgen receptors and its antagonists	**13**
3	Marketed androgen receptor inhibitors	**14**
4	Representing structures of arylpiperazine-based derivatives	**17**
5	Androgen inhibitors based on bicalutamide	**18**
6	Flavonoid based antiandrogen inhibitors	**20**
7	Benzamide based derivatives	**21**
8	Triazoles as antiprostate cancer agents	**22**
9	Derivatives based on furanocoumarin, curcumin and piperazine	**23**
10	Disubstituted oxadiazoles derivatives	**24**
11	Oxadiazoles representatives as anti-prostate cancer agents	**26**
12	Representative structures of 1,2,4-oxadiazoles	**27**
13	Oxadiazole based derivatives	**28**
14	*N*-containing compounds as anti-prostate cancer agents	**29**
15	Miscellaneous derivatives against prostate cancer	**30**
16	Designing of proposed molecules	**32**
17	Basic Structure of the both designed series	**33**
18	Docked structure of co-crystallized ligand for validation	**37**
19	Designing rationale for 3,5-diphenyl-1,2,4-oxadiazoles	**39**
20	Fragmentation Pattern of MS03 (one of the representatives of MS01-MS15)	**47**
21	Graphical representation of percentage inhibition of PC-3 cells	**48**
22	2D and 3D interactions of few representatives of the series MS01-MS15	**52**
23	MS14-induced ROS production in a dose-dependent manner	**58**
24	Inhibition of androgen receptor expression in a dose-dependent manner	**59**
25a	Androgen receptor expression measured by immunofluorescence	**60**

	assay	
25b	Graphical representation of mean fluorescence intensity (MFI) of control, MS14 at 150 & 300 nm and bicalutamide at 200 nm	**60**
26	Designing rationale of the compound SP01-SP25.	**66**
27	Mass fragmentation of SP04 (One of the representations of SP01-SP25)	**78**
28	Graphical presentation of Percentage inhibition of PC-3 cell lines	**79**
29	2D and 3D interactions of few representatives of the series SP01-SP25	**84**
30	SP04-induced ROS production in a dose-dependent manner	**90**
31	Inhibition of androgen receptor (AR) expression in a dose-dependent manner	**91**
32a	Androgen receptor expression measured by immunofluorescence assay	**92**
32b	Graphical representation of mean fluorescence intensity (MFI) of control, SP04 at 100 & 200 nm and bicalutamide at 200 nm	**92**

LIST OF TABLES

Table Number	Table Title	Page Number
1	Inherited genes associated with prostate cancer	**4**
2	Stages of prostate cancer	**6**
3	Treatment options for prostate cancer	**7**
4	List of drugs for prostate cancer treatment	**10-12**
5	Percentage Inhibition and inhibitory concentration of MS01-MS15	**48-49**
6	Binding affinities and interaction pattern of synthesized compounds and bicalutamide	**50-51**
7	MFI for compound MS14 and Bicalutamide at different concentrations	**57**
8	ADME Properties of compound MS01-MS15 and bicalutamide	**62**
9	Toxicity analysis of MS01-MS15 and bicalutamide	**64**
10	IC_{50} values and percentage inhibition of SP01-SP25 and bicalutamide	**79-80**
11	Binding affinities and interactions of synthesized compounds against 1Z95	**81-83**
12	Mean Fluorescence Intensity for SP04 at different concentrations along with bicalutamide	**89**
13	ADME properties of the synthesized compounds and bicalutamide	**93-94**
14	Toxicity analysis of the SP01-SP25 and bicalutamide	**96-97**

LIST OF SCHEMES

Scheme Number	Scheme Title	Page Number
1	Reaction for Synthesis of *N'*-hydroxybenzimidamide	**40**
2	Mechanism for Synthesis of *N'*-hydroxybenzimidamide	**41**
3	Synthesis of *N'*-(benzoyloxy)benzimidamide	**41**
4	Mechanism for Synthesis of *N'*-(benzoyloxy)benzimidamide	**42**
5	Reaction for Synthesis of 3,5-diphenyl-1,2,4-oxadiazoles MS01-MS15	**42**
6	Mechanism for Synthesis of 3,5-diphenyl-1,2,4-oxadiazoles MS01-MS15	**43**
7	Synthesis of *N'*-hydroxybenzimidamide	**67**
8	Mechanism of reaction of substituted *N'*-hydroxybenzimidamide	**67**
9	Synthesis of *N'*-(cinnamoyloxy)benzimidamide	**68**
10	Reaction Mechanism for *N'*-(cinnamoyloxy)benzimidamide	**68**
11	Synthesis of target molecule 3-phenyl-5-styryl-1,2,4-oxadiazoles SP01-SP25	**69**
12	Mechanism of reaction for target molecule 3-phenyl-5-styryl-1,2,4-oxadiazoles SP01-SP25	**70**

LIST OF ABBREVIATIONS

Abbreviation	Full Form
ADME	Absorption Distribution Metabolism Excretion
ADT	Androgen Deprivation Therapy
AR	Androgen Receptor
ATM	Ataxia Telangiectasia Mutated
BBB	Blood Brain Barrier
BPH	Benign Prostatic Hyperplasia
BRCA1	Breast Cancer gene 1
BRCA2	Breast Cancer gene 2
CHEK2	Checkpoint Kinase 2
CT	Computed Tomography
DBD	DNA Binding Domain
DHT	Dihydro Testosterone
DMEM	Dulbecco's Modified Eagle Medium
DMSO	Dimethyl Sulfoxide
DNA	Deoxy Ribonucleic Acid
DRE	Digital Rectal Examination
EBRT	External-Beam Radiation Therapy
ECF	Ethyl Chloroformate
EDGs	Electron Donating Group
EWG	Electron Withdrawing Group
GI	Gastro Intestinal
HNPCC	Hereditary Non-Polyposis Colorectal Cancer
HPC	Human Prostate Cancer
IGF	Insulin-Like Growth Factor
IL	Interleukin
IR	Infra-Red
LD	Lethal Dose
LH-RH	Luteinizing Hormone-Releasing Hormone

m/z	Mass to Charge Ratio
MFI	Mean Fluorescence Intensity
MLH1	MutL Homolog 1
MM2	Molecular Mechanic
MOA	Mechanism of Action
MP	Melting Point
MRI	Magnetic Resonance Imaging
MSH2	MutS Homolog 2
MSH6	MutS Homolog 6
MTD	Max Tolerated Dose
NMR	Nuclear Magnetic Resonance
ORAT	Oral Rat Acute Toxicity
PALB2	Partner and Localizer of BRCA2
PARP	Poly Adenosine Diphosphate-Ribose Polymerase
PC	Prostate Cancer
PDB	Protein Data Bank
PMS2	Postmeiotic Segregation Increased 2
PPM	Parts Per Million
PSA	Prostate Specific Antigens
RAD51D	RAD51 Homolog D
RMSD	Root Mean Square Deviation
ROS	Reactive Oxygen Species
SAR	Structure-Activity Relationship
TEA	Tri Ethyl Amine
TLC	Thin Layer Chromatography
TNF	Tumour Necrosis Factor
TRUS	Transrectal Ultrasound

LISTS OF APPENDIXES

Appendix Number	Title	Page No
Appendix I	Letter of Candidacy For Ph.D	116
Appendix II	1^{H} & 13^{C} NMR and Mass Spectra	117-149
Appendix III	Publication Details	150-153
Appendix V	Allied Publication Details	154
Appendix VI	Conference Attended Details	155-158

CHAPTER 1

1. Introduction

Health challenges cause major implications on the population's economic standards, life expectancy and mortality. These health challenges also impact healthcare spending patterns, workforce productivity, and overall economic growth [1]. The complex relationship between health and economics leads to increased burdens and decreased efficiency of healthcare systems. Moreover, higher mortality rates and shorter life expectancies lead to a decline in capital, which hampers societal development [2]. Among these health challenges, cancer stands out as a concern causing approximately 14 million new cases each year and causing deaths of nearly 8 million people. The severity of the impact caused by cancer emphasizes the need for prevention measures robust early detection protocols and advancements in treatment options [3].

Cancer is characterized by cell growth due to a breakdown, in the mechanism that normally stops cells from dividing [4]. This abnormal cell growth becomes invasive spreading to tissues and other parts of the body a process known as metastasis. Cancer cells' continued advancement and the challenges they bring in their treatment are closely linked to their nature [5]. Cancer manifests in various forms, distinguished by their point of origin. For instance, if a cancer emerges from epithelial tissues, it falls under carcinomas. This group encompasses lung, breast, prostate, and colorectal cancers, collectively comprising a significant portion of cancer cases [6]. On the other hand, if a cancer originates in the lymphatic system, it is referred to as lymphoma [7]. Prostate cancer is one of the most prevalent cancers in men leading to the second most death-causing cancer in men. It predominantly emerges between the ages of 45 and 60 and constitutes a primary contributor to mortality, particularly in Western nations. According to 2020 GLOBACON data, approximately 1.4 million individuals worldwide are diagnosed with prostate cancer annually, resulting in around 375,304 deaths globally [8]. The incidence of prostate cancer varies significantly across different geographical regions. In Asia, a total of 371,225 cases of prostate cancer reported annually while approx. 120 thousand of people demise due to prostate cancer [9]. Developed countries, where awareness regarding cancer and prostate-specific antigen (PSA) testing is more widespread, observe higher instances of prostate cancer.

Approximately 1 in 9 males receive a prostate cancer diagnosis, with 1 in 40 facing fatal progression. On time screenings and early detection contribute to lower mortality rates. Most cases (about 60%) occur in men aged 65 and above, while occurrences are rare in those under 40 [10]. Localized prostate cancer boasts a high 10-year survival rate, often resulting in cures. Thus far, metastatic cases carry a grim prognosis, yielding a meagre 5-year survival rate of around 30% and a median survival of about 3 years, despite rigorous treatments [11].

1.1. Anatomy of Prostate Gland

The prostate gland measures around 3 cm in length, approximately the size of a walnut and weighs about 20 g. It contributes about 1/3rd of the seminal fluid. Positioned amidst the male pelvic region and the base of the penis (radix), it lies beneath the urinary bladder and anterior to the rectum as shown in **Figure 1** [12].

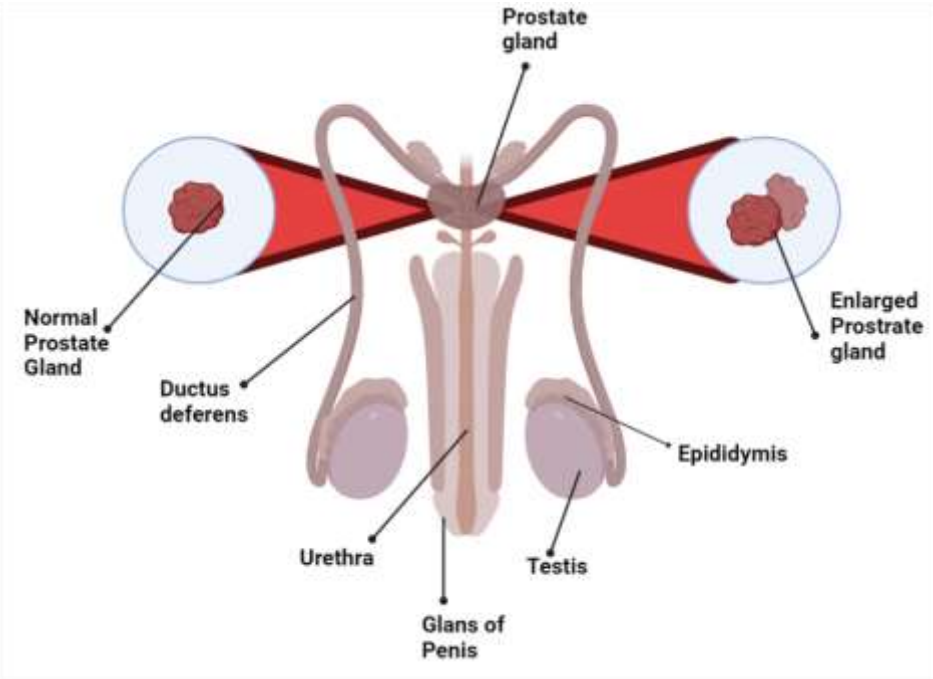

Figure 1: Showing anatomy of prostate gland

Enveloping the posterior part of the urethra, and distinguishing its exact posterior, prostatic, and proximal segments is challenging, as they share a similar internal lining. Comprising glandular tissue, the prostate generates a fluid that supports sperm nutrition and helps maintain an alkaline pH within the semen [13]. Notably, the

remaining seminal fluid is produced by seminal vesicles. Proper functionality of the prostate necessitates androgens, primarily testosterone. Consequently, hormonal therapy proves highly effective. Enlargement of the prostate gland is the major concern of prostate cancer [14].

1.2. Causes of Prostate Cancer

The cause of prostate cancer remains unclear to medical professionals. However, it is known that prostate cancer initiates when there are alterations in the DNA of prostate cells. DNA serves as a cell's instruction manual, dictating its activities. These DNA changes speedup the affected cells to proliferate and divide at a faster rate than healthy cells. Unlike typical cells, these abnormal cells persist and do not undergo the natural cell death process. Over time, these accumulating abnormal cells cluster together to form a tumor which has the potential to invade nearby tissues. Furthermore, some of these aberrant cells may eventually break away and disseminate (metastasize) to other parts of the body [15].

1.2.1. Inherited Gene Mutations: In approximately 10% of prostate cancer cases, inherited gene mutations play a crucial role, a phenomenon known as hereditary cancer [16]. These hereditary mutated genes encompass various crucial functions. Breast cancer (BRCA1 and BRCA2), responsible for DNA repair, are commonly linked to breast and ovarian cancer, with specific changes in BRCA2 associated with certain instances of prostate cancer [17]. DNA repair genes like CHEK2, ATM, PALB2, and RAD51D can undergo mutations, contributing to specific cases of prostate cancer. DNA mismatch repair genes, including MSH2, MSH6, MLH1, and PMS2, are pivotal in fixing DNA mismatches arising during cell division. Mutations in these genes lead to lynch syndrome, also known as hereditary non-polyposis colorectal cancer (HNPCC), elevating the risk not only for prostate cancer but also for other malignancies[18].

RNASEL (HPC1) holds the role of triggering cell death in response to internal cellular issues. Inherited mutations in this gene extend the lifespan of abnormal cells, subsequently heightening the risk of prostate cancer Additionally, HOXB13, essential for prostate gland development, exhibits mutations linked to early-onset prostate

cancer, often observed in specific family lines, though such mutations remain relatively uncommon (**Table 1**) [19].

Table 1: Inherited genes associated with the prostate cancer [17-19]

Sr. No.	Gene	Function	Associated Cancers	Conditions/Mutations
1.	BRCA1 and BRCA2	DNA repair	Breast, Ovarian, Prostate	Mutations in BRCA2 linked to some Prostate
2.	CHEK2	DNA repair	Prostate	DNA repair gene mutation
3.	ATM	DNA repair	Prostate	DNA repair gene mutation
4.	PALB2	DNA repair	Prostate	DNA repair gene mutation
5.	RAD51D	DNA repair	Prostate	DNA repair gene mutation
6.	Mismatch Repair	Fixes DNA mismatches during cell division	Prostate, Lynch Syndrome, Other Cancers	Mutations in MSH2, MSH6, MLH1, PMS2
7.	RNASEL (HPC1)	Induces cell death when problems arise in the cell	Increased Prostate Cancer Risk	Inherited mutations increase cancer risk
8.	HOXB13	Essential for prostate gland development	Early-Onset Prostate Cancer, Runs in Some	Mutations linked to early-onset cancer

Sr. No.	Gene	Function	Associated Cancers	Conditions/Mutations
			Families	

1.2.2. Acquired Gene Mutation: Further consideration of genetic influence lies in acquired gene mutations, which result from random occurrences influenced by factors such as diet, lifestyle, exposure to radiation, etc. For example, androgens, which stimulate prostate cell growth, can elevate cancer risk with higher androgen levels in certain patients. Additionally, research indicates a potential link between elevated levels of insulin-like growth factor-1 (IGF-1) and increased risk in specific patient groups aged more than 50 years. These acquired genetic changes further contribute to the complex landscape of prostate cancer development [20].

1.3. Diagnosis of Prostate Cancer

Prostate cancer is often detected at later stages, leading to higher death rates due to treatment challenges [21]. Currently, there is not a single specific test available for diagnosis. Traditional methods are often adopted for the diagnosis which include Digital Rectal Examination (DRE), PSA blood tests, MRI and CT scans, and biopsies [22].

1.3.1. Prostate Specific Antigen (PSA)

Prostate gland produces PSA protein and is found in the blood in small quantities, which keep increasing with age. A blood sample is analyzed with a PSA cutoff of 4 ng/mL. If the PSA level in blood exceeds 4 ng/mL, more examination is required. The specificity of PSA is to prostate gland but it is not specific to prostate cancer, so raised levels of PSA can indicate diseases such as prostatitis and Benign Prostatic Hyperplasia (BPH) [23]. However, the likelihood of prostate cancer is only 50%, as increased PSA levels are also seen in individuals without prostate cancer. When PSA levels rise, additional tests like biopsy confirm the cancer [24].

1.3.2. Digital Rectal Examination (DRE)

A gloved finger is introduced in to the rectum of the patient in a digital rectal examination. The size of the prostate gland is assessed by the finger and detects any anomalies. While DRE can aid in prostate cancer detection, it's especially valuable for diagnosing prostate enlargement due to benign prostatic hyperplasia [25, 26].

1.3.3. Magnetic Resonance Imaging (MRI)

MRI proves valuable for diagnosing prostate enlargement. An MRI scan produces a detailed image of the prostate gland, facilitating the assessment of abnormalities. Additionally, transrectal ultrasound (TRUS) aids in cancer staging based on its spread and the evaluation of bone metastasis, complementing MRI in diagnostic capabilities. If the results of the PSA, DRE test, and MRI are negative, additional multiparametric MRI can also be conducted [27, 28].

1.3.4. Biopsy

Biopsy (such as liquid biopsy, prostate fusion biopsy) is a highly reliable technique for diagnosing prostate cancer. During this procedure, tissue is extracted and examined under a microscope to determine the presence, cause, or extent of disease. Biopsy also helps assess the rapid spread of cancer cells. Detection of cancerous cells leads to a positive diagnosis, while absence of such cells results in a negative finding for prostate cancer [29].

1.3.5. Staging of Prostate

The staging of prostate cancer involves the utilization of grade groups and PSA levels, which are outcomes of both diagnostic and staging tests. Tissue biopsy is employed to ascertain the Gleason score, a scale ranging from 2 to 10 that microscopically describes cancer cells and assesses the tumor's potential for spread; scores lower than 6 are uncommon. The grade group is determined by the Gleason score and is categorized as follows: grading group 1 comprises individuals with a Gleason score of 6 or below, while grading group 2 or 3 is associated with a Gleason score of 7. Grading Group 4 is linked to a Gleason score of 8, and Grading Group 5 encompasses individuals with a Gleason score of 9 or 10 (**Table 2**) [30].

Table 2: Stages of Prostate Cancer

Gleason Score	Grade Group	Stages	Severity
2 to 6	1	I	Low
7	2 or 3	II	Medium
8	4	III	High

9 or 10	5	IV	Severe

1.4. Treatment Available Against Prostate Cancer

When experiencing symptoms like weak urine flow, blood in urine, frequent urination, painful urination, and incomplete bladder emptying, considering a diagnosis for prostate cancer becomes prudent. Assessment of PSA levels, biopsy, and gleason score can confirm the condition. Positive results in these aspects can lead to treatment. For stages I-III, choices include active surveillance, radiotherapy, and prostatectomy. In advanced stages like IV or high-risk stage III, androgen ablation through surgical or pharmacological castration is utilized [31]. The treatment options against prostate cancer involve employing the first generation of anti-androgens for example flutamide and bicalutamide. Various strategies for the treatment of the prostate cancer has been enlisted below in **Table 3** [32].

Table 3: Treatment options for prostate cancer according to stage of cancer

Stage	**Options for Treatment**
Stage I	Vigilant or active observation/active monitoring EBRT Radical prostatectomy Implanting radioisotopes in intestine
Stage II	Active monitoring Interstitial implantation of radioisotopes Radical prostatectomy EBRT with or without hormonal therapy
Stage III	Active monitoring EBRT along hormonal therapy Radical prostatectomy Hormonal manipulations with or without radiation therapy Chemotherapy
Stage IV	Active monitoring Palliative radiation therapy

Stage	Options for Treatment
	Chemotherapy Surgery with TURP Hormonal manipulations
Recurrent Cancer	Radiopharmaceutical therapy Chemotherapy for hormone-resistant prostate cancer Immunotherapy

1.4.1. Active Monitoring

Active monitoring is a structured approach involving ongoing monitoring and selective intervention for prostate cancer management. It is particularly suitable for patients with low cancer risk or shorter life expectancy. Guidelines were adopted to surveillance the characteristics of the disease, the general health of the patient, potential side effects, and patient preferences. Simultaneously, they consistently monitor PSA levels and other relevant indicators. The benefits include cost-efficiency, the prevention of unnecessary treatments for slow-growing cancers, and the preservation of erectile function. However, drawbacks include potential cancer metastasis before treatment, missed treatment chances, heightened patient anxiety, and the need for complex therapies with multiple side effects [33, 34].

1.4.2. Cryotherapy

This technique involves surgically inserting cryoprobes into the prostate gland under ultrasound guidance. The gland is frozen to temperatures between -100°C and -200°C for about 10 minutes [35]. Possible side effects can include urinary incontinence, erectile dysfunction, rectal discomfort, and urinary retention [36].

1.4.3. Radiation

Radiation therapy stands as a highly effective approach, employing intense radiation to eliminate prostate cancer cells [37]. Various techniques, including brachytherapy (seeds placed internally) and external beams (energy projected through the skin), deliver radiation to cancer sites. This method focuses on targeting prostate cells exclusively with high-energy rays or particles, sparing normal tissues. Particularly

suitable for patients unsuitable for surgery, radiation therapy delivers a targeted and viable treatment solution [38].

1.4.4. Brachytherapy

Brachytherapy entails directly inserting radioactive sources into the prostate using techniques like seeds, injections, or wires, guided by transrectal ultrasound. This method commonly encompasses two strategies: low dose and high dose rates. Low dose involves permanently implanting seeds that gradually lose radioactivity, while high dose administers radiation to the prostate with possible leakage risk to surrounding organs. Brachytherapy offers the advantage of swift completion within a day or less [39].

1.4.5. External Beam Radiation Therapy (EBRT)

EBRT is a widely employed technique for prostate cancer treatment. This approach utilizes strong X-rays to precisely target prostate tissue while minimizing exposure to surrounding areas. It is particularly effective for managing intermediate to high-risk prostate cancer cases and offers distinct advantages over surgical methods [40].

1.4.6. Radical Prostatectomy

Radical Prostatectomy involves the removal of the prostate gland through either open surgery or laparoscopic surgery techniques. This procedure is employed to treat prostate cancer by eliminating the affected gland. It is a significant intervention in the management of the disease [41].

1.4.7. Hormonal Therapy

Therapy using hormones, referred to as androgen deprivation therapy (ADT), is utilized to treat advanced or metastasized prostate cancer. It operates by obstructing testosterone and other male hormone production, impeding their role in the growth of prostate cancer cells. This therapy significantly lowers male hormone levels, impeding the impact of androgens on the androgen receptor [42].

1.4.8. Immunotherapy

Immunotherapy, alternatively referred to as biological therapy, functions by regulating the immune system's response. This method utilizes vaccines to cooperate with the patient's immune system in combatting cancerous cells. An example of such a vaccine is Sipuleucel-T (Provenge), which is specifically tailored for individuals with advanced and metastatic prostate cancer that has become resistant to hormone therapy [43].

1.4.9. Chemotherapy

Chemotherapy employs anticancer medications to suppress the growth of cancer cells. Decades of genetic research, diagnostics, and treatment understanding have led to advancements in prostate cancer management [44]. **Table 4** enlisted the various drugs for the treatment of the prostate cancer.

Table 4: Most common drugs for prostate cancer treatment [45-47]

Drug	Structure	MOA	Side Effects
Docetaxel	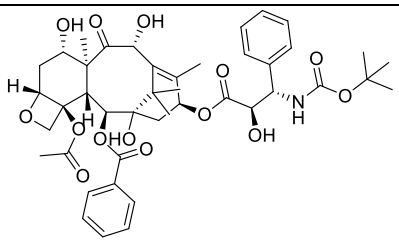	Bind to β-tubulin subunit of microtubules and antagonize disassembly of the microtubule protein	Cause severe allergic reactions, Peripheral neuropathy
Cabazitaxel	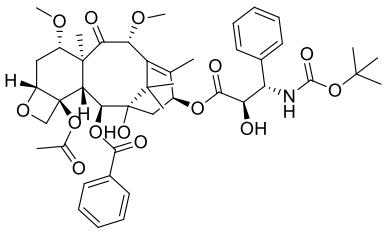	Bind to tubulin protein and promotes its assembly inside microtubules and cause mitotic interference	Cause severe allergic reactions, Peripheral neuropathy

Mitoxantrone	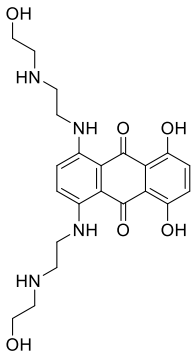	Inhibits the proliferation of B, T cells and of macrophages Impairment in secretion of interferon-γ, TNFα, and IL-2	Can cause leukemia (after several year of use)
Estramustine	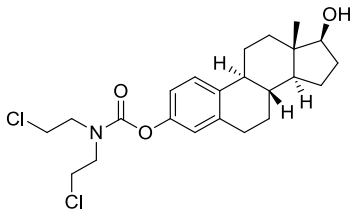	Nitrogen-mustard moiety of this compound becomes active and participates in the alkylation of DNA or other cellular components.	Blood clotting risks
Bicalutamide	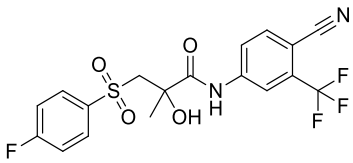	Binds with the allosteric site on the AR and induces conformational changes in the co-activator binding site and alters its transcriptional activity	Hepatoxicity, Muscle weakness, Weight loss,
Flutamide	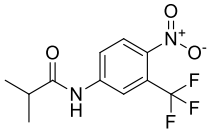	Binds to AR and prevents binding of androgens	Gynacomastia, Impotence, Hot flashes
Nilutamide	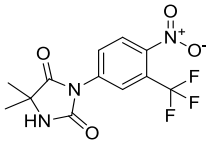	Binds to AR and prevents binding of androgens	Impotence, Vision changes,
Abiraterone acetate	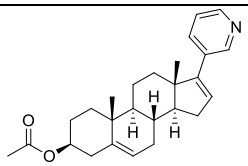	Inhibits the activity of steroid 17 α-monooxygenase,	Diarrhea, Joint pain, Hot flushes

		which is used for testosterone synthesis	
Apalutamide	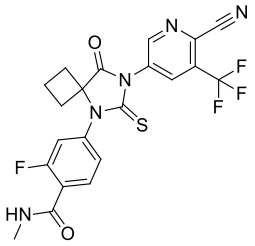	Binds to AR ligand-binding domain, hindering nuclear translocation, preventing DNA binding, and inducing alterations in transcription.	Peripheral edema, Thyroid dysfunction
Rucaparib camsylate	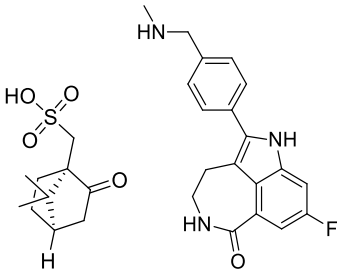	Binds with PARP1, 2 and 3 and inhibits PARP-mediated DNA repair which leads to cell cycle arrest and apoptosis	Vomiting, Constipation

1.5. Role of Androgen Receptor in Prostate Cancer

Prostate cancer progression is closely linked to the androgen receptor (AR). AR signaling drives the growth of prostate cancer cells. Initially, cancer is androgen-dependent, responding to androgen deprivation therapy. However, it often progresses to castration-resistant prostate cancer (CRPC), where AR signaling persists despite low androgen levels, promoting tumor growth. Androgens, including testosterone and dihydrotestosterone (DHT), represent the essential male sex hormones necessary for the formation of the male reproductive system and the development of secondary sexual characteristics. The conversion of testosterone into DHT is facilitated by the enzyme 5α-reductase. The DHT then effectively activates the AR, which is responsible for mediating these hormonal effects. Notably, DHT exhibits a binding affinity for the AR that is twice as strong as that of testosterone. The AR is situated on the X chromosome and is expressed in various tissues including bone, prostate, muscle, adipose tissue, and the reproductive organs. In terms of structure, the AR

consists of three primary functional domains: the *N*-terminal transcriptional regulation domain which promotes transcriptional activities, the DNA binding domain (DBD) recognizes the specific DNA sequence and facilitate binding, and the ligand binding domain (LBD) facilitates the binding of androgen ligands [31]. The AR plays a significant role in promoting cellular proliferation, particularly evident in its stimulation of cell growth within the prostate gland as shown in **Figure 2** [48].

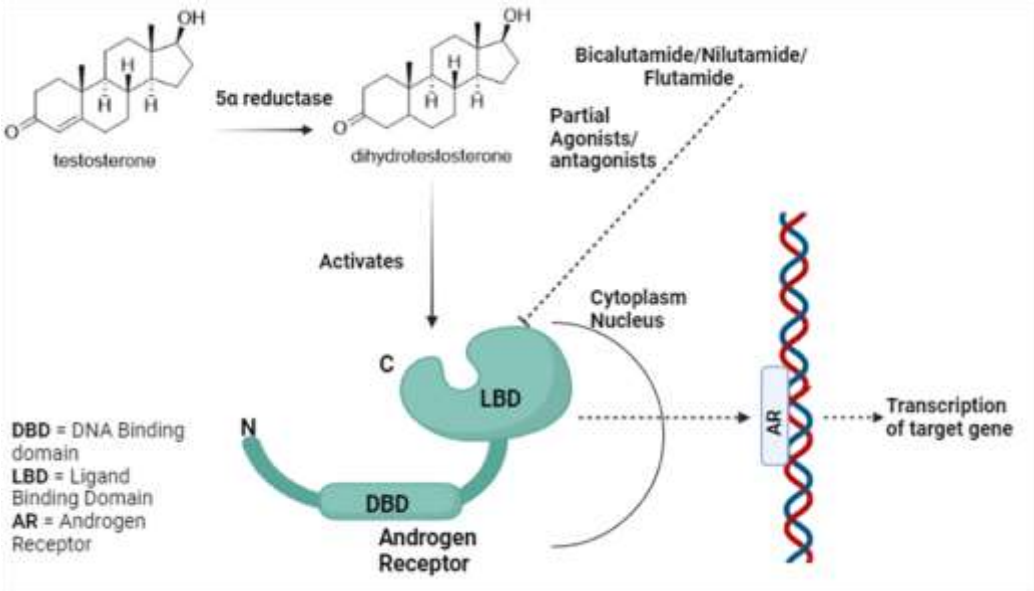

Figure 2: Role of androgen receptors and its antagonists

The androgen receptor has a significant role in promoting cell growth, made this a main target for prostate cancer treatment. Antiandrogens compititevly binds to LBD and inhibit the function of androgen receptor. Two types of antiandrogen drugs are available in the market *viz* steroid-based anti-androgen agents and non-steroidal anti-androgen agents for prostate cancer treatment. Some marketed steroidal antagonists for prostate cancer treatment include oxendolone, cyproterone, spironolactone, etc. However, these agents have various limitations, such as poor oral bioavailability and pharmacokinetics, potential hepatotoxicity, lack of tissue selectivity, cross-reactions with other steroids, and limited structural modifications due to their rigidity. On the other hand, non-steroidal antagonists like flutamide, nilutamide, *R*-bicalutamide, etc., as shown in **Figure 3** [49] are available in the market and are more favorable for clinical applications. These agents offer several advantages over steroidal antagonists, such as good tissue selectivity, favourable pharmacokinetic profiles, androgen

receptor specificity, absence of steroidal-related adverse effects, and flexibility for structural modifications [50]. However, non-steroidal antagonists still have limitations in clinical applications due to side effects like gynecomastia and hepatotoxicity with long-term administration. Furthermore, non-steroidal antagonists are not purely antagonistic as they also exhibit partial agonistic activity. Till date, enzalutamide and apalutamide have emerged as pure antagonists for the androgen receptor; however, they do exhibit side effects similar to other non-steroidal antiandrogen drugs [48, 51].

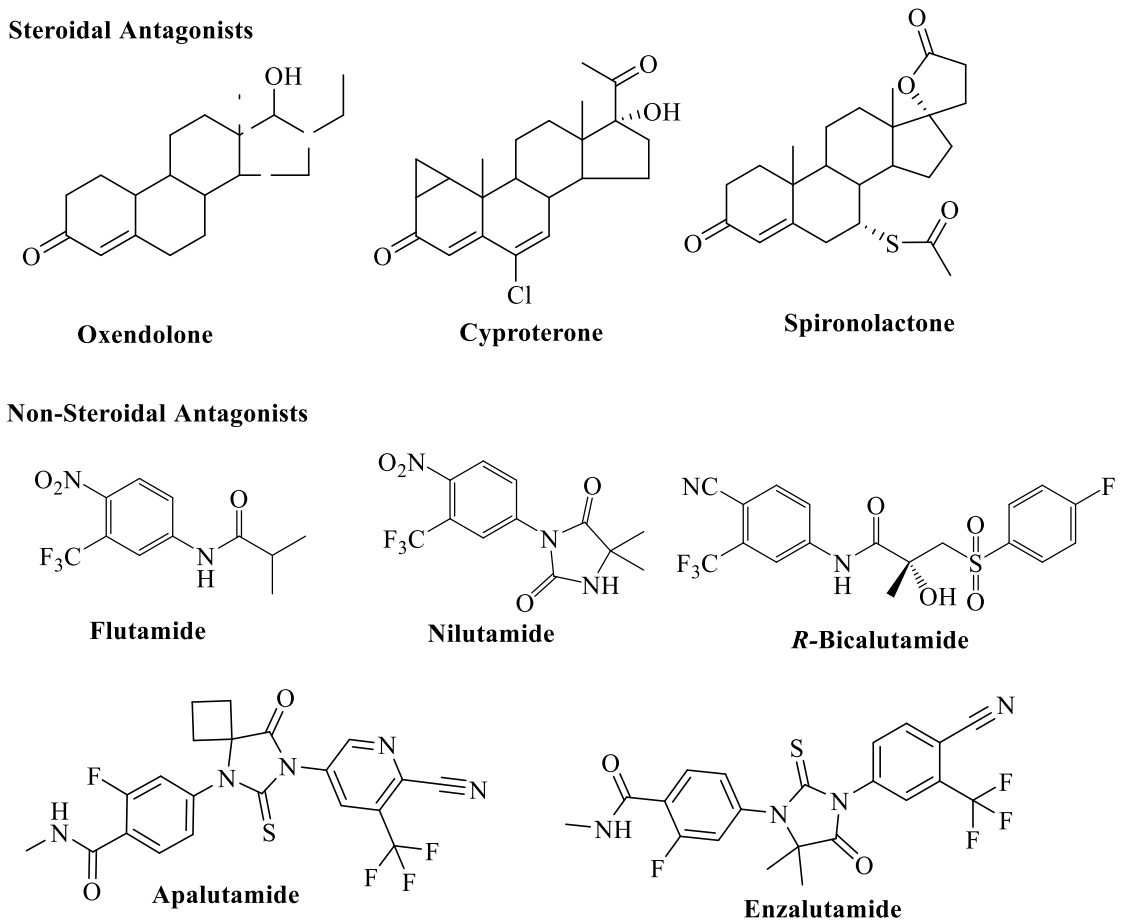

Figure 3: Marketed androgen receptor inhibitors

CHAPTER 2

2. Review of Literature

Prostate cancer remains highly prevalent among men worldwide, significantly impacting public health. Over the past decade, extensive research has focused on exploring prostate cancer development and progression, alongside the search of innovative therapeutic approaches to combat this challenging disease effectively. This comprehensive literature review explores into the progress achieved in prostate cancer research in the last decade. Various research on prostate cancer emphasizes the vital role of chemical moieties as fundamental building blocks in drug discovery, significantly contributing to the development of precise and potent anticancer agents. Among these few moieties like arylpiperazines, carboxamides, bicalutamides, oxadiazoles, triazoles, flavanol moieties, and other miscellaneous categories have showed promising activity against prostate cancer. The mentioned chemical classes exhibit distinct molecular interactions and pharmacological properties, rendering them attractive candidates for crafting innovative therapeutic interventions. Despite promising results, developing anticancer agents like arylpiperazines, carboxamides, and others faces challenges such as drug resistance, toxicity, and limited specificity. Future research should focus on overcoming these issues through targeted delivery systems, combination therapies, and personalized medicine approaches to enhance efficacy and reduce adverse effects [52].

2.1. Arylpiperazine Based Derivatives

Compounds containing arylpiperazine moieties often exhibit various bioactivities like antiarrhythmic, antiallergic, antidepressant, anxiolytic effects and many more. An arylpiperazine based drug Naftopidil is one of the drug used for the treatment of prostate cancer by targeting the androgen receptor [53]. Xu and colleagues, new arylpiperazine derivatives were designed and synthesized. These were tested against two androgen-dependent HPC cell lines (PC-3 and LNCaP) and one androgen-independent HPC cell line (DU145). Compound **1** displayed the highest potency against tested cell lines, with IC_{50} values of 6.69, 6.07, and 5.83 μM, respectively. Their study concluded that benzylpiperazine derivatives exhibited greater activity compared to phenylpiperazine derivatives. Substitution with *m*-CH_3 and *chloro* groups on the phenyl ring showed strong activity against LNCaP cell lines but less potency against PC-3 and DU145, respectively. On the other hand, *o*-substitution with an electron-withdrawing group on

the phenyl ring reduced activity against all tested cell lines. Additionally, methyl sulfonyl substitution at *ortho* of the phenyl established potent activity against LNCaP [54]. Continuing from their previous work, the same research team has further explored arylpiperazine clubbed amide derivatives against HPC cell lines (PC-3, LNCaP, and DU145). Among these, Compound **2** emerged as the most potent against PC-3, LNCaP, and DU145, with IC_{50} values of 1.18, 6.23, and 1.23 μM, respectively. The study also revealed that adding hydrophobic groups to the aryl position resulted in increased activity against all tested cell lines. Introducing the α-indolyl group enhanced activity against PC-3 but reduced it against LNCaP and DU145. Incorporating heteroaryl derivatives at the aryl position exhibited potent activity against DU145 while showing weaker activity against LNCaP and PC-3 [55]. Chen *et al.,* further explored arylpiperazines clubbed with saccharin against PC-3, LNCaP, and DU145 cancer cell lines. Among all the synthesized compounds, **3** was the most potent compound against the DU145 with IC_{50} value of 1.28 μM while having moderate activity against Compound other two cell lines (PC-3 and LNCaP) with IC_{50} value of >50 μM as compared to standard drug Naftopidil [56]. The same authors have synthesized a series of compounds by combining an aromatic phenol ring and an arylpiperazine tail. They tested these compounds on three types of HPC cells: PC-3, LNCaP, and DU145. Compound **4**, showed the best results against all three cell types. It worked even better than the standard drug Naftopidil (showed in **Figure 4**), with IC_{50} values of 9.23 μM, 8.74 μM, and 8.51 μM for the three cell lines, respectively. Compound **4** has also showed decrease in androgen receptors activity by 50.1% [57]. Further, same research group synthesized naftopidil based arylpiperazine derivatives and compound **5** has showed promising activity with IC_{50} value of 46.72, 17.33 and 0.86 μM against PC-3, LNCaP and DU145, respectively as compared to naftopidil. It has been found that aryl substituent has exhibited selective cytotoxic activity against LNCaP as heteroaryl (pyridine) has showed selective cytotoxic activity against DU145 [58]. Further, they explored arylpiperazine clubbed 4-amino-2*H*-benzo[*h*]chromen-2-one derivative against the two cancers cell lines PC-3 and LNCaP and compound **6** was found to be the most potent derivative against LNCaP. Moreover, compound **6** has weak activity against PC-3 as compared to naftopidil. Compound **6** was also found to have AR (androgen receptor) antagonistic activity by 72.1% [59]. Same research group also

designed, synthesized piperazine clubbed bromophenol moiety (compound **7**,) and evaluated them against HPC cell line PC-3 and LNCaP. Results depicted out compound **7** as the most potent compound against both of the tested cancer cell lines as compared to standard drug naftopidil with IC_{50} value of 0.05 and 0.18 µM respectively [60].

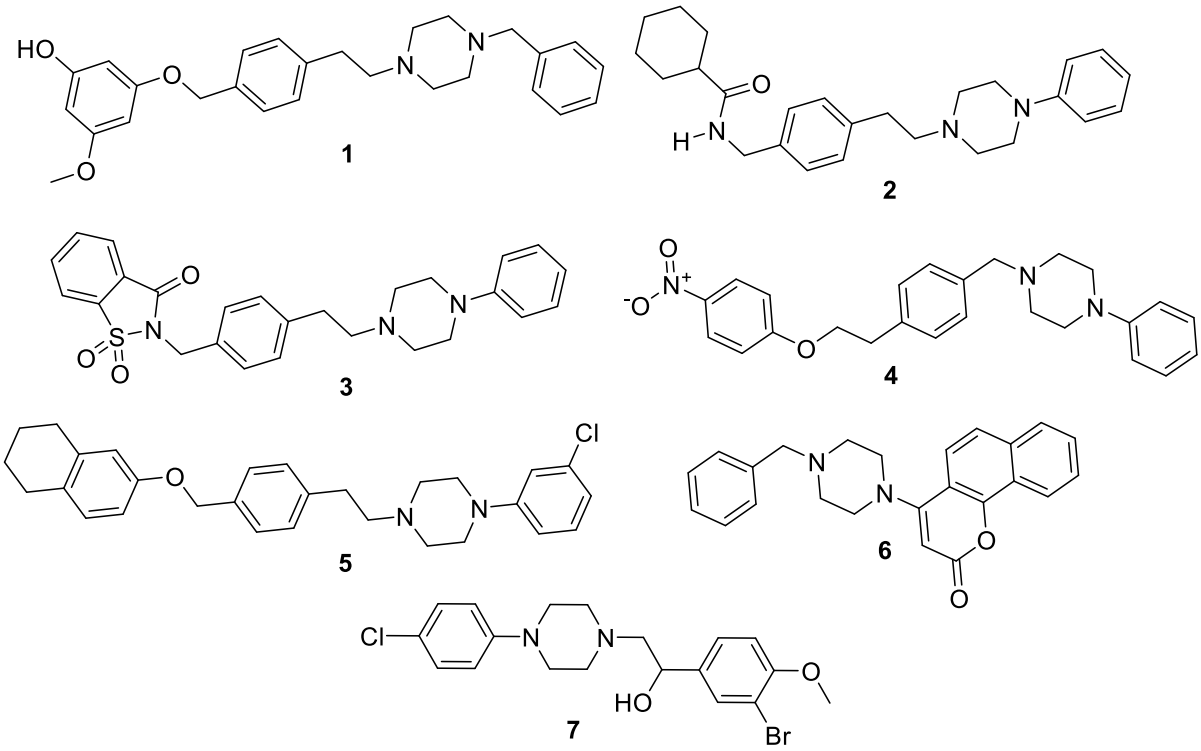

Figure 4: Representing structures of arylpiperazine-based derivatives

2.2. Bicalutamide Based Derivatives

Bicalutamide is one of the non-steroidal based anti-androgen drugs which is widely used for the treatment of PC [61]. So, designing derivatives of bicalutamide is one of the good approaches to find the new molecules of bicalutamide and a potential drug against prostate cancer.

Kandil and co-authors explored novel deshydroxy bicalutamide compounds prostate cancer cell line LNCaP. From *in vitro* assay it was revealed that compound **8** was established as most potent compound against tested cell line by IC_{50} value of 0.43 µM. It has been reported that presence of sulfur showed potent inhibition as compared to suphone. Apart from this, substitution of *o*-CF_3 has showed potent inhibition as compared to *m*-CF_3 [62]. Same research group evaluated anticancer property against of bicalutamide derivatuves against HPC cell lines (22Rv1, DU-145, LNCaP and VCaP).

The result of *in vitro* assay revealed that compound **9** was the most potent compound compared to all the tested cancerous cell lines by IC_{50} values of 6.59-10.86 µM. In these synthesized analogues, sulfur was found to be most appropriate group because oxidation of sulfur to the corresponding sulfoxide (or sulfone) lost the biological activity [63]. Pertusati *et al.,* designed and synthesized a new series based on bicalutamide and evaluated against HPC cell lines VCaP, LNCaP, 22Rv1and Du-145. From the results, it was found that Compound **10** was the most potent compound against all the tested cancerous cell line [64]. Novel anti-prostate cancer agents bearing 3,5-bis-trifluoromethylphenyl moiety was designed and synthesized by Ferla and coworkers. They evaluated all the compounds against four HPC cell lines 22Rv1, DU-145, LNCaP and VCaP. Compound **11** was the most potent compound against all the tested cancerous cell lines with IC_{50} value in the range of 2.5-6.36 µM (**Figure 5**). It has been observed 3,5-bis-trifluoromethyl substituent at aromatic ring and CN group along with CF_3 gives better activity as compared to other EWGs substituent [65].

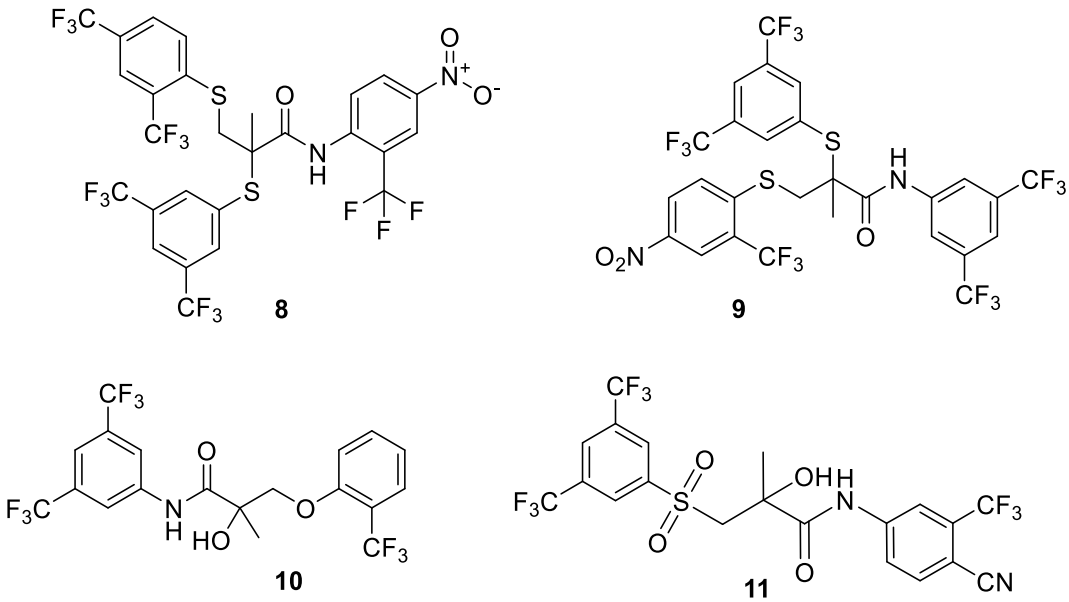

Figure 5: Androgen inhibitors based on bicalutamide

2.3. Flavonoid Based Derivatives

Flavonoid is best known for its prostate cancer and can be treated with the help of flavonoid enriched diet. Apart from this, it was also known that flavonoid-based compounds like quercetin and dehydro-silybin are the best-known compounds against

the prostate cancer [66]. So, various researchers has evaluated compound based upon the flavonoid against prostate cancer and these efforts are discussed below:

Li and co-authors evaluated the anticancer activity of several 3-*O*-substituted-3',4',5'-trimethoxyflavonols against PC-3, DU-145 and LNCaP. Compound **12**, (**Figure 6**) was found one of the potent compound by IC_{50} values of 32.1, 27.2 and 14.7 μM (PC-3, DU-145 and LNCaP, respectively). It has been noted that modifications at -OH groups in parent molecule gives more potent derivatives and as chain length increases activity decreases [67].

Rajaram and his research team evaluated the antiprostate cancer protentional of novel nitrogen-containing derivatives of *O*-tetramethyl quercetin against PC-3, LNCaP and DU145. From the results, it was depicted that Compound **13** demonstrated the best potent activity against all the tested HPC cell lines. It has been concluded that 5-*O*-aminoalkyl derivatives are more potent than 3-*O*-aminoalkyl derivatives against PC [68].

Vue *et al.,* explored 7-OH in silibinin and 2,3-dehydrosilibinin against cell lines (LNCaP, DU-145 and PC-3). Their study revealed that Compound **14** as one of the best compound with IC_{50} of 2.76, 7.92 and 2.39 μM against LNCaP, DU-145 and PC-3, respectively. Moreover, 2,3-dehydrosilibinin derivatives were more potent silibinins and alkylation at 7-OH of silibinin enhances potency against prostate cancer [69]. Further, the same authors explored the effect of trimethyl-2,3-dehydrosilybin via an appropriate linker as potential anti-cancer agents against PC-3, DU145 and LNCaP. Their study revealed that compound **15** was the most potent compound against PC-3, DU145 and LNCaP with IC_{50} values of 1.40, 1.84 and 1.82 μM, respectively. Furthermore, substitution of hydroxyl group on 2,3-dehydrosilybin increase potency [70].

Jian and his colleagues designed, synthesized 23-*O*-substituted-2,3-Dehydrosilybins derivatives and evaluated their anticancer potential upon LNCaP, DU145 and PC-3. The results of their study stated that compound **16** had good activity compared to all of these tested cancerous cell lines (**Figure 6**) [71].

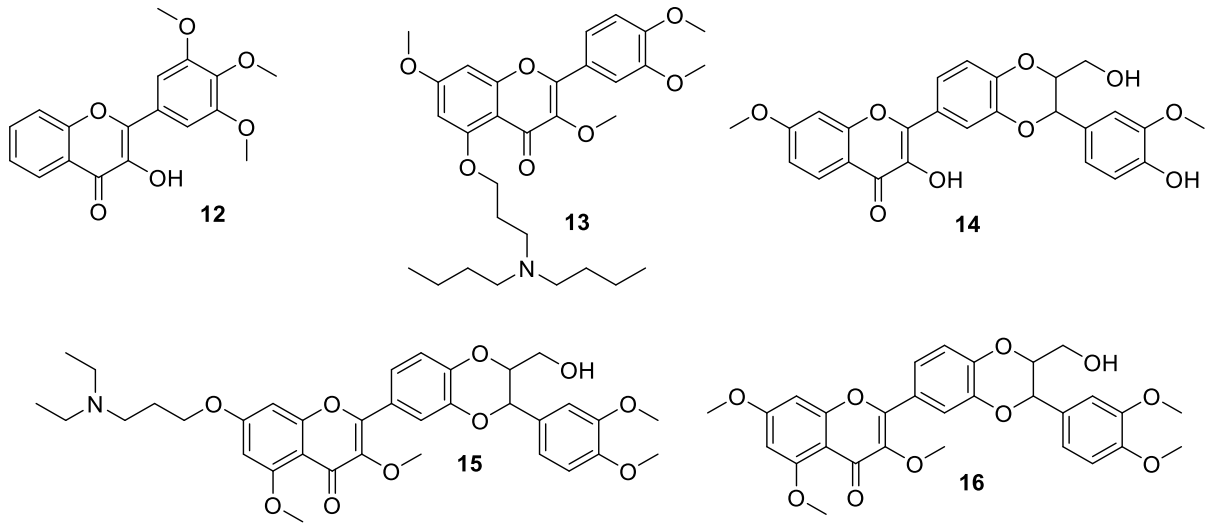

Figure 6: Flavonoid based antiandrogen inhibitors

2.4. Benzamide Based Derivatives

Benzamide group are found to be potent compound against prostate cancer by targeting the androgen receptor. Impact of phenylsulfonyl-benzamides derivatives on HPC cell lines LNCaP, 22Rv1, VCaP and DU145 were elaborated by Bassetto *et al*. Researchers have designed and synthesized derivative of phenylsulfonyl-benzamides and concluded that compound **17** was the most potent compound against all the tested cancerous cell lines LNCaP, 22Rv1, VCaP and DU145 with IC_{50} values of 5.95, 9.66, 5.73 and 10.58 μM, respectively. The replacement of the SF_5 group with CF_3 moiety at *para* or *meta* position improves activity whereas *ortho* trifluoromethyl group decrease the activity of derivatives [72].

Bindu and colleagues explored anticancer potential of *N*-(benzo[d]thiazol-2-yl)-2-hydroxyquinoline-4-carboxamides against HPC cell lines PC-3 and LNCaP. *In vitro* results revealed that compound **18** was most potent compound against both the tested cancerous cell lines [73].

Research team of Kazui reported synthesis of 4-[4-(benzoylamino)phenoxy]phenol derivative and evaluated their anticancer activity against HPC cell line LNCaP and PC-3. Their study stated that compound **19** was potent compound against both cancer cell lines (**Figure 7**). Fluorine (mostly) or chlorine substitution on aryl ring increases the activity as compared to bromine and iodine substitution [74].

Soliman and colleagues exploared novel *N*-(4-3-(phenyl)-1-prop-2-en-1-one phenyl) benzamides against HPC cell line PC-3. *In Vitro* assay revealed that Compound **20** was potent against PC-3 cell lines by IC_{50} value of 5.59 µM (**Figure 7**). It has been observed that EWGs like Cl- at *ortho* and *para* position of ring A increase activity against the tested cell lines[75].

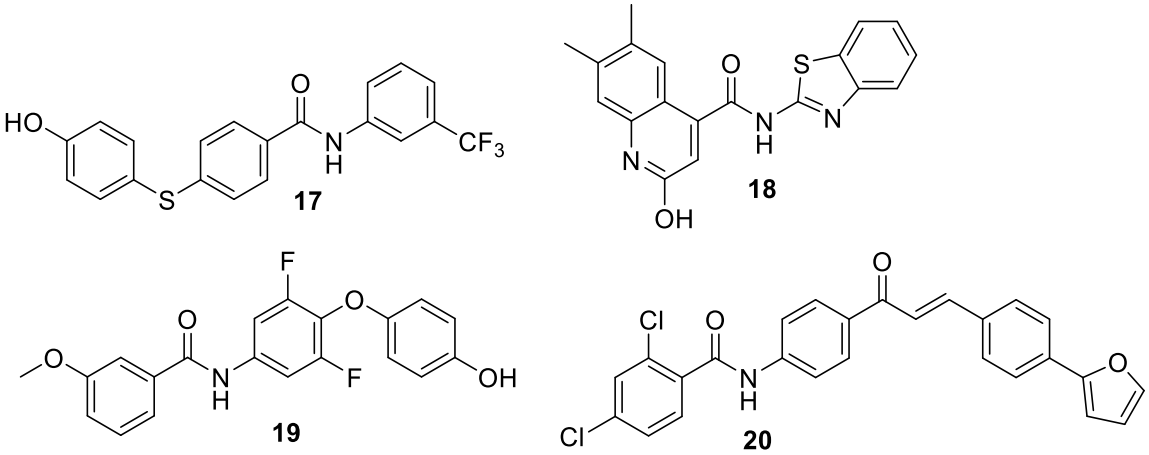

Figure 7: Benzamide based derivatives

2.5. Triazole Based Derivatives

Triazole scaffold bearing molecules are widely used for the treatment of various fungal, bacterial and different types of cancers including prostate by targeting the androgen receptor, respectively. In continuation, Kumar and his colleagues prepared and evaluated a series of Alkyne–azide conjugates with triazoles nucleus against PC-3 HPC cell line. Their study results revealed that compound **21** have showed significant promising activity with an IC_{50} value of 2.04 µM. Further, they have also stated that *ortho* substituted aryl ring position with mainly EDGs like methyl enhances their anticancer potential as compare to *m* and *p* substituted analogues [76]. Another group also synthesised and evaluated 1,3,4-thiadiazoles and 1,2,4-triazoles derivatives linked to pyrazolyl coumarin ring against HPC cell lines LNCaP and PC-3, respectively. Their study results concluded that triazole substituted analogues were more potent with respect thaidiazole derivatives. The most promising compound **22** exhibited significant activities with an IC_{50} values of 0.24 and 1.37 µM against LNCaP and PC-3 cell lines (**Figure 8**) [77].

Xie and his team members evaluated selective AR degraders (SARDs) with different linkers against PC-3, LNCaP and WPMY-1 cell lines. They have found that compound

23 was effective molecule against the LNCaP with IC_{50} value of 1.75 µM in comparison to other synthesized derivatives with excellent AR degradation activity as well. In addition, compound **23** has showed weaker activity against the other two tested cell lines (PC-3 and WPMY-1) with IC_{50} values more than 80 µM (**Figure 8**) [78].

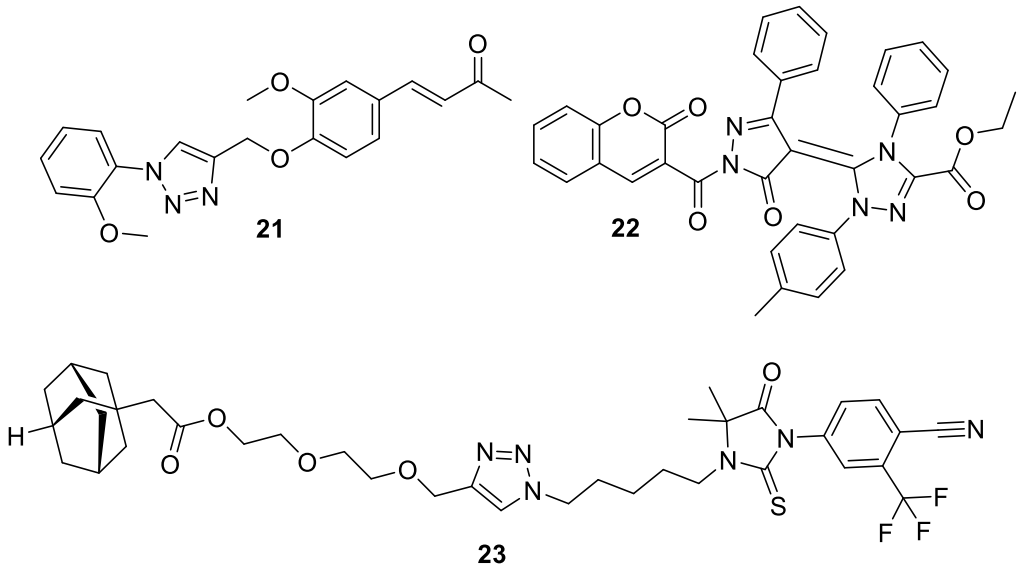

Figure 8: Triazoles as antiprostate cancer agents

2.6. Furanocumarin/ Curcumin/piperazine Based Derivatives

Chauthe and colleagues synthesized and checked twenty two furanocoumarin derivatives for cytotoxicity and structure activity relationship of the substituted compounds was also studied (**Figure 9**). Among synthesized compounds, compound **24** depicted promising antiproliferative activity in MCF-7 cell line (Breast cancer) and PC-3 cell line. In respect to structural modification, it has been found that biological activity improves with *N*,*N*'- alkylation substitution while aryl and acyl substitution decrease the activity [79]. Zhang and co-authors has synthesized various 1,9-diarylnona1,3,6,8-tetraen-5-ones (curcumin analogues) using wittig reaction. This study concluded that these analogues can be used as a potential scaffold for anti-prostate cancer agents . Compounds **25** and **26**, decreased PC-3 cell proliferation by stimulating apoptosis process and by striking the cell cycle (G0/G1 phase) [80]. Bhati and coworkers. designed piperazine linked thiohydantoin derivatives that were debveloped using AutoDock 4.2. All derivatives obeyed Lipinski's rule and showed good oral bioavailability. The results depicted that binding energy was in between -11.1 and -9.30

kcal/mol and the inhibition constant was in between 7.25-152.11 nM. compound **27** is a potential androgen antagonist due to its stability and better interaction with a receptor (**Figure 9**) [81].

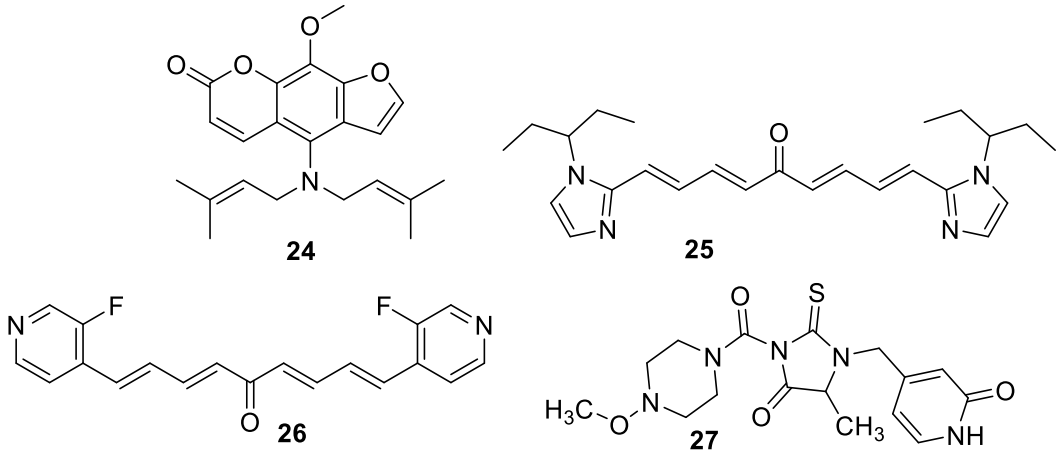

Figure 9: Derivatives based on furanocoumarin, curcumin and piperazine

2.7. Oxadiazole Based Derivatives

Oxadiazole has a wide range of activities like antidiabetic, antibacterial, etc. Advancement in the oxadiazole based derivatives against prostate cancer agents by targeting androgen receptors are discussed below:

Ticona and the group have synthesized novel pyridinyl-based 1,2,4-oxadiazole compounds and evaluated their anticancer activity against the prostate cancer cell line (DU-145). From the *in vitro* assay, it was assessed that compound **28** was the most potent compound with an IC_{50} value of 1.57 µM. SAR analysis assessed that substituting the 5th place of the 1,2,4-oxadiazole with thiophene proved to be the most favorable modification for enhancing the compounds' activity. On the other hand, when furan or azole substitutions were employed, the resulting compounds exhibited reduced potency compared to those with thiophene substitutions [82].

Oggu and the research group have designed, synthesized, and evaluated the anti-prostate cancer activity of 1,2,3-triazole incorporated 1,3,4-oxadiazole-Triazine ragainst PC-3 and DU-145 cell lines. Results revealed that among all the synthesized compounds pyridine-4-yl substituted compound **29** has showed the best action with an IC_{50} of 0.17 µM (PC-3 cell lines) and 0.16 µM (DU-145 cell lines) as compared to

standard drug etoposide (2.39 µM PC-3 and 1.97 µM DU-145). An analysis of the SAR revealed that heterocyclic rings resembling pyridine demonstrated significantly higher potency compared to phenyl rings, regardless of the presence of electron-donating groups (EDGs) or electron-withdrawing groups (EWGs) as substitutions [83].

Biological evaluation of 1,3,4-oxadiazole-bearing pyrimidine-pyrazine against HPC cell lines PC-3 and DU145 were conducted by Rachala and co-workers. Compound **30** was potent compound with an IC_{50} of 0.13 and 0.11 µM (PC-3 and DU-145, respectively). The IC_{50} for the standard drug etoposide were found to be 2.39 µM against PC-3 and 1.97 µM against DU-145 cell lines. Moreover, it was also assessed that substitution with EDGs containing phenyl ring has showed potent results as compared to compound containing phenyl ring with EWGs (**Figure 10**) [84].

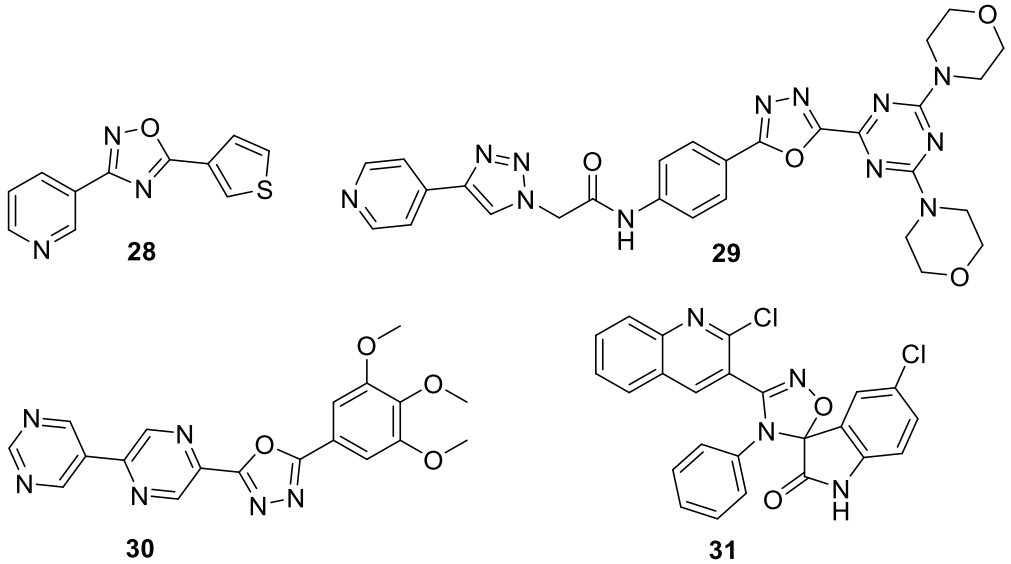

Figure 10: Disubstituted oxadiazoles derivatives

Kanchrana *et al.* evaluated the anticancer potential of spirooxindolo-1,2,4-oxadiazoles derivatives against the DU-145 HCP cell line. All the compounds were synthesized using a cycloaddition reaction. Results suggested that compound **31** has showed modest anti-prostate cancer action with IC_{50} of 19.27 µM while standard drug doxorubicin has showed an IC_{50} of 1.89 µM. Substitution with EWGs like halogens was more favourable for activity than substitution with the EDGs (**Figure 10**) [85].

Naaz and coauthors has evaluated the antiprostate cancer potential of newly synthesized 1,3,4-oxadiazole clubbed indole derivatives. Results of *in vitro* assay suggested that compound **32** has the most potent activity with IC_{50} value of 2.42 µM against PC-3 cell lines as compared to standard drug doxorubicin (IC_{50} 6.31 µM). Moreover, it was also assessed that compound **32** induced cyclic capture at G0/G1 phase along disruption of mitochondrial membrane. From the SAR analysis, it was observed that 1,3,4-oxadiazole has a better influence on anticancer activity as compared to 1,2,4-triazole [86].

Various 1,2,4-oxadiazole clubbed 1,2,3-triazole-pyrazole derivatives were evaluated against PC-3 and DU145 prostate cancer cell lines by Mohan *et al.* Results of the MTT assay revealed that compound **33** exhibited potent activity against both cell lines with IC_{50} of 0.01 µM and 0.081 µM, respectively. Phenyl substituted with EWGs at the 3rd position of 1,2,4-oxadiazole has showed enhanced activity as compared to EDGs substituted phenyl [87].

Al-Wahaibi *et al.,* evaluated 1,3,4-Oxadiazole *N*-Mannich Bases against PC-3. Compound **34** was most potent compound against PC-3 with an IC_{50} of 23.92 µM as compared to doxorubicin (IC_{50} = 8.87 µM). From the SAR interpretation, it was observed that substitution with benzyl at piperazine has showed promising anticancer activity as compared to substituted benzyl group [88].

Alam and coworkers have designed, synthesized and anti-prostate cancer activity of new eugenol derivatives containing 1,3,4-oxadiazole against PC-3 cell lines. *In vitro* assay revealed that **35** has most promising activity with IC_{50} of 0.26 µM as compared to doxorubicin 2.61 µM. Mercapto linker with acyclic chain substitution has showed promising activity as compared to cyclic substitution at mercapto linker. Moreover, ADMET confirm the favourable drug likeness properties of synthesized compounds (**Figure 11**) [89].

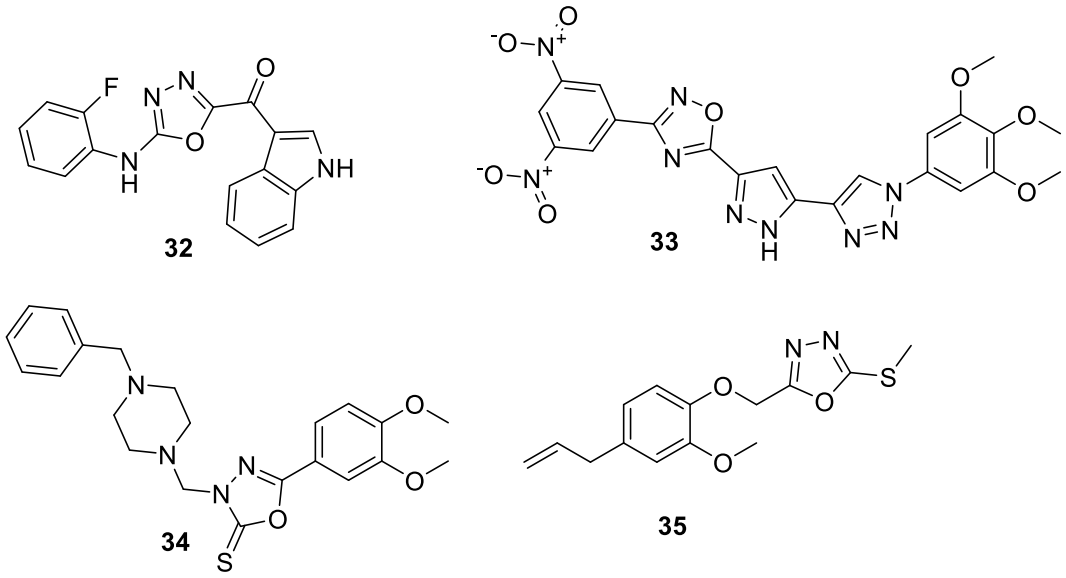

Figure 11: Oxadiazoles representatives as anti-prostate cancer agents

Bommera and colleagues have reported anticancer activity of 5-fluorouracil clubbed 1,2,4-oxadiazoles derivatives against DU-145. Compound **37** was one of the most potent compounds against prostate cancer with IC_{50} of 0.017 µM against DU-145 cell line as compared to etoposide (IC_{50} = 1.97 µM). Moreover, molecular docking suggested that compound **37** had occupied the active cavity of AR. ADMET analysis revealed compound **37** has promising physicochemical properties. SAR suggested EDGs substitution on phenyl ring has resulted in potent activity as compared to EWGs [90].

Quinazoline linked 1,2,4- oxadiazole-isoxazole derivatives were designed, and synthesized by Srinivas and coworkers. Authors have evaluated the antiprostate cancer potential of all the compounds against DU145 and revealed that compound **38** has the most promising activity against DU-145 (IC_{50} of 0.011 µM) as compared to standard drug etoposide (IC_{50} = 1.97 µM). Substitution with EDGs has showed promising anti-prostate cancer activity as compared to EWGs substitution [91].

The research team of Nagaraju reported the one-pot synthesis of 1,2,4-oxadiazole-1,4-Benzoxazine hybrids and evaluated their anti-prostate cancer potential against PC3 cell lines. Compound **39** has showed promising activity with IC_{50} 3.41 µM as compared to standard drug etoposide (IC_{50} = 2.39 µM). Analysis of SAR data revealed that

substituting EWGs (like CN) has accounted for antiprostate cancer effect as compared to EDGs [92]. Vaidya *et al.,* reported anticancer potential of 1,2,4-oxadiazoles against PC-3. The *in vitro* data established compound **40** has found to be a moderate active molecule against prostate cancer with an IC_{50} value of 15.7 µM as compared to the standard drug mitomycin (IC_{50} = 1.5 µM). Substitution with EDGs like hydroxy has resulted in better activity as compared to substitution with EWGs (**Figure 12**) [93].

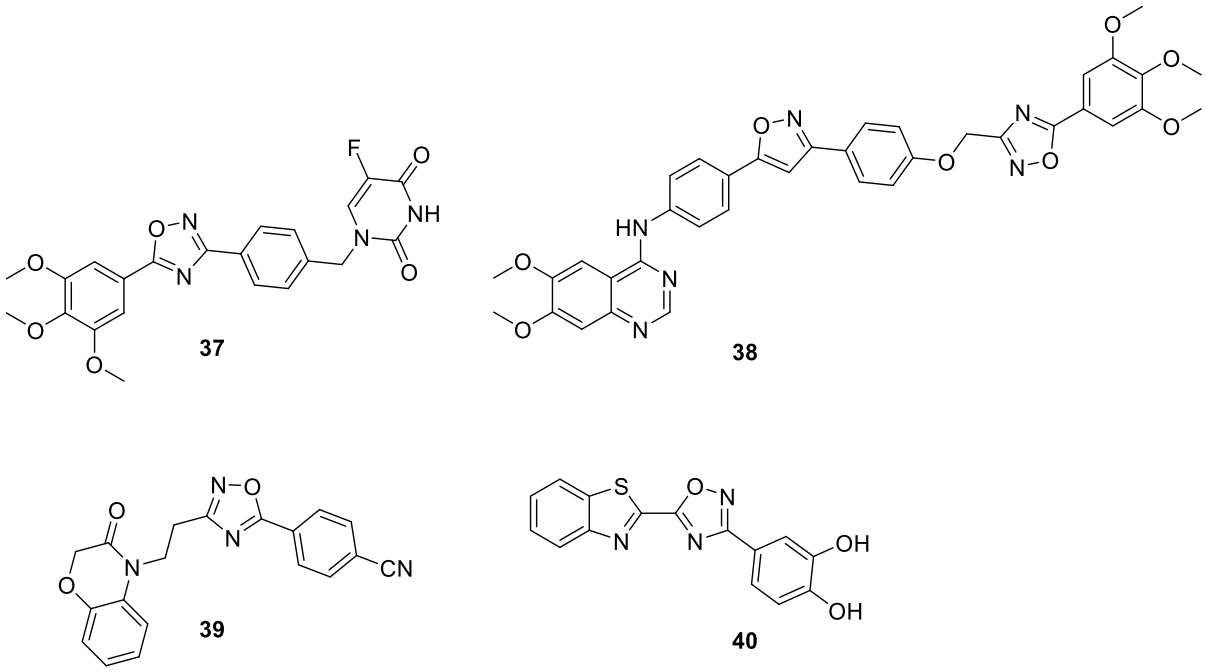

Figure 12: Representative structures of 1,2,4-oxadiazoles

Mochona and research team designed and synthesized oxadiazole derivatives and evaluated their anticancer activity against HPC cell line (PC-3 and LNCaP. It was found that compound **41** was the most potent compound against both tested cell lines with IC_{50} values of 0.22, 1.3 µM respectively). It has been summarized that substitution of CF_3 at *para* position at ring A increase the activity but any group substitution at B ring led to decrease in the activity. Similarly, substitution with aryl ring at both A and B decrease the activity. Amide linkage also plays important role to increase the drug efficacy [94].

Gamal El-Din M.M. and colleagues designed, and synthesized diarylamides and diarylureas possessing 1,3,4-oxadiazole and evaluated anticancer potential against HPC cell line PC-3 (**Figure 13**). From the results, it was obtained that Compound **42** was

found to be the most potent compound against PC-3 with IC_{50} = 0.80 µM. Chemically, it has been found that bis 3, 5- CF_3 as well as aryl substitution at are essential for the activity while aliphatic chain decrease the activity. EWGs like halogen especially chlorine at para position is better for activity as compared to EDGs [95].

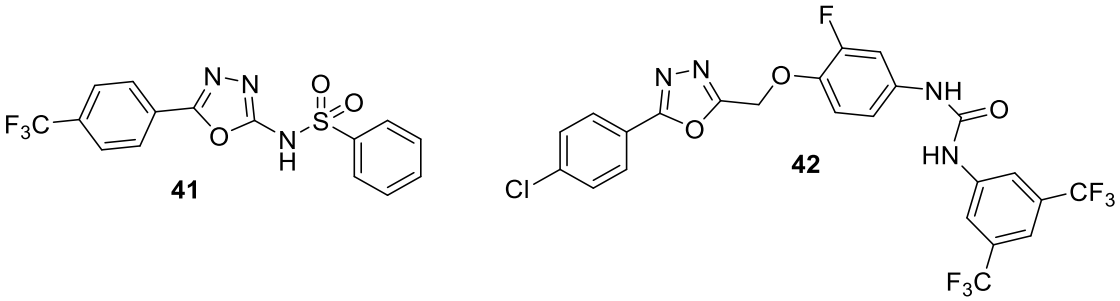

Figure 13: Oxadiazole based derivatives

2.8. Miscellaneous Agents

Arjun and coauthors has designed, synthesized some benzohydrazide and evaluated against HPC cell lines LNCaP and PC-3. Compound **43** was found to be most potent compound against LNCaP while having moderate activity against PC-3 [96]. Novel benzothiazole derivatives were synthesized by Cao *et al.* Further, authors have evaluated all the compounds against DU145 and PC-3 (**Figure 14**). From the results, it was depicted that Compound **44** was the most potent compound against both the tested cancer cell line with nanomolar range of IC_{50} [97].

Gomha and coworkers., designed, and synthesized isoxazolopyrimidinethione derivatives and evaluated them against LNCaP and PC-3. Results revealed that Compound **45** was found to be the most potent compound against LNCaP while it has moderate activity against PC-3 [98]. Mohareb and his research team designed, and synthesized tetrahydropyrazolo-quinazoline and tetrahydropyrazolo-pyrimidocarbazole derivatives and evaluated their anticancer potential against HPC cell line PC-3. Compound **46** was potent compound (PC-3 with IC_{50} of 0.42 µM) [99]. Saravanan K. *et al.,* evaluated isoindoline based compounds against two cell lines PC-3 and LNCaP with IC_{50} value of 43.12, 5.96 respectively. *In vitro* assay showed that Compound **47** was the most potent compound against LNCaP and weaker activity against PC-3 [100].The research team of Szumilak has designed, synthesized, and evaluated some novel polyamine derivatives. PC-3 and DU145 were utilized for

prostate cancer study and results suggested that Compound **48** has weaker activity against both of the cell lines (**Figure 14**) [101].

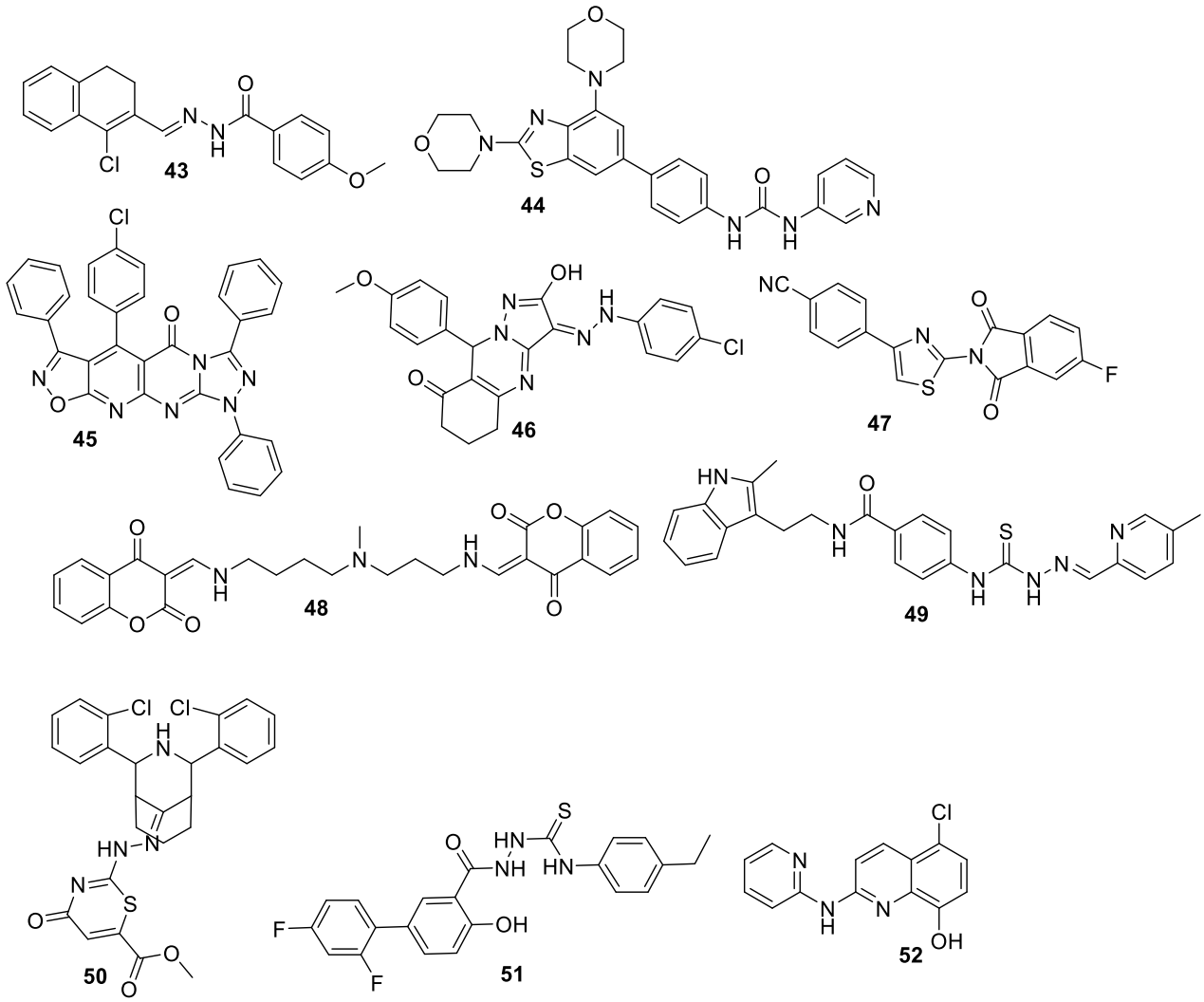

Figure 14: *N*-containing compounds as anti-prostate cancer agents

He *et al.*, evaluated new thiosemicarbazone-indole analogues and evaluated against PC-3 and WPMY-1. Results yielded Compound **49** as the potent compound against PC-3 with IC_{50} of 0.054 µM while it has moderate activity against WPMY-1 with IC_{50} value of 19.47 µM [102]. Anand and coworkers recently reported the design, synthesis and anti-prostate cancer activity of some novel thiazinones and thiosemicarbazones derivatives. Compounds were evaluated against the LNCaP and compound **50** was most potent with IC_{50} of 30.4 µM [103]. Coskun and colleagues designed and synthesized novel thiosemicarbazide derivatives and evaluated against HPC cell line PC-3. The study results revealed that Compound **51** was potent (PC-3 IC_{50} of 11.7 µM) as

compared to standard drug cisplatin [104]. Quinoline derivatives were synthesized by Li *et al*. and tested against PC-3 cell line. Results revealed compound **52** was potent compound against PC-3 with GI_{50} = 1.29 µM (**Figure 14)** [105].

Britton *et al.* synthesized flavonol analogues and evaluated against 22rn1(prostate cancer cell line) out of which compound **53** with IC_{50} 2.6 mM were more potent in comparison to the lead compound 3' ,4' ,5' -trimethoxyflavonol (compound **54**) (IC_{50}= 3.1 mM) (**Figure 15**) and also superior to quercetin and fisetin with IC_{50}>15 mM (for both). Results depicted the presence of either hydroxy (OH) or methoxy at 3' ,4' ,5' position was essential for activity and that containing moieties may be superior [106].

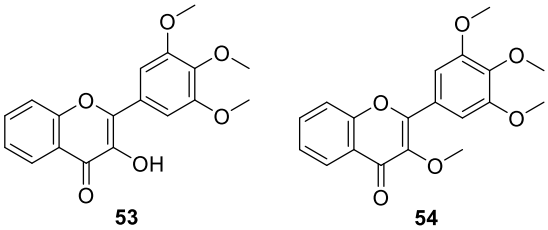

Figure 15: Miscellaneous derivatives against prostate cancer

CHAPTER 3

3. Rationale, Aim and Objectives

3.1. Rationale

In current investigation, we employed a pharmacophore-based designing strategy to facilitate the development of 1,2,4-Oxadiazole-based novel compounds. Initially, we have explored the molecular structure of bicalutamide (**1**), a prostate cancer drug available in the market. This analysis unveiled a distinctive structural motif consisting of two aromatic rings linked by a sulfonyl-2-hydroxy-2-methylpropanamide spacer within the bicalutamide molecule [107].

This structural insight led to incorporating dual aromatic rings, **A** and **B**, into the proposed framework, supported by a literature review highlighting numerous compounds with similar two-ring systems. [108]. In this context, we emphasized the example of the imidazo[1,2-α]pyridine-oxadiazole based compound **2**. This compound was designed, synthesized, evaluated as a potent anticancer agent with IC_{50} value of 3.45 µM by Sigalapilli *et al* [109]. Additionally, Oliveira and co-authors has also synthesized 3,5-disubstituted-1,2,4-oxadiazole derivatives based compound **3** demonstrating promising anticancer activity with IC_{50} value of 14.9 µM [110].

Furthermore, Gamal El-Din and colleagues reported the design and synthesis of diaryl-based 1,3,4-oxazoles based compound **4** as efficacious anti-prostate cancer agents with IC_{50} value of 0.8 µM [95]. Similarly, Pertusati *et al*. made significant advancements by identifying a series of bicalutamide-derived inhibitors compound **5** with robust anti-prostate cancer properties [64]. Moreover, Khatik and his group reported a novel series of 3,5-disubstituted 1,2,4-oxadiazole derivatives **6** showcasing proven activity against prostate cancer [111]. The dual-ring structural motif observed in prior studies guided our adoption of a similar bivalent ring system (**Figure 16**). Rings in bicalutamide and compounds **2**, **3**, **4**, and **6** were linked by a 5-membered ring or a five-atom chain. Docking analysis revealed oxadiazole's potent activity against the androgen receptor [112].

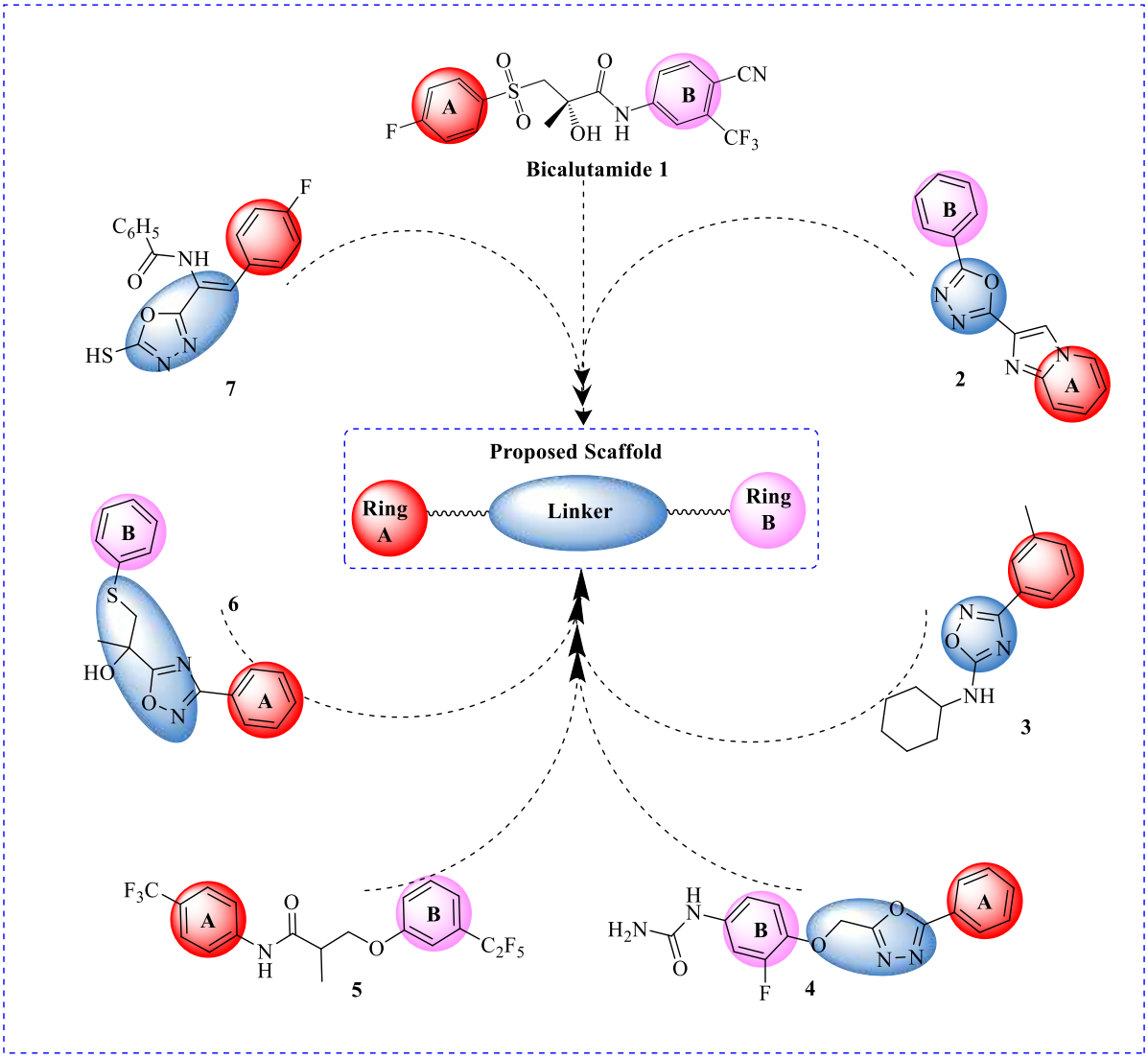

Figure 16: Designing of proposed molecules

A thorough exploration of the literature revealed the dominant use of the oxadiazoles by various researchers in the synthesis of potent compounds, as evidenced in compounds **2-4** and **6-7**. Moreover, we have also observed that compounds **5** and bicalutamide featured an aliphatic chain-type linker. Vinjavarapu *et al*. discovered 2-mercapto-5-substituted styryl-1,3,4-oxadiazoles compound **7** for prostate cancer, featuring a linker based on a 5-styryl substituted oxadiazole[113, 114]. Moreover, compounds **2** and **3** displayed an oxadiazole linker directly attached to the aryl ring and compound **6** showcased a mercapto-2-(1,2,4-oxadiazol-5-yl)propan-2-ol linker (**Figure 16)**. Considering these factors, we elected to replace the sulfonyl-2-hydroxy-2-methylpropanamide spacer in bicalutamide using a bioisoster replacement approach.

We proposed two linkers: one involving a 1,2,4-oxadiazole ring directly connected to both aryl rings and the other involving a 5-vinyl 1,2,4-oxadiazole ring connected to two aryl rings. This rationale led to the design of two series, namely **MS01-MS15** (3,5-diphenyl-1,2,4-oxadiazole) and **SP1-SP25** (3-substituted phenyl-5-substituted styryl-1,2,4-oxadiazole) and (**Figure 17**).

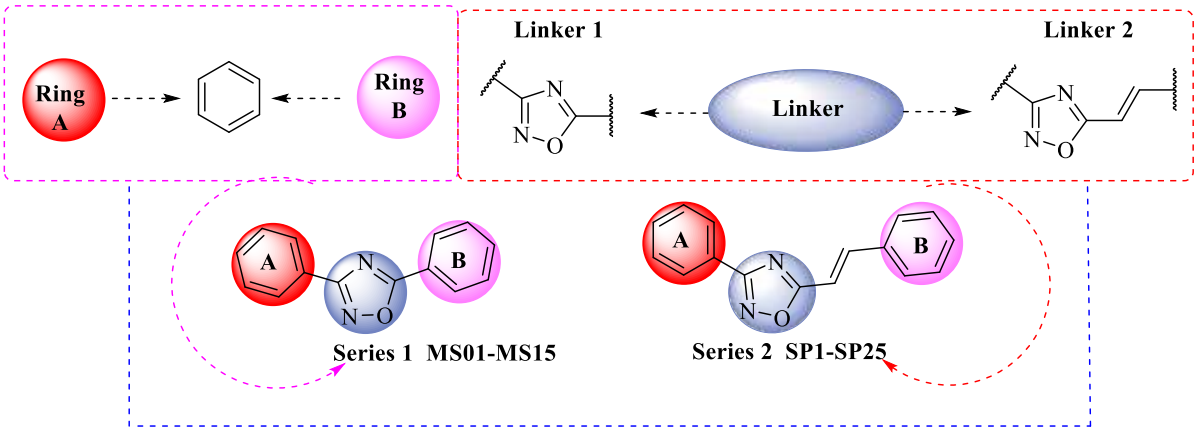

Figure 17: Basic Structure of the both designed series

3.2. Aim

Synthesis, Characterization and Evaluation of Some Novel Non-Steroidal Molecules for the Treatment of Prostate Cancer

3.3. Objectives:

- Identify novel 5-styryl-1,2,4-oxadiazoles/triazoles derivatives as the potential nonsteroidal heterocyclic derivatives for the treatment of prostate cancer through molecular docking.
- Synthesis of most potent compounds as identified through molecular docking.
- Characterization of synthesized compounds (NMR, MASS).
- *In vitro* studies of test compounds on human prostate cancer cell line (PC-3) for determining affinity and efficacy.

CHAPTER 4

4. Material and Methods

Synthetic grade chemicals and reagents were utilized and acquired from various vendors such as BLD Pharm, Loba Chemie, and Merck, as well as local suppliers. Analytical grade pure solvents were employed. Characterization of synthesized compounds accomplished following recrystallization and purification through column chromatography. The ^{1}H NMR and ^{13}C NMR spectra were obtained using the Avance III HD series from Bruker at frequencies of 400 MHz and the chemical shifts were recorded in ppm. Mass spectra within the range of 0 to 700 m/z were recorded using a Gas Chromatograph-Mass Spectrometer and the Shimadzu model specifically GCMS-TQ8040 NCI. Melting points were checked using melting point device. Autodock 1.5.6 was employed for performing the docking study, and the results were presented as binding affinity (kcal/mol). The 2D/3D interaction poses obtained through the use of the Discover Studio Visualizer. SwissADME was utilized for calculating the in silico ADME profile, while pkCSM was employed for analysing the toxicity profile.

4.1. Procedure of *In Vitro* Study Upon PC-3:

4.1.1. Cell Viability Assay: -

In vitro assay was performed in triplicate for cell inhibition study. PC3 cells expressing AR-WILD TYPE [WT-1] cells were derived from NCBI, Pune. Then, PC-3 cells were cultivated with 10% foetal bovine serum and high-glucose DMEM (Dulbecco's modified Eagle Medium) with 5% carbon dioxide. After this, "9×10^{4} cells" plated in 96 well plates and kept at 37 °C for 24 hour. After 24h of incubation, the cells were treated with Bicalutamide and **SP01** to **SP25**, **MS01** to **MS15** with concentrations of 0, 10, 50, 100, 200, 400, 600, 800, and 1000 nM. To test PC-3 cell viability, 10 µL of 5mg/mL MTT in 96 well plates were applied to the cells and incubated for two hours at 37 °C. MTT is the tetrazolium salt MTT undergoes a conversion into an insoluble formazan compound through the action of mitochondrial dehydrogenases in viable cells. Formazan solublized in DMSO, and the absorbance was quantified at two different wavelengths (550 and 630) , using an ELISA plate spectrophotometer provided of Biotrek. Microsoft excel was used to calculate the mean and IC_{50} values while SPSS was used to plot the graph between concentration and inhibition percentage [115-118].

4.1.2. Reactive Oxygen Species (ROS) Measurement-

A total of 1×10^5 PC-3 cells were seeded onto 12-well plates and treated with selected compounds and standard to determine their effect on total ROS production. After 24 hours of treatment, plates were treated with selected compound at different concentrations (100, 150, 200, 300 nM) and Bicalutamide with concentration of 100nM, followed by supplemented with a final concentration of 10 µM of the sensitive fluorescent probe DCFH-DA, and the mixture was incubated for 30 minutes at 37 °C. At last, the results were analysed using flow cytometry after the cells got stained and washed [119-122].

4.1.3. Androgen Receptor Inhibition Assay

A cell population of $1x10^5$ PC-3 cells were seeded and cultured in separate wells of 12-well plates and then treated with selected compound at different concentrations and Bicalutamide at a concentration of 200 nM for a duration of 24 hours. After the 24-hour incubation period, the cells were collected, pelleted, and the supernatant was discarded. To fix the cell pellets, they were immersed in 100 µl of 4% formaldehyde and left for 15 minutes. The fixed pellet was then centrifuged, and any residual formaldehyde was removed by washing with 1X PBS (concentrated Phosphate Buffer Saline). Subsequently, the cells were permeated with cold 100% methanol, followed by two washes with 1X PBS. In the immunostaining procedure, cells were incubated for 30 minutes and then suspended in 100 µl of a primary antibody solution, specifically the Androgen Receptor Rabbit (GTX100056). After undergoing three additional washes in 1X PBS, the samples underwent centrifugation for five minutes at 1500×g. Subsequent to centrifugation and two more PBS washes, cells were treated with 100 µl of a diluted fluorochrome-conjugated secondary antibody, Alexa Fluor 488, at a 1:25 dilution for 30 minutes at room temperature. The cells were once again centrifuged, underwent a PBS wash, and the supernatant was removed. Finally, the cells were reconstituted in 200-500 µl of 1X PBS for flow cytometric analysis, and the resulting data were analyzed using the Flowjo V10 program. [123-125].

4.1.4. Immunofluorescence Study for AR Inhibition

In a 35 mm high glass bottom dish, 1×10^5 PC-3 cells were planted to examine the inhibition of androgen receptor expression. Cells were treated with different concentrations of selected compounds and 200 nM Bicalutamide and after 24h cells were fixed with 4% paraformaldehyde and permeabilized with 0.2% triton X in 1X PBS. Following a 24h treatment with androgen receptor rabbit (GTX100056) primary antibody at a dilution of 1:50, the cells underwent a series of washing steps to remove any excess, unbound primary antibody. Specifically, the cells were washed three times with 1X PBS. Subsequently, the cells were subjected to an additional incubation step, this time with Anti-rabbit Alexa Fluor 488 secondary antibody (catalog number 4412) at a dilution of 1:100. This secondary antibody incubation was carried out for a duration of 1 hour. Cells expression of androgen receptor was analysed, using fluorescence microscopy imaging using an Olympus CFX41. The imaging technique involved fluorescence microscopy using an Olympus CFX41 microscope. Quantification methods likely included image analysis software to measure fluorescence intensity or cell counts. Data analysis involved comparing fluorescence intensity or cell counts between different treatment groups, possibly using statistical methods to assess significance [126, 127].

4.2. Computational Studies

Autodock Tool Vina 1.5.6 software was employed to evaluate the activity in terms of binding affinity (kcal/mol). Subsequently, the binding affinity scores for the best docked configurations were compared with bicalutamide [128, 129]. ChemBioDraw Ultra 2D was utilized to depict the 2D structure of the newly designed compound, which was then converted to a 3D structure using ChemBioDraw 3D. To ensure the compounds were in a readable format for the AutoDock Vina interface, energy minimization was performed using the MM2 method to optimize the newly designed compounds. For the identification of a potential antiprostate cancer agent, protein **1Z95** was selected and downloaded from the Protein Data Bank using https://www.rcsb.org/. The results from AutoDock Vina were analysed to determine close contacts, hydrogen bonds, and hydrophilic and hydrophobic interactions. Furthermore, pharmacokinetics

and toxicities of the potent compounds were predicted using SwissADME and pkCSM, respectively [130].

4.2.1. Protein Selection and Preparation

The androgen receptors protein with the PDB code **1Z95** was obtained from the official Protein Data Bank website (https://www.rcsb.org/) for the purpose of this research [131, 132]. Subsequently, the protein was imported into AutoDock to extract the ligand and protein separately. The objective for using this software was to assess the binding affinity and optimize the ligands to identify the best lead molecule for anti-prostate cancer agents.

4.2.2. Validation of Protein for Docking

The co-crystallized ligand of PDBID: **1Z95**, was extracted from the original androgen receptor protein. Afterwards, the ligand was redocked into its corresponding binding site. To assess the validation of method, the RMSD of the ligand atoms in the redocked conformation was compared to the crystallographic conformation (**Figure 18**) [112].

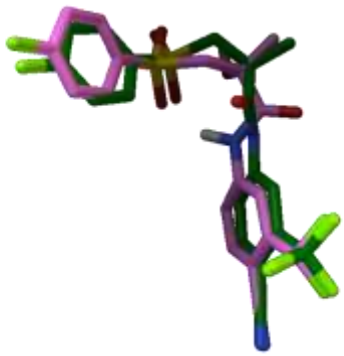

Figure 18: Docked structure of co-crystallized ligand for validation

4.2.3. Molecular Docking Program

Compounds were analysed using docking software to identify the AR inhibition. The selected protein, **1Z95**, was ready by categorizing its binding site. Initially, the protein's validity was confirmed by removing the ligand and saving it in pdb format. Subsequently, the protein in pdb format was loaded into AutoDock Vina and prepared

for the docking study [133]. This involved removing water and other extraneous structures, repairing missing atoms, adding polar hydrogen, and subsequently applying the Kollman charges. The autodock tool vina molecular docking was performed using the command "program files\the scripps research institute\vina\vina.exe -config conf.txt -log log.txt" in the command prompt. This generated an output file with the docking score/binding affinity measured in kcal/mol. Similarly, all the newly designed compounds were studied, and their binding affinities were recorded in a tabular form. Finally, Discovery Studio was used to analyse the 2D interactions [134].

4.3. Absorption, Distribution, Metabolism and Excretion (ADME) Analysis

All compounds were further screened and evaluated using the SwissADME server at http://www.swissadme.ch [135]. Initially, the compounds were converted to their respective SMILES IDs using ChemDraw 2D and then pasted into the SwissADME portal. Subsequently, the results were predicted in terms of various physicochemical properties, including interactions with p-glycoprotein, adherence to the Lipinski rule of 5 (indicating drug-likeness), the number of hydrogen bond acceptors and donors, and the prediction of drug penetration through the blood-brain barrier and gastrointestinal absorption, as indicated by the BOILED-egg method [136].

4.4. Toxicity Analysis

Following the prediction of ADME (Absorption, Distribution, Metabolism, and Elimination), these compounds undertook further toxicity prediction using online portals such as pkCSM. The pkCSM online tool was used to predict the toxicity of **MS01-MS15**, **SP01-SP25** and bicalutamide. Maximum Tolerated Dose (MTD) for humans using pkCSM was predicted. hERG, or the human ether-a-go-go-related gene, plays a significant role in cardiac depolarization and repolarization. Inhibition of hERG can lead to certain cardiac diseases. Therefore, inhibitory effects on hERG I and II was also predicted along with toxicity in rats, including the median lethal dose (LD_{50}). Additionally, predictions for parameters such as hepatotoxicity and skin sensitization were also made. Furthermore, pkCSM was also utilized to predict toxic doses for the inhibition of growth in *Tetrahymena pyriformis* (*T. pyriformis*) and estimated minnow toxicity to assess aquatic toxicity [137-139].

CHAPTER 5

5.1. Designing of 3,5-Diphenyl-1,2,4-Oxadiazoles (MS01-MS15)

The rationale for designing 3,5-diphenyl-1,2,4-oxadiazole derivatives has been previously discussed in chapter 3. However, we are now exploring another aspect of the rationale behind their design. In the field of prostate cancer treatment, three majors' drugs-bicalutamide, Apalutamide, and Enzalutamide hold significance. But bicalutamide does not function as a pure androgen receptor antagonist, unlike Apalutamide and Enzalutamide. The latter two drugs are regarded as pure antagonists due to the presence of a hydrophobic-interaction-inducing heterocyclic ring positioned between two rings, in contrast to bicalutamide, which possesses an acyclic section between its rings (depicted in **Figure 19**). Moreover, an extensive literature review has unveiled the potent anti-prostate cancer activity of 3,5-disubstituted oxadiazole-based compounds like **28** and **30**.

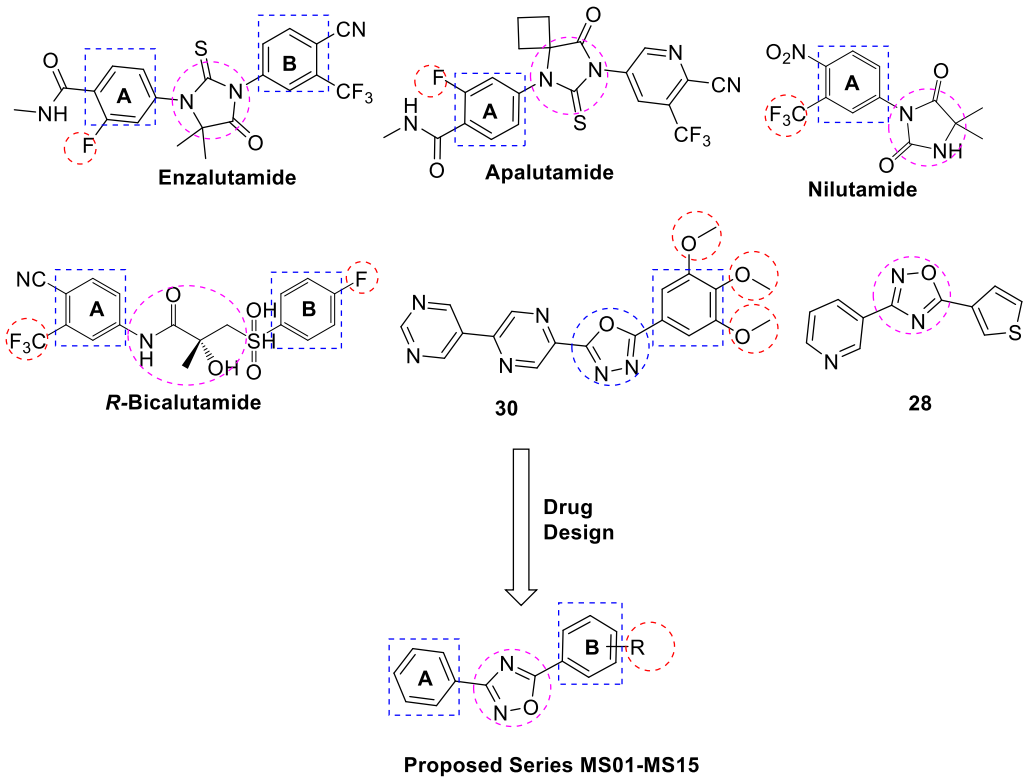

Figure 19: Designing rationale for 3,5-diphenyl-1,2,4-oxadiazole

This discovery prompted the idea of replacing the imidazole ring found in Flutamide, Enzalutamide and Apalutamide with an oxadiazole ring. This substitution was motivated by the well-documented major side effects associated with Enzalutamide

and Apalutamide, such as gynecomastia and hepatotoxicity. Alongside the incorporation of the oxadiazole moiety, the objective was to assess the influence of various EDGs and EWGs on the phenyl ring. Taking these factors into consideration, a series of compounds **MS01-MS15** were designed for prostate cancer treatment.

5.2. Chemistry

5.2.1. General Synthesis of 3,5-Diphenyl-1,2,4-Oxadiazoles (MS01-MS15)

MS01-MS15 were synthesized in three steps. Initially, benzonitrile (**1**) was used to synthesize *N'*-hydroxybenzimidamide (**2**). Subsequently, substituted aromatic acids (**3a-3o**) were reacted with the *N'*-hydroxybenzimidamide (**2**) to yield *N'*-(benzoyloxy)benzimidamides (**4a-4o**). Further, *N'*-(benzoyloxy) benzimidamides was cyclized into 3,5-disubstituted oxadiazoles (**MS01-MS15**). A detailed procedure and characterization were given below:

5.2.2. Procedure For Synthesis of *N'*-hydroxybenzimidamide (2)

In 100 mL round bottom flask, benzonitrile **1** (9.69 mmol) was added to 15 mL of ethanol along with hydroxylamine hydrochloride (48.45 mmol), and stirred at r.t. for20 minutes. After the stipulated time, equivalents of sodium bicarbonate (29.07 mmol) were added gradually, and mixture was refluxed for 2 h. The reaction progression was monitored by TLC, and once the nitriles were completely consumed, then solvent was evaporated using rota evaporator. An excess amount of distilled water was added which resulted in a viscous solution, and mixture was partitioned using ethyl acetate. Then, ethyl acetate layer was separated, and the solvent evaporated under vacuum distillation to obtain the corresponding *N'*-hydroxybenzimidamide **2** (**Scheme 1**) and mechanism of the reaction was also shown in **Scheme 2**. The synthesis of *N'*-hydroxybenzimidamide was validated through literature reports that support its structural confirmation [140, 141].

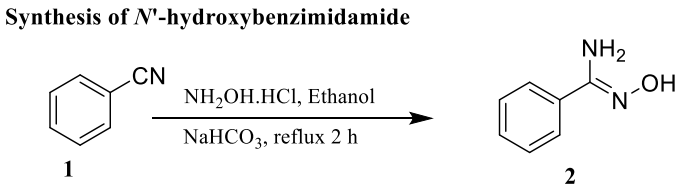

Scheme 1: Reaction for synthesis of *N'*-hydroxybenzimidamide

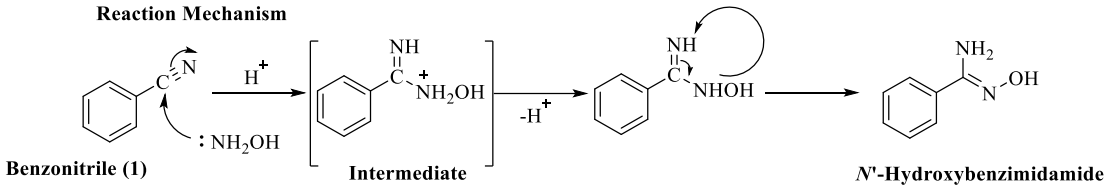

Scheme 2: Mechanism for synthesis of *N'*-hydroxybenzimidamide

5.2.3. Procedure for Synthesis of *N'*-(benzoyloxy)benzimidamide (4a-4o)

In 100 mL round bottom flask, a reaction mixture was prepared by mixing substituted aromatic acid **3a-3o** (1.8 mmol) with 5 mL of 1,4-dioxane and triethylamine (3 mmol), respectively. 3 mmol of Ethyl chloroformate was then added in a dropwise manner to the mixture. The mixture was stirred at r.t. for 15 minutes. To the above reaction mixture, a solution of *N'*-hydroxybenzimidamide **2** (2.5 mmol) in 5 mL of 1,4-dioxane was added, and stirred at r.t. for a duration of 30 minutes. Once the reaction had reached completion, the reaction mixture was concentrated using vacuum distillation. It was subsequently diluted with 25 mL of cold water to obtain solid. This solid was subjected to filtration, then washing with water, and then allowed to dry at room temperature. The resulting solid was further purified by column chromatography, eluting it with mixture *n*-hexane and ethyl acetate. This purification process yielded pure compounds presented in the **scheme 3** with reaction mechanism in **scheme 4**) [142].

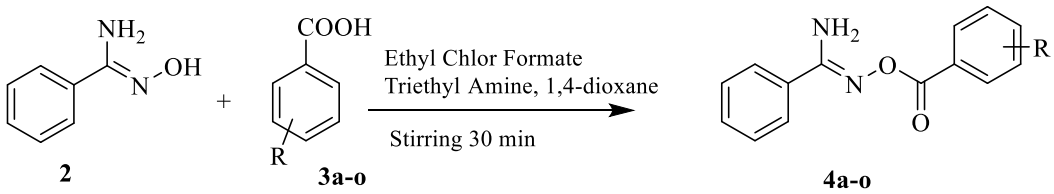

Scheme 3: Synthesis of *N'*-(benzoyloxy)benzimidamide

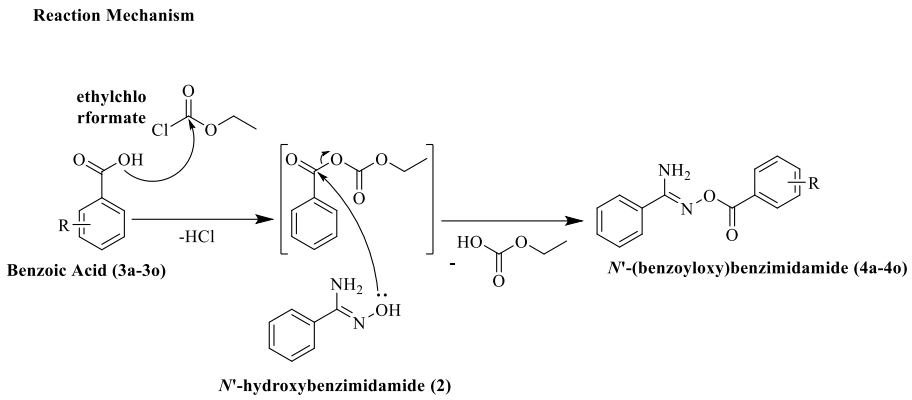

Scheme 4: Mechanism for synthesis of *N*'-(benzoyloxy)benzimidamide

5.2.4. Procedure For Synthesis of Substituted 3,5-Diphenyl-1,2,4-Oxadiazoles (MS01-MS15)

A suspension was prepared by stirring 1.5 mmol of potassium hydroxide in 5 mL of dimethyl sulfoxide (DMSO). To this suspension, *N*'-(benzoyloxy)benzimidamide **4a-4o (**1.5 mmol) was added, respectively. Following the addition of the reactants, the reaction mixture was stirred for 30 minutes with continuous monitoring of the reaction progress using TLC. Once the reaction reached its completion, the mixture was diluted with 25 mL of cold water, resulting in the formation of a precipitate. This precipitate was subsequently filtered, washed with water, and allowed to air-dry at room temperature. The obtained solid was then subjected to purification using column chromatography, employing a mixture of ethyl acetate and *n*-hexane as the eluent, to isolate the pure compound as depicted in **Schemes 5** and **6**. [143].

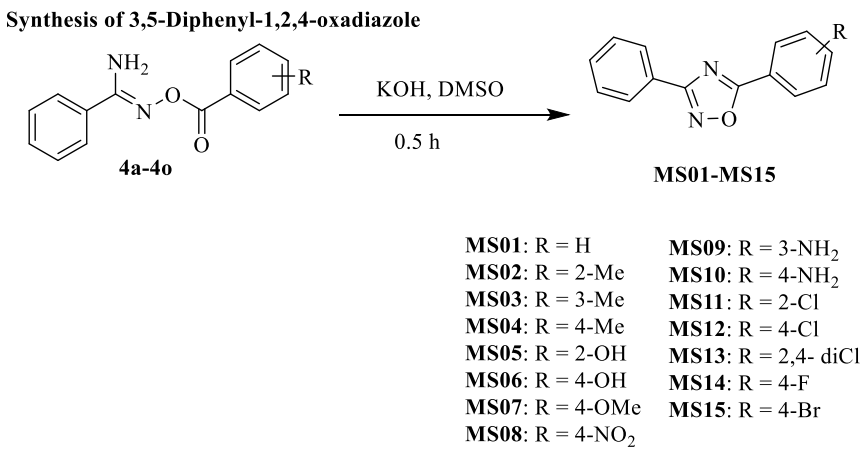

Scheme 5: Reaction for synthesis of 3,5-diphenyl-1,2,4-oxadiazoles

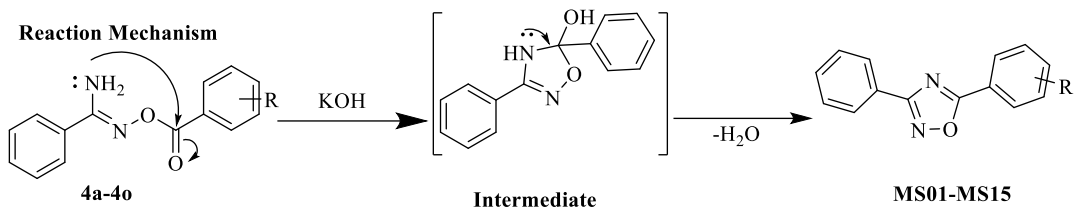

Scheme 6: Mechanism for synthesis of 3,5-diphenyl-1,2,4-oxadiazoles

Following the successful synthesis of all compounds, characterization was performed using IR, ^{1}H NMR, ^{13}C NMR, and Mass Spectroscopy. The corresponding data is presented below:

5.3. Spectral Characterization of Compounds

"**3,5-Diphenyl-1,2,4-oxadiazole (MS01)**: Yield 63%, White powder, mp 121-123 °C. **IR (KBr) (cm^{-1})**: 2918 (C=C-H str.), 1603 (C=C str.), 1323 (C-O str.), 1056 (C-N str.); **^{1}H NMR (400 MHz, DMSO-*d*$_6$), δ (ppm)**: 7.37 (d, Ar-*H*, 3H), 7.50 (m, Ar-*H*, 3H), 7.94 (m, Ar-*H*, 2H), 8.00 (m, Ar-*H*, 2H); **^{13}C NMR (100 MHz, DMSO-*d*$_6$), δ (ppm)**: 126.12 (Ar-C, 1C), 128.26 (Ar-C, 1C), 129.84 (Ar-C, 2C), 129.97 (Ar-C, 2C), 129.98 (Ar-C, 2C), 130.01 (Ar-C, 2C), 131.69 (Ar-C, 1C), 136.95 (Ar-C, 1C), 169.26 (Ar-C, 1C), 173.61 (Ar-C, 1C); **ESI-MS m/z**: 228 [M+H]$^{+}$."

"**3-Phenyl-5-(*o*-tolyl)-1,2,4-oxadiazole (MS02)**: Yield 73%, Pale Yellow powder, mp 145-147 °C. **IR (KBr) (cm^{-1})**: 2938 (C=C-H str.), 1609 (C=C str.), 1303 (C-O str.), 1106 (C-N str.); **^{1}H NMR (400 MHz, DMSO-*d*$_6$), δ (ppm)**: 2.36 (s, -C*H*$_3$, 3H), 7.28 (d, Ar-*H*, 2H, *J* = 8 Hz), 7.50 (m, Ar-*H*, 3H), 7.94 (m, Ar-*H*, 2H), 7.96 (m, Ar-*H*, 2H); **^{13}C NMR (100 MHz, DMSO-*d*$_6$), δ (ppm)**: 21.25 (Ar-C, 1C), 126.78 (Ar-C, 1C), 128.26 (Ar-C, 1C), 128.42 (Ar-C, 2C), 129.92 (Ar-C, 2C) 129.98, (Ar-C, 2C), 130.10, (Ar-C, 2C), 131.69 (Ar-C, 1C) , 142.23 (Ar-C, 1C), 169.27 (Ar-C, 1C), 173.32 (Ar-C, 1C); **ESI-MS m/z**: 237 [M+H]$^{+}$."

"**3-Phenyl-5-(*m*-tolyl)-1,2,4-oxadiazole (MS03)**: Yield 77%, Yellow powder, mp 151-153 °C. **IR (KBr) (cm^{-1})**: 2983 (C=C-H str.), 1611 (C=C str.), 1309 (C-O str.), 1103 (C-N str.); **^{1}H NMR (400 MHz, DMSO-*d*$_6$), δ (ppm)**: 2.36 (s, -C*H*$_3$, 3H), 7.28 (d, Ar-*H*, 2H, *J* = 8 Hz), 7.50 (m, Ar-H, 3H), 7.94 (m, Ar-H, 2H), 7.96 (m, Ar-H, 2H); **^{13}C NMR (100 MHz, DMSO-*d*$_6$), δ (ppm)**: 21.25 (Ar-C, 1C), 126.78 (Ar-C, 1C),

128.26 (Ar-C, 1C), 128.42 (Ar-C, 2C), 129.92 (Ar-C, 2C), 129.98 (Ar-C, 2C), 130.10 (Ar-C, 2C), 131.69 (Ar-C, 1C), 142.23 (Ar-C, 1C), 169.27 (Ar-C, 1C), 173.32 (Ar-C, 1C); **ESI-MS m/z**: 237 $[M+H]^+$."

"**3-Phenyl-5-(*p*-tolyl)-1,2,4-oxadiazole (MS04)**: Yield 83%, Pale Yellow powder, mp 153-155 °C. **IR (KBr) (cm^{-1})**: 3436 (O-H str.), 2900 (C=C-H str.), 1588 (C=C str.), 1318 (C-O str.), 1098 (C-N str.); **^{1}H NMR (400 MHz, DMSO-d_6), δ (ppm)**: 2.36 (s, -CH_3, 3H), 7.28 (d, Ar-*H*, 2H, *J* = 8 Hz), 7.50 (m, Ar-*H*, 3H), 7.94 (m, Ar-*H*, 2H), 7.96 (m, Ar-*H*, 2H); **^{13}C NMR (100 MHz, DMSO-d_6), δ (ppm)**: 21.25 (-CH_3, 1C), 126.78 (Ar-C, 1C), 128.26 (Ar-C, 1C), 128.42 (Ar-C, 2C), 129.92 (Ar-C, 2C), 129.98 (Ar-C, 2C), 130.10 (Ar-C, 2C), 131.69 (Ar-C, 1C), 142.23 (Ar-C, 1C), 169.27 (Ar-C, 1C), 173.32 (Ar-C, 1C); **ESI-MS m/z**: 237 $[M+H]^+$."

"**2-(3-Phenyl-1,2,4-oxadiazol-5-yl)phenol (MS05)**: Yield 87%, Off White powder, mp 133-135 °C. **IR (KBr) (cm^{-1})**: 3436 (O-H str.), 2900 (C=C-H str.), 1588 (C=C str.), 1318 (C-O str.), 1098 (C-N str.); **^{1}H NMR (400 MHz, DMSO-d_6), δ (ppm)**: 6.90 (d, Ar-*H*, 2H, *J* = 8 Hz), 7.50 (m, Ar-*H*, 3H), 7.83 (m, Ar-*H*, 2H), 7.93 (m, Ar-*H*, 2H), 8.23 (s, O*H*, 1H); **^{13}C NMR (100 MHz, DMSO-d_6), δ (ppm)**: 117.17 (Ar-C, 1C), 117.48 (Ar-C, 1C), 128.26 (Ar-C, 1C), 129.92 (Ar-C, 4C), 130.35 (Ar-C, 2C), 131.69 (Ar-C, 1C), 160.56 (Ar-C, 1C), 169.26 (Ar-C, 1C), 173.40 (Ar-C, 1C); **ESI-MS m/z**: 239 $[M+H]^+$."

"**4-(3-Phenyl-1,2,4-oxadiazol-5-yl)phenol (MS06)**: Yield 77%, Off White powder, mp 137-139 °C. **IR (KBr) (cm^{-1})**: 3436 (O-H str.), 2900 (C=C-H str.), 1588 (C=C str.), 1318 (C-O str.), 1098 (C-N str.); **^{1}H NMR (400 MHz, DMSO-d_6), δ (ppm)**: 6.90 (d, Ar-*H*, 2H, *J* = 8 Hz), 7.50 (m, Ar-*H*, 3H), 7.83 (m, Ar-*H*, 2H), 7.93 (m, Ar-*H*, 2H), 8.23 (s, O*H*, 1H); **^{13}C NMR (100 MHz, DMSO-d_6), δ (ppm)**: 117.17 (Ar-C, 2C), 117.48 (Ar-C, 1C), 128.26 (Ar-C, 1C), 129.92 (Ar-C, 4C), 130.35 (Ar-C, 2C), 131.69 (Ar-C, 1C), 160.56 (Ar-C, 1C), 169.26 (Ar-C, 1C), 173.40 (Ar-C, 1C); **ESI-MS m/z**: 239 $[M+H]^+$."

"**5-(4-Methoxyphenyl)-3-phenyl-1,2,4-oxadiazole (MS07)**: Yield 87%, Yellowish White powder, mp 167-169 °C. **IR (KBr) (cm^{-1})**: 2900 (C=C-H str.), 1608 (C=C str.), 1308 (C-O str.), 1113 (C-N str.); **^{1}H NMR (400 MHz, DMSO-d_6), δ (ppm)**: 3.80 (s, -

OC*H*$_3$, 3H), 6.98 (d, Ar-*H*, 2H, *J* = 8 Hz), 7.50 (m, Ar-*H*, 3H), 7.88 (m, Ar-*H*, 2H), 7.96 (m, Ar-*H*, 2H); **^{13}C NMR (100 MHz, DMSO-*d*$_6$), δ (ppm)**: 55.35 (O-CH$_3$, 1C), 115.11 (Ar-C, 2C), 119.37 (Ar-C, 1C), 128.26 (Ar-C, 1C), 129.92 (Ar-C, 2C), 129.98 (Ar-C, 2C), 130.13 (Ar-C, 2C), 131.69 (Ar-C, 1C), 162.94 (Ar-C, 1C), 168.07 (Ar-C, 1C), 169.26 (Ar-C, 1C); **ESI-MS m/z**: 251 [M-H]$^+$."

"5-(4-Nitrophenyl)-3-phenyl-1,2,4-oxadiazole (MS08): Yield 89%, Pale Yellow powder, mp 165-167 °C. **IR (KBr) (cm^{-1})**: 2900 (C=C-H str.), 1588 (C=C str.), 1318 (C-O str.), 1098 (C-N str.); **^{1}H NMR (400 MHz, DMSO-*d*$_6$), δ (ppm)**: 7.49 (d, Ar-*H*, 3H, *J* = 8 Hz), 7.95 (m, Ar-*H*, 2H), 8.22 (m, Ar-*H*, 4H); **^{13}C NMR (100 MHz, DMSO-*d*$_6$), δ (ppm)**: 125.03 (Ar-C, 2C), 128.26 (Ar-C, 1C), 129.58 (Ar-C, 2C), 129.92 (Ar-C, 5C), 130.36 (Ar-C, 1C), 131.69 (Ar-C, 1C), 149.13 (Ar-C, 1C), 169.26 (Ar-C, 1C), 173.78 (Ar-C, 1C); **ESI-MS m/z**: 268 [M+H]$^+$."

"**3-(3-Phenyl-1,2,4-oxadiazol-5-yl)aniline (MS09)**: Yield 67%, Pale Yellow powder, mp 139-141 °C. **IR (KBr) (cm^{-1})**: 3395 (N-H str.), 3259 (N-H str.), 2962 (C=C-H str.), 1591 (C=C str.), 1286 (C-O str.), 1023 (C-N str.); **^{1}H NMR (400 MHz, DMSO-*d*$_6$), δ (ppm)**: 4.60 (s, -N*H*$_2$, 2H), 6.83 (m, Ar-*H*, 2H), 7.50 (m, Ar-*H*, 3H), 7.84 (m, Ar-*H*, 2H), 7.95 (m, Ar-*H*, 2H); **^{13}C NMR (100 MHz, DMSO-*d*$_6$), δ (ppm)**: 115.85 (Ar-C, 2C), 117.48 (Ar-C, 1C), 128.26 (Ar-C, 1C), 129.48 (Ar-C, 1C), 129.92 (Ar-C, 2C), 129.98 (Ar-C, 2C), 131.69 (Ar-C, 1C), 151.85 (Ar-C, 1C), 169.27 (Ar-C, 1C), 173.04 (Ar-C, 1C); **ESI-MS m/z**: 238 [M+H]$^+$."

"**4-(3-Phenyl-1,2,4-oxadiazol-5-yl)aniline (MS10)**: Yield 67%, Pale Yellow powder, mp 143-145 °C. **IR (KBr) (cm^{-1})**: 3391 (N-H str.), 3233 (N-H str.), 2912 (C=C-H str.), 1581 (C=C str.), 1266 (C-O str.), 1093 (C-N str.); **^{1}H NMR (400 MHz, DMSO-*d*$_6$), δ (ppm)**: 4.60 (s, -N*H*$_2$, 2H), 6.83 (d, Ar-*H*, 2H, *J* = 8 Hz), 7.50 (m, Ar-*H*, 3H), 7.84 (m, Ar-*H*, 2H), 7.95 (m, Ar-*H*, 2H); **^{13}C NMR (100 MHz, DMSO-*d*$_6$), δ (ppm)**: 115.85 (Ar-C, 2C), 117.48 (Ar-C, 1C), 128.26 (Ar-C, 1C), 129.48 (Ar-C, 2C), 129.92 (Ar-C, 2C), 129.98 (Ar-C, 2C), 131.69 (Ar-C, 1C), 151.85 (Ar-C, 1C), 169.27 (Ar-C, 1C), 173.04 (Ar-C, 1C); **ESI-MS m/z**: 238 [M+H]$^+$."

"**5-(2-Chlorophenyl)-3-phenyl-1,2,4-oxadiazole (MS11)**: Yield 79%, White powder, mp 157-159 °C. **IR (KBr) (cm^{-1})**: 2932 (C=C-H str.), 1596 (C=C str.), 1276 (C-O

str.), 1033 (C-N str.); **^{1}H NMR (400 MHz, DMSO-*d*$_6$), δ (ppm)**: 7.37 (d, Ar-*H*, 2H, *J* = 8 Hz), 7.50 (m, Ar-*H*, 3H), 7.94 (m, Ar-*H*, 2H), 8.00 (m, Ar-*H*, 2H); **^{13}C NMR (100 MHz, DMSO-*d*$_6$), δ (ppm)**: 126.12 (Ar-C, 1C), 128.26 (Ar-C, 1C), 129.84 (Ar-C, 2C), 129.97 (Ar-C, 2C), 129.98 (Ar-C, 3C), 130.01 (Ar-C, 1C), 131.69 (Ar-C, 1C), 136.95 (Ar-C, 1C), 169.26 (Ar-C, 1C), 173.61 (Ar-C, 1C); **ESI-MS m/z**: 258 $[M+H]^+$."

"**5-(4-Chlorophenyl)-3-phenyl-1,2,4-oxadiazole (MS12)**: Yield 43%, White powder, mp 161-163 °C. **IR (KBr) (cm^{-1})**: 2953 (C=C-H str.), 1581 (C=C str.), 1236 (C-O str.), 1073 (C-N str.); **^{1}H NMR (400 MHz, DMSO-*d*$_6$), δ (ppm)**: 7.37 (d, Ar-*H*, 2H, *J* = 8 Hz), 7.50 (m, Ar-*H*, 3H), 7.94 (m, Ar-H, 2H), 8.00 (m, Ar-*H*, 2H); **^{13}C NMR (100 MHz, DMSO-*d*$_6$), δ (ppm)**: 126.12 (Ar-C, 1C), 128.26 (Ar-C, 1C), 129.84 (Ar-C, 1C), 129.97 (Ar-C, 2C), 129.98 (Ar-C, 3C), 130.01 (Ar-C, 1C), 131.69 (Ar-C, 1C), 136.95 (Ar-C, 1C), 169.26 (Ar-C, 1C), 173.61 (Ar-C, 1C); **ESI-MS m/z**: 258 $[M+H]^+$."

"**5-(2,4-Dichlorophenyl)-3-phenyl-1,2,4-oxadiazole (MS13)**: Yield 83%, White powder, mp 167-169 °C. **IR (KBr) (cm^{-1})**: 2954 (C=C-H str.), 1591 (C=C str.), 1286 (C-O str.), 1023 (C-N str.); **^{1}H NMR (400 MHz, DMSO-*d*$_6$), δ (ppm)**: 7.37 (d, Ar-*H*, 2H, *J* = 8 Hz), 7.50 (m, Ar-*H*, 2H), 7.94 (m, Ar-*H*, 2H), 8.00 (m, Ar-*H*, 2H); **^{13}C NMR (100 MHz, DMSO-*d*$_6$), δ (ppm)**: 126.12 (Ar-C, 1C), 128.26 (Ar-C, 1C), 129.84 (Ar-C, 1C), 129.97 (Ar-C, 2C), 129.98 (Ar-C, 3C), 130.01 (Ar-C, 1C), 131.69 (Ar-C, 1C), 136.95 (Ar-C, 1C), 169.26 (Ar-C, 1C), 173.61 (Ar-C, 1C); **ESI-MS m/z**: 292 $[M+H]^+$."

"**5-(4-Fluorophenyl)-3-phenyl-1,2,4-oxadiazole (MS14)**: Yield 71%, White powder, mp 171-173 °C. **IR (KBr) (cm^{-1})**: 2918 (C=C-H str.), 1603 (C=C str.), 1323 (C-O str.), 1056 (C-N str.); **^{1}H NMR (400 MHz, DMSO-*d*$_6$), δ (ppm)**: 7.27 (d, Ar-*H*, 2H, *J* = 8 Hz), 7.50 (m, Ar-*H*, 3H), 7.94 (m, Ar-*H*, 2H), 8.00 (m, Ar-*H*, 2H); **^{13}C NMR (100 MHz, DMSO-*d*$_6$), δ (ppm)**: 116.42 (Ar-C, 1C), 116.60 (Ar-C, 1C), 122.72 (Ar-C, 1C), 122.75 (Ar-C, 1C), 128.26 (Ar-C, 2C), 129.92 (Ar-C, 2C), 130.67 (Ar-C, 2C), 131.69 (Ar-C, 1C), 164.33 (Ar-C, 1C), 169.26 (Ar-C, 1C), 173.77 (Ar-C, 1C); **ESI-MS m/z**: 241 $[M+H]^+$."

"**5-(4-bromophenyl)-3-phenyl-1,2,4-oxadiazole (MS15)**: Yield 75%, Yellowish White powder, mp 149-151 °C. **IR (KBr) (cm^{-1})**: 2900 (C=C-H str.), 1608 (C=C str.), 1308 (C-O str.), 1113 (C-N str.) **^{1}H NMR (400 MHz, DMSO-d_6), δ (ppm)**: 7.49 (d, Ar-*H*, 3H, *J* = 8 Hz), 7.62 (m, Ar-*H*, 2H), 7.92 (m, Ar-*H*, 1H), 7.95 (m, Ar-*H*, 3H); **^{13}C NMR (100 MHz, DMSO-d_6), δ (ppm)**: 124.98 (Ar-C, 1C), 126.93 (Ar-C, 1C), 128.26 (Ar-C, 1C), 129.57 (Ar-C, 2C), 129.92 (Ar-C, 2C), 129.98 (Ar-C, 2C), 131.69 (Ar-C, 1C), 132.63 (Ar-C, 2C), 169.26 (Ar-C, 1C), 173.41 (Ar-C, 1C); **ESI-MS m/z**: 300 $[M-H]^+$."

The mass fragmentation of the compound **MS03** was investigated and is presented in **Figure 20**.

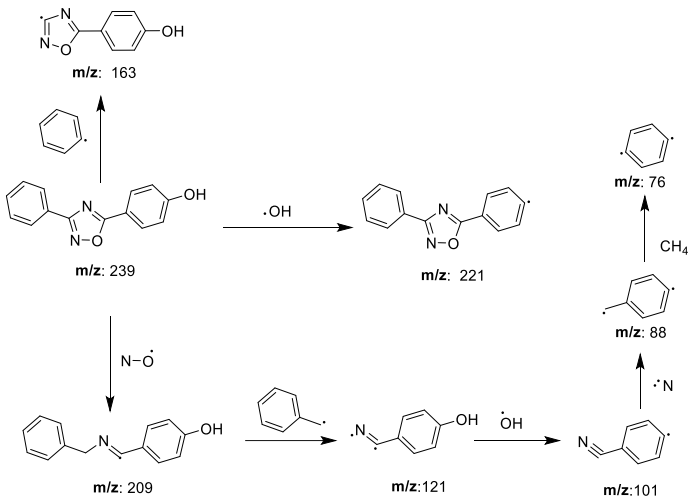

Figure 20: Fragmentation pattern of **MS03** (one of the representatives of **MS01-MS15**)

5.4. Results

5.4.1. Cell Viability Assay

To assess the cytotoxic effects of **MS01-MS15**, the MTT assay was performed using the bicalutamide. The *in vitro* assay was performed in triplicate *for* cell inhibition study against PC-3 cell lines expressing AR-WILD TYPE [WT-1] cells, derived from NCBI, Pune. Cell viability was subsequently determined through the MTT assay, and the findings were graphically represented in **Figure 21**. The results of the MTT assay conducted on PC-3 cell lines expressing wild-type androgen receptors, using a series

of compounds **MS01-MS15**, revealed a remarkable inhibitory effect on cell viability. The percentage inhibition ranged up to 97.32% within the series, with corresponding IC_{50} values spanning from 370.37 nM to 838.14 nM against PC3 cell lines. In comparison, the reference compound bicalutamide exhibited an IC_{50} value of 158.03 nM and a percentage inhibition of 98.11%. Significantly, the utilization of various concentrations of **MS01-MS15** and bicalutamide resulted in a dose-dependent decrease in the viability of PC3 cells, as illustrated in **Table 5**.

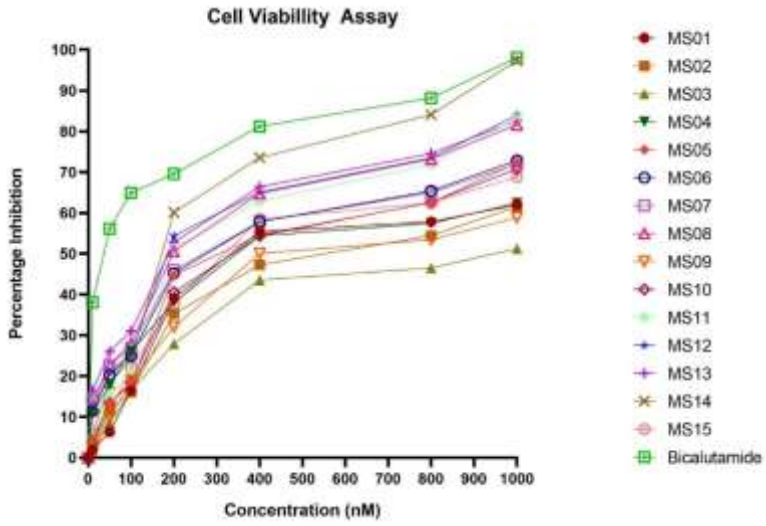

Figure 21: Graphical representation of percentage inhibition of PC-3 cells

Table 5: Percentage Inhibition and inhibitory concentration of MS01-MS15 and bicalutamide

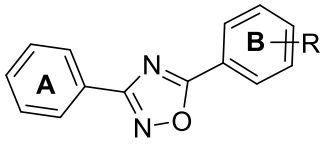

MS01-MS15

Sr. No.	Compound	R	Percentage Inhibition (%)	IC_{50} (nM)
1.	**Bicalutamide**		98.11	158.03
2.	**MS01**	H	62.03	645.37
3.	**MS02**	2-Me	61.56	687.92

4.	**MS03**	3-Me	51.25	838.14
5.	**MS04**	4-Me	62.41	627.38
6.	**MS05**	2-OH	72.31	562.69
7.	**MS06**	4-OH	72.91	520.45
8.	**MS07**	4-OMe	72.01	515.73
9.	**MS08**	4-NO_2	81.62	436.34
10.	**MS09**	3-NH_2	58.89	706.74
11.	**MS10**	4-NH_2	70.77	575.22
12.	**MS11**	2-Cl	83.15	464.84
13.	**MS12**	4-Cl	83.99	430.29
14.	**MS13**	2,4-diCl	82.64	409.52
15.	**MS14**	4-F	97.32	370.37
16.	**MS15**	4-Br	68.85	578.3

5.4.2. Molecular Docking Analysis

After conducting *in vitro* analysis of synthesized compounds, molecular docking investigations were carried out using Autodock Vina 1.5.6. The androgen receptor protein (**PDBID: 1Z95**) was obtained from the Protein Data Bank, and subsequent docking analysis results were analyzed. Following these outcomes, Discovery Studio was employed to examine the 2D and 3D interactions of all synthesized compounds (**Figure 22**). The results of the study indicated that compounds **MS01-MS15** demonstrated varying binding affinities, ranging from -6.5 to -9.0 kcal/mol within the active site of androgen receptor. In contrast, the reference compound bicalutamide exhibited a remarkably strong binding affinity of -11.1 kcal/mol. Synthesized compounds has shown hydrogen bond, π- π T Shaped, π-alkyl/alkyl, π-σ and π-sulphur types of interactions in the active site of the receptors as shown in **Table 6.**

Table 6: Binding affinities and interaction pattern of synthesized compounds MS01-MS15 and bicalutamide.

Compound	Binding affinity (kcal/mol)	*H*-Bond	π- π T Shaped	π-alkyl/alkyl	π-σ	π-sulphur
Bicalutamide	-11.1	Arg752 Gln711 Asn705 His874	Phe764	--	Met742	Met745
MS01	-7.4	--	Phe764	Leu701 Leu704 Met749	--	Met745 Met780
MS02	-7.1	--	Phe764 Leu704	Met749 Met745 Val746	Met895	Met745
MS03	-6.5	--	Phe764 Leu704	Met749 Met787	Met895	--
MS04	-7.5	--	Phe764	Met749 Phe876 Leu880 Phe891	Met895	Met742 Met745
MS05	-7.9	Gln711	Phe764	Met749 Met895 Leu704	Asn705	Met745
MS06	-8	Arg752	Phe764	Met745 Met749	Leu704	Met780
MS07	-8	Gln711	Phe764	Met745 Leu707 Met749 Leu704 Phe876	Met745	Met780
MS08	-8.3	Arg752 Gln711	Phe764	Ile899	Thr877	Met742
MS09	-7		Leu704 Phe764	Met749	--	Met780
MS10	-7.7	Arg752	Phe764	Leu704 Met749	Met895	Met742
MS11	-8.2	Gln711	Leu704 Phe764	Met749		Met745

MS12	-8.3	Arg752 Gln711	Phe764	Met749 Met895 Leu704 Phe876 Leu701 Leu880	Met745	Met780 Met745
MS13	-8.7	Arg752 Gln711	Phe764	Met745 Met749 Leu704 Leu873 Met742		Met745 Met742
MS14	-9	Arg752 Gln711	Phe764	Met749 Leu704	Met895 Met745	Met745 Met780
MS15	-7.8	--	Phe764	Met749 Leu704	--	Met780

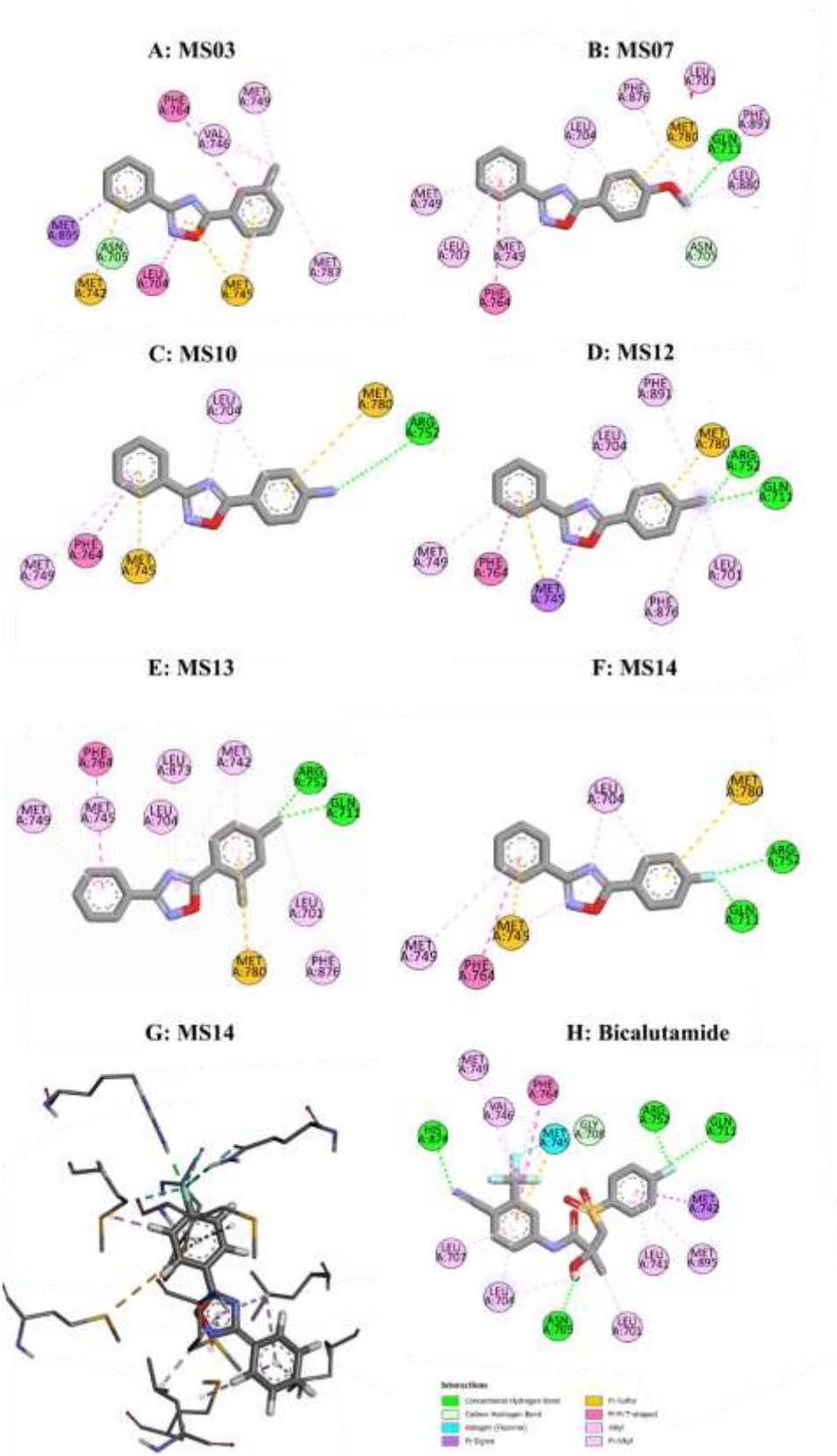

Figure 22: 2D and 3D interactions of few representatives of the series MS01-MS15

5.5. Discussion

The choice of substituents and their positioning on the aromatic ring can significantly impact the compound's anticancer activity. The synthesized aromatic oxadiazoles substituted with electron-withdrawing and electron-donating groups exhibited different anti-prostate cancer activities due to their effects on the chemical and biological properties of the aromatic compound. The results of *in vitro* assay and docking analysis of **MS01-MS15** have shown percentage inhibition up to 97.32 % and IC_{50} values in the range from 370.37 nM to 838.14 nM against PC3 cell lines, respectively. The compounds **MS01-MS15** exhibited varying binding affinities, ranging from -6.5 to -9.0 kcal/mol within active site of **PDB ID: 1Z95**. In contrast, the reference compound, bicalutamide, displayed an IC_{50} value of 158.03 nM and a robust binding affinity of -11.1 kcal/mol. This strong binding was attributed to the formation of four H-bond with amino acids Arg752, Asn705, Gln711, and His874.

The first synthesized compound, **MS01**, features an unsubstituted bivalent ring system (comprising rings A and B) connected by an oxadiazole linker. **MS01** exhibited a dock score of -7.4 kcal/mol. Notably, the phenyl ring A engaged in π-alkyl/alkyl and π-π T-shaped interactions with the amino acids Met749 and Phe764, respectively. Meanwhile, the phenyl ring B displayed an interaction with Leu701. Additionally, the -NH group of the oxadiazole linker formed a π-π type interaction with the amino acid Leu704. **MS01** demonstrated a significant inhibitory effect on the growth of prostate cancer cells, with an IC_{50} value of 645.37 nM.

Following the synthesis of compound **MS01**, three derivatives (**MS02-MS04**) were developed, featuring electron-donating group methyl substitution at the *ortho, meta,* and *para* positions of phenyl ring B. Remarkably, all three compounds exhibited a substantial inhibitory effect on the growth of prostate cancer cells, achieving up to 62.41% inhibition. But, none of these compounds formed hydrogen bond interactions within the active site, and their dock scores ranged from -6.5 to -7.5 kcal/mol. While their hydrophobic interactions resembled those of **MS01**, the *p*-substituted analogue, **MS04**, uniquely engaged in π-alkyl interactions with amino acids Leu880 and Phe891. Furthermore, compound **MS04** also demonstrated a noteworthy improvement in inhibitory efficacy against prostate cancer cell growth, boasting an IC_{50} value of

627.38 nM. Out of these three compounds (**MS02-MS04)**, it was observed that compound **MS03** exhibited the least activity. This could be attributed to the presence of a methyl group at the *meta* position, potentially impeding the molecule's optimal binding to the target and consequently diminishing its anti-cancer activity.

Further, to explore the impact of structural modifications on compounds **MS02** and **MS04**, in the pursuit of enhancing their potential against PC3 cell lines, two new analogues, **MS05** and **MS06**, were synthesized via incorporating hydroxyl groups at the *ortho* and *para* positions of the phenyl ring B. The findings from these *in vitro* studies indicate that both compounds **MS05** and **MS06** have a significant inhibitory impact on the growth of prostate cancer cells, achieving a remarkable 72.91% inhibition. Specifically, compounds **MS05** and **MS06** exhibited binding affinities of -7.9 and -8.0 kcal/mol, respectively, forming hydrogen bonding interactions with amino acids Gln711 and Arg752. Compound **MS05** demonstrated an IC_{50} value of 627.38 nM, while compound **MS06** displayed an even higher activity with an IC_{50} value of 520.45 nM. The increased activity of compound **MS06** may be attributed to its hydrogen bond interaction with the Arg752 residue in the receptor's pocket and the comparatively lower steric hindrance of the hydroxyl group at the para position. Upon substituting the hydroxyl group with a methoxy group in compound **MS07**, a marginal boost in activity was also observed, evident in the reduced IC_{50} value of 515.73 nM compared to compound **MS06**. This improved activity could be attributed to the potential impact on the electronic properties of the compound or the lipophilicity introduced by the para-substituted methoxy group. Such alterations may influence the cellular uptake of compound **MS07**, thereby enhancing its overall efficacy in inhibiting the growth of prostate cancer cells. Following this, the evaluation of para-nitro substituted compound **MS08** revealed an enhanced activity with an IC_{50} value of 436.34 nM. Compound **MS08** exhibited prominent interactions, forming two hydrogen bonds with Arg752 and Gln711, and displayed a binding affinity of -8.3 kcal/mol. The significant improved activity of compound **MS08** can be attributed to its electron-withdrawing nature. It was hypothesised that the introduction of the para-nitro substituent induces electronic effects that contribute to the improved activity by influencing the compound's interactions with the biological target.

Subsequently, two compounds, **MS09** and **MS10** was synthesized, wherein the nitro group was reduced to an amino group, strategically placed at the *meta* and *para* positions. However, the results revealed a notable difference in activity between these two (**MS09** and **MS10**). The compound **MS09** exhibited weaker activity, with an IC_{50} value of 706.74 nM, in comparison to compound **MS10**. The binding affinity of compound **MS09** was found to be -7.0 kcal/mol, with no discernible hydrogen bond interactions. This outcome can be attributed to the electron-donating property of the amino group at the meta position, which exerted steric hindrance on ring B, ultimately diminishing the compound's activity. On the other hand, compound **MS10** demonstrated improved activity, boasting an IC_{50} value of 575.22 nM. The introduction of the amino group at the para position resulted in reduced steric hindrance, contributing to an enhanced performance. The binding affinity of compound **MS10** also increased to -7.7 kcal/mol, accompanied by a notable hydrogen bond interaction with Arg752. Despite these advancements, it is noteworthy that the activity of compound **MS10** did not surpass that of the nitro substitution analogue **MS08**. The electron-donating nature of the amino group, as opposed to the electron-withdrawing property of the nitro group, played a role in this disparity. Nonetheless, these findings provide valuable insights into the intricate relationship between substituent effects and compound activity.

Next, the impact of electron-withdrawing group (EWG) substitutions in compounds **MS11** and **MS12** was examined by strategically introducing chlorine groups at the *ortho* and *para* positions of phenyl ring B. The results from *in vitro* studies reveal a substantial inhibitory effect on prostate cancer cell growth, with both compounds **MS11** and **MS12** exhibiting an impressive 83.99% inhibition rate. Notably, **MS11** demonstrated a good dock score of -8.2 kcal/mol, establishing hydrogen bonding interactions with amino acid Gln711. In cell-based assays, compound **MS11** exhibited an IC_{50} value of 464.84 nM. On the other hand, compound **MS12** displayed an enhanced activity, boasting an IC_{50} value of 430.29 nM and a binding affinity of -8.3 kcal/mol. This heightened activity can be attributed to the electron-withdrawing nature of the chloro substituent and reduced steric hindrance at the para position compared to the ortho position. Furthermore, compound **MS12** formed two crucial

hydrogen bonding interactions with amino acids Arg752 and Gln711. These findings underscore the potential therapeutic significance of these compounds in targeting prostate cancer cells.Building on the promising outcomes of compounds **MS11** and **MS12**, compound **MS13**, featuring dichloro substitution at the *ortho* and *para* positions of phenyl ring B was synthesized. Notably, compound **MS13** exhibited a compelling dock score of -8.7 kcal/mol, establishing hydrogen bonding interactions with amino acids Arg752 and Gln711 residues. This interaction likely contributes to the an enhanced activity observed, with an IC_{50} of 409.52 nM against PC3 cell lines. The improved activity of dichloro-substituted analogue **MS13** compared to mono chloro-substituted compounds (**MS11** and **MS12**) is often attributed to an enhanced electronic properties and a more optimal spatial arrangement, both of which contribute to better interactions with biological targets. Following these results, compound **MS14**, introducing a fluorine atom, the most electronegative, at the *para* position on ring B was investigated. The remarkable electronegativity of fluorine contributed to the maximum activity, yielding an IC_{50} value of 370.37 nM. Compound **MS14** emerged as the most potent compound in the series, displaying an increased binding affinity of -9.0 kcal/mol and engaging in two hydrogen bond interactions with Arg752 and Gln711, respectively. Finally, the investigation of compound **MS15**, with a less electronegative bromine atom at the para position, led to a decrease in activity due to reduced electronegativity and the bulkier nature of bromine. The binding affinity dropped to -7.8 kcal/mol, and no H-bond interactions were observed. In summary, compound **MS14** emerged as the standout compound in the series, featuring the highly electronegative fluorine at the para position of ring B. Consequently, compound **MS14** has been chosen for further analysis, including investigations into ROS and androgen receptor inhibition.

At last, compound **MS15** with least electronegative atom bromo at the *para* position was synthesized. Compound **MS15** has shown decrease in the activity as compared to fluoro substituted compound because of the decrease in the electronegativity and bulkier nature of bromo. The binding affinity was also decreased to -7.8 kcal/mol and no H-bond interaction was observed. Overall, compound **MS14** was the best compound of the series with the most electronegative element fluoro at *para* position

of ring B. Thus, compound **MS14** was selected for further analysis like ROS and androgen receptor inhibition.

5.6. ROS Production Assay in PC3 Cell Lines

ROS (Reactive oxygen species) play a crucial role in beginning oxidative stress within cancer cells. This escalated oxidative stress, in turn, triggers apoptotic pathways, effectively facilitating the demise of cancerous cells. The oxidative stress induced by ROS presents a promising therapeutic approach for precisely targeting and eradicating cancer cells, while preserving the integrity of healthy ones. For the assessment of intracellular ROS induction by compound **MS14** and bicalutamide in PC-3 cells, flow cytometry analysis was employed to quantify reactive oxygen species levels, utilizing the H2DCFDA (2',7'-dichlorodihydrofluorescein diacetate) dye (**Figure 23**).

Table 7: MFI for compound MS14 and bicalutamide at different concentrations

Sr. No	**Sample**	**MFI**
1	Control	3078
2	MS-14 (150 nM)	10409
3	MS-14 (300 nM)	31551
4	Bicalutamide (200 nM)	60778

In this experiment, PC-3 cell lines were subjected to different treatments, including a control group, compound **MS14** at concentrations of 150 nM and 300 nM, and bicalutamide at 200 nM. The results indicated a dose-dependent increase in the percentage of ROS. The mean fluorescence intensity (MFI) values were as follows: 60778 for bicalutamide at 200 nM, 31551 for compound **MS14** at 300 nM, 10409 for compound **MS14** at 150 nM, and 3078 for the control group (**Table 7**).

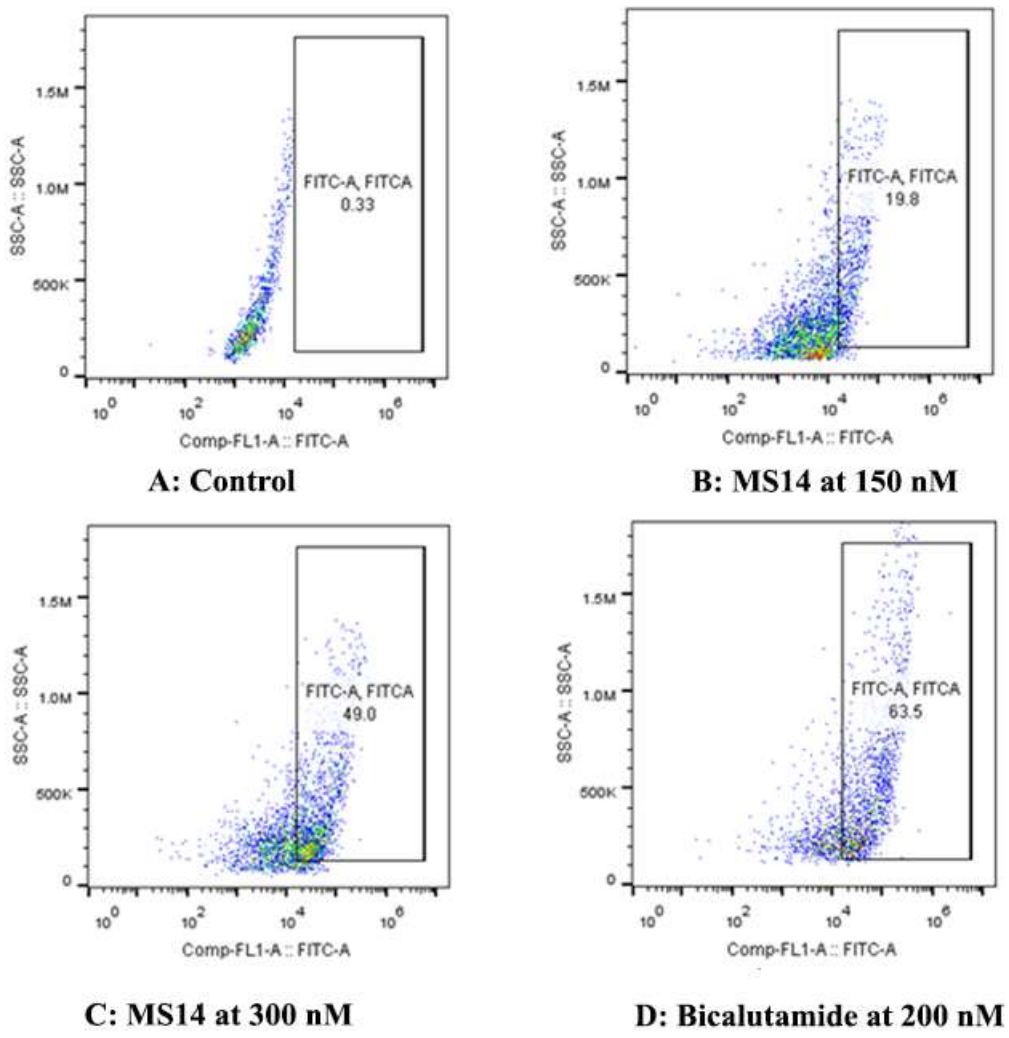

Figure 23: MS14 induced ROS production in a dose dependent manner

Compound **MS14** exhibited a significant increase in ROS percentage, with a 19.8% at 150 nM and a remarkable 49% increase at 300 nM compared to the control group, which had a baseline ROS level of 0.33%. In contrast, bicalutamide displayed a substantial increase in ROS percentage, marking a 63.5% rise compared to the control. These findings emphasize the potent impact of compound **MS14** and bicalutamide in inducing intracellular ROS production, with compound **MS14** showing a distinguished dose-dependent manner effect (**Figure 23**).

5.7. Androgen Receptor Inhibition Assay

To conduct a more comprehensive analysis of their mechanisms, compound **MS14** and bicalutamide were subjected to mechanistic study. As mentioned in the rationale these compounds were designed with the specific goal of inhibiting the androgen receptor.

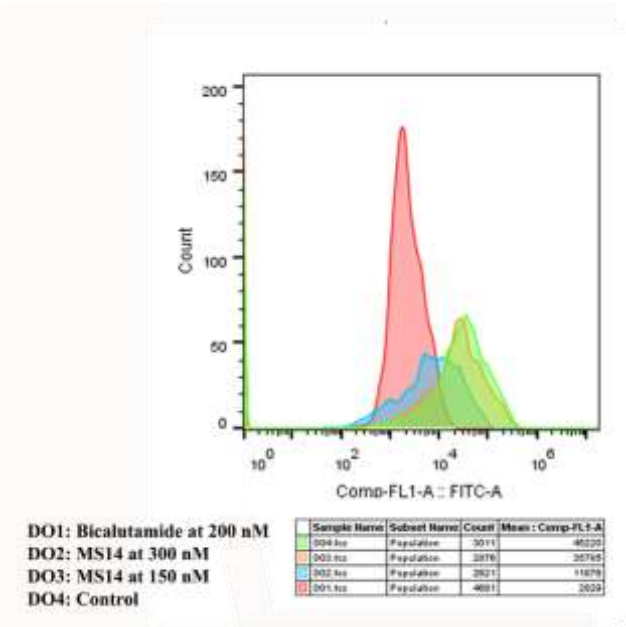

Figure 24: Inhibition of androgen receptor (AR) expression in a dose-dependent manner

So, in accordance with the same, we have conducted an investigation into their capability to effectively suppress androgen receptor expression within the PC-3 cell lines. In this study, both Flow Cytometry and Immunofluorescence assays was employed to assess androgen receptor protein expression. Compound **MS14** was administered at concentrations of 150 nM and 300 nM, while bicalutamide was provided at a concentration of 200 nM. The findings from the Flow Cytometry assay demonstrated a dose-dependent reduction in prostate cancer cells when treated with compound **MS14**, implying a corresponding dose-dependent inhibition of androgen receptor expression by compound **MS14**. After 24h of treatment with compound **MS14** has shown MFI of 35785 at 150 nM concentration and 11876 at 300 nM concentration suggesting a decrease of androgen receptor expression *via* dose-

dependent manner while the MFI was 2829 and 45220 for bicalutamide at 200 nM and control, respectively (**Figure 24**).

Furthermore, Immunofluorescence assay was also conducted to assess the inhibition of the androgen receptor. Similar to previous findings, a dose-dependent inhibition of androgen receptor expression was observed. **MS14** was administered at concentrations of 150 nM and 300 nM, while bicalutamide was given at a concentration of 200 nM.

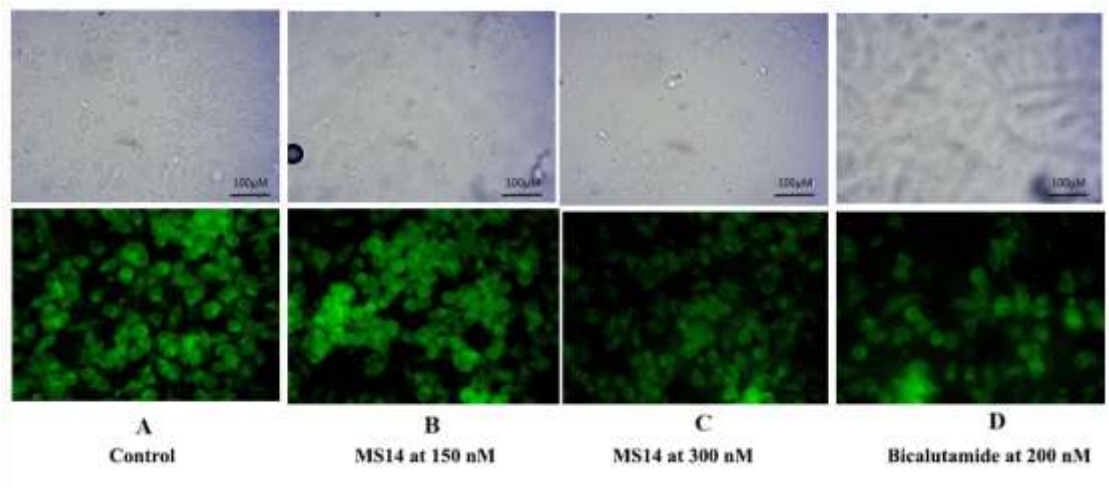

Figure 25a: Androgen receptor expression measured by immunofluorescence assay -

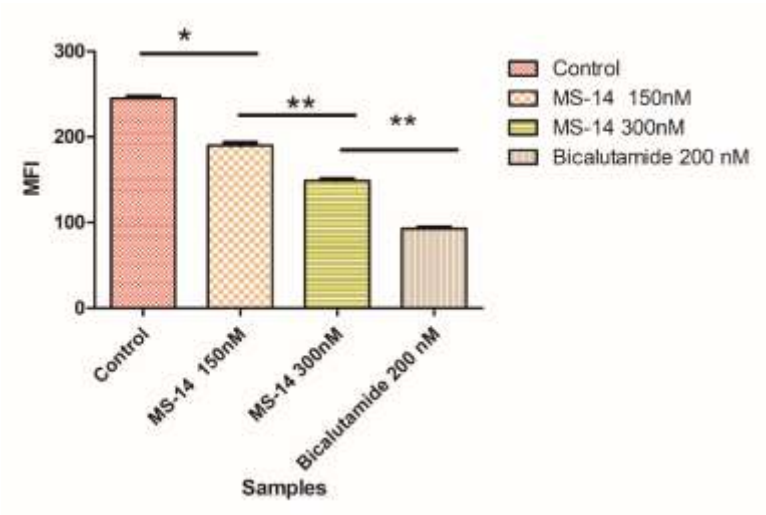

Figure 25b: Graphical representation of mean fluorescence intensity (MFI) of control, MS14 at 150 and 300 nM and bicalutamide at 200 nM

The results indicate that treatment with compound **MS14** resulted in a dose-dependent decrease in androgen receptor expression compared to the control group (**Figure 25**). The Mean Fluorescence Intensity (MFI) was measured at 193 for compound **MS14** at 150 nM, 148 for compound **MS14** at 300 nM, and 245 for the control group. Bicalutamide exhibited an MFI of 95 at a concentration of 200 nM. Based on these findings, it was evident that compound **MS14** reduces androgen receptor expression in a dose-dependent manner.

5.8. Absorption, Distribution, Metabolism, and Excretion (ADME) Analysis of Synthesized Compounds MS01-MS15 And Bicalutamide

Physicochemical properties play a pivotal role in determining the potential of a compound as a drug candidate. To evaluate the ADME (absorption, distribution, metabolism, and excretion) properties of the synthesized compounds and bicalutamide, they were subjected to analysis using SWISSADME. Various parameters such as LogP (partition coefficient), H-bond acceptors and donors, gastrointestinal (GI) absorption, blood-brain barrier (BBB) permeation, Lipinski's rule of 5, and lead likeness properties were predicted. The results revealed that only all compounds including bicalutamide have shown ideal drug-likeness properties with no violation of Lipinski’s rule of 5. Further, lead likeness properties for all the compounds was also predicted and it has been observed that except compounds **MS07** and **MS08**, all other compounds (including bicalutamide) have shown the least 1 violation of lead likeness properties. Moreover, it was also observed that compounds **MS01**, **MS02**, **MS03** and **MS04** have shown two violations of lead likeness properties.

Furthermore, the majority of compounds exhibited high GI absorption, signifying their advantageous uptake within the gastrointestinal tract, except for bicalutamide. Moreover, Except compound **MS08** and bicalutamide have shown no permeation for the blood-brain barrier and apart from that other compounds have demonstrated the potential to permeate the blood-brain barrier (BBB), implying their capacity to traverse this crucial physiological barrier. However, compounds that violated lead likeness properties, including bicalutamide, did not display BBB permeation. This suggests that while these compounds obey Lipinski's rule of five and also, they

remain safe for human administration due to their inability to breach the BBB. The bioavailability of all the compounds, as well as bicalutamide, was determined to be 0.55, which is considered an optimum value. Bioavailability is a critical factor in assessing the fraction of an administered dose of a drug that reaches the systemic circulation unchanged, and an optimal value is desirable for effective drug delivery (**Table 8**).

Table 8: ADME Properties of compound MS01-MS15 and bicalutamide

Molecules	**MW**	**#H-bond acceptors**	**#H-bond donors**	**Consensus Log P**	**GI absorption**	**BBB permeant**	**Lipinski #violations**	**Bioavailability Score**	**Leadlikeness #violations**
Bicalutamide	430.37	9	2	3.06	Low	No	0	0.55	1
MS01	222.24	3	0	3.3	High	Yes	0	0.55	2
MS02	236.27	3	0	3.5	High	Yes	0	0.55	2
MS03	236.27	3	0	3.56	High	Yes	0	0.55	2
MS04	236.27	3	0	3.55	High	Yes	0	0.55	2
MS05	238.24	4	1	2.74	High	Yes	0	0.55	1
MS06	238.24	4	1	2.76	High	Yes	0	0.55	1
MS07	252.27	4	0	3.17	High	Yes	0	0.55	0
MS08	267.24	5	0	2.57	High	No	0	0.55	0
MS09	237.26	3	1	2.62	High	Yes	0	0.55	1
MS10	237.26	3	1	2.61	High	Yes	0	0.55	1
MS11	256.69	3	0	3.69	High	Yes	0	0.55	1
MS12	256.69	3	0	3.71	High	Yes	0	0.55	1
MS13	291.13	3	0	4.21	High	Yes	0	0.55	1
MS14	240.23	4	0	3.49	High	Yes	0	0.55	1
MS15	301.14	3	0	3.8	High	Yes	0	0.55	1

5.9. Toxicity Analysis of MS01-MS15 compounds and Bicalutamide

Furthermore, the pkCSM online tool was utilized to predict the toxicity of compounds **MS01-MS15** and bicalutamide. Maximum Tolerated Dose (MTD) for humans using pkCSM was calculated. hERG, or the human ether-a-go-go-related gene, plays a significant role in cardiac depolarization and repolarization. Inhibition of hERG can lead to certain cardiac diseases. Therefore, the inhibitory effects on hERG I and II, acute toxicity in rats, including the median lethal dose (LD_{50}) was also predicted. Additionally, we made predictions for parameters such as hepatotoxicity and skin sensitization along with toxic doses for the inhibition of growth in *Tetrahymena pyriformis* (*T. pyriformis*) and estimated minnow toxicity to assess aquatic toxicity.

The predicted parameters, as listed in **Table 9**, were analyzed using pkCSM to assess toxicity. The results of this analysis revealed that, with the exception of compounds **MS05**, **MS06**, **MS11**, **MS13**, and **MS14**, all other compounds exhibited positive results for AMES toxicity. This suggests that several compounds in the study may possess mutagenic and carcinogenic properties. The Maximum Tolerated Dose (MTD) for humans was found to vary within the range of -0.047 to 0.402 log mg/kg/day. Higher log MTD values, as observed in compounds **MS07** and **MS10**, indicate a greater tolerance in humans, while lower values raise potential safety concerns, particularly at lower doses. Notably, all the compounds showed negative results for inhibitory effects on hERG I and II, implying a lack of cardiotoxicity potential across the board. Regarding acute toxicity, compounds with lower values of the Oral Rat Acute Toxicity (ORAT) parameter, such as compound **MS07**, suggest higher toxicity in rats, whereas higher values, exemplified by compounds **MS08** and **MS01**, indicate lower toxicity levels in this species. All synthesized compounds demonstrated negative results for hepatotoxicity and skin sensitization, suggesting a low likelihood of causing skin allergies or liver damage upon exposure. However, it's important to note that bicalutamide exhibited positive results for hepatotoxicity. The values obtained for *T. pyriformis* toxicity fell within the range of 0.369 to 0.653 µg/mL. Lower values in this range indicate potential toxicity to *T. pyriformis*, which could have environmental implications. Most compounds showed values close to zero for minnow toxicity, indicating a low risk to aquatic life. However, bicalutamide stood

out as having the potential for a higher risk to aquatic organisms. Compound **MS14**, identified as a potent candidate through in vitro analysis, exhibits favorable ADME (Absorption, Distribution, Metabolism, and Excretion) properties and manageable levels of toxicity.

Table 9: Toxicity analysis of substituted 3,5-diphenyl 1,2,4-oxadiazoles and bicalutamide

Compound Code	**MTD (human) log mg/kg /day**	**hERG I inhibitor**	**hERG II inhibitor**	**ORAT (LD_{50}) mol/kg**	**Hepatotoxicity**	**Skin Sensitisation**	***T. Pyriformis* toxicity log µg/mL**	**minnow toxicity (log mM)**
Bicalutamide	0.233	No	No	2.484	Yes	No	0.484	0.824
MS01	0.284	No	No	1.934	No	No	0.563	0.171
MS02	0.011	No	No	1.904	No	No	0.638	0.197
MS03	0.146	No	No	1.94	No	No	0.575	0.342
MS04	0.273	No	No	1.959	No	No	0.517	0.153
MS05	-0.047	No	No	1.918	No	No	0.608	0.638
MS06	0.22	No	No	1.96	No	No	0.5	0.594
MS07	0.402	No	No	2.05	No	No	0.433	-0.607
MS08	0.039	No	No	2.732	No	No	0.421	-0.14
MS09	0.071	No	No	2.382	No	No	0.391	0.796
MS10	0.201	No	No	2.412	No	No	0.369	0.606
MS11	0.008	No	No	1.956	No	No	0.653	-0.021
MS12	0.276	No	No	2.019	No	No	0.52	-0.65
MS13	0.177	No	No	2.119	No	No	0.58	-0.667
MS14	0.249	No	No	1.978	No	No	0.506	0.268
MS15	0.278	No	No	2.03	No	No	0.52	-0.211

CHAPTER 6

6.1. Designing of 3-Phenyl-5-Styryl-1,2,4-Oxadiazoles (SP01-SP25)

From the results of the previous series, it was observed that fluoro-substituted compound **MS14** was found to be the most potent among the **MS01-MS15** series. It was observed that compounds substituted with Electron-Withdrawing Groups (EWGs) had a more significant effect compared to compounds substituted with Electron-Donating Groups (EDGs). Furthermore, upon analysing the structures of bicalutamide, enzalutamide, and apalutamide, it was noticed that both rings in these compounds were substituted with EWGs. Additionally, a literature survey revealed that several potent compounds were also substituted with EWGs, such as compound **4**. To know the reason behind this, the active site of the androgen receptor was deeply studied and found that active site of the AR LBD (ligand binding domain) is well characterized as a hydrophobic pocket with two polar patches Arg752 and Gln711 at one end and Thr877 and Asn705 at the other end of the site. Compounds substituted with electron-withdrawing groups like Br, Cl, F interact with amino acids like Arg752, and Gln711 present in the active site of the protein target site via their stronger electrostatic interactions. It was believed that EWG substitutions withdraw electrons from the aromatic ring, reducing electron density and obtaining a negative charge on it by creating a positive charge on the ring. This leads to the interaction of EWGs with residues present in the active site of targeted protein of cancer cells or within their microenvironment, potentially enhancing anticancer activity. This was further clarified by the literature review where it was observed that multiple studies done by various research groups yielded the compounds substituted with EWGs have shown potent activity. Consequently, the decision was made to substitute both rings surrounding the oxadiazole with EWGs at the *para* position. Moreover, it was thought to extend the linker to increase the hydrophobic interactions. In bicalutamide, the spacer consists of an approximately 5-atom long chain, while in **MS01-MS15**, it comprises only an oxadiazole. Additionally, the heterocyclic rings in apalutamide and enzalutamide are substituted with alkyl groups, contributing to hydrophobic interactions.

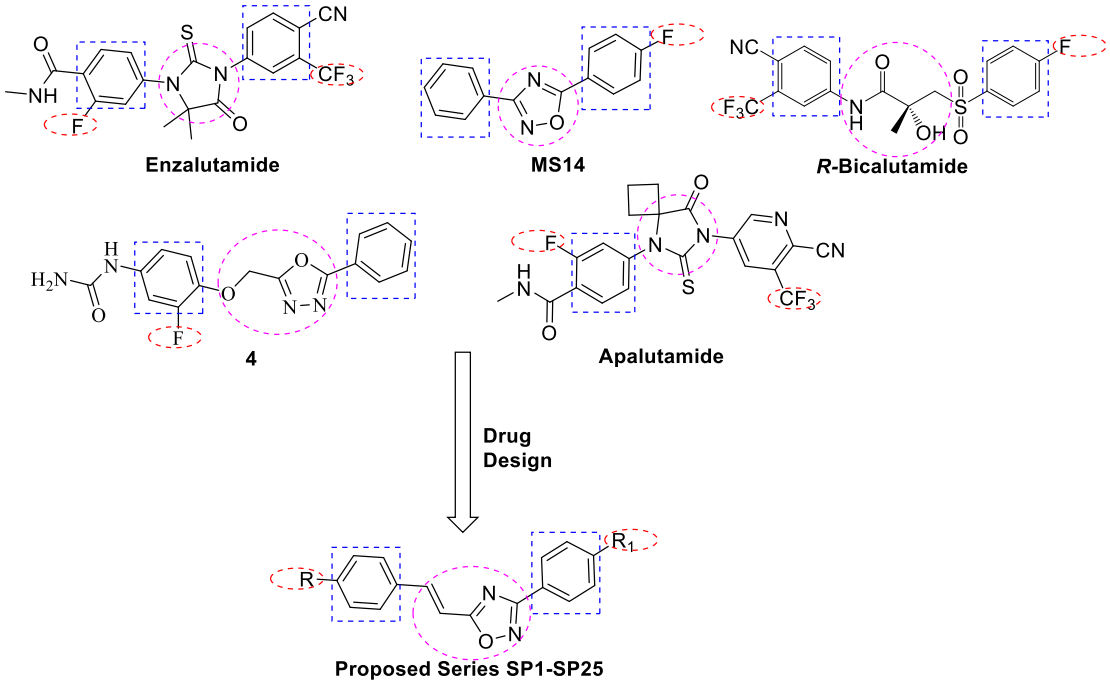

Figure 26: Designing rationale of the compound SP01-SP25.

Examining compound **4**, an extra spacer of methyl ether (-O-CH_2-) was noted. This led to the idea of introducing a replacement of -O-CH_2- with a vinyl group (-CH=CH-) between the oxadiazole and one of the rings because alkene can produce more hydrophobic interaction by introducing π- π interaction. Consequently, another series was designed, known as **SP01-SP25** (**Figure 26**), aimed at prostate cancer treatment by inhibiting the androgen receptor and functioning as pure antagonists of AR.

6.2. Chemistry

6.2.1. General Synthesis of 3-Phenyl-5-Styryl-1,2,4-Oxadiazoles (SP01-SP25)

The synthesis of 3-phenyl-5-styryl-1,2,4-oxadiazoles was carried out in three steps. First, substituted *N'*-hydroxybenzimidamide (**2a-2e**) were synthesized from their corresponding substituted benzonitriles (**1a-1e**). Next, substituted cinnamic acids (**3a-3e**) were reacted with *N'*-hydroxybenzimidamide to yield *N'*-(cinnamoyloxy)benzimidamide (**4a-4y**), and finally, *N'*-(cinnamoyloxy)benzimidamide was cyclized to yield 3-phenyl-5-styryl-1,2,4-oxadiazoles (**SP01-SP25**).

6.2.2. Procedure For Synthesis of *N*'-hydroxybenzimidamide (2a-2e)

In 100 mL round bottom flask, benzonitriles **1a-1e** (9.69 mmol) were added to 15 mL of ethanol, along with hydroxylamine hydrochloride (48.45 mmol), and stirred at r.t. for 15 minutes, respectively. In 100 mL round bottom flask, benzonitriles **1a-1e** (9.69 mmol) were added to 15 mL of ethanol, along with hydroxylamine hydrochloride (48.45 mmol), and stirred at r.t. for 15 minutes, respectively. Upon completion of time, sodium bicarbonate (29.07 mmol) was gradually introduced, and the mixture was refluxed for a period of 2 hours. The progression of the reaction was continuously monitored via TLC. Once the nitriles were entirely consumed, the solvent was removed through vacuum distillation. A surplus of distilled water was added, resulting in the formation of a viscous solution. The mixture was then partitioned using ethyl acetate. Subsequently, the ethyl acetate layer was separated, and the solvent was evaporated under vacuum distillation, yielding the corresponding *N*'-hydroxybenzimidamides (**2a-2e**) **Scheme 7** and the reaction mechanism was also discussed in **Scheme 8** [140, 141].

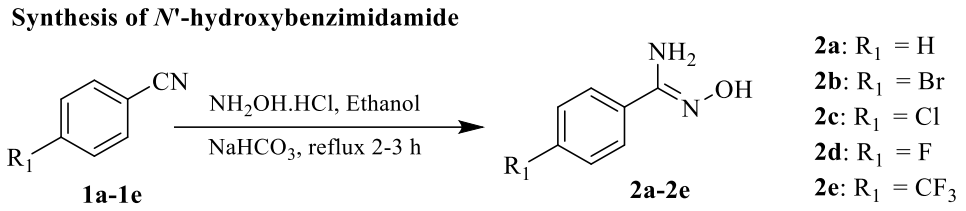

Scheme 7: Synthesis of *N*'-hydroxybenzimidamide

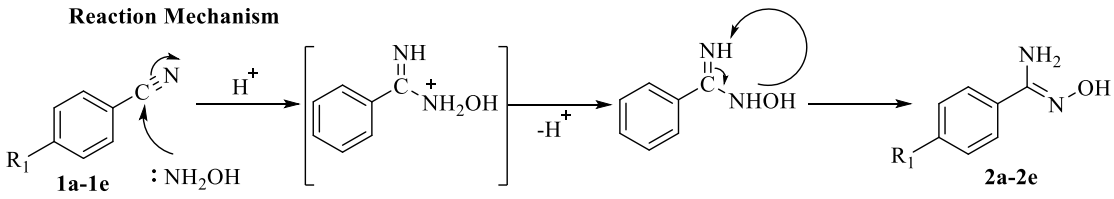

Scheme 8: Mechanism of reaction of substituted *N*'-hydroxybenzimidamides

6.2.3. Procedure For Synthesis of Substituted *N*'-(cinnamoyloxy)benzimidamide (4a-4y)

In a 100 mL of round bottom flask, cinnamic acid **3a-3e** (1.8 mmol), along with TEA (3 mmol), was mixed in 5 mL of 1,4-dioxane, respectively. Subsequently, ethyl chloroformate (3 mmol) was added drop by drop to the mixture. The resulting reaction

mixture was stirred at r.t. for 15 minutes. Following this, a solution containing *N'*-hydroxybenzimidamides (**2a-2e**) (2.5 mmol) in 5 mL of 1,4-dioxane was introduced into the reaction mixture, respectively, and the resulting mixture was stirred at r.t. for a duration of 30 minutes. Once the reaction had completed, the reaction mixture was subjected to concentration through vacuum distillation. It was then diluted with 25 mL of cold water, which resulted in the formation of a precipitate. This precipitate was carefully filtered, washed with cold water, and subsequently dried at r.t. The solid that resulted from this process was further purified using silica gel column chromatography, with elution carried out by ethyl acetate and *n*-hexane. This purification method yielded the pure compounds (**Scheme 9**) and reaction mechanism was discussed in **Scheme 10** [144].

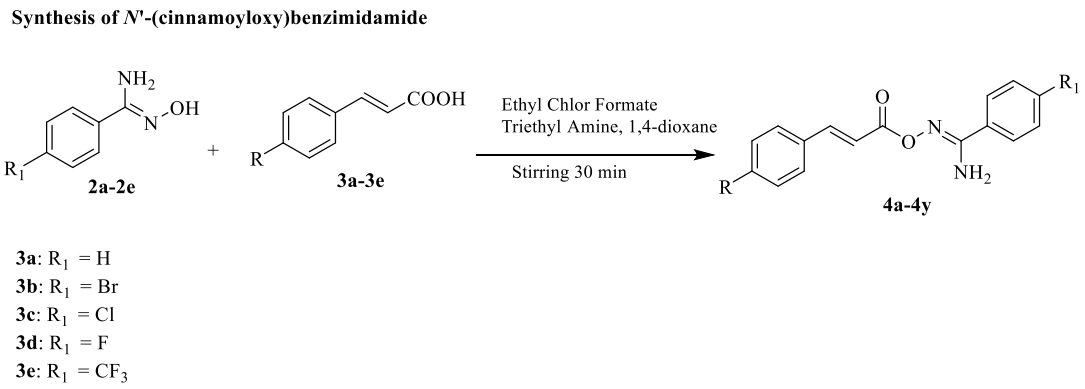

Scheme 9: Synthesis of *N'*-(cinnamoyloxy)benzimidamides

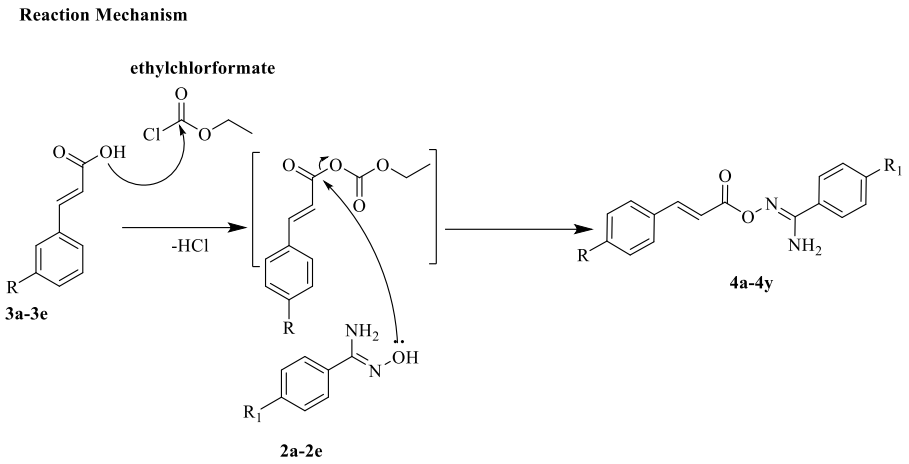

Scheme 10: Reaction Mechanism for *N'*-(cinnamoyloxy)benzimidamides

6.2.4. Procedure For Synthesis of Substituted 3-phenyl-5-styryl-1,2,4-oxadiazoles (SP01-SP25)

A suspension of potassium hydroxide (1.5 mmol) in 5 mL of dimethyl sulfoxide (DMSO) was prepared by stirring. To this suspension, *N'*-(cinnamoyloxy)benzimidamides **4a-4y** (1.5 mmol) was added, respectively. After stirring the reaction mixture for 20 minutes, the progress of the reaction was continuously monitored by TLC. Upon completion of the reaction, the mixture was diluted with 25 mL of cold water, resulting in the formation of a precipitate. This precipitate was meticulously filtered, washed with water, and permitted to air-dry at room temperature. Following this, the obtained solid underwent purification through silica gel column chromatography, employing a mixture of ethyl acetate and n-hexane as the eluent. This process ultimately resulted in the isolation of the pure compound, as depicted in **Schemes 11** and **12** [145-146].

Synthesis of substituted 3-phenyl-5-styryl-1,2,4-oxadiazole

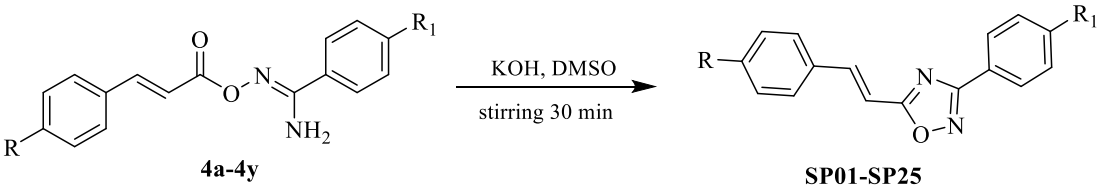

4a-4y **SP01-SP25**

SP01: R = H ; R_1 = H
SP02: R = Br ; R_1 = H
SP03: R = Cl ; R_1 = H
SP04: R = F ; R_1 = H
SP05: R = CF_3; R_1 = H
SP06: R = H ; R_1 = Br
SP07: R = Br ; R_1 = Br
SP08: R = Cl ; R_1 = Br
SP09: R = F ; R_1 = Br
SP10: R = CF_3; R_1 = Br
SP11: R = H ; R_1 = Cl
SP12: R = Br ; R_1 = Cl
SP13: R = Cl ; R_1 = Cl
SP14: R = F ; R_1 = Cl
SP15: R = CF_3; R_1 = Cl
SP16: R = H ; R_1 = F
SP17: R = Br ; R_1 = F
SP18: R = Cl ; R_1 = F
SP19: R = F ; R_1 = F
SP20: R = CF_3; R_1 = F
SP21: R = H ; R_1 = CF_3
SP22: R = Br ; R_1 = CF_3
SP23: R = Cl ; R_1 = CF_3
SP24: R = F ; R_1 = CF_3
SP25: R = CF_3; R_1 = CF_3

Scheme 11: Synthesis of target molecule 3-phenyl-5-styryl-1,2,4-oxadiazoles

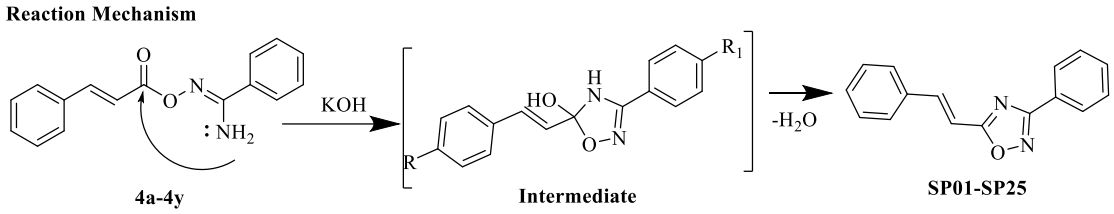

Scheme 11: Mechanism of reaction for target molecule 3-phenyl-5-styryl-1,2,4-oxadiazoles

Following the successful synthesis of all compounds, characterization was performed using IR, ^{1}H NMR, ^{13}C NMR, and Mass Spectroscopy. The corresponding data is presented below:

6.3. Spectral Characterization of Compounds

"**3-Phenyl-5-styryl-1,2,4-oxadiazole (SP01)**: Yield 72%, White powder, mp 133-135 °C. **IR (KBr) (cm^{-1})**: 3087 (C=C-H str.), 2960 (Ar, C=C-H, str.), 1607 (C=C str.), 1246 (C-O str.), 1033 (C-N str.); **^{1}H NMR (400 MHz, DMSO-*d*$_6$), δ (ppm)**: 7.06 (d, -C*H*=, 1H, *J* = 12 Hz), 7.17 (d, -C*H*=, 1H, *J* = 12 Hz), 7.21 (m, Ar-*H*, 1H), 7.32 (m, Ar-*H*, 2H), 7.49 (m, Ar-*H*, 3H), 7.52 (m, Ar-*H*, 2H), 7.94 (m, Ar-*H*, 2H); **^{13}C NMR (100 MHz, DMSO-*d*$_6$), δ (ppm)**: 114.70 (C=C, 1C), 127.31 (C=C, 1C), 127.94 (Ar-C, 2C), 128.26 (Ar-C, 2C), 128.95 (Ar-C, 2C), 129.40 (Ar-C, 1C), 129.98 (Ar-C, 2C), 131.69 (Ar-C, 1C), 135.09 (Ar-C, 1C), 136.62 (Ar-C, 1C), 168.28 (Ar-C, 1C), 169.06 (Ar-C, 1C); **ESI-MS m/z**: 249 [M+H]$^{+}$."

"**3-(4-Bromophenyl)-5-styryl-1,2,4-oxadiazole (SP02)**: Yield 67%, Light yellow powder, mp 178-180 °C. **IR (KBr) (cm^{-1})**: 3082 (C=C-H str.), 2839 (Ar, C=C-H, str.), 1630 (C=C str.), 1257 (C-O str.), 1042 (C-N str.); **^{1}H NMR (400 MHz, DMSO-*d*$_6$), δ (ppm)**: 7.06 (d, -C*H*=, 1H, *J* = 12 Hz), 7.21 (d, -C*H*=, 1H, *J* = 12 Hz), 7.36 (m, Ar-*H*, 3H), 7.42 (m, Ar-*H*, 2H), 7.40 (m, Ar-*H*, 2H), 7.94 (m, Ar-*H*, 2H); **^{13}C NMR (100 MHz, DMSO-*d*$_6$), δ (ppm)**: 114.19 (C=C, 1C), 121.81 (C=C, 1C), 127.31 (Ar-C, 2C), 127.94 (Ar-C, 2C), 129.54 (Ar-C, 2C), 129.98 (Ar-C, 2C), 131.69 (Ar-C, 2C), 134.12 (Ar-C, 1C), 135.50 (Ar-C, 1C), 168.28 (Ar-C, 1C), 169.06 (Ar-C, 1C); **ESI-MS m/z**: 328 [M+H]$^{+}$."

"**3-(4-Chlorophenyl)-5-styryl-1,2,4-oxadiazole (SP03)**: Yield 69%, Pale Yellow powder, mp 158-160 °C. **IR (KBr) (cm^{-1})**: 3081 (C=C-H str.), 2958 (Ar, C=C-H, str.),

1630 (C=C str.), 1257 (C-O str.), 1042 (C-N str.); **^{1}H NMR (400 MHz, DMSO-*d*$_6$), δ (ppm)**: 7.08 (d, -C*H*=, 1H, *J* = 12 Hz), 7.21 (d, -C*H*=, 1H, *J* = 12 Hz), 7.31 (m, Ar-*H*, 2H), 7.46 (m, Ar-*H*, 2H), 7.50 (m, Ar-*H*, 3H), 7.94 (m, Ar-*H*, 2H); **^{13}C NMR (100 MHz, DMSO-*d*$_6$), δ (ppm)**: 114.19 (C=C, 1C), 127.31 (C=C, 1C), 127.94 (Ar-C, 1C), 129.28 (Ar-C, 2C), 129.54 (Ar-C, 2C), 129.98 (Ar-C, 2C), 131.69 (Ar-C, 2C), 133.60 (Ar-C, 1C), 134.62 (Ar-C, 1C), 135.35 (Ar-C, 1C), 168.28 (Ar-C, 1C), 169.06 (Ar-C, 1C); **ESI-MS m/z**: 283 [M+H]$^+$."

"**3-(4-Fluorophenyl)-5-styryl-1,2,4-oxadiazole (SP04)**: Yield 90%, Creamy White powder, mp 151-153 °C. **IR (KBr) (cm^{-1})**: 3087 (C=C-H str.), 2958 (Ar, C=C-H, str.), 1607 (C=C str.), 1246 (C-O str.), 1033 (C-N str.); **^{1}H NMR (400 MHz, DMSO-*d*$_6$), δ (ppm)**: 7.08 (d, -C*H*=, 1H, *J* = 12 Hz), 7.17 (d, -C*H*=, 1H, *J* = 12 Hz), 7.23 (m, Ar-*H*, 1H), 7.33 (m, Ar-*H*, 2H), 7.37 (m, Ar-*H*, 2H), 7.50 (m, Ar-*H*, 2H), 7.84 (m, Ar-*H*, 2H); **^{13}C NMR (100 MHz, DMSO-*d*$_6$), δ (ppm)**: 114.76 (C=C, 1C), 115.77 (C=C, 1C), 115.95 (Ar-C, 1C), 123.77 (Ar-C, 1C), 128.31 (Ar-C, 2C), 128.96 (Ar-C, 2C), 129.39 (Ar-C, 2C), 129.46.17 (Ar-C, 1C), 135.27 (Ar-C, 2C), 163.62 (Ar-C, 1C), 168.51 (Ar-C, 1C), 169.18 (Ar-C, 1C); **ESI-MS m/z**: 267 [M+H]$^+$."

"**5-Styryl-3-(4-(trifluoromethyl)phenyl)-1,2,4-oxadiazole (SP05)**: Yield 71%, White powder, mp 205-207 °C. **IR (KBr) (cm^{-1})**: 3073 (C=C-H str.), 2948 (Ar, C=C-H, str.), 1601 (C=C str.), 1226 (C-O str.), 1023 (C-N str.); **^{1}H NMR (400 MHz, DMSO-*d*$_6$), δ (ppm)**: 7.09 (d, -C*H*=, 1H, *J* = 12 Hz), 7.24 (d, -C*H*=, 1H, *J* = 12 Hz), 7.31 (m, Ar-*H*, 3H), 7.45 (m, Ar-*H*, 2H), 7.79 (m, Ar-*H*, 2H), 8.05 (m, Ar-*H*, 2H); **^{13}C NMR (100 MHz, DMSO-*d*$_6$), δ (ppm)**: 114.16 (C=C, 1C), 120.64 (C=C, 1C), 122.82 (CF_3, 1C), 124.99 (Ar-C, 2C), 125.98 (Ar-C, 2C), 126.02 (Ar-C, 2C), 127.17 (Ar-C, 1C), 128.12 (Ar-C, 1C), 129.15 (Ar-C, 1C), 132.31 (Ar-C, 1C), 133.60 (Ar-C, 1C), 135.35 (Ar-C, 1C), 167.94 (Ar-C, 1C), 169.06 (Ar-C, 1C); **ESI-MS m/z**: 317 [M+H]$^+$."

"**5-(4-Bromostyryl)-3-phenyl-1,2,4-oxadiazole (SP06)**: Yield 61%, Light Orange powder, mp 168-170 °C. **IR (KBr) (cm^{-1})**: 3073 (C=C-H str.), 2918 (Ar, C=C-H, str.), 1593 (C=C str.), 1233 (C-O str.), 1013 (C-N str.); **^{1}H NMR (400 MHz, DMSO-*d*$_6$), δ (ppm)**: 7.09 (d, -C*H*=, 1H, *J* = 12 Hz), 7.24 (d, -C*H*=, 1H, *J* = 12 Hz), 7.39 (m, Ar-*H*, 3H), 7.44 (m, Ar-*H*, 2H), 7.50 (m, Ar-*H*, 2H), 7.94 (m, Ar-*H*, 2H); **^{13}C NMR (100 MHz, DMSO-*d*$_6$), δ (ppm)**: 114.19 (C=C, 1C), 121.81 (C=C, 1C), 127.31 (Ar-C, 1C), 127.94

(Ar-C, 1C), 129.54 (Ar-C, 2C), 129.98 (Ar-C, 2C), 131.69 (Ar-C, 3C), 134.12 (Ar-C, 2C), 135.50 (Ar-C, 1C), 168.28 (Ar-C, 1C), 169.06 (Ar-C, 1C); **ESI-MS m/z**: 326 $[M-H]^+$."

"**3-(4-Bromophenyl)-5-(4-bromostyryl)-1,2,4-oxadiazole (SP07)**: Yield 58%, Light Green powder, mp 207-209 °C. **IR (KBr) (cm^{-1})**: 3057 (C=C-H str.), 2932 (Ar, C=C-H, str.), 1587 (C=C str.), 1226 (C-O str.), 1043 (C-N str.); **^{1}H NMR (400 MHz, DMSO-*d*$_6$), δ (ppm)**: 7.09 (d, -C*H*=, 1H, *J* = 12 Hz), 7.21 (d, -C*H*=, 1H, *J* = 12 Hz), 7.39 (m, Ar-*H*, 2H), 7.44 (m, Ar-*H*, 2H), 7.83 (m, Ar-*H*, 2H), 7.85 (m, Ar-*H*, 2H); **^{13}C NMR (100 MHz, DMSO-*d*$_6$), δ (ppm)**: 114.15 (C=C, 1C), 121.82 (C=C, 1C), 125.40 (Ar-C, 1C), 126.90 (Ar-C, 1C), 129.16 (Ar-C, 2C), 129.70 (Ar-C, 2C), 131.70 (Ar-C, 2C), 131.95 (Ar-C, 2C), 134.29 (Ar-C, 1C), 134.82 (Ar-C, 1C), 168.12 (Ar-C, 1C), 169.16 (Ar-C, 1C); **ESI-MS m/z**: 407 $[M+H]^+$."

"**5-(4-Bromostyryl)-3-(4-chlorophenyl)-1,2,4-oxadiazole (SP08)**: Yield 43%, Off White powder, mp 198-200 °C. **IR (KBr) (cm^{-1})**: 3072 (C=C-H str.), 2942 (Ar, C=C-H, str.), 1593 (C=C str.), 1221 (C-O str.), 1023 (C-N str.); **^{1}H NMR (400 MHz, DMSO-*d*$_6$), δ (ppm)**: 7.09 (d, -C*H*=, 1H, *J* = 12 Hz), 7.21 (d, -C*H*=, 1H, *J* = 12 Hz), 7.39 (m, Ar-*H*, 2H), 7.42 (m, Ar-*H*, 2H), 7.50 (m, Ar-*H*, 2H), 7.88 (m, Ar-*H*, 2H); **^{13}C NMR (100 MHz, DMSO-*d*$_6$), δ (ppm)**: 114.19 (C=C, 1C), 121.81 (C=C, 1C), 127.36 (Ar-C, 1C), 129.28 (Ar-C, 2C), 129.54 (Ar-C, 2C), 131.93 (Ar-C, 2C), 134.12 (Ar-C, 2C), 135.50 (Ar-C, 1C), 135.58 (Ar-C, 2C), 168.37 (Ar-C, 1C), 169.06 (Ar-C, 1C); **ESI-MS m/z**: 362 $[M+H]^+$."

"**5-(4-Bromostyryl)-3-(4-fluorophenyl)-1,2,4-oxadiazole (SP09)**: Yield 75%, Light Brown powder, mp 202-204 °C. **IR (KBr) (cm^{-1})**: 3073 (C=C-H str.), 2925 (Ar, C=C-H, str.), 1583 (C=C str.), 1229 (C-O str.), 1019 (C-N str.); **^{1}H NMR (400 MHz, DMSO-*d*$_6$), δ (ppm)**: 7.08 (d, -C*H*=, 1H, *J* = 12 Hz), 7.21 (d, -C*H*=, 1H, *J* = 12 Hz), 7.35 (m, Ar-*H*, 2H), 7.40 (m, Ar-*H*, 2H), 7.44 (m, Ar-*H*, 2H), 7.84 (m, Ar-*H*, 2H); **^{13}C NMR (100 MHz, DMSO-*d*$_6$), δ (ppm)**: 114.19 (C=C, 1C), 115.77 (C=C, 1C), 115.95 (Ar-C, 2C), 121.81 (Ar-C, 2C), 123.77 (Ar-C, 2C), 129.39 (Ar-C, 2C), 129.46 (Ar-C, 1C), 129.54 (Ar-C, 1C), 131.93 (Ar-C, 1C), 134.12 (Ar-C, 1C), 135.50 (Ar-C, 1C), 163.62 (Ar-C, 1C), 168.43 (Ar-C, 1C), 168.91 (Ar-C, 1C); **ESI-MS m/z**: 346 $[M+H]^+$."

"**3-(4-Fluorophenyl)-5-(4-(trifluoromethyl)styryl)-1,2,4-oxadiazole (SP10)**: Yield 63%, Dark Yellow powder, mp 184-186 °C. **IR (KBr) (cm^{-1})**: 3067 (C=C-H str.), 2943 (Ar, C=C-H, str.), 1590 (C=C str.), 1249 (C-O str.), 1029 (C-N str.); **^{1}H NMR (400 MHz, DMSO-*d*$_6$), δ (ppm)**: 7.09 (d, -C*H*=, 1H, *J* = 12 Hz), 7.21 (d, -C*H*=, 1H, *J* = 12 Hz), 7.35 (m, Ar-*H*, 2H), 7.67 (m, Ar-*H*, 2H), 7.78 (m, Ar-*H*, 2H), 7.84 (m, Ar-*H*, 2H); **^{13}C NMR (100 MHz, DMSO-*d*$_6$), δ (ppm)**: 114.19 (CF_3, 1C), 115.77 (C=C, 1C), 115.95 (C=C, 1C), 120.85 (CF_3, 1C), 123.77 (Ar-C, 1C), 125.19 (Ar-C, 2C), 125.93 (Ar-C, 1C), 128.73 (Ar-C, 1C), 129.39 (Ar-C, 1C), 129.46 (Ar-C, 1C), 130.66 (Ar-C, 1C), 134.93 (Ar-C, 1C), 135.30 (Ar-C, 1C), 161.65 (Ar-C, 1C), 168.43 (Ar-C, 1C), 168.91 (Ar-C, 1C); **ESI-MS m/z**: 333 $[M-H]^+$."

"**5-(4-Chlorostyryl)-3-phenyl-1,2,4-oxadiazole (SP11)**: Yield 89%, Yellow powder, mp 161-163 °C. **IR (KBr) (cm^{-1})**: 3059 (C=C-H str.), 2943 (Ar, C=C-H, str.), 1597 (C=C str.), 1237 (C-O str.), 1037 (C-N str.); **^{1}H NMR (400 MHz, DMSO-*d*$_6$), δ (ppm)**: 7.08 (d, -C*H*=, 1H, *J* = 12 Hz), 7.21 (d, -C*H*=, 1H, *J* = 12 Hz), 7.31 (m, Ar-*H*, 2H), 7.46 (m, Ar-*H*, 2H), 7.50 (m, Ar-*H*, 3H), 7.94 (m, Ar-*H*, 2H); **^{13}C NMR (100 MHz, DMSO-*d*$_6$), δ (ppm)**: 114.19 (C=C, 1C), 127.31 (C=C, 1C), 127.94 (Ar-C, 1C), 129.28 (Ar-C, 2C), 129.54 (Ar-C, 1C), 129.98 (Ar-C, 2C), 131.69 (Ar-C, 2C), 133.60 (Ar-C, 2C), 134.62 (Ar-C, 1C), 135.35 (Ar-C, 1C), 168.28 (Ar-C, 1C), 169.06 (Ar-C, 1C); **ESI-MS m/z**: 283 $[M+H]^+$."

"**3-(4-Bromophenyl)-5-(4-chlorostyryl)-1,2,4-oxadiazole (SP12)**: Yield 83%, Off White powder, mp 200-202 °C. **IR (KBr) (cm^{-1})**: 3063 (C=C-H str.), 2938 (Ar, C=C-H, str.), 1591 (C=C str), 1246 (C-O str.), 1033 (C-N str.); **^{1}H NMR (400 MHz, DMSO-*d*$_6$), δ (ppm)**: 7.09 (d, -C*H*=, 1H, *J* = 12 Hz), 7.21 (d, -C*H*=, 1H, *J* = 12 Hz), 7.39 (m, Ar-*H*, 2H), 7.42 (m, Ar-*H*, 2H), 7.50 (m, Ar-*H*, 2H), 7.88 (m, Ar-*H*, 2H); **^{13}C NMR (100 MHz, DMSO-*d*$_6$), δ (ppm)**: 114.19 (C=C, 1C), 121.81 (C=C, 1C), 127.36 (Ar-C, 1C), 129.28 (Ar-C, 2C), 129.54 (Ar-C, 2C), 129.98 (Ar-C, 2C), 131.93 (Ar-C, 1C), 134.12 (Ar-C, 2C), 135.50 (Ar-C, 1C), 135.58 (Ar-C, 1C), 168.37 (Ar-C, 1C), 169.06 (Ar-C, 1C); **ESI-MS m/z**: 362 $[M+H]^+$."

"**3-(4-Chlorophenyl)-5-(4-chlorostyryl)-1,2,4-oxadiazole (SP13)**: Yield 88%, Light Yellow powder, mp 191-193 °C. **IR (KBr) (cm^{-1})**: 3051 (C=C-H str.), 2931 (Ar, C=C-H, str.), 1612 (C=C str.), 1256 (C-O str.), 1073 (C-N str.); **^{1}H NMR (400 MHz, DMSO-**

***d*6), δ (ppm)**: 7.06 (d, -C*H*=, 1H, *J* = 12 Hz), 7.24 (d, -C*H*=, 1H, *J* = 12 Hz), 7.36 (m, Ar-*H*, 2H), 7.48 (m, Ar-*H*, 2H), 7.89 (m, Ar-*H*, 2H), 7.89 (m, Ar-*H*, 2H); **^{13}C NMR (100 MHz, DMSO-*d*6), δ (ppm)**: 114.15 (C=C, 1C), 121.82 (C=C, 1C), 125.40 (Ar-C, 1C), 126.90 (Ar-C, 1C), 129.16 (Ar-C, 1C), 129.70 (Ar-C, 2C), 131.70 (Ar-C, 1C), 131.95 (Ar-C, 2C), 134.29 (Ar-C, 2C), 134.82 (Ar-C, 2C), 168.12 (Ar-C, 1C), 169.16 (Ar-C, 1C); **ESI-MS m/z**: 318 $[M+H]^+$."

"**5-(4-Chlorostyryl)-3-(4-fluorophenyl)-1,2,4-oxadiazole (SP14)**: Yield 83%, Off White powder, mp 208-210 °C. **IR (KBr) (cm^{-1})**: 3072 (C=C-H str.), 2918 (Ar, C=C-H, str.), 1617 (C=C str.), 1226 (C-O str.), 1043 (C-N str.); **^{1}H NMR (400 MHz, DMSO-*d*6), δ (ppm)**: 7.09 (d, -C*H*=, 1H, *J* = 12 Hz), 7.21 (d, -C*H*=, 1H, *J* = 12 Hz), 7.35 (m, Ar-*H*, 2H), 7.48 (m, Ar-*H*, 2H), 7.53 (m, Ar-*H*, 2H), 7.83 (m, Ar-*H*, 2H); **^{13}C NMR (100 MHz, DMSO-*d*6), δ (ppm)**: 114.19 (C=C, 1C), 121.81 (C=C, 1C), 127.36 (Ar-C, 1C), 129.28 (Ar-C, 2C), 129.54 (Ar-C, 2C), 129.98 (Ar-C, 2C), 131.93 (Ar-C, 1C), 134.12 (Ar-C, 1C), 135.50 (Ar-C, 1C), 135.58 (Ar-C, 2C), 168.37 (Ar-C, 1C), 169.06 (Ar-C, 1C); **ESI-MS m/z**: 301 $[M+H]^+$."

"**5-(4-Chlorostyryl)-3-(4-(trifluoromethyl)phenyl)-1,2,4-oxadiazole (SP15)**: Yield 81%, Creamy White powder, mp 213-215 °C. **IR (KBr) (cm^{-1})**: 3062 (C=C-H str.), 2933 (Ar, C=C-H, str.), 1619 (C=C str.), 1223 (C-O str.), 1033 (C-N str.); **^{1}H NMR (400 MHz, DMSO-*d*6), δ (ppm)**: 7.09 (d, -C*H*=, 1H, *J* = 12 Hz), 7.24 (d, -C*H*=, 1H, *J* = 12 Hz), 7.66 (m, Ar-*H*, 2H), 7.78 (m, Ar-*H*, 1H), 7.80 (m, Ar-*H*, 1H), 7.83 (m, Ar-*H*, 2H), 7.85 (m, Ar-*H*, 2H); **^{13}C NMR (100 MHz, DMSO-*d*6), δ (ppm)**: 114.19 (C=C, 1C), 120.85 (C=C, 1C), 125.19 (Ar-C, 2C), 126.90 (Ar-C, CF_3, 2C), 128.70 (Ar-C, 2C), 129.16 (Ar-C, 1C), 130.15 (Ar-C, 2C), 131.70 (Ar-C, 2C), 134.93 (Ar-C, 2C), 135.30 (Ar-C, 2C), 168.07 (Ar-C, 1C), 169.06 (Ar-C, 1C); **ESI-MS m/z**: 350 $[M-H]^+$."

"**5-(4-Fluorostyryl)-3-phenyl-1,2,4-oxadiazole (SP16)**: Yield 90%, Creamy White powder, mp 151-153 °C. **IR (KBr) (cm^{-1})**: 3081 (C=C-H str.), 2960 (Ar, C=C-H, str.), 1633 (C=C str.), 1263 (C-O str.), 1058 (C-N str.); **^{1}H NMR (400 MHz, DMSO-*d*6), δ (ppm)**: 7.08 (d, -C*H*=, 1H, *J* = 12 Hz), 7.17 (d, -C*H*=, 1H, *J* = 12 Hz), 7.23 (m, Ar-*H*, 1H), 7.33 (m, Ar-*H*, 2H), 7.37 (m, Ar-*H*, 2H), 7.50 (m, Ar-*H*, 2H), 7.84 (m, Ar-*H*, 2H); **^{13}C NMR (100 MHz, DMSO-*d*6), δ (ppm)**: 114.76 (C=C, 1C), 115.77 (Ar-C, 1C), 123.77 (Ar-C, 2C), 128.31 (Ar-C, 2C), 127.31 (Ar-C, 2C), 128.96(Ar-C, 1C), 129.39

(Ar-C, 1C), 129.46 (Ar-C, 1C), 135.17 (Ar-C, 1C), 135.27 (Ar-C, 1C), 163.62 (Ar-C, 1C), 168.51 (Ar-C, 1C), 169.18 (Ar-C, 1C); **ESI-MS m/z**: 267 $[M+H]^+$."

"**3-(4-Bromophenyl)-5-(4-fluorostyryl)-1,2,4-oxadiazole (SP17)**: Yield 75%, Light Yellow powder, mp 212-214 °C. **IR (KBr) (cm^{-1})**: 3031 (C=C-H str.), 2919 (Ar, C=C-H, str.), 1613 (C=C str.), 1301 (C-O str.), 1107 (C-N str.); **^{1}H NMR (400 MHz, DMSO-*d*$_6$), δ (ppm)**: 7.08 (d, -C*H*=, 1H, *J* = 12 Hz), 7.21 (d, -C*H*=, 1H, *J* = 12 Hz), 7.38 (m, Ar-*H*, 2H), 7.42 (m, Ar-*H*, 2H), 7.48 (m, Ar-*H*, 2H), 7.89 (m, Ar-*H*, 2H); **^{13}C NMR (100 MHz, DMSO-*d*$_6$), δ (ppm)**: 114.19 (C=C, 1C), 115.95 (C=C, 1C), 121.81 (Ar-C, 1C), 123.77 (Ar-C, 1C), 129.39 (Ar-C, 2C), 129.46 (Ar-C, 2C), 129.54 (Ar-C, 2C), 131.93 (Ar-C, 2C), 134.12 (Ar-C, 1C), 135.50 (Ar-C, 1C), 163.62 (Ar-C, 1C), 168.43 (Ar-C, 1C), 168.91 (Ar-C, 1C); **ESI-MS m/z**: 346 $[M+H]^+$."

"**3-(4-Chlorophenyl)-5-(4-fluorostyryl)-1,2,4-oxadiazole (SP18)**: Yield 79%, White powder, mp 212-214 °C. **IR (KBr) (cm^{-1})**: 3081 (C=C-H str.), 2992 (Ar, C=C-H, str.), 1609 (C=C str.), 1273 (C-O str.), 1093 (C-N str.); **^{1}H NMR (400 MHz, DMSO-*d*$_6$), δ (ppm)**: 7.06 (d, -C*H*=, 1H, *J* = 12 Hz), 7.24 (d, -C*H*=, 1H, *J* = 12 Hz), 7.32 (m, Ar-*H*, 2H), 7.43 (m, Ar-*H*, 2H), 7.50 (m, Ar-*H*, 2H), 7.81 (m, Ar-*H*, 2H); **^{13}C NMR (100 MHz, DMSO-*d*$_6$), δ (ppm)**: 114.19 (C=C, 1C), 121.81 (C=C, 1C), 127.36 (Ar-C, 1C), 129.28 (Ar-C, 2C), 129.54 (Ar-C, 2C), 129.98 (Ar-C, 1C), 131.93 (Ar-C, 2C), 134.12 (Ar-C, 2C), 135.50 (Ar-C, 2C), 135.58 (Ar-C, 1C), 168.37 (Ar-C, 1C), 169.06 (Ar-C, 1C); **ESI-MS m/z**: 301 $[M+H]^+$."

"**3-(4-Fluorophenyl)-5-(4-fluorostyryl)-1,2,4-oxadiazole (SP19)**: Yield 85%, Dark Yellow powder, mp 197-199 °C. **IR (KBr) (cm^{-1})**: 3082 (C=C-H str.), 2839 (Ar, C=C-H, str.), 1630 (C=C str.), 1325 (C-O str.), 1042 (C-N str.); **^{1}H NMR (400 MHz, DMSO-*d*$_6$), δ (ppm)**: 7.05 (d, -C*H*=, 1H, *J* = 12 Hz), 7.21 (d, -C*H*=, 1H, *J* = 12 Hz), 7.33 (m, Ar-*H*, 2H), 7.41 (m, Ar-*H*, 2H), 7.80 (m, Ar-*H*, 2H), 7.84 (m, Ar-*H*, 2H); **^{13}C NMR (100 MHz, DMSO-*d*$_6$), δ (ppm)**: 114.15 (C=C, 1C), 121.82 (C=C, 1C), 125.40 (Ar-C, 1C), 126.90 (Ar-C, 1C), 129.16 (Ar-C, 1C), 129.70 (Ar-C, 2C), 131.70 (Ar-C, 2C), 131.95 (Ar-C, 2C), 134.29 (Ar-C, 2C), 134.82 (Ar-C, 1C), 168.12 (Ar-C, 1C), 169.16 (Ar-C, 1C); **ESI-MS m/z**: 285 $[M+H]^+$."

"**5-(4-Fluorostyryl)-3-(4-(trifluoromethyl)phenyl)-1,2,4-oxadiazole (SP20)**: Yield 63%, Dark Yellow powder, mp 184-186 °C. **IR (KBr) (cm^{-1})**: 3062 (C=C-H str.), 2933 (Ar, C=C-H, str.), 1619 (C=C str.), 1223 (C-O str.), 1033 (C-N str.); **^{1}H NMR (400 MHz, DMSO-*d*$_6$), δ (ppm)**: 7.09 (d, -C*H*=, 1H, *J* = 12 Hz), 7.24 (d, -C*H*=, 1H, *J* = 12 Hz), 7.32 (m, Ar-*H*, 2H), 7.61 (m, Ar-*H*, 2H), 7.71 (m, Ar-*H*, 2H), 7.81 (m, Ar-*H*, 2H); **^{13}C NMR (100 MHz, DMSO-*d*$_6$), δ (ppm)**: 114.19 (C=C, 1C), 115.95 (C=C, 1C), 120.85 (CF_3, 1C), 123.02 (Ar-C, 1C), 123.77 (Ar-C, 1C), 125.19 (Ar-C, 1C), 125.93 (Ar-C, 1C), 128.73 (Ar-C, 1C), 129.39 (Ar-C, 1C), 129.46 (Ar-C, 1C), 130.66 (Ar-C, 2C), 134.93 (Ar-C, 1C), 135.30 (Ar-C, 1C), 161.65 (Ar-C, 1C), 168.43 (Ar-C, 1C), 168.91 (Ar-C, 1C); **ESI-MS m/z**: 335 $[M+H]^+$."

"**3-Phenyl-5-(4-(trifluoromethyl)styryl)-1,2,4-oxadiazole (SP21)**: Yield 84%, White powder, mp 215-217 °C. **IR (KBr) (cm^{-1})**: 3072 (C=C-H str.), 2942 (Ar, C=C-H, str.), 1593 (C=C str.), 1221 (C-O str.), 1023 (C-N str.); **^{1}H NMR (400 MHz, DMSO-*d*$_6$), δ (ppm)**: 7.09 (d, -C*H*=, 1H, *J* = 12 Hz), 7.24 (d, -C*H*=, 1H, *J* = 12 Hz), 7.31 (m, Ar-*H*, 3H), 7.45 (m, Ar-*H*, 2H), 7.79 (m, Ar-*H*, 2H), 8.05 (m, Ar-*H*, 2H); **^{13}C NMR (100 MHz, DMSO-*d*$_6$), δ (ppm)**: 114.16 (C=C, 1C), 120.64 (C=C, 1C), 122.82 (CF_3, 1C), 124.99 (Ar-C, 1C), 126.02 (Ar-C, 1C), 128.12 (Ar-C, 1C), 129.15 (Ar-C, 2C), 132.31 (Ar-C, 1C), 132.82 (Ar-C, 1C), 131.95 (Ar-C, 1C), 133.60 (Ar-C, 2C), 134.62 (Ar-C, 1C), 135.35 (Ar-C, 1C), 167.94 (Ar-C, 1C), 169.06 (Ar-C, 1C); **ESI-MS m/z**: 317 $[M+H]^+$."

"**3-(4-Bromophenyl)-5-(4-(trifluoromethyl)styryl)-1,2,4-oxadiazole (SP22)**: Yield 91%, Off White powder, mp 223-225 °C. **IR (KBr) (cm^{-1})**: 3073 (C=C-H str.), 2918 (Ar, C=C-H, str.), 1593 (C=C str.), 1233 (C-O str.), 1013 (C-N str.); **^{1}H NMR (400 MHz, DMSO-*d*$_6$), δ (ppm)**: 7.09 (d, -C*H*=, 1H, *J* = 12 Hz), 7.24 (d, -C*H*=, 1H, *J* = 12 Hz), 7.66 (m, Ar-*H*, 2H), 7.78 (m, Ar-*H*, 1H), 7.80 (m, Ar-*H*, 1H), 7.83 (m, Ar-*H*, 2H), 7.85 (m, Ar-*H*, 2H); **^{13}C NMR (100 MHz, DMSO-*d*$_6$), δ (ppm)**: 114.19 (C=C, 1C), 120.85 (C=C, 1C), 123.02 (CF_3, 1C), 125.19 (Ar-C, 1C), 126.90 (Ar-C, 1C), 128.70 (Ar-C, 1C), 129.16 (Ar-C, 2C), 130.15 (Ar-C, 1C), 130.92 (Ar-C, 1C), 131.70 (Ar-C, 1C), 134.93 (Ar-C, 2C), 135.30 (Ar-C, 2C), 168.07 (Ar-C, 1C), 169.06 (Ar-C, 1C); **ESI-MS m/z**: 396 $[M+H]^+$."

"**3-(4-Chlorophenyl)-5-(4-(trifluoromethyl)styryl)-1,2,4-oxadiazole (SP23)**: Yield 71%, White powder, mp 219-221 °C. **IR (KBr) (cm^{-1})**: 3081 (C=C-H str.), 2960 (Ar,

C=C-H, str.), 1633 (C=C str.), 1263 (C-O str.), 1058 (C-N str.); **^{1}H NMR (400 MHz, DMSO-*d*$_6$), δ (ppm)**: 7.09 (d, -C*H*=, 1H, *J* = 12 Hz), 7.24 (d, -C*H*=, 1H, *J* = 12 Hz), 7.31 (m, Ar-*H*, 2H), 7.45 (m, Ar-*H*, 2H), 7.79 (m, Ar-*H*, 2H), 8.05 (m, Ar-*H*, 2H); **^{13}C NMR (100 MHz, DMSO-*d*$_6$), δ (ppm)**: 114.16 (C=C, 1C), 120.64 (C=C, 1C), 122.82 (CF_3, 1C), 124.99 (Ar-C, 1C), 125.98 (Ar-C, 1C), 126.02 (Ar-C, 1C), 127.17 (Ar-C, 1C), 128.12 (Ar-C, 1C), 129.15 (Ar-C, 1C), 129.54 (Ar-C, 1C), 132.31 (Ar-C, 1C), 132.82 (Ar-C, 1C), 133.60 (Ar-C, 1C), 134.62 (Ar-C, 1C), 135.35 (Ar-C, 1C), 167.94 (Ar-C, 1C), 169.06 (Ar-C, 1C); **ESI-MS m/z**: 349 $[M-H]^+$."

"**3-(4-Fluorophenyl)-5-(4-(trifluoromethyl)styryl)-1,2,4-oxadiazole (SP24)**: Yield 89%, Yellow powder, mp 194-196 °C. . **IR (KBr) (cm^{-1})**: 3072 (C=C-H str.), 2918 (Ar, C=C-H, str.), 1617 (C=C str.), 1226 (C-O str.), 1043 (C-N str.); **^{1}H NMR (400 MHz, DMSO-*d*$_6$), δ (ppm)**: 7.09 (d, -C*H*=, 1H, *J* = 12 Hz), 7.21 (d, -C*H*=, 1H, *J* = 12 Hz), 7.35 (m, Ar-*H*, 2H), 7.67 (m, Ar-*H*, 2H), 7.78 (m, Ar-*H*, 2H), 7.84 (m, Ar-*H*, 2H); **^{13}C NMR (100 MHz, DMSO-*d*$_6$), δ (ppm)**: 114.19 (C=C, 1C), 115.77 (C=C, 1C), 115.95 (CF_3, 1C), 120.85 (Ar-C, 1C), 123.02 (Ar-C, 1C), 123.77 (Ar-C, 1C), 125.19 (Ar-C, 2C), 125.93 (Ar-C, 2C), 128.73 (Ar-C, 1C), 129.39 (Ar-C, 1C), 130.66 (Ar-C, 1C), 134.93 (Ar-C, 1C), 161.65 (Ar-C, 1C), 168.43 (Ar-C, 1C), 168.91 (Ar-C, 1C); **ESI-MS m/z**: 335 $[M+H]^+$."

"**3-(4-(Trifluoromethyl)phenyl)-5-(4-(trifluoromethyl)styryl)-1,2,4-oxadiazole (SP25)**: Yield 69%, Off White powder, mp 219-221 °C. **IR (KBr) (cm^{-1})**: 3062 (C=C-H str.), 2933 (Ar, C=C-H, str.), 1619 (C=C str.), 1223 (C-O str.), 1033 (C-N str.); **^{1}H NMR (400 MHz, DMSO-*d*$_6$), δ (ppm)**: 7.09 (d, -C*H*=, 1H, *J* = 12 Hz), 7.24 (d, -C*H*=, 1H, *J* = 12 Hz), 7.67 (m, Ar-*H*, 2H), 7.78 (m, Ar-*H*, 2H), 7.81 (m, Ar-*H*, 2H), 8.08 (m, Ar-*H*, 2H); **^{13}C NMR (100 MHz, DMSO-*d*$_6$), δ (ppm)**: 114.19 (C=C, 1C), 120.64 C=C, 1C), 122.82 (CF_3, 1C), 123.02 (CF_3, 1C), 124.99 (Ar-C, 1C), 125.89 (Ar-C, 1C), 125.98 (Ar-C, 1C), 127.37 (Ar-C, 1C), 128.80 (Ar-C, 1C), 129.15 (Ar-C, 1C), 130.15 (Ar-C, 1C), 132.05 (Ar-C, 1C), 132.56 (Ar-C, 1C), 132.82 (Ar-C, 1C), 134.93 (Ar-C, 1C), 135.30 (Ar-C, 1C), 167.94 (Ar-C, 1C), 169.06 (Ar-C, 1C); **ESI-MS m/z**: 385 $[M+H]^+$."

The mass fragmentation of the compound **SP04** has been discussed above:

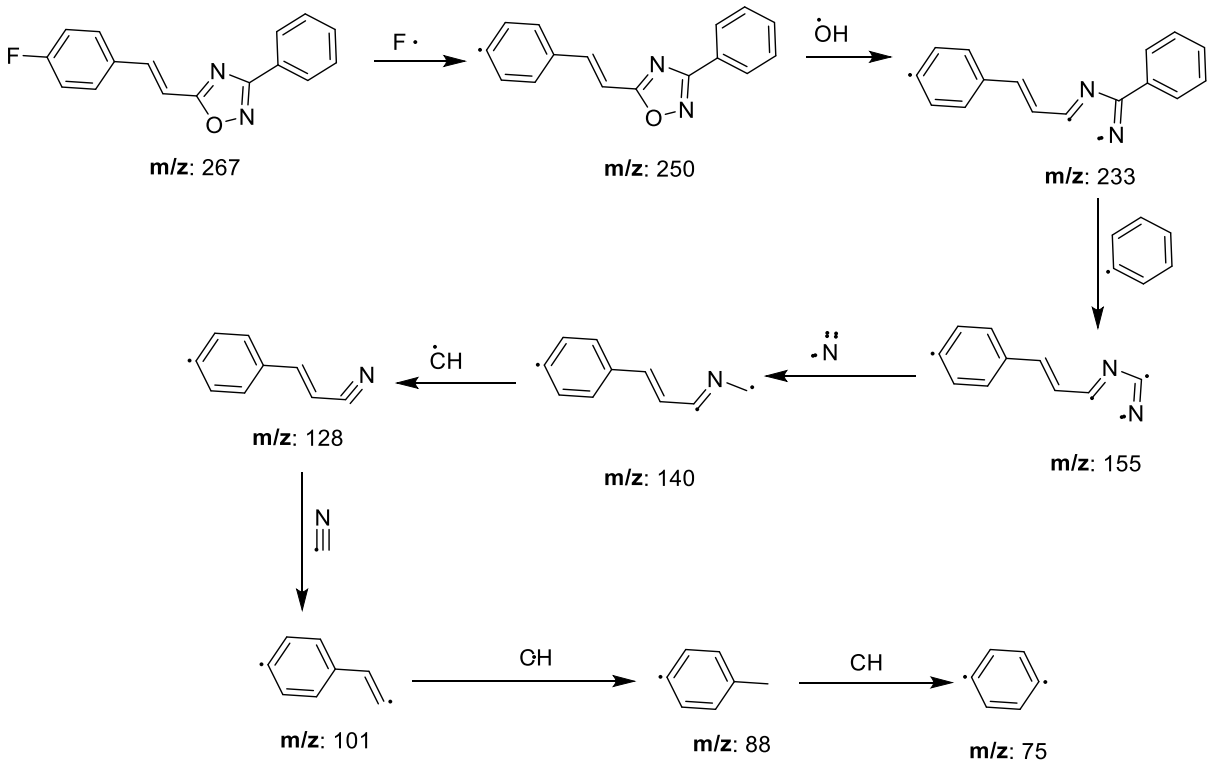

Figure 27: Mass fragmentation of SP04 (One of the representations of SP01-SP25)

6.4. Results

6.4.1. Cell Viability Assay

To assess the cytotoxic effects of synthesized substituted 3-phenyl-5-styryl-1,2,4-oxadiazole derivatives (**SP01-SP25**), the MTT assay was performed using the bicalutamide. The *in vitro* assay was performed in triplicate for cell inhibition study against PC-3 cell lines expressing AR-WILD TYPE [WT-1] cells, derived from NCBI, Pune. Cell viability was subsequently determined through the MTT assay, and the findings were graphically represented in **Figure 28**. The results of the MTT assay conducted on PC-3 cell lines expressing wild-type androgen receptors, using a series of compounds **SP01-SP25**, revealed a remarkable inhibitory effect on cell viability. The percentage inhibition ranged up to 89.99% within the series, with corresponding IC_{50} values spanning from 238.18 nM to 1645 nM against PC3 cell lines. In comparison, the reference compound bicalutamide exhibited an IC_{50} value of 158.03 nM and a percentage inhibition of 98.11%. Significantly, the utilization of various concentrations

of compounds **SP01-SP25** and bicalutamide resulted in a dose-dependent decrease in the viability of PC3 cells, as illustrated in **Table 10**.

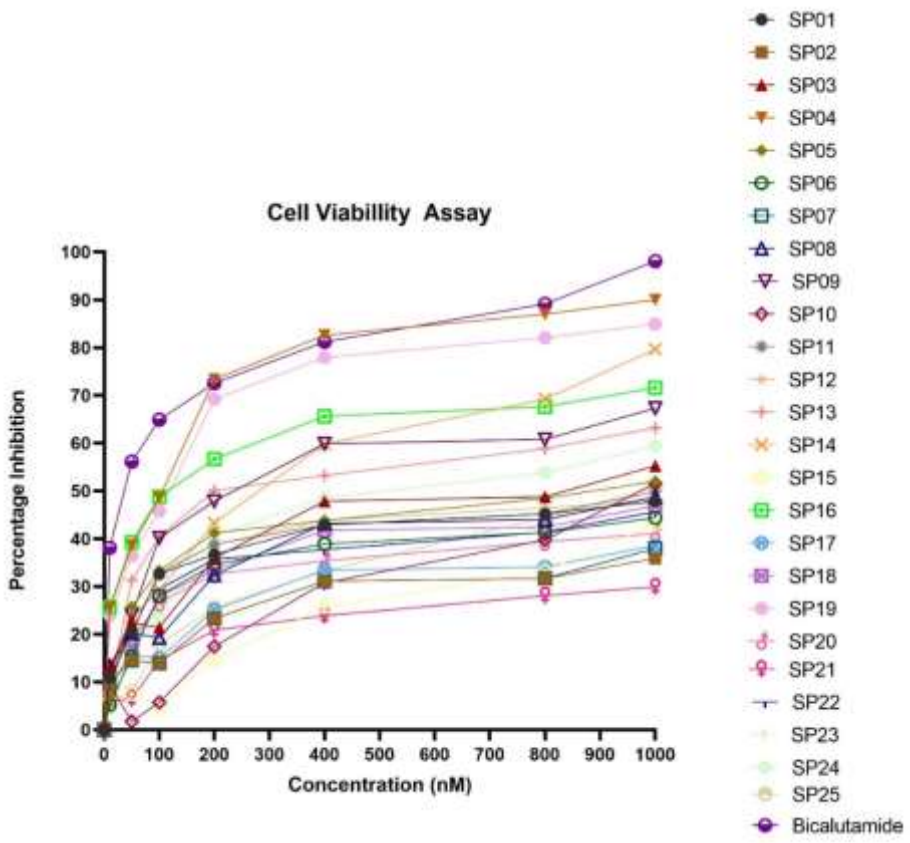

Figure 28: Graphical presentation of Percentage inhibition of PC-3 cell lines

Table 10: IC_{50} values and percentage inhibition of **SP01-SP25** and bicalutamide

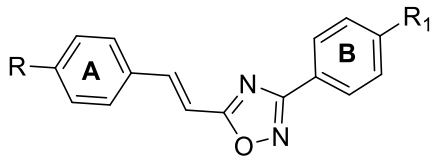

SP01-SP25

Sr. No	Compounds	Ring A	Ring B	IC_{50} (nM)	Percentage inhibition (%)
1.	**Bicalutamide**	--		158.03	98.11
2.	**SP01**	H	H	887.5	47.83
3.	**SP02**	H	Br	1375	35.89

4.	**SP03**	H	Cl	758.71	55.23
5.	**SP04**	H	F	238.13	89.99
6.	**SP05**	H	CF_3	790.18	52.01
7.	**SP06**	Br	H	991.08	44.35
8.	**SP07**	Br	Br	1395	37.97
9.	**SP08**	Br	Cl	893.42	48.73
10.	**SP09**	Br	F	526.39	67.28
11.	**SP10**	Br	CF_3	950.01	51.58
12.	**SP11**	Cl	H	854.04	49.85
13.	**SP12**	Cl	Br	883.35	48.04
14.	**SP13**	Cl	Cl	680.55	63.2
15.	**SP14**	Cl	F	556.33	79.63
16.	**SP15**	Cl	CF_3	951.14	43.11
17.	**SP16**	F	H	348.72	71.61
18.	**SP17**	F	Br	934.02	38.6
19.	**SP18**	F	Cl	884.03	46.95
20.	**SP19**	F	F	281.42	84.9
21.	**SP20**	F	CF_3	1271.1	41.09
22.	**SP21**	CF_3	H	1645	29.91
23.	**SP22**	CF_3	Br	1245.8	45.65
24.	**SP23**	CF_3	Cl	1129	49.86
25.	**SP24**	CF_3	F	784.77	59.39
26.	**SP25**	CF_3	CF_3	1017.8	50.71

6.4.2. Molecular Docking Analysis

After conducting *in vitro* analysis of synthesized compounds, molecular docking investigations were carried out using Autodock Vina 1.5.6. The androgen receptor protein (**PDBID: 1Z95**) was obtained from the Protein Data Bank, and subsequent docking analysis results presented in **Table 11**. Following these outcomes, Discovery Studio was employed to examine the 2D and 3D interactions of all synthesized compounds (**Figure 29**). Compounds **SP01-SP25** demonstrated varying binding

affinities, ranging from -6.5 to -9.5 kcal/mol within the active site of androgen receptor. In contrast, the reference compound bicalutamide exhibited a remarkably strong binding affinity of -11.1 kcal/mol. Synthesized compounds has shown hydrogen bond, π- π T Shaped, π-alkyl/alkyl, π-σ and π-sulphur types of interactions in the active site of the receptors as shown in **Table 11**.

Table 11: Binding affinities and interactions of synthesized compounds against 1Z95

Compounds	Binding Affinity (kcal/mol)	H-Bond	π - π T Shaped	π -cation	π -σ	Alkyl/ π-alkyl
Bicalutamide	-11.1	Arg752 Gln711 Asn705 His874	Phe764	--	Met742	--
SP01	-8	--	Trp718	Arg752 Lys808	Val715	Ala748 Pro682 Leu744
SP02	-6.6	--	Arg752 Trp718	Arg752 Lys808	Val715	Ala748 Pro682 Leu744
SP03	-8.2	--	Trp718	Arg752 Lys808	Val715	Ala748 Pro682 Leu744
SP04	-9.5	Arg752 Gln711 Lys808	Trp718	Arg752 Lys808	Val715	Ala748 Pro682 Leu744
SP05	-8	Lys808	Trp751	Arg752	Pro682	Ala748 Val715
SP06	-7.2	--	Trp718	Lys808	Val715	Ala748 Pro682 Leu744
SP07	-6.5	--	--	Arg752	Val684	Ala748 Pro682 Leu744 Trp718 Val715 Lys808
SP08	-8.3	Arg752	Trp718	Arg752 Lys808	Val715 Ala748	Leu744 Pro682
SP09	-8.7	Arg752	Trp718	Arg752 Lys808	Val715	Ala748 Pro682 Leu744 Val684

SP10	-8.4	Lys808	--	Arg752	--	Ala748 Pro682 Trp718 Val715 Val684
SP11	-8.2	Arg752	Trp751	Arg752	--	Ala748 Pro682 Leu744 Trp718 Val715
SP12	-8.1	--	Trp718	Arg752 Lys808	Val715	Ala748 Pro682 Leu744
SP13	-8.4	--	--	Arg752	Val684	Ala748 Pro682 Leu744 Trp718 Val715 Lys808
SP14	-8.6	Arg752	Trp718	Lys808	Val715	Ala748 Pro682 Leu744 Val684
SP15	-7.7	Lys808	--	Arg752	--	Ala748 Pro682 Leu744 Trp718 Val715 Val684
SP16	-8.9	Arg752 Gln711	Trp718	Lys808	Val715	Ala748 Pro682 Leu744
SP17	-8	Arg752	--	Arg752	Val684	Ala748 Pro682 Leu744 Trp718 Val715 Lys808 Val685
SP18	-8.2	Arg752	Trp718	Arg752 Lys808	Ala748 Val715	Pro682 Leu744
SP19	-9.1	Arg752 Gln711	Trp718	Arg752 Lys808	Val715 Ala748	Pro682 Leu744

SP20	-6.7	--	--	Arg752	--	Ala748 Pro682 Leu744 Trp718 Val715 Val684
SP21	-6.1	--	--	Arg752	Val684	Ala748 Pro682 Leu744 Val715 Trp718 Val685
SP22	-6.8	--	--	Arg752	Val684	Ala748 Pro682 Trp718
SP23	-6.8	Lys808	--	Arg752	--	Ala748 Pro682 Leu744 Trp718 Val715
SP24	-8.1	--	--	Arg752	Val684	Ala748 Pro682 Trp718 Val715 Val685
SP25	-7.1	Lys808 Asn756	--	Arg752	Val684	Ala748 Pro682 Trp718 Val685

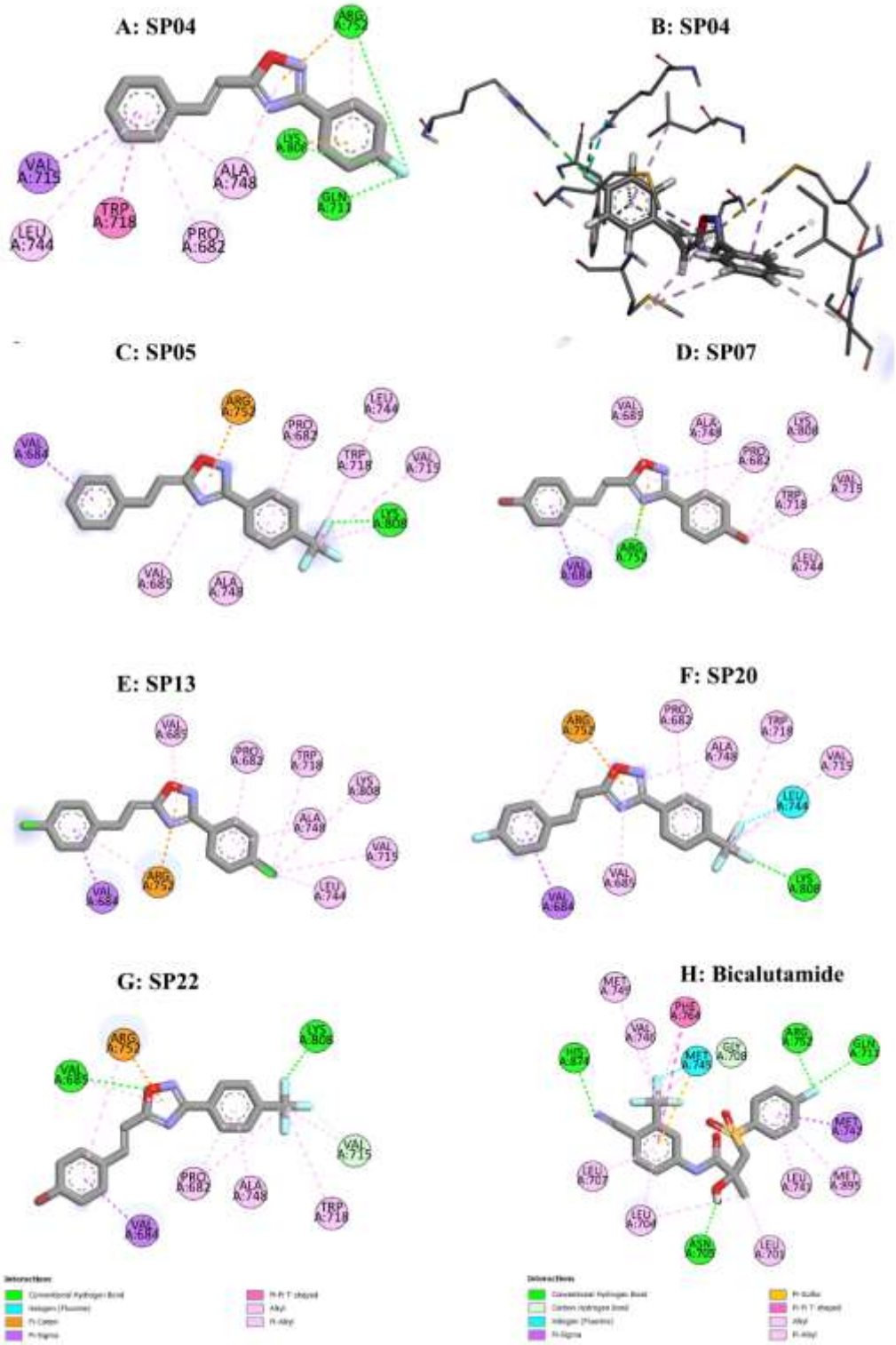

Figure 29: 2D and 3D interactions of few representatives of the series SP01-SP25

6.5. Discussion

The first series of 3,5-diphenyl-1,2,4-oxadiazoles (**MS01-MS15**) revealed that compounds with electron-withdrawing group (EWG) substitutions exhibited potent activity comparable to those with electron-donating group (EDG) substitutions. The active site of the androgen receptor's ligand binding domain (AR LBD) features a hydrophobic pocket with polar patches, facilitating strong electrostatic interactions with EWG-substituted compounds. Leveraging the framework of existing antiandrogen drugs like bicalutamide, oxadiazole analogs were developed with EWG substitutions at key positions, resulting in promising anticancer activity. Compound MS14, with a fluoro substituent, was particularly potent. In the present series, 3-phenyl-5-styryl-1,2,4-oxadiazoles (**SP01-SP25**) were synthesized with EWGs strategically placed on both rings A and B, while a vinyl bridge was introduced to enhance interactions with the receptor's active site. Here, bicalutamide was also used as a reference compound and in *in vitro* analysis it inhibited the growth of PC3 cell lines with an IC_{50} value of 158.03 nM. Initially, unsubstituted compound **SP01** was synthesized and found that it exhibited 47.83 % inhibition of PC3 cell lines using a cell proliferation assay. The binding affinity of compounds **SP01** was -8.0 kcal/mol. It was found to show π-π T shape interaction with Trp718 (by phenyl ring A) whereas ring B and - NH group of the oxadiazole ring showed π-alkyl/alkyl as well as π-cation type of interactions with the Ala748, Pro682, and Leu744 in the active site of the receptor. Conspicuously, the NH group of the oxadiazole ring of the compound **SP01** has shown π-cation type of interaction with the Arg752 and Lys808. Meanwhile, ring A of compound **SP01** was engaged in π-π T-shape interaction with Trp718 and ring B showed π-alkyl/alkyl interactions with the Ala748, Pro682, and Leu744 in the active site of the receptor. MTT assay revealed that compound **SP01** has shown a decrease in prostate cancer cell lines with an IC_{50} value of 887.5 nM.

Following the synthesis of compound **SP01**, we aimed to enhance the electronegativity on phenyl ring B by substituting hydrogen groups with halide groups (**SP02-SP05**) at the *p* position. Subsequently, their biological activities was assessed, determining IC_{50} values ranging from 238.13 to 1375 nM against a prostate cancer cell line. The binding affinities fell within the range of -6.6 to -9.5 kcal/mol, featuring

similar π-alkyl/alkyl, π-π T shape, and π-cation interactions as observed in compound **SP01**. The findings revealed that the bromine-substituted compound **SP02** (dock score of -6.6 kcal/mol) exhibited poor activity with an IC_{50} value of 1375 nM. This diminished activity could be attributed to its lower electronegativity, steric hindrance, and the absence of H-bond interactions. Remarkably, among the analogs, compound **SP04**, substituted with a fluoro group, demonstrated the highest activity with an IC_{50} value of 238.13 nM. It formed three hydrogen bonding interactions with amino acid residues Arg752, Gln711, and Lys808, boasting a binding affinity of -9.5 kcal/mol. Conversely, compounds **SP03** (substituted with a chlorine group) and **SP05** (substituted with a trifluoromethyl group) exhibited comparatively weaker activities, with IC_{50} values of 758.71 and 991.08 nM, and binding affinities of -8.2 and -8.0 kcal/mol, respectively.

Further, bromine group at the *p* position of styryl ring A was substituted to explore the effect of the EWGs by evaluating the biological activities of analogues (**SP06-SP10**) substituted with H, Br, Cl, F, and CF_3 groups at p position of ring B. *In vitro* assay results revealed that compounds **SP06-SP10** exhibited their inhibitory activities (IC_{50} values) in the range of 526.39-1395 nM with dock score of -6.5 to -8.7 kcal/mol, respectively. Compound **SP08** with chlorine at ring B has shown good activity with an IC_{50} value of 526.39 nM and binding affinity of -8.7 kcal/mol among **SP06-SP10**. The presence of chlorine at ring A and H-bond with Arg752 caused good activity of compound **SP08** while among compounds **SP06-SP10**, dibromo substituted compound **SP07** has shown weak activity with an IC_{50} value of 1395 nM and binding affinity of -6.6 kcal/mol. The presence of bromine at both rings A and B caused steric hindrance and thus, compound **SP07** has shown weak activity. Moreover, **SP07** also has weak binding affinity and no H-bond interaction which can be another reason for the less activity. Apart from that other compounds like **SP06**, **SP09,** and **SP10** has shown moderate activity.

Due to the hindrance caused by the bulky bromine group, there is a negative impact on the anti-cancer activity of the Oxadiazoles. In light of this, the focus shifted towards exploring alternative substitutions, specifically introducing a chlorine group

at the *p* position of styryl ring A. The objective was to enhance the therapeutic performance of the compounds. Subsequently, compounds **SP11-SP15** were synthesized, involving an increase in electronegativity at ring A by incorporating a chloro group. Various substitutions were introduced at the *p* position of ring B, including atoms such as H, Br, Cl, F, and CF3. The study findings disclosed that compounds **SP11-SP15** demonstrated prominent anti-prostate cancer activities, with IC_{50} values ranging from 556.33 to 951.14 nM and binding affinities falling within the range of -8.6 to -7.7 kcal/mol. Among these, three compounds *viz*: **SP11**, characterized by an unsubstituted phenyl ring B, and compounds **SP12** and **SP13**, featuring substitutions with bromine and chlorine atoms at the *p* position of the phenyl ring B. These compounds displayed moderate activity, with IC_{50} values of 854.04, 883.35, and 680.55 nM and binding affinities in the range of -8.1 to -8.4 kcal/mol, respectively. Furthermore, compound **SP14**, substituted with fluorine at the phenyl ring B, demonstrated significant improved activity, showcasing an IC_{50} value of 556.33 nM against PC3 cell lines. It also exhibited a hydrogen bonding interaction with amino acid residue Arg752, resulting in a dock score of -8.6 kcal/mol. However, among these compounds, compound **SP15** exhibited weaker activity, with an IC_{50} value of 951.14 nM and a binding affinity of -7.7 kcal/mol. The presence of the least electronegative atom CF_3 at the *p* position of phenyl ring B in compound **SP15**, coupled with the absence of H-bond interactions with key amino acid residues like Arg752, may account for this diminished activity.

Fluorine is frequently considered as a bioisostere for hydrogen due to its comparable size and shape. This implies that substituting a hydrogen atom on styryl ring A at the *p* position with fluorine in a molecule can enhance its pharmacological properties without significantly altering its overall structure. Based on this concept, five compounds (**SP16-SP20**) were synthesized and assessed against PC3 cell lines in the study. The results revealed an overall enhancement in the biological activities of compounds **SP16-SP20**, with IC_{50} values ranging from 281.42 to 1271.1 nM, and the binding affinity falling within the range of -6.7 to -9.1 kcal/mol, respectively. Specifically, compound **SP16**, featuring an unsubstituted ring B, demonstrated inhibitory activity against the PC3 cell line with an IC_{50} value of 348.72 nM. It also

exhibited two hydrogen bonding interactions with amino acid residues Arg 752 and Gln 711, accompanied by a binding affinity of -8.9 kcal/mol. In contrast, the introduction of bulky bromo (compound **SP17**) and chloro (compound **SP18**) substituents at the *p* position of phenyl ring B resulted in a loss of biological activities, with IC_{50} values of 934.02 and 884.03 nM, respectively. Notably, compound **SP19**, featuring a fluoro group substitution at *p* positions of both ring A and B, demonstrated improved biological activity (IC_{50} 281.42 nM) and binding affinity (-9.1 kcal/mol) within the active site. Compound **SP19** also displayed two hydrogen bonding interactions with amino acid residues Arg752 and Gln711, contributing to an increase in the therapeutic efficacy of the drug. The introduction of a less electronegative $-CF_3$ atom (Compound **SP20**) at the *p* positions of ring B results in the absence of hydrogen bonding interactions. This alteration also correlates with a reduction in the inhibitory activity against the PC3 cell line, as evidenced by the IC_{50} value of 1271.1 nM

The introduction of a *p*-fluoro substituent, either on the styryl ring A or the phenyl ring B, enhances the binding affinity of the compound to the active site of protein **PDB ID**:**1Z95**. This enhancement may lead to increased potency against prostate cancer cell lines, potentially achieved through improved receptor binding or modulation of intracellular signalling cascades. Following this rationale, the exploration of derivatives (**SP21-SP25**) with a less electronegative $-CF_3$ at the styryl ring A and various substitutions at the phenyl ring B can further optimize the anti-prostate cancer activity. The compounds **SP21-SP25** have demonstrated inhibitory activities within IC_{50} values ranging from 784.77 to 1645 nM against PC3 cell lines, accompanied by binding affinities ranging from -8.1 to -6.1 kcal/mol, respectively. Notably, compound **SP21**, with an unsubstituted phenyl ring B, emerged as the least potent, displaying an IC_{50} value of 1645 nM and a binding affinity of -6.1 kcal/mol. Unfortunately, with the exception of compound **SP24** (substituted with a fluoro group at the *p* position of ring B), none of the molecules exhibited promising anti-prostate cancer cell activity. Compound **SP24** demonstrated moderate anti-prostate cancer activity with an IC_{50} value of 784.77 nM. It is hypothesized that the introduction of a less electronegative $-CF_3$ group at the styryl ring A might result in either the introduction of steric hindrance or a decrease in the overall electron density of the

molecule compared to fluoro-substituted analogs.

Among all the compounds, compound **SP04** (with a fluoro group substitution) emerged as the most potent molecule. The assumption was that the highly electronegative fluoro group at the *p* position of ring B enhances electronic effects, influencing the molecule's reactivity and biological interactions. Consequently, compound **SP04** was selected for further analysis of ROS production and androgen receptor inhibition.

6.6. ROS Production Assay in PC3 Cell Lines

Reactive oxygen species (ROS) play a critical role in initiating oxidative stress within cancer cells. This escalated oxidative stress, in turn, triggers apoptotic pathways, effectively facilitating the demise of cancerous cells. The oxidative stress induced by ROS presents a promising therapeutic approach for precisely targeting and eradicating cancer cells, while preserving the integrity of healthy ones. For the assessment of intracellular ROS induction by compound **SP04** and bicalutamide in PC-3 cells, flow cytometry analysis was employed to quantify reactive oxygen species levels, utilizing the H2DCFDA (2',7'-dichlorodihydrofluorescein diacetate) dye.

Table 12: Mean Fluorescence Intensity for SP04 at different concentrations along with bicalutamide

Sr. No	Sample	MFI
1	Control	3203
2	SP04 100	21295
3	SP04 200	53921
4	Bicalutamide 200	81131

In this experiment, PC-3 cell lines were subjected to different treatments, including a control group, compound **SP04** at concentrations of 100 nM and 200 nM, and bicalutamide at a concentration of 200 nM. The results indicated a dose-dependent increase in the percentage of ROS. The mean fluorescence intensity (MFI) values were as follows: 81131 for bicalutamide at 200 nM, 53921 for compound **SP04** at 200 nM, 21295 for compound **SP04** at 100 nM, and 3203 for the control group (**Table 12**).

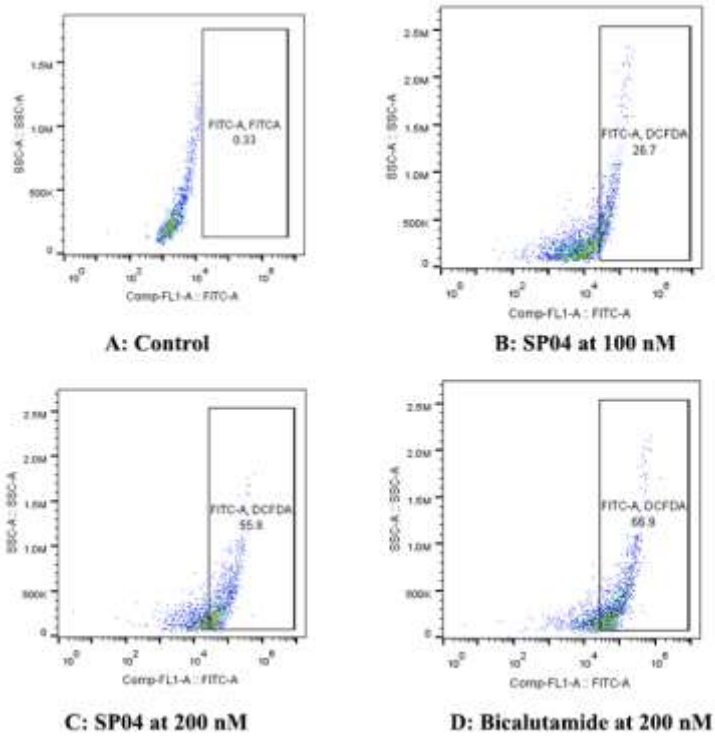

Figure 30: SP04 induced ROS production in a dose dependent manner

Compound **SP04** exhibited a significant increase in ROS percentage, with a 26.7% at 100 nM and a remarkable 55.9% increase at 200 nM compared to the control group, which had a baseline ROS level of 0%. In contrast, bicalutamide displayed a substantial increase in ROS percentage, marking a 66.9% rise compared to the control. These findings emphasize the potent impact of compound **SP04** and bicalutamide in inducing intracellular ROS production, with compound **SP04** showing a distinguished dose-dependent manner effect (**Figure 30**).

6.7. Androgen Receptor Inhibition Assay

To conduct a more comprehensive analysis of their mechanisms, compound **SP04** and bicalutamide were subjected to mechanistic study. As mentioned in the rationale these compounds were designed with the specific goal of inhibiting the androgen receptor. So, in accordance with the same, we have conducted an investigation into their capability to effectively suppress androgen receptor expression within the PC-3 cell lines.

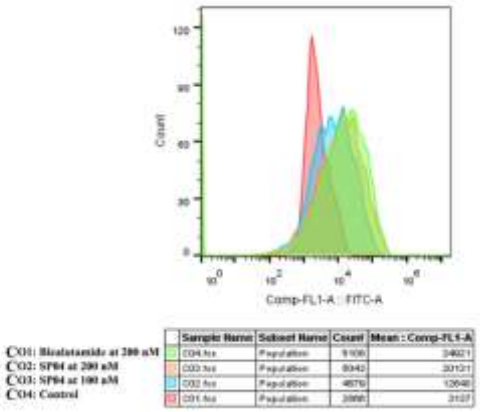

Figure 31: Inhibition of androgen receptor (AR) expression in a dose-dependent manner

In this study, both Flow Cytometry and Immunofluorescence assays was employed to assess androgen receptor protein expression. Compound **SP04** was administered at concentrations of 100 nM and 200 nM, while bicalutamide was provided at a concentration of 200 nM. The findings from the Flow Cytometry assay demonstrated a dose-dependent reduction in prostate cancer cells when treated with compound **SP04**, implying a corresponding dose-dependent inhibition of androgen receptor expression by compound **SP04**. After 24h of treatment with compound **SP04** has shown MFI of 20131 at 100 nM concentration and 12640 at 200 nM concentration suggesting a decrease of androgen receptor expression in a dose-dependent manner while the MFI was found to be 24921 and 3137 for control and bicalutamide at 200 nM, respectively (**Figure 31**). Furthermore, Immunofluorescence assay was also conducted to assess the inhibition of the androgen receptor. Similar to the previous findings, a dose-dependent inhibition was observed. Compound **SP04** was administered at concentrations of 100 nM and 200 nM, while bicalutamide was given at a concentration of 200 nM. The results indicate that treatment with compound **SP04** resulted in a dose-dependent decrease in androgen receptor expression compared to the control group (**Figure 32**). The Mean Fluorescence Intensity (MFI) was measured at 160 for compound **SP04** at 100 nM, 140 for compound **SP04** at 200 nM, and 230 for the control group. Bicalutamide exhibited an MFI of 95 at a concentration of 200 nM. Based on these findings, it was evident that compound **SP04** reduces androgen receptor expression in a dose-dependent manner.

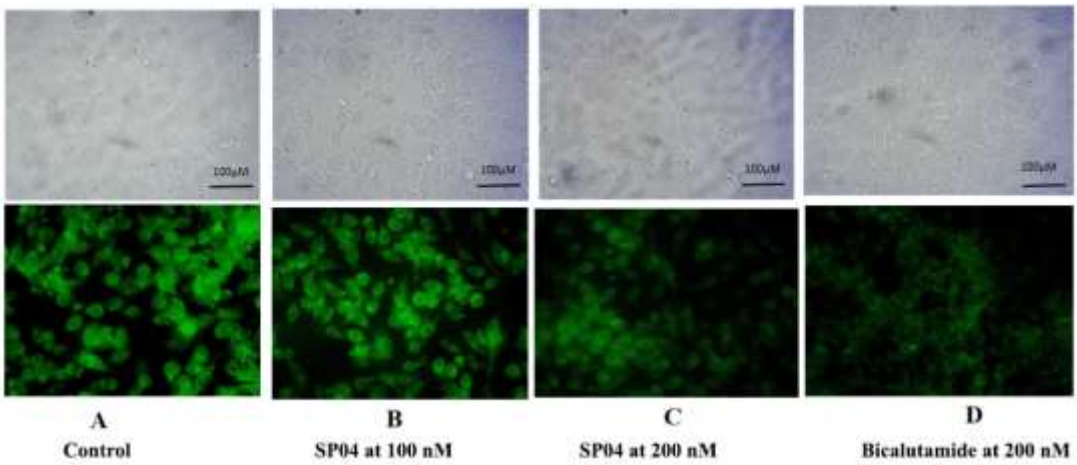

Figure 32a: Androgen receptor expression measured by immunofluorescence assay

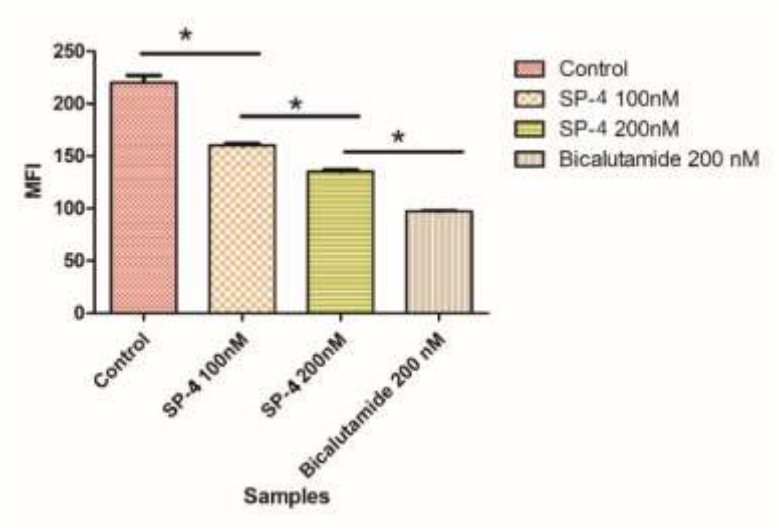

Figure 32b: Graphical representation of mean fluorescence intensity (MFI) of control, **SP04** at 100 & 200 nM and bicalutamide at 200 nM

6.8. Absorption, Distribution, Metabolism, and Excretion (ADME) Analysis of SP01-SP25 And Bicalutamide

Physicochemical properties play a pivotal role in determining the potential of a compound as a drug candidate. To evaluate the ADME (absorption, distribution, metabolism, and excretion) properties of the synthesized compounds and bicalutamide, they were subjected to analysis using SWISSADME. Various parameters such as LogP (partition coefficient), H-bond acceptors and donors, gastrointestinal (GI) absorption, blood-brain barrier (BBB) permeation, Lipinski's rule of 5, and lead likeness properties

were predicted. The results revealed that almost all compounds exhibited drug-like properties, as they adhered to Lipinski's rule of 5 without any violations except compounds **SP15**, **SP20**, **SP22**, **SP23**, **SP24** & **SP25** (as these compounds has shown one violation of Lipinski's rule of five). Notably, bicalutamide also demonstrated compliance with Lipinski's rule of 5 (**Table 13**). Lipinski's rule of 5 assesses a compound's drug-likeness based on parameters related to molecular weight, lipophilicity, and hydrogen bonding.

Furthermore, the majority of compounds exhibited high GI absorption, signifying their advantageous uptake within the gastrointestinal tract, except for compound **SP25** and bicalutamide. Moreover, several compounds demonstrated the potential to permeate the blood-brain barrier (BBB), implying their capacity to traverse this crucial physiological barrier except compounds **SP10**, **SP15**, **SP20**, **SP22**, **SP23**, **SP24**, and **SP25**. The bioavailability of all the compounds, as well as bicalutamide, was determined to be 0.55, which is considered an optimum value. Bioavailability is a critical factor in assessing the fraction of an administered dose of a drug that reaches the systemic circulation unchanged, and an optimal value is desirable for effective drug delivery.

Lead likeness violations provide insight into a compound's alignment with properties commonly found in lead compounds. In this context, the majority of the compounds, including the bicalutamide, have one violation of lead likeness properties. The exceptions were compounds **SP01**, **SP14**, **SP15**, **SP18**, **SP19**, **SP20**, **SP23**, **SP24**, and **SP25**, which exhibit two violations of lead likeness properties.

Table 13: ADME properties of the synthesized compounds SP01-SP25 and bicalutamide

Compound code	MW	#H-bond acceptors	#H-bond donors	Log P	GI absorption	BBB permeant	Bioavailability Score	Lipinski #violations	Leadlikeness #violations
Bicalutamide	430.37	9	2	3.06	Low	No	0.55	0	1
SP01	248.28	3	0	3.6	High	Yes	0.55	0	2

SP02	327.18	3	0	4.18	High	Yes	0.55	0	1
SP03	282.72	3	0	4.09	High	Yes	0.55	0	1
SP04	266.27	4	0	3.87	High	Yes	0.55	0	1
SP05	316.28	6	0	4.59	High	Yes	0.55	0	1
SP06	327.18	3	0	4.27	High	Yes	0.55	0	1
SP07	406.07	3	0	4.81	High	Yes	0.55	0	2
SP08	361.62	3	0	4.72	High	Yes	0.55	0	2
SP09	345.17	4	0	4.5	High	Yes	0.55	0	1
SP10	395.17	6	0	5.3	High	No	0.55	1	2
SP11	282.72	3	0	4.18	High	Yes	0.55	0	1
SP12	361.62	3	0	4.72	High	Yes	0.55	0	2
SP13	317.17	3	0	4.64	High	Yes	0.55	0	1
SP14	300.71	4	0	4.41	High	Yes	0.55	0	1
SP15	350.72	6	0	5.21	High	No	0.55	1	2
SP16	266.27	4	0	3.95	High	Yes	0.55	0	1
SP17	345.17	4	0	4.49	High	Yes	0.55	0	1
SP18	300.71	4	0	4.41	High	Yes	0.55	0	1
SP19	284.26	5	0	4.18	High	Yes	0.55	0	1
SP20	334.27	7	0	4.98	High	No	0.55	1	1
SP21	316.28	6	0	4.67	High	Yes	0.55	0	1
SP22	395.17	6	0	5.23	High	No	0.55	1	2
SP23	350.72	6	0	5.14	High	No	0.55	1	2
SP24	334.27	7	0	4.91	High	No	0.55	0	1
SP25	384.28	9	0	5.68	Low	No	0.55	1	2

6.9. Toxicity Analysis of SP01-SP25 and bicalutamide

Furthermore, pkCSM online tool was utilized to predict the toxicity of compounds **SP01-SP25** and bicalutamide. The data obtained predictions for various parameters using the pkCSM tool, including calculated the Maximum Tolerated Dose (MTD) for humans using pkCSM. hERG, or the human ether-a-go-go-related gene, plays a significant role in cardiac depolarization and repolarization. Inhibition of hERG can lead to certain cardiac diseases. Therefore, the inhibitory effects on hERG I and II, acute toxicity in rats, including the median lethal dose (LD_{50}) were predicted. Additionally, predictions were made for parameters such as hepatotoxicity and skin sensitization. Furthermore, pkCSM was also used to predict toxic doses for the inhibition of growth in *Tetrahymena pyriformis* (*T. pyriformis*) and estimated minnow toxicity to assess aquatic toxicity.

These parameters have been predicted and are listed in **Table 14**. The results of the pkCSM-mediated toxicity analysis revealed that compounds **SP01-SP5**, **SP17**, **SP18**, **SP21**, **SP24**, and **bicalutamide** have exhibited positive results for AMES toxicity. Therefore, the study suggests that these compounds may possess mutagenic and carcinogenic properties. Notably, the potent compound **SP06** did not show AMES toxicity, indicating its potential safety in this regard. The Maximum Tolerated Dose (MTD) for humans was found to range from 0.071 to 0.674 log mg/kg/day. Higher log MTD values, as observed in compound **SP19** and **SP14**, imply a greater tolerance, while lower values raise concerns about potential safety issues at lower doses. All the compounds demonstrated negative results for inhibitory effects on hERG I, suggesting no risk of cardiotoxicity. However, compounds **SP07-SP11**, **SP13-SP16**, and **SP19-SP20** showed positive results for the less common isoform, hERG II, indicating a need for vigilance in assessing their cardiac safety. The Oral Rat Acute Toxicity (ORAT) values showed variations, with lower values, such as those of compounds **SP06**, indicating higher toxicity in rats, while higher values, exemplified by compound **SP24** and **SP25**, suggest lower toxicity levels in this species.

Several compounds, including bicalutamide, exhibited indications of hepatotoxicity. However, the potent compound **SP6** was found to be non-hepatotoxic, highlighting its potential as a safer option. All synthesized compounds displayed negative results for

skin sensitization, suggesting a low likelihood of causing skin allergies. The values obtained for *T. pyrifor*mis toxicity ranged from 0.514 to 1.162 µg/mL, indicating potential toxicity to *T. pyriformis* and potential environmental implications. Most compounds had minnow toxicity values close to zero, indicating a low risk to aquatic life. However, **bicalutamide**, **SP01**, and **SP10** stood out with the potential for a higher risk to aquatic organisms.

In summary, the analysis revealed that compound **SP06**, the most potent compound, demonstrated compliance with ADME properties and tolerable toxicities. This suggests that further clinical exploration of **SP06** may yield a superior compound for prostate cancer treatment.

Table 14: Toxicity analysis of the SP01-SP25 and bicalutamide.

Compound Code	MTD (human) log mg/kg/day	hERG I inhibitor	hERG II inhibitor	ORAT (LD50) mol/kg	Hepatotoxicity	Skin Sensitisation	*T. Pyriformis* toxicity log µg/mL	minnow toxicity (log mM)
Bicalutamide	0.233	No	No	2.484	Yes	No	0.484	0.824
SP01	0.636	No	No	2.039	No	No	0.662	0.85
SP02	0.662	No	Yes	2.195	Yes	No	0.582	0.315
SP03	0.659	No	Yes	2.181	No	No	0.584	0.461
SP04	0.368	No	No	2.038	No	No	0.7	0.176
SP05	0.358	No	No	2.28	Yes	No	0.691	0.044
SP06	0.436	No	No	2.191	No	No	0.733	-1.138
SP07	0.674	No	Yes	2.35	Yes	No	0.562	-0.145
SP08	0.671	No	Yes	2.336	Yes	No	0.564	0.001
SP09	0.639	No	Yes	2.29	No	No	0.559	0.334
SP10	0.409	No	No	2.557	Yes	No	0.652	-1.251
SP11	0.433	No	No	2.176	No	No	0.734	-0.992

SP12	0.443	No	No	2.342	No	No	0.716	-1.452
SP13	0.668	No	Yes	2.321	No	No	0.566	0.147
SP14	0.636	No	Yes	2.275	Yes	No	0.56	0.48
SP15	0.111	No	No	2.231	No	No	1.162	-0.995
SP16	0.398	No	No	2.122	No	No	0.713	-659
SP17	0.407	No	No	2.292	No	No	0.701	-1.119
SP18	0.404	No	No	2.277	Yes	No	0.702	-0.973
SP19	0.433	No	Yes	2.298	No	No	0.559	-0.274
SP20	0.071	No	No	2.186	Yes	No	1.092	-0.661
SP21	0.395	No	No	2.404	Yes	No	0.693	-0.791
SP22	0.646	No	Yes	2.536	Yes	No	0.515	0.202
SP23	0.643	No	Yes	2.522	Yes	No	0.517	0.348
SP24	0.61	No	Yes	2.481	Yes	No	0.514	0.681
SP25	0.238	No	No	2.623	Yes	No	0.645	-0.515

CHAPTER 7

7. Conclusion

Prostate cancer, one of the most prevalent cancers in men, arises due to complex molecular alterations that disrupt normal cellular processes within the prostate gland. The development of this cancer involves multiple genetic and molecular changes, often initiated by mutations in specific genes such as the tumor suppressor genes (e.g., CHEK2) or oncogenes (e.g., RAD51D). These mutations can lead to uncontrolled growth and division of prostate cells, forming tumors. Androgen receptor signaling plays a pivotal role in prostate cancer progression, as the prostate cells depend on androgen hormones like testosterone for growth and survival. Dysregulation of androgen receptor signalling, through mechanisms like amplification of the androgen receptor gene or alterations in co-regulatory proteins, contributes to cancer progression and treatment resistance.

Despite the availability of various androgen receptor antagonists, the cure of prostate cancer is not affective. Steroidal antagonists, like abiraterone acetate, have been valuable in treating prostate cancer by inhibiting androgen production. However, they come with their limitations. One significant drawback is the potential for side effects. While these medications effectively reduce testosterone levels, they can also impact other hormonal pathways, leading to adverse effects such as hypertension, fluid retention, and electrolyte imbalances. Additionally, some patients might not respond optimally to steroidal antagonists due to the development of resistance over time. Cancer cells can adapt and find alternative pathways to produce androgens, rendering these medications less effective. Furthermore, steroidal antagonists often require combination therapies or sequential treatments to enhance their efficacy, adding complexity to the treatment regimen and potentially increasing the risk of side effects or drug interactions. Thus, while steroidal antagonists offer substantial benefits in managing prostate cancer, their limitations underscore the ongoing need for further research and the development of alternative strategies to improve patient outcomes.

Designing non-steroidal antagonists, specifically oxadiazole analogues, for treating prostate cancer stems from the necessity to target the androgen receptor (AR) pathway effectively. Oxadiazole analogs offer promising advantages over existing therapies for prostate cancer by addressing unmet clinical needs. Their strategic design targets specific molecular pathways, potentially overcoming drug resistance. Combining oxadiazoles with existing therapies or personalized treatment strategies could enhance efficacy while minimizing adverse effects, heralding a new era in prostate cancer management. Prostate cancer progression is often fueled by the activation of AR signalling, even in the absence of testosterone. Traditional treatments, like androgen deprivation therapy (ADT), lose efficacy as cancer cells develop resistance, necessitating the development of novel therapeutics. Oxadiazole analogues offer a promising alternative due to their unique structural features, which allow for precise interactions with the AR ligand-binding domain. Here, we have used a pharmacophore-based approach and designed the compounds **MS1-MS15** series, comprised of 15 molecules with diverse electron-donating (EDGs) and electron-withdrawing groups (EWGs) on 3,5-diphenyl substituted Oxadiazoles. After successful synthesis and characterization, we conducted MTT assays on PC-3 cells. Compounds **MS1-MS15** has shown lower potency as compared to bicalutamide and compound **MS14** was the most potent compound of the series with an IC_{50} of 370.37 nM and percentage inhibition of 97.32% of cancer cells. Compound **MS14** was further investigated for its ROS-inducing ability, demonstrating dose-dependent manner increase in ROS production (19.8% at 150 nM, 49% at 300 nM). The androgen receptor inhibition assay revealed that compound **MS14** dose-dependently reduced receptor expression. Our docking study showed hydrophobic interactions within the androgen receptor's active site. ADMET analyses identified compounds with favorable physicochemical properties and manageable toxicity profiles, including compound **MS14**. These findings highlight compound **MS14**'s significant anti-prostate cancer potential, inhibiting the androgen receptor and inducing ROS production. Further, we developed a second series based on insights from our literature survey and our study's findings. We observed that compounds with electron-withdrawing groups (EWGs) were more effective, aligning with previous studies. This led us to design of the compounds **SP1-SP25** series, featuring EWGs in both rings and a vinyl group for enhanced hydrophobic

interactions. We successfully synthesized and characterized these 25 molecules, and they demonstrated dose-dependent reductions in cell viability in MTT assays. Notably, **SP04** exhibited remarkable potency, as compared to other molecules and even compound **MS14**. Compound **SP04** stood out with an impressive IC_{50} value of 238.13 nM and an 89.99% inhibition of PC-3 cells, showing its potential. Further investigations into compound **SP04**'s mechanisms revealed a dose-dependent manner increase in ROS production, indicating its potential for promoting cell death. Compound **SP04** also displayed a dose-dependent reduction in androgen receptor expression, disrupting the androgen receptor pathway, similar to bicalutamide. Docking study highlighted hydrophobic interactions of compound **SP04** within the androgen receptor's active site. ADMET analysis has verified favourable characteristics and controllable toxicity profiles for compound **SP04** and the accompanying compounds.

In the future, the development of substituted non-steroidal antagonists containing an oxadiazole nucleus will hold great promise for advancing prostate cancer treatment. We will actively explore modifications to the oxadiazole structure to enhance efficacy while reducing toxicity. Our efforts will focus on finely tuning the molecular design to improve specificity towards the androgen receptor (AR) and minimize off-target effects, thus reducing overall toxicity. Furthermore, advancements in understanding the molecular pathways involved in prostate cancer will offer opportunities to design agents targeting specific mutations or resistance mechanisms, ensuring enhanced effectiveness. Additionally, conducting *in vivo* studies with **SP04** will validate these findings. Moreover, further expanding these molecule designs to incorporate a three-ring system followed by amide coupling, potentially enhancing therapeutic efficacy. This research could potentially unveil pure androgen receptor antagonists, significantly impacting prostate cancer treatment and improving patient outcomes.

CHAPTER 8

8. References

(1) Miller, J. D.; Foley, K. A.; Russell, M. W. Current challenges in health economic modeling of cancer therapies: a research inquiry. *American Health and Drug Benefits* **2014**, *7* (3), 153-162.

(2) Park, H. J.; Kim, K. W.; Won, S. E.; Yoon, S.; Chae, Y. K.; Tirumani, S. H.; Ramaiya, N. H. Definition, incidence, and challenges for assessment of hyperprogressive disease during cancer treatment with immune checkpoint inhibitors: a systematic review and meta-analysis. *JAMA Network Open* **2021**, *4* (3), e211136-e211136.

(3) Gandaglia, G.; Leni, R.; Bray, F.; Fleshner, N.; Freedland, S. J.; Kibel, A.; Stattin, P.; Van Poppel, H.; La Vecchia, C. Epidemiology and prevention of prostate cancer. *European Urology Oncology* **2021**, *4* (6), 877-892.

(4) Quon, H.; Loblaw, A.; Nam, R. Dramatic increase in prostate cancer cases by 2021. *BJU International* **2011**, *108* (11), 1734-1738.

(5) Chen, J.; Zhang, D.; Yan, W.; Yang, D.; Shen, B. Translational bioinformatics for diagnostic and prognostic prediction of prostate cancer in the next-generation sequencing era. *BioMed Research International* **2013**, *2013*, 1-13.

(6) Termini, D.; Den Hartogh, D. J.; Jaglanian, A.; Tsiani, E. Curcumin against prostate cancer: current evidence. *Biomolecules* **2020**, *10* (11), 1536-1575.

(7) Gurunathan, S.; Qasim, M.; Kang, M. H.; Kim, J. H. Role and therapeutic potential of melatonin in various type of cancers. *OncoTargets and Therapy* **2021**, *14*, 2019-2052.

(8) Banerjee, R.; Bandopadhyay, D.; Abilash, V. Epidemiology, pathology, types and diagnosis of soft tissue sarcoma: A research review. *Asian Journal of Pharmaceutical and Clinical Research* **2013**, *6* (suppl 3), 18-25.

(9) Bray, F.; Ferlay, J.; Soerjomataram, I.; Siegel, R. L.; Torre, L. A.; Jemal, A. Global cancer statistics 2018: GLOBOCAN estimates of incidence and mortality worldwide for 36 cancers in 185 countries. *CA: A Cancer Journal for Clinicians* **2018**, *68* (6), 394-424.

(10) Reddy, S.; Shapiro, M.; Morton, R.; Brawley, O. W. Prostate cancer in black and white Americans. *Cancer and Metastasis Reviews* **2003**, *22*, 83-86.

(11) Stenman, U. H.; Leinonen, J.; Zhang, W. M.; Finne, P. Prostate-specific antigen. In *Seminars in Cancer Biology: Academic Press* **1999**, *9* (2), 83-93.

(12) Post, P.; Stockton, D.; Davies, T.; Coebergh, J. W. Striking increase in incidence of prostate cancer in men aged< 60 years without improvement in prognosis. *British Journal of Cancer* **1999**, *79* (1), 13-17.

(13) Wilson, A. The prostate gland: a review of its anatomy, pathology, and treatment. *JAMA:Open Network* **2014**, *312* (5), 562-562.

(14) Hammerich, K. H.; Ayala, G. E.; Wheeler, T. M. Anatomy of the prostate gland and surgical pathology of prostate cancer. *Cambridge University, Cambridge Press: Chapter 1,* **2009**, 1-10.

(15) Walz, J.; Epstein, J. I.; Ganzer, R.; Graefen, M.; Guazzoni, G.; Kaouk, J.; Menon, M.; Mottrie, A.; Myers, R. P.; Patel, V. A critical analysis of the current knowledge of surgical anatomy of the prostate related to optimisation of cancer control and preservation of continence and erection in candidates for radical prostatectomy: an update. *European Urology* **2016**, *70* (2), 301-311.

(16) Chan, J. M.; Stampfer, M. J.; Giovannucci, E. L. What causes prostate cancer? A brief summary of the epidemiology. In *Seminars in cancer biology*: *Academic Press* **1998** *8* (2), 263-273.

(17) Visakorpi, T. The molecular genetics of prostate cancer. *Urology* **2003**, *62* (5), 3-10.

(18) Pritchard, C. C.; Mateo, J.; Walsh, M. F.; De Sarkar, N.; Abida, W.; Beltran, H.; Garofalo, A.; Gulati, R.; Carreira, S.; Eeles, R. Inherited DNA-repair gene mutations in men with metastatic prostate cancer. *New England Journal of Medicine* **2016**, *375* (5), 443-453.

(19) Cybulski, C.; Wokołorczyk, D.; Kluźniak, W.; Jakubowska, A.; Górski, B.; Gronwald, J.; Huzarski, T.; Kashyap, A.; Byrski, T.; Dębniak, T. An inherited NBN mutation is associated with poor prognosis prostate cancer. *British Journal of Cancer* **2013**, *108* (2), 461-468.

(20) Rökman, A.; Ikonen, T.; Seppälä, E. H.; Nupponen, N.; Autio, V.; Mononen, N.; Bailey Wilson, J.; Trent, J.; Carpten, J.; Matikainen, M. P. Germline alterations of the RNASEL gene, a candidate HPC1 gene at 1q25, in patients and families with prostate cancer. *The American Journal of Human Genetics* **2002**, *70* (5), 1299-1304.

(21) Choudhury, A. D.; Eeles, R.; Freedland, S. J.; Isaacs, W. B.; Pomerantz, M. M.; Schalken, J. A.; Tammela, T. L.; Visakorpi, T. The role of genetic markers in the management of prostate cancer. *European Urology* **2012**, *62* (4), 577-587.

(22) Buttigliero, C.; Tucci, M.; Bertaglia, V.; Vignani, F.; Bironzo, P.; Di Maio, M.; Scagliotti, G. V. Understanding and overcoming the mechanisms of primary and acquired resistance to abiraterone and enzalutamide in castration resistant prostate cancer. *Cancer Treatment Reviews* **2015**, *41* (10), 884-892.

(23) Hessels, D.; Schalken, J. A. The use of PCA3 in the diagnosis of prostate cancer. *Nature Reviews Urology* **2009**, *6* (5), 255-261.

(24) Barry, M. J. Prostate-specific–antigen testing for early diagnosis of prostate cancer. *New England Journal of Medicine* **2001**, *344* (18), 1373-1377.

(25) Caplan, A.; Kratz, A. Prostate-specific antigen and the early diagnosis of prostate cancer. *Pathology Patterns Reviews* **2002**, *117* (suppl_1), S104-S108.

(26) Naji, L.; Randhawa, H.; Sohani, Z.; Dennis, B.; Lautenbach, D.; Kavanagh, O.; Bawor, M.; Banfield, L.; Profetto, J. Digital rectal examination for prostate cancer screening in primary care: a systematic review and meta-analysis. *The Annals of Family Medicine* **2018**, *16* (2), 149-154.

(27) Chodak, G. W.; Keller, P.; Schoenberg, H. W. Assessment of screening for prostate cancer using the digital rectal examination. *The Journal of Urology* **1989**, *141* (5), 1136-1138.

(28) Shukla Dave, A.; Hricak, H. Role of MRI in prostate cancer detection. *NMR in Biomedicine* **2014**, *27* (1), 16-24.

(29) Chen, V. H.; Mouraviev, V.; Mayes, J. M.; Sun, L.; Madden, J. F.; Moul, J. W.; Polascik, T. J. Utility of a 3-dimensional transrectal ultrasound-guided prostate biopsy system for prostate cancer detection. *Technology in Cancer Research and Treatment* **2009**, *8* (2), 99-103.

(30) Shariat, S. F.; Roehrborn, C. G. Using biopsy to detect prostate cancer. *Reviews in Urology* **2008**, *10* (4), 262.

(31) Egevad, L.; Granfors, T.; Karlberg, L.; Bergh, A.; Stattin, P. Prognostic value of the Gleason score in prostate cancer. *BJU International* **2002**, *89* (6), 538-542.

(32) Wirth, M. P.; Hakenberg, O. W.; Froehner, M. Antiandrogens in the treatment of prostate cancer. *European Urology* **2007**, *51* (2), 306-314.

(33) Daniyal, M.; Siddiqui, Z. A.; Akram, M.; Asif, H.; Sultana, S.; Khan, A. Epidemiology, etiology, diagnosis and treatment of prostate cancer. *Asian Pacific Journal of Cancer Prevention* **2014**, *15* (22), 9575-9578.

(34) Choo, R.; Klotz, L.; Danjoux, C.; Morton, G. C.; DeBoer, G.; Szumacher, E.; Fleshner, N.; Bunting, P.; Hruby, G. Feasibility study: watchful waiting for localized low to intermediate grade prostate carcinoma with selective delayed intervention based on prostate specific antigen, histological and/or clinical progression. *The Journal of Urology* **2002**, *167* (4), 1664-1669.

(35) Van den Bergh, R. C.; Roemeling, S.; Roobol, M. J.; Aus, G.; Hugosson, J.; Rannikko, A. S.; Tammela, T. L.; Bangma, C. H.; Schröder, F. H. Outcomes of men with screen-detected prostate cancer eligible for active surveillance who were managed expectantly. *European Urology* **2009**, *55* (1), 1-8.

(36) Mouraviev, V.; Polascik, T. J. Update on cryotherapy for prostate cancer in 2006. *Current Opinion in Urology* **2006**, *16* (3), 152-156.

(37) Shah, S.; Young, H. N.; Cobran, E. K. Comparative effectiveness of conservative management compared to cryotherapy in localized prostate cancer patients. *American Journal of Men's Health* **2018**, *12* (5), 1681-1691.

(38) Luzzago, S.; Suardi, N.; Dell'Oglio, P.; Cardone, G.; Gandaglia, G.; Esposito, A.; De Cobelli, F.; Cristel, G.; Kinzikeeva, E.; Freschi, M. Mp77-20 multiparametric mri represents an added value but not a substitute of follow-up biopsies in patients on active surveillance for low-risk prostate cancer. *The Journal of Urology* **2017**, *197* (4S), e1029-e1029.

(39) Potosky, A. L.; Legler, J.; Albertsen, P. C.; Stanford, J. L.; Gilliland, F. D.; Hamilton, A. S.; Eley, J. W.; Stephenson, R. A.; Harlan, L. C. Health outcomes after prostatectomy or radiotherapy for prostate cancer: results from the Prostate Cancer Outcomes Study. *Journal of the National Cancer Institute* **2000**, *92* (19), 1582-1592.

(40) Keyes, M.; Crook, J.; Morton, G.; Vigneault, E.; Usmani, N.; Morris, W. J. Treatment options for localized prostate cancer. *Canadian Family Physician* **2013**, *59* (12), 1269-1274.

(41) Haikerwal, S. J.; Hagekyriakou, J.; MacManus, M.; Martin, O. A.; Haynes, N. M. Building immunity to cancer with radiation therapy. *Cancer Letters* **2015**, *368* (2), 198-208.

(42) Costello, A. J. Considering the role of radical prostatectomy in 21st century prostate cancer care. *Nature Reviews Urology* **2020**, *17* (3), 177-188.

(43) Sharifi, N.; Gulley, J. L.; Dahut, W. L. Androgen deprivation therapy for prostate cancer. *JAMA: Open Network* **2005**, *294* (2), 238-244.

(44) Mellman, I.; Coukos, G.; Dranoff, G. Cancer immunotherapy comes of age. *Nature* **2011**, *480* (7378), 480-489.

(45) Gilligan, T.; Kantoff, P. W. Chemotherapy for prostate cancer. *Urology* **2002**, *60* (3), 94-100.

(46) Cevik, O.; Acidereli, H.; Turut, F. A.; Yildirim, S.; Acilan, C. Cabazitaxel exhibits more favorable molecular changes compared to other taxanes in androgen-independent prostate cancer cells. *Journal of Biochemical and Molecular Toxicology* **2020**, *34* (9), e22542.

(47) Capper, C. P.; Rae, J. M.; Auchus, R. J. The metabolism, analysis, and targeting of steroid hormones in breast and prostate cancer. *Hormones and Cancer* **2016**, *7*, 149-164.

(48) Xiang, W.; Wang, S. Therapeutic strategies to target the androgen receptor. *Journal of Medicinal Chemistry* **2022**, *65* (13), 8772-8797.

(49) Fujita, K.; Nonomura, N. Role of androgen receptor in prostate cancer: a review. *The World Journal of Men's Health* **2019**, *37* (3), 288-295.

(50) Sharifi, N. Steroid receptors aplenty in prostate cancer. *New England Journal of Medicine* **2014**, *370* (10), 970-971.

(51) Tan, M.; Li, J.; Xu, H. E.; Melcher, K.; Yong, E. l. Androgen receptor: structure, role in prostate cancer and drug discovery. *Acta Pharmacologica Sinica* **2015**, *36* (1), 3-23.

(52) Kaur P.; Khatik, G. K. *A*dvancements in non-steroidal antiandrogens as potential therapeutic agents for the treatment of prostate cancer. *Mini-Reviews in Medicinal Chemistry* **2016**, 16 (7), 531-546.

(53) Sharma, V.; Das, R.; Sharma, D.; Mujwar, S.; Mehta, D. K. Green chemistry approach towards Piperazine: anticancer agents. *Journal of Molecular Structure* **2023**, *1292*, 136089.

(54) Xu, F.; Chen, H.; Xu, J.; Liang, X.; He, X.; Shao, B.; Sun, X.; Li, B.; Deng, X.; Yuan, M. Synthesis, structure–activity relationship and biological evaluation of novel

arylpiperzines as α1A/1D-AR subselective antagonists for BPH. *Bioorganic and Medicinal Chemistry* **2015**, *23* (24), 7735-7742.

(55) Chen, H.; Xu, F.; Xu, B. B.; Xu, J. Y.; Shao, B. H.; Huang, B. Y.; Yuan, M. Design, synthesis and biological evaluation of novel arylpiperazine derivatives on human prostate cancer cell lines. *Chinese Chemical Letters* **2016**, *27* (2), 277-282.

(56) Chen, H.; Xu, B. B.; Sun, T.; Zhou, Z.; Ya, H. Y.; Yuan, M. Synthesis and antitumor activity of novel arylpiperazine derivatives containing the saccharin moiety. *Molecules* **2017**, *22* (11), 1857.

(57) Chen, H.; Yu, Y. Z.; Tian, X. M.; Wang, C. L.; Qian, Y. N.; Deng, Z. A.; Zhang, J. X.; Lv, D.-J.; Zhang, H. B.; Shen, J. L. Synthesis and biological evaluation of arylpiperazine derivatives as potential anti-prostate cancer agents. *Bioorganic and Medicinal Chemistry* **2019**, *27* (1), 133-143.

(58) Chen, H.; Wang, C. L.; Sun, T.; Zhou, Z.; Niu, J. X.; Tian, X. M.; Yuan, M. Synthesis, biological evaluation and SAR of naftopidil-based arylpiperazine derivatives. *Bioorganic and Medicinal Chemistry Letters* **2018**, *28* (9), 1534-1539.

(59) Chen, H.; Zhang, J.; Hu, P.; Qian, Y.; Li, J.; Shen, J. Synthesis, biological evaluation and molecular docking of 4-Amino-2H-benzo [h] chromen-2-one (ABO) analogs containing the piperazine moiety. *Bioorganic & Medicinal Chemistry* **2019**, *27* (20), 115081.

(60) Chen, H.; Qian, Y.; Jia, H.; Yu, Y.; Zhang, H.; Shen, J.; Zhao, S. Synthesis and pharmacological evaluation of naftopidil-based arylpiperazine derivatives containing the bromophenol moiety. *Pharmacological Reports* **2020**, *72*, 1058-1068.

(61) Schellhammer, P. F. An evaluation of bicalutamide in the treatment of prostate cancer. *Expert Opinion on Pharmacotherapy* **2002**, *3* (9), 1313-1328.

(62) Kandil, S.; Lee, K. Y.; Davies, L.; Rizzo, S. A.; Dart, D. A.; Westwell, A. D. Discovery of deshydroxy bicalutamide derivatives as androgen receptor antagonists. *European Journal of Medicinal Chemistry* **2019**, *167*, 49-60.

(63) Kandil, S. B.; McGuigan, C.; Westwell, A. D. Synthesis and biological evaluation of bicalutamide analogues for the potential treatment of prostate cancer. *Molecules* **2020**, *26* (1), 56-69.

(64) Pertusati, F.; Ferla, S.; Bassetto, M.; Brancale, A.; Khandil, S.; Westwell, A. D.; McGuigan, C. A new series of bicalutamide, enzalutamide and enobosarm derivatives

carrying pentafluorosulfanyl (SF_5) and pentafluoroethyl (C_2F_5) substituents: Improved antiproliferative agents against prostate cancer. *European Journal of Medicinal Chemistry* **2019**, *180*, 1-14.

(65) Ferla, S.; Bassetto, M.; Pertusati, F.; Kandil, S.; Westwell, A. D.; Brancale, A.; McGuigan, C. Rational design and synthesis of novel anti-prostate cancer agents bearing a 3, 5-bis-trifluoromethylphenyl moiety. *Bioorganic and Medicinal Chemistry Letters* **2016**, *26* (15), 3636-3640.

(66) Ghasemi, S.; Lorigooini, Z. A review of significant molecular mechanisms of flavonoids in prevention of prostate cancer. *Journal of Chemistry Pharmaceutical Sciencec* **2016**, *9* (4), 3388-3394.

(67) Li, X.; Lee, M.; Chen, G.; Zhang, Q.; Zheng, S.; Wang, G.; Chen, Q. H. 3-O-Substituted-3′, 4′, 5′-trimethoxyflavonols: Synthesis and cell-based evaluation as anti-prostate cancer agents. *Bioorganic and Medicinal Chemistry* **2017**, *25* (17), 4768-4777.

(68) Rajaram, P.; Jiang, Z.; Chen, G.; Rivera, A.; Phasakda, A.; Zhang, Q.; Zheng, S.; Wang, G.; Chen, Q.-H. Nitrogen-containing derivatives of O-tetramethylquercetin: Synthesis and biological profiles in prostate cancer cell models. *Bioorganic chemistry* **2019**, *87*, 227-239.

(69) Vue, B.; Zhang, S.; Zhang, X.; Parisis, K.; Zhang, Q.; Zheng, S.; Wang, G.; Chen, Q. H. Silibinin derivatives as anti-prostate cancer agents: Synthesis and cell-based evaluations. *European Journal of Medicinal Chemistry* **2016**, *109*, 36-46.

(70) Vue, B.; Zhang, S.; Vignau, A.; Chen, G.; Zhang, X.; Diaz, W.; Zhang, Q.; Zheng, S.; Wang, G.; Chen, Q. H. O-Aminoalkyl-O-trimethyl-2, 3-dehydrosilybins: Synthesis and in vitro effects towards prostate cancer cells. *Molecules* **2018**, *23* (12), 3142-3157.

(71) Jiang, Z.; Sekhon, A.; Oka, Y.; Chen, G.; Alrubati, N.; Kaur, J.; Orozco, A.; Zhang, Q.; Wang, G.; Chen, Q. H. 23-O-Substituted-2, 3-dehydrosilybins selectively suppress androgen receptor-positive LNCaP prostate cancer cell proliferation. *Natural Product Communications* **2020**, *15* (5), 1-10.

(72) Bassetto, M.; Ferla, S.; Giancotti, G.; Pertusati, F.; Westwell, A. D.; Brancale, A.; McGuigan, C. Rational design and synthesis of novel phenylsulfonyl-benzamides as anti-prostate cancer agents. *MedChemComm* **2017**, *8* (7), 1414-1420.

(73) Bindu, B.; Vijayalakshmi, S.; Manikandan, A. Discovery, synthesis and molecular substantiation of N-(benzo [d] thiazol-2-yl)-2-hydroxyquinoline-4-carboxamides as anticancer agents. *Bioorganic Chemistry* **2019**, *91*, 103171.

(74) Kazui, Y.; Fujii, S.; Yamada, A.; Ishigami-Yuasa, M.; Kagechika, H.; Tanatani, A. Structure-activity relationship of novel (benzoylaminophenoxy) phenol derivatives as anti-prostate cancer agents. *Bioorganic and Medicinal Chemistry* **2018**, *26* (18), 5118-5127.

(75) Soliman, D. H.; Farrag, A. M.; Omran, O. Design, synthesis and in-silico studies of novel chalcones as anti-prostate cancer and cathepsin B inhibitors. *Journal of Applied Pharmaceutical Science* **2017**, *7* (7), 010-020.

(76) Kumar, C.; Rasool, R. U.; Iqra, Z.; Nalli, Y.; Dutt, P.; Satti, N. K.; Sharma, N.; Gandhi, S. G.; Goswami, A.; Ali, A. Alkyne–azide cycloaddition analogues of dehydrozingerone as potential anti-prostate cancer inhibitors via the PI3K/Akt/NF-kB pathway. *MedChemComm* **2017**, *8* (11), 2115-2124.

(77) Gomha, S. M.; Abdel-aziz, H. M.; Badrey, M. G.; Abdulla, M. M. efficient synthesis of some new 1, 3, 4-thiadiazoles and 1, 2, 4-triazoles linked to pyrazolylcoumarin ring system as potent 5α-reductase inhibitors. *Journal of Heterocyclic Chemistry* **2019**, *56* (4), 1275-1282.

(78) Xie, H.; Liang, J. J.; Wang, Y. L.; Hu, T. X.; Wang, J. Y.; Yang, R. H.; Yan, J. K.; Zhang, Q. R.; Xu, X.; Liu, H. M. The design, synthesis and anti-tumor mechanism study of new androgen receptor degrader. *European Journal of Medicinal Chemistry* **2020**, *204*, 112512.

(79) Chauthe, S. K.; Mahajan, S.; Rachamalla, M.; Tikoo, K.; Singh, I. P. Synthesis and evaluation of linear furanocoumarins as potential anti-breast and anti-prostate cancer agents. *Medicinal Chemistry Research* **2015**, *24*, 2476-2484.

(80) Zhang, X.; Wang, R.; Perez, G. R.; Chen, G.; Zhang, Q.; Zheng, S.; Wang, G.; Chen, Q. H. Design, synthesis, and biological evaluation of 1, 9-diheteroarylnona-1, 3, 6, 8-tetraen-5-ones as a new class of anti-prostate cancer agents. *Bioorganic and Medicinal Chemistry* **2016**, *24* (19), 4692-4700.

(81) Bhati, S.; Kaushik, V.; Singh, J. In silico identification of piperazine linked thiohydantoin derivatives as novel androgen antagonist in prostate cancer treatment. *International Journal of Peptide Research and Therapeutics* **2019**, *25*, 845-860.

(82) Ticona, L. A.; Sánchez-Corral, J. S.; Sepúlveda, A. F.; Vázquez, C. S.; Vieco, C. H.; Sánchez, Á. R. Novel 1, 2, 4-oxadiazole compounds as PPAR-α ligand agonists: a new strategy for the design of antitumour compounds. *RSC Medicinal Chemistry* **2023**, *7*, 1-12.

(83) Oggu, S.; Akshinthala, P.; Katari, N. K.; Nagarapu, L. K.; Malempati, S.; Gundla, R.; Jonnalagadda, S. B. Design, synthesis, anticancer evaluation and molecular docking studies of 1, 2, 3-triazole incorporated 1, 3, 4-oxadiazole-Triazine derivatives. *Heliyon* **2023**, *9* (5), e15935.

(84) Rachala, M. R.; Maringanti, T. C.; Syed, T.; Eppakayala, L. Synthesis and biological evaluation of 1, 3, 4-oxadiazole bearing pyrimidine-pyrazine derivatives as anticancer agents. *Synthetic Communications* **2023**, *2023*, 1-7.

(85) Kanchrana, M.; Allaka, B. S.; Krishna, G. R.; Basavoju, S. An ultrasound assisted synthesis of spirooxindolo-1, 2, 4-oxadiazoles via [3+ 2] cycloaddition reaction and their anti-cancer activity. *Arkivoc* **2023**, *6*, S1-S46.

(86) Naaz, F.; Ahmad, F.; Lone, B. A.; Pokharel, Y. R.; Fuloria, N. K.; Fuloria, S.; Ravichandran, M.; Pattabhiraman, L.; Shafi, S.; Yar, M. S. Design and synthesis of newer 1, 3, 4-oxadiazole and 1, 2, 4-triazole based Topsentin analogues as anti-proliferative agent targeting tubulin. *Bioorganic Cchemistry* **2020**, *95*, 103519.

(87) Mohan, G.; Sridhar, G.; Laxminarayana, E.; Chary, M. T. Synthesis and biological evaluation of 1, 2, 4-oxadiazole incorporated 1, 2, 3-triazole-pyrazole derivatives as anticancer agents. *Chemical Data Collections* **2021**, *34*, 100735.

(88) Al-Wahaibi, L. H.; Mohamed, A. A.; Tawfik, S. S.; Hassan, H. M.; El-Emam, A. A. 1, 3, 4-Oxadiazole N-Mannich bases: synthesis, antimicrobial, and anti-proliferative activities. *Molecules* **2021**, *26* (8), 2110-2121.

(89) Alam, M. M.; Elbehairi, S. E. I.; Shati, A. A.; Hussien, R. A.; Alfaifi, M. Y.; Malebari, A. M.; Asad, M.; Elhenawy, A. A.; Asiri, A. M.; Mahzari, A. M. Design, synthesis and biological evaluation of new eugenol derivatives containing 1, 3, 4-oxadiazole as novel inhibitors of thymidylate synthase. *New Journal of Chemistry* **2023**, *47* (10), 5021-5032.

(90) Bommera, R. K.; Kethireddy, S.; Govindapur, R. R.; Eppakayala, L. Synthesis, biological evaluation and docking studies of 1, 2, 4-oxadiazole linked 5-fluorouracil derivatives as anticancer agents. *BMC chemistry* **2021**, *15*, 1-12.

(91) Srinivas, M.; Satyaveni, S.; Ram, B. Design, synthesis, and biological evaluation of 1, 2, 4-oxadiazole-isoxazole linked quinazoline derivatives as anticancer agents. *Russian Journal of General Chemistry* **2019**, *89* (12), 2492-2497.

(92) Nagaraju, A.; Kumar Nukala, S.; Narasimha Swamy Thirukovela, T.; Manchal, R. In Vitro Anticancer and In Silico Studies of Some 1, 4-Benzoxazine-1, 2, 4-oxadiazole Hybrids. *ChemistrySelect* **2021**, *6* (14), 3318-3321.

(93) Vaidya, A.; Jain, S.; Prashantha Kumar, B.; Singh, S. K.; Kashaw, S. K.; Agrawal, R. K. Synthesis of 1, 2, 4-oxadiazole derivatives: anticancer and 3D QSAR studies. *Monatshefte für Chemie-Chemical Monthly* **2020**, *151*, 385-395.

(94) Mochona, B.; Qi, X.; Euynni, S.; Sikazwi, D.; Mateeva, N.; Soliman, K. F. Design and evaluation of novel oxadiazole derivatives as potential prostate cancer agents. *Bioorganic and Medicinal Chemistry Letters* **2016**, *26* (12), 2847-2851.

(95) El-Din, M. M. G.; El-Gamal, M. I.; Abdel-Maksoud, M. S.; Yoo, K. H.; Oh, C.-H. Synthesis and broad-spectrum antiproliferative activity of diarylamides and diarylureas possessing 1, 3, 4-oxadiazole derivatives. *Bioorganic and Medicinal Chemistry Letters* **2015**, *25* (8), 1692-1699.

(96) Arjun, H.; Elancheran, R.; Manikandan, N.; Lakshmithendral, K.; Ramanathan, M.; Bhattacharjee, A.; Lokanath, N.; Kabilan, S. Design, synthesis, and biological evaluation of (*E*)-*N*'-((1-chloro-3, 4-dihydronaphthalen-2-yl) methylene) benzohydrazide derivatives as anti-prostate cancer agents. *Frontiers in Chemistry* **2019**, *7*, 474.

(97) Cao, S.; Cao, R.; Liu, X.; Luo, X.; Zhong, W. Design, synthesis and biological evaluation of novel benzothiazole derivatives as selective PI3Kβ inhibitors. *Molecules* **2016**, *21* (7), 876-891.

(98) Gomha, S. M.; Badry, M. G.; Abdalla, M. M. Isoxazolopyrimidinethione and Isoxazolopyridopyrimidinethione Derivatives: Key Intermediates for Synthesis of Novel Fused Triazoles as Potent 5α-Reductase Inhibitors and Anti-Prostate Cancer. *Journal of Heterocyclic Chemistry* **2016**, *53* (2), 558-565.

(99) Mohareb, R. M.; Abbas, N. S.; Mohamed, A. A. Synthesis of tetrahydropyrazolo-quinazoline and tetrahydropyrazolo-pyrimidocarbazole derivatives as potential anti-prostate cancer agents and Pim-1 kinase inhibitors. *Medicinal Chemistry Research* **2017**, *26*, 1073-1088.

(100) Saravanan, K.; Elancheran, R.; Divakar, S.; Anand, S. A. A.; Ramanathan, M.; Kotoky, J.; Lokanath, N.; Kabilan, S. Design, synthesis and biological evaluation of 2-(4-phenylthiazol-2-yl) isoindoline-1, 3-dione derivatives as anti-prostate cancer agents. *Bioorganic and Medicinal Chemistry Letters* **2017**, *27* (5), 1199-1204.

(101) Szumilak, M.; Galdyszynska, M.; Dominska, K.; Stanczak, A.; Piastowska-Ciesielska, A. Anticancer activity of some polyamine derivatives on human prostate and breast cancer cell lines. *Acta Biochimica Polonica* **2017**, *64* (2), 307-313.

(102) He, Z.-X.; Huo, J.-L.; Gong, Y. P.; An, Q.; Zhang, X.; Qiao, H.; Yang, F. F.; Zhang, X. H.; Jiao, L. M.; Liu, H. M. Design, synthesis and biological evaluation of novel thiosemicarbazone-indole derivatives targeting prostate cancer cells. *European Journal of Medicinal Chemistry* **2021**, *210*, 112970.

(103) Anand, S. A. A.; George, K.; Thomas, N. S.; Kabilan, S. Synthesis, characterization and antitumor activities of some novel thiazinones and thiosemicarbazones derivatives. *Phosphorus, Sulfur, and Silicon and the Related Elements* **2020**, *195* (10), 821-829.

(104) Coşkun, G. P.; Djikic, T.; Hayal, T. B.; Türkel, N.; Yelekçi, K.; Şahin, F.; Küçükgüzel, Ş. G. Synthesis, molecular docking and anticancer activity of diflunisal derivatives as cyclooxygenase enzyme inhibitors. *Molecules* **2018**, *23* (8), 1969-1987.

(105) Li, K.; Li, Y.; Zhou, D.; Fan, Y.; Guo, H.; Ma, T.; Wen, J.; Liu, D.; Zhao, L. Synthesis and biological evaluation of quinoline derivatives as potential anti-prostate cancer agents and Pim-1 kinase inhibitors. *Bioorganic and Medicinal Chemistry* **2016**, *24* (8), 1889-1897.

(106) Britton, R. G.; Horner Glister, E.; Pomenya, O. A.; Smith, E. E.; Denton, R.; Jenkins, P. R.; Steward, W. P.; Brown, K.; Gescher, A.; Sale, S. Synthesis and biological evaluation of novel flavonols as potential anti-prostate cancer agents. *European Journal of Medicinal Chemistry* **2012**, *54*, 952-958.

(107) Bohl, C. E.; Gao, W.; Miller, D. D.; Bell, C. E.; Dalton, J. T. Structural basis for antagonism and resistance of bicalutamide in prostate cancer. *Proceedings of the National Academy of Sciences* **2005**, *102* (17), 6201-6206.

(108) Li, W.; Hwang, D. J.; Cremer, D.; Joo, H.; Kraka, E.; Kim, J.; Ross, C. R.; Nguyen, V. Q.; Dalton, J. T.; Miller, D. D. Structure determination of chiral sulfoxide in diastereomeric bicalutamide derivatives. *Chirality: The Pharmacological,*

Biological, and Chemical Consequences of Molecular Asymmetry **2009**, *21* (6, 578-583.

(109) Sigalapalli, D. K.; Kiranmai, G.; Devi, G. P.; Tokala, R.; Sana, S.; Tripura, C.; Jadhav, G. S.; Kadagathur, M.; Shankaraiah, N.; Nagesh, N. Synthesis and biological evaluation of novel imidazo [1, 2-α] pyridine-oxadiazole hybrids as anti-proliferative agents: Study of microtubule polymerization inhibition and DNA binding. *Bioorganic and Medicinal Chemistry* **2021**, *43*, 116277.

(110) De Oliveira, V. N. M.; Dos Santos, F. G.; Ferreira, V. P. G.; Araújo, H. M.; do Ó Pessoa, C.; Nicolete, R.; de Oliveira, R. N. Focused microwave irradiation-assisted synthesis of N-cyclohexyl-1, 2, 4-oxadiazole derivatives with antitumor activity. *Synthetic Communications* **2018**, *48* (19), 2522-2532.

(111) Khatik, G. L.; Kaur, J.; Kumar, V.; Tikoo, K.; Nair, V. A. 1, 2, 4-Oxadiazoles: A new class of anti-prostate cancer agents. *Bioorganic and Medicinal Chemistry Letters* **2012**, *22* (5), 1912-1916.

(112) Vinjavarapu, A. K.; Begum, S.; Koganti, B. Synthesis, evaluation, and in silico studies of 2-mercapto-5-substituted styryl-1, 3, 4-oxadiazoles as potential cytotoxic agents. *The Thai Journal of Pharmaceutical Sciences* **2020**, *44* (1), 52-65.

(113) Madhu, S.; Yamini, G.; Divya, K.; Padmavathi, V.; Padmaja A. Synthesis and bioassay of a new class of disubstituted 1, 3, 4-oxadiazoles, 1, 3, 4-thiadiazoles and 1, 2, 4-triazoles. *Medicinal Chemistry Research* **2019**, *28* (1), 1049-1062.

(114) Ahmad, M.; Akhtar, J.; Hussain, A.; Arshad, M.; Mishra, A. Development of a new rutin nanoemulsion and its application on prostate carcinoma PC3 cell line. *Excli Journal* **2017**, *16*, 810-823.

(115) Hua, X.; Xiao, Y.; Pan, W.; Li, M.; Huang, X.; Liao, Z.; Xian, Q.; Yu, L. miR-186 inhibits cell proliferation of prostate cancer by targeting GOLPH3. *American Journal of Cancer Research* **2016**, *6* (8), 1650-1660.

(116) Zhu, S.; Jiao, W.; Xu, Y.; Hou, L.; Li, H.; Shao, J.; Zhang, X.; Wang, R.; Kong, D. Palmitic acid inhibits prostate cancer cell proliferation and metastasis by suppressing the PI3K/Akt pathway. *Life Sciences* **2021**, *286*, 120046.

(117) bilir, E. K.; Tutun, H.; Sevin, S.; Kismali, G.; Yarsan, E. Cytotoxic effects of Rhododendron ponticum L. extract on prostate carcinoma and adenocarcinoma cell line (DU145, PC3). *Kafkas Üniversitesi Veteriner Fakültesi Dergisi* **2018**, *24* (3), 1-7.

(118) Eruslanov, E.; Kusmartsev, S. Identification of ROS using oxidized DCFDA and flow-cytometry. *Advanced Protocols in Oxidative Stress II* **2010**, 57-72.

(119) Yoon, D. S.; Lee, M. H.; Cha, D. S. Measurement of intracellular ROS in Caenorhabditis elegans using 2', 7'-dichlorodihydrofluorescein diacetate. *Bio Protocol* **2018**, *8* (6), e2774-e2774.

(120) Sarasija, S.; Norman, K. R. Measurement of ROS in Caenorhabditis elegans using a reduced form of fluorescein. *Bio-protocol* **2018**, *8* (7), e2800-e2810.

(121) Jambunathan, N. Determination and detection of reactive oxygen species (ROS), lipid peroxidation, and electrolyte leakage in plants. *Plant Stress Tolerance: Methods and Protocols: Humana Press* **2010**, 291-297.

(122) Ishioka, T.; Tanatani, A.; Nagasawa, K.; Hashimoto, Y. Anti-androgens with full antagonistic activity toward human prostate tumor LNCaP cells with mutated androgen receptor. *Bioorganic and Medicinal Chemistry Letters* **2003**, *13* (16), 2655-2658.

(123) Lallous, N.; Snow, O.; Sanchez, C.; Parra Nuñez, A. K.; Sun, B.; Hussain, A.; Lee, J.; Morin, H.; Leblanc, E.; Gleave, M. E. Evaluation of darolutamide (Odm201) efficiency on androgen receptor mutants reported to date in prostate cancer patients. *Cancers* **2021**, *13* (12), 2939-2349.

(124) Jan, Y. J.; Yoon, J.; Chen, J. F.; Teng, P. C.; Yao, N.; Cheng, S.; Lozano, A.; Chu, G. C.; Chung, H.; Lu, Y.-T. A circulating tumor cell-RNA assay for assessment of androgen receptor signaling inhibitor sensitivity in metastatic castration-resistant prostate cancer. *Theranostics* **2019**, *9* (10), 2812-2826.

(125) Sabeur, K.; Edwards, D. P.; Meizel, S. Human sperm plasma membrane progesterone receptor (s) and the acrosome reaction. *Biology of Reproduction* **1996**, *54* (5), 993-1001.

(126) Simental, J.; Sar, M.; Lane, M.; French, F.; Wilson, E. Transcriptional activation and nuclear targeting signals of the human androgen receptor. *Journal of Biological Chemistry* **1991**, *266* (1), 510-518.

(127) Eweas, A. F.; Maghrabi, I. A.; Namarneh, A. I. Advances in molecular modeling and docking as a tool for modern drug discovery. *Der Pharma Chemica* **2014**, *6* (6), 211-228.

(128) Aminpour, M.; Montemagno, C.; Tuszynski, J. A. An overview of molecular modeling for drug discovery with specific illustrative examples of applications. *Molecules* **2019**, *24* (9), 1693-1722.

(129) Kumar, S.; Khatik, G. L.; Mittal, A. In silico molecular docking study to search new SGLT2 inhibitor based on dioxabicyclo [3.2. 1] octane scaffold. *Current Computer-Aided Drug Design* **2020**, *16* (2), 145-154.

(130) Liu, H.; An, X.; Li, S.; Wang, Y.; Li, J.; Liu, H. Interaction mechanism exploration of R-bicalutamide/S-1 with WT/W741L AR using molecular dynamics simulations. *Molecular BioSystems* **2015**, *11* (12), 3347-3354.

(131) Bohl, C. E.; Wu, Z.; Miller, D. D.; Bell, C. E.; Dalton, J. T. Crystal structure of the T877A human androgen receptor ligand-binding domain complexed to cyproterone acetate provides insight for ligand-induced conformational changes and structure-based drug design. *Journal of Biological Chemistry* **2007**, *282* (18), 13648-13655.

(132) Kumar, S.; Arora, P.; Wadhwa, P.; Kaur, P. A Rationalized Approach to Design and Discover Novel Non-steroidal Derivatives through Computational Aid for the Treatment of Prostate Cancer. *Current computer-aided drug design* **2024**, *20* (5), 575-589.

(133) Dorice, M. H. C.; Khurana, N.; Sharma, N.; Khatik, G. L. Identification of Possible Molecular Targets of Potential Anti-Parkinson Drugs by Predicting Their Binding Affinities Using Molecular Docking. *Asian Journal of Pharmaceutical and Clinical Research* **2018**, *11* (2) 1-5.

(134) Jejurikar, B. L.; Rohane, S. H. Drug designing in discovery studio. **2021**, 135-138.

(135) Mishra, S.; Dahima, R. In vitro ADME studies of TUG-891, a GPR-120 inhibitor using SWISS ADME predictor. *Journal of Drug Delivery and Therapeutics* **2019**, *9* (2-s), 366-369.

(136) Daina, A.; Michielin, O.; Zoete, V. SwissADME: a free web tool to evaluate pharmacokinetics, drug-likeness and medicinal chemistry friendliness of small molecules. *Scientific Reports* **2017**, *7* (1), 42717-42729.

(137) Banerjee, P.; Dehnbostel, F. O.; Preissner, R. Prediction balancing act: Importance of sampling methods to balance sensitivity and specificity of predictive models based on imbalanced chemical data. *Frontiers in Chemistry* **2018**, *362* (6), 1-11.

(138) Pires, D. E.; Blundell, T. L.; Ascher, D. B. pkCSM: predicting small-molecule pharmacokinetic and toxicity properties using graph-based signatures. *Journal of Medicinal Chemistry* **2015**, *58* (9), 4066-4072.

(139) Azzam, K. A. SwissADME and pkCSM webservers predictors: An integrated online platform for accurate and comprehensive predictions for in silico ADME/T properties of artemisinin and its derivatives. *Kompleksnoe Ispolzovanie Mineralnogo Syra= Complex Use of Mineral Resources* **2023**, *325* (2), 14-21.

(140) Tarasenko, M.; Sidneva, V.; Belova, A.; Romanycheva, A.; Sharonova, T.; Baykov, S.; Shetnev, A.; Kofanov, E.; Kuznetsov, M. An efficient synthesis and antimicrobial evaluation of 5-alkenyl-and 5-styryl-1, 2, 4-oxadiazoles. *Arkivoc* **2018**, *2018* (7), 458-470.

(141) Sahyoun, T.; Arrault, A.; Schneider, R. Amidoximes and oximes: Synthesis, structure, and their key role as NO donors. *Molecules* **2019**, *24* (13), 2470-2488.

(142) Sangshetti, J. N.; Shinde, D. B. Synthesis of some novel 3-(1-(1-substitutedpiperidin-4-yl)-1H-1, 2, 3-triazol-4-yl)-5-substituted phenyl-1, 2, 4-oxadiazoles as antifungal agents. *European Journal of Medicinal Chemistry* **2011**, *46* (4), 1040-1044.

(143) Santos Ballardo, L.; Garcia-Paez, F.; Picos Corrales, L. A.; Ochoa Teran, A.; Bastidas, P.; Calderón-Zamora, L.; Rendon-Maldonado, G.; Osuna-Martínez, U.; Sarmiento-Sánchez, J. I. Synthesis, biological evaluation and molecular docking of 3-substituted quinazoline-2, 4 (1 H, 3 H)-diones. *Journal of Chemical Sciences* **2020**, *132*, 1-10.

(144) Hatsuda, M.; Kuroda, T.; Seki, M. An improved synthesis of (*E*)-cinnamic acid derivatives via the Claisen–Schmidt condensation. *Synthetic Communications* **2003**, *33* (3), 427-434.

(145) Biernacki, K.; Dasko M.; Ciupak O.; Kubinski K.; Rachon J.; Demkowicz S. 1, 2, 4-oxadiazole derivatives in drug discovery. *Pharmaceuticals* **2020** *13* (6) 111-156.

(146) Kumar, S.; Wadhwa P. Synthesis, molecular docking and biological evaluation of 1,2,4-oxadiazole based novel non-steroidal derivatives against prostate cancer. *Bioorganic chemistry* **2024**, *143*, 107029.

Lists of Appendix

List of Appendix

I. Letter of Candidacy

LOVELY PROFESSIONAL UNIVERSITY

Centre for
Research Degree Programmes

LPU/CRDP/PHD/EC/20210802/001235

Dated: 19 May 2021

Shubham Kumar
Registration Number: 42000292
Programme Name: Doctor of Philosophy (Pharmaceutical Chemistry)

Subject: Letter of Candidacy for Ph.D.

Dear Candidate,

We are very pleased to inform you that the Department Doctoral Board has approved your candidacy for the Ph.D. Programme on 19 May 2021 by accepting your research proposal entitled: "Synthesis, Characterization and Evaluation of some novel non steroidal molecules for the treatment of Prostate cancer"

As a Ph.D. candidate you are required to abide by the conditions, rules and regulations laid down for Ph.D. Programme of the University, and amendments, if any, made from time to time.

We wish you the very best!!

In case you have any query related to your programme, please contact Centre of Research Degree Programmes.

Head

Centre for Research Degree Programmes

Note:-This is a computer generated certificate and no signature is required. Please use the reference number generated on this certificate for future conversations.

Jalandhar-Delhi G.T.Road, Phagwara, Punjab (India) - 144411
Ph : +91-1824-444594 E-mail : drp@lpu.co.in website : www.lpu.in

II. NMR and Mass Spectra for Series 1 (MS01-MS15) and Series 2 (SP01-SP25)

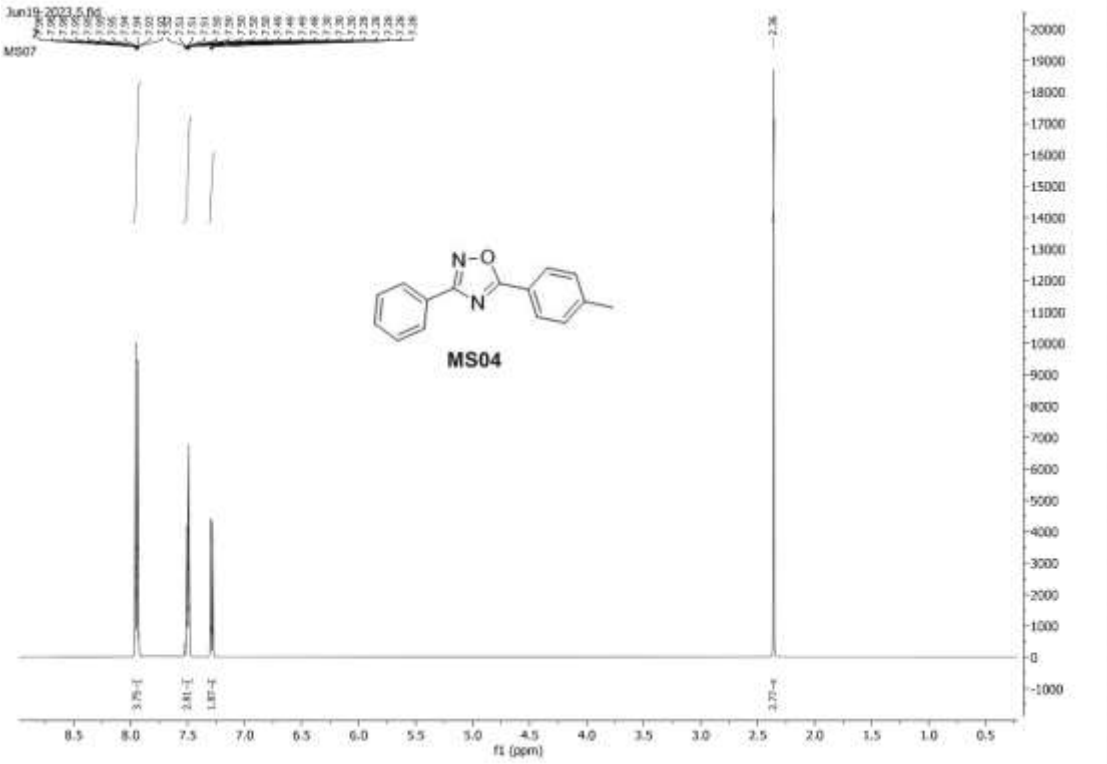

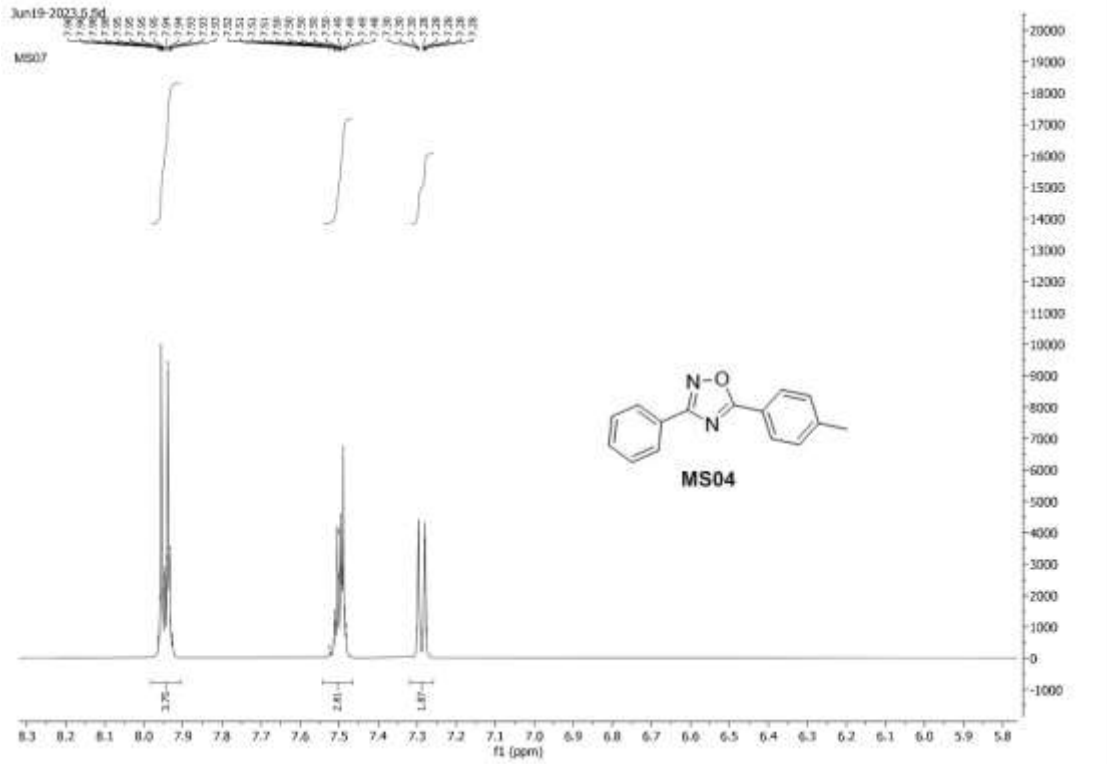

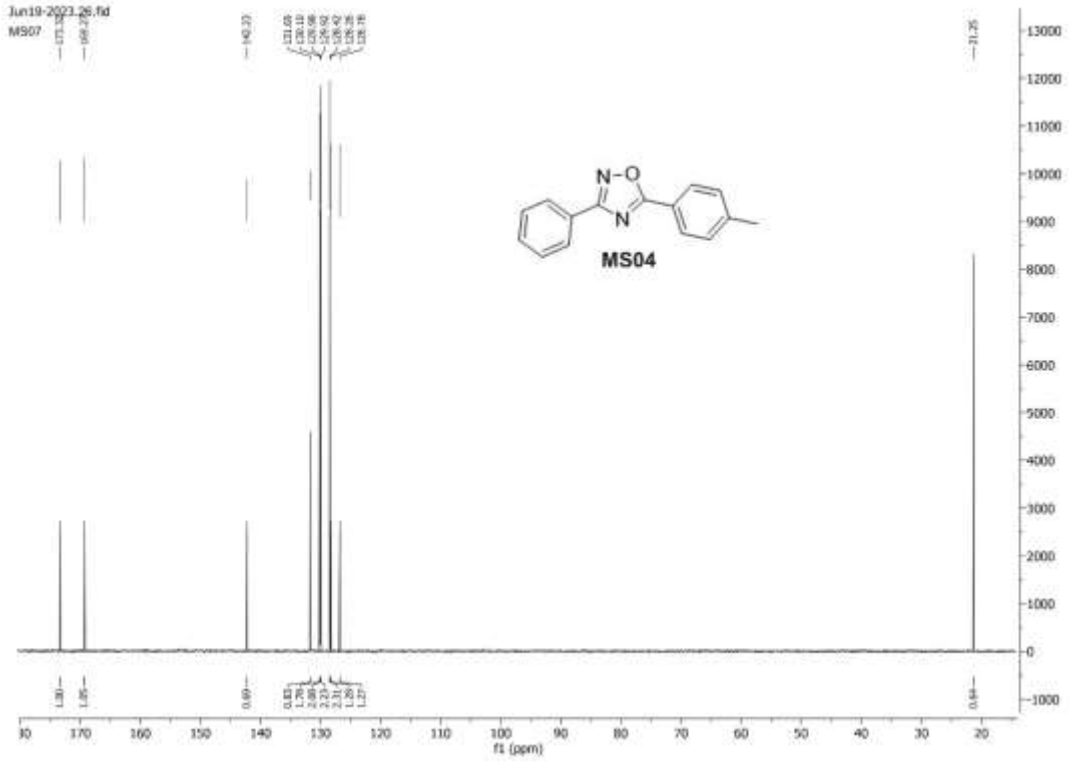
Jun19-2023.26.fid
MS07
MS04
f1 (ppm)

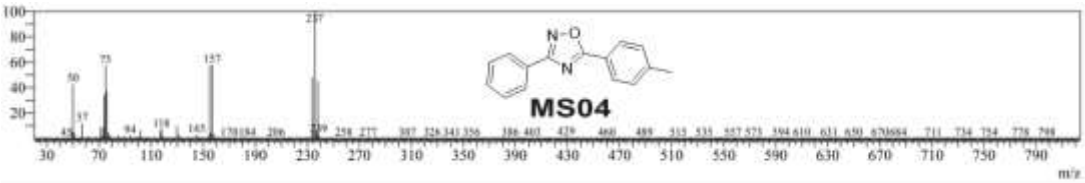
MS04
m/z

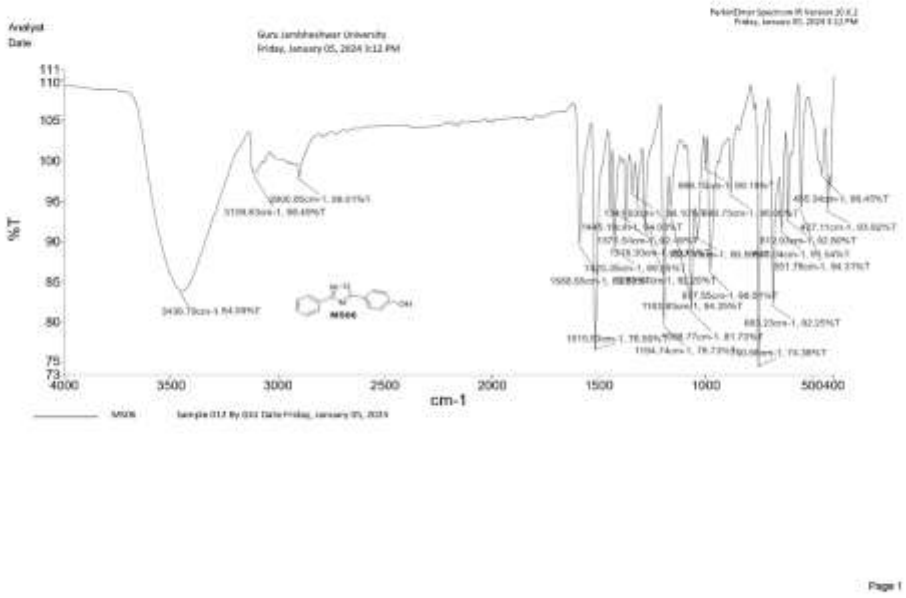
Analyst
Date
Guru Jambheshwar University
Friday, January 05, 2024 3:12 PM
%T
cm-1
MS06

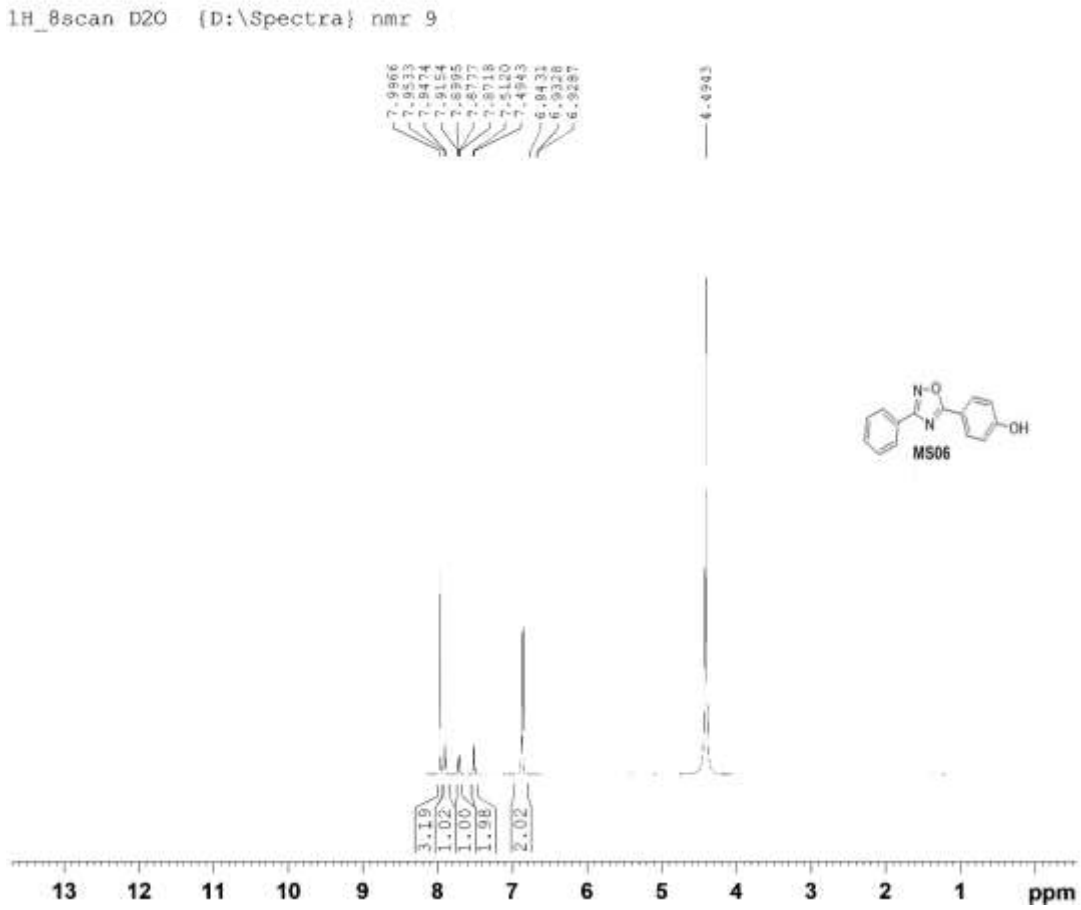
1H_8scan D2O {D:\Spectra} nmr 9
MS06
ppm

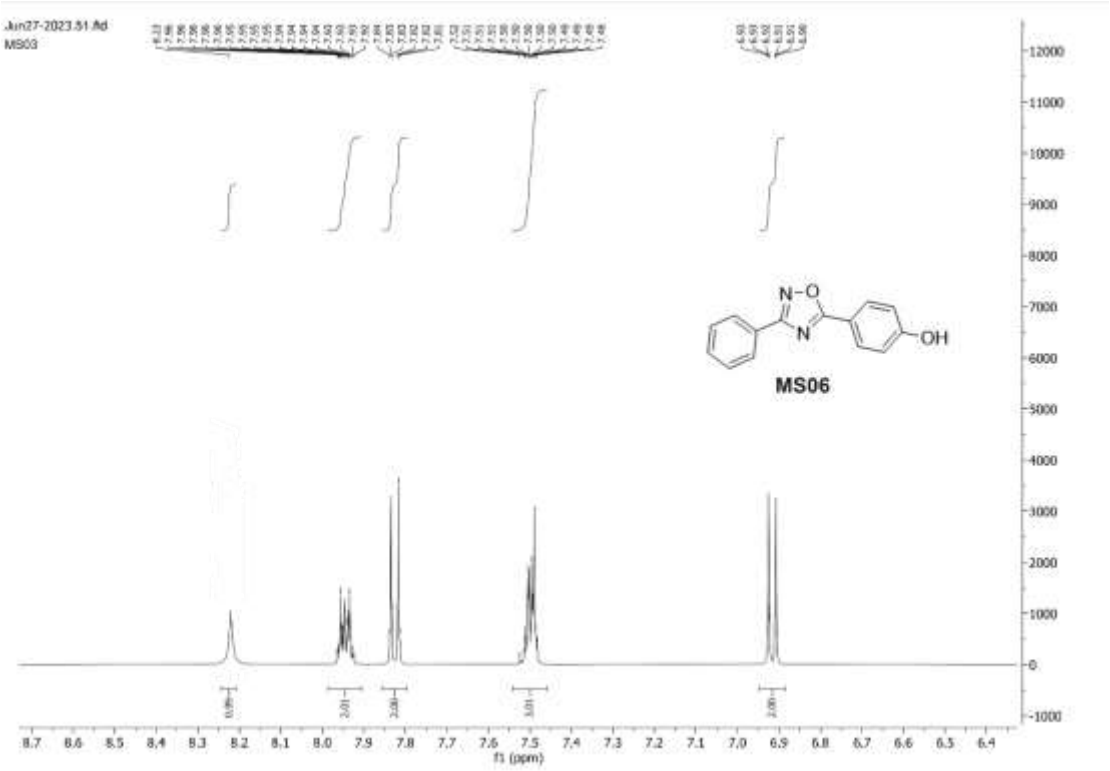
Jun27-2023.51.fid
MS03
MS06
f1 (ppm)

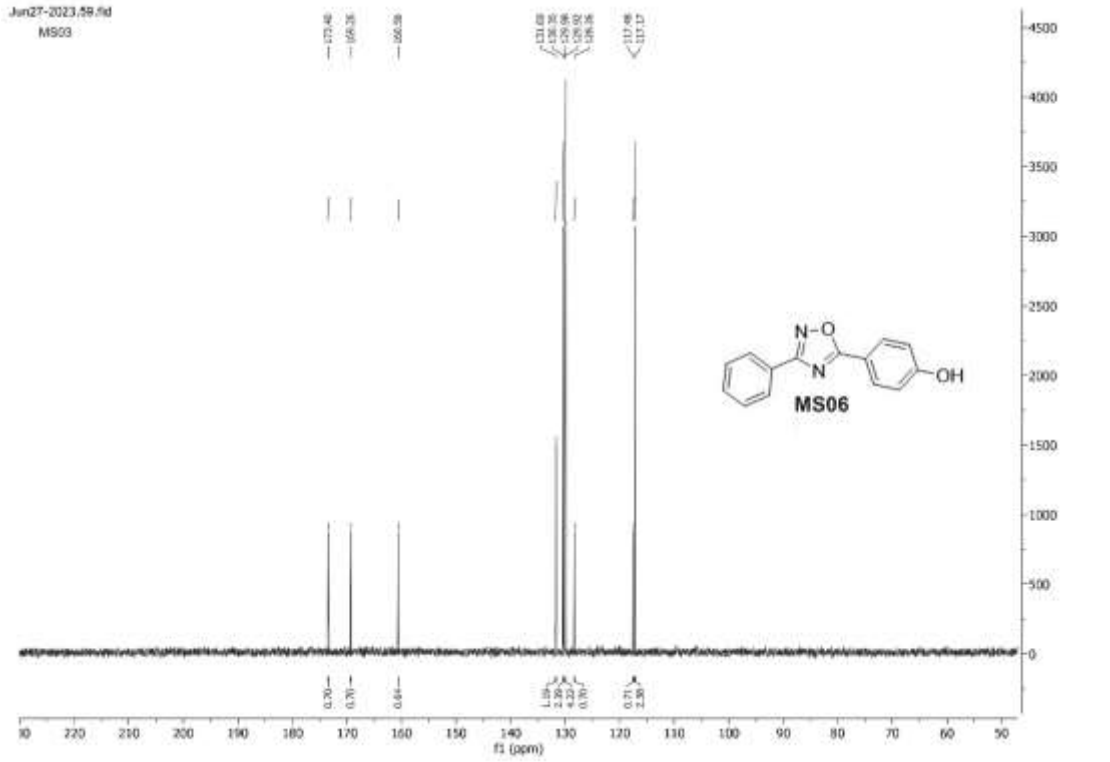
Jun27-2023.59.fid
MS03
MS06
f1 (ppm)

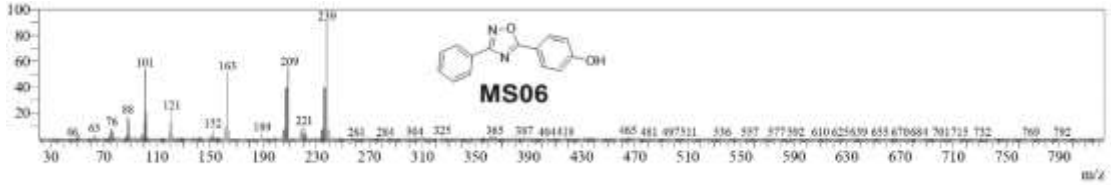
MS06
OH
m/z

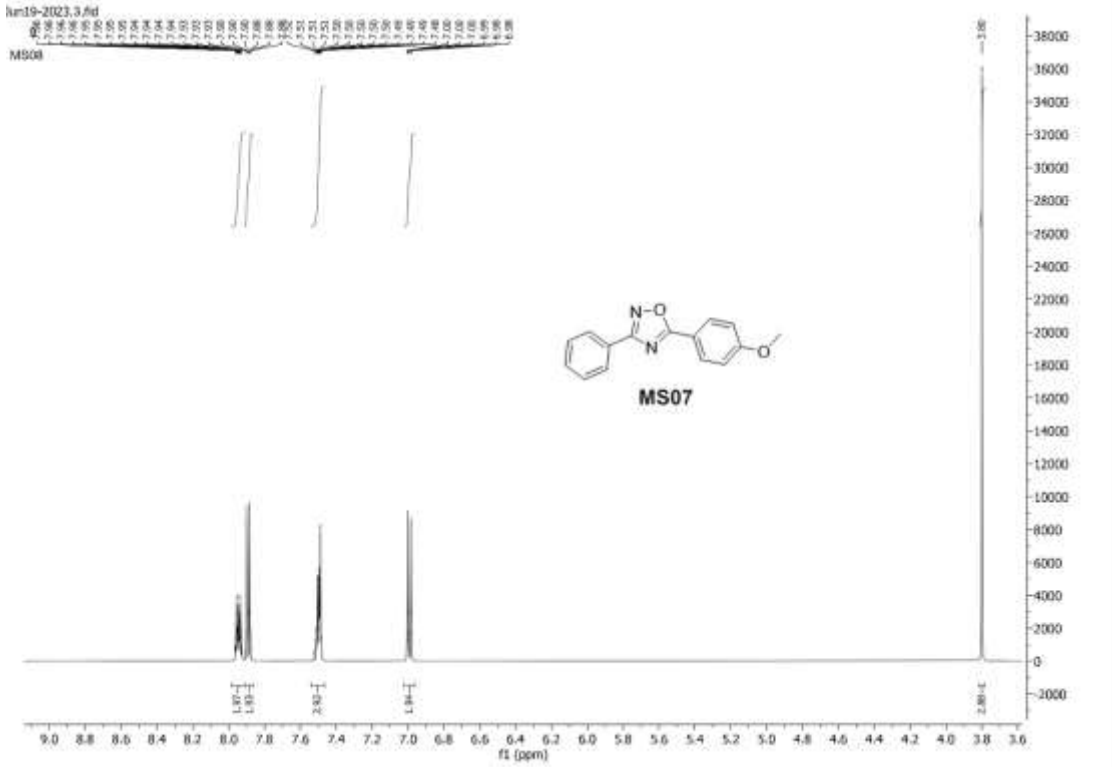
MS08
MS07
f1 (ppm)

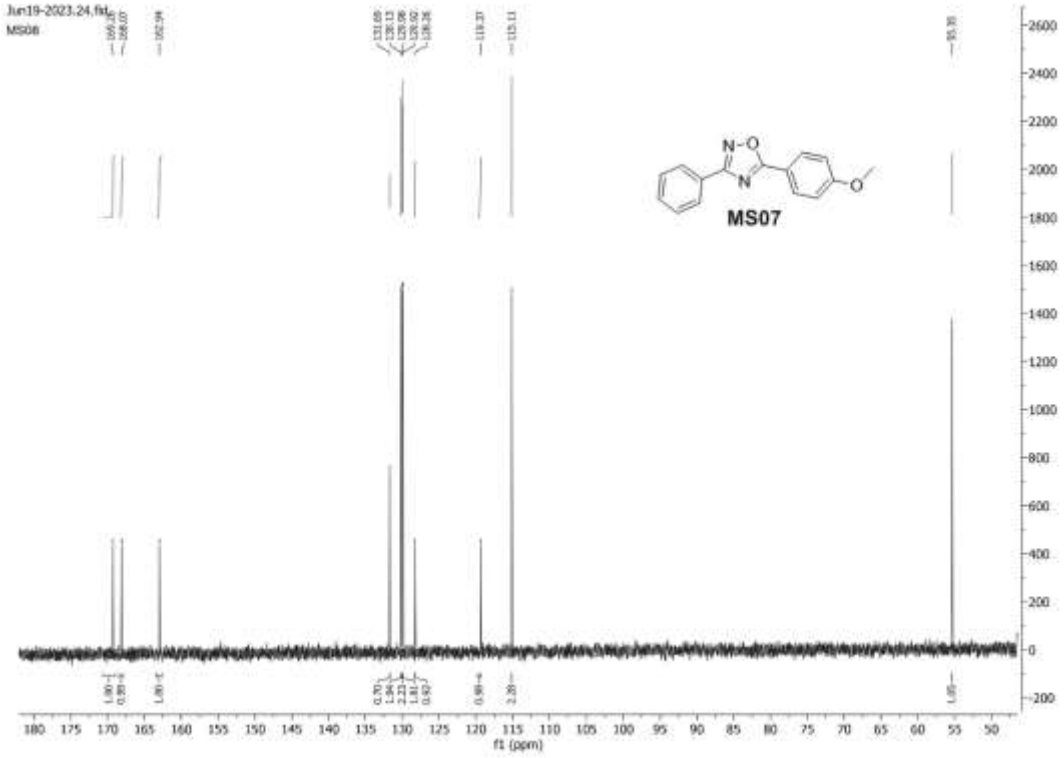
Jun19-2023.24.fid
MS08
MS07
f1 (ppm)

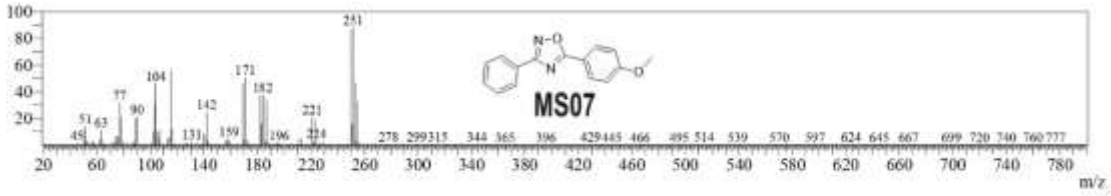
MS07
m/z

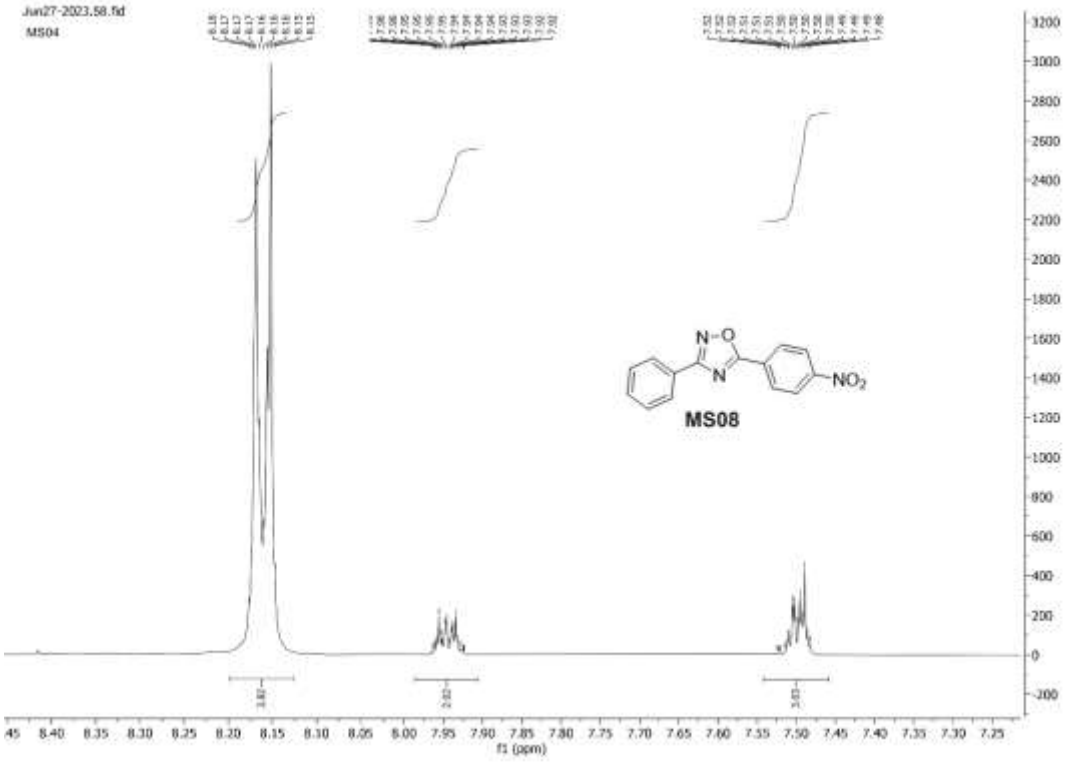
Jun27-2023.58.fid
MS04
MS08
f1 (ppm)

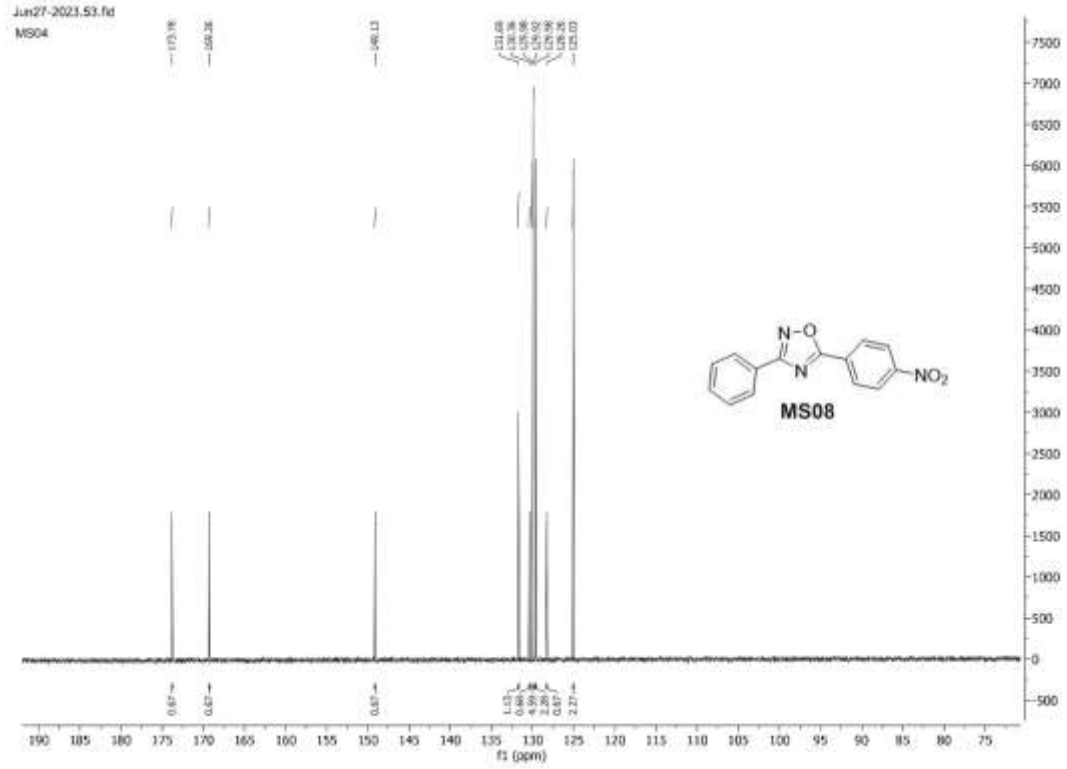
Jun27-2023.53.fid
MS04
MS08
f1 (ppm)

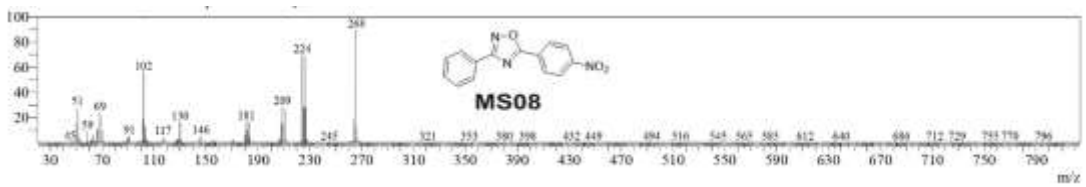
MS08
m/z

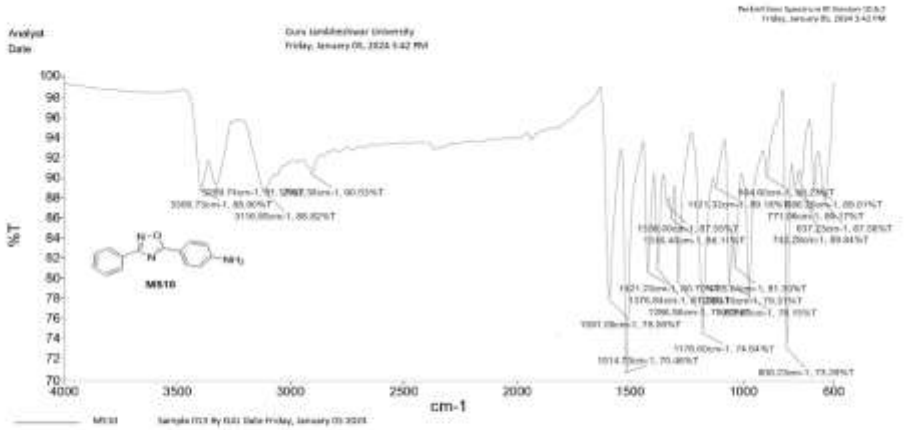
Analyst
Date
%T
cm-1
MS10

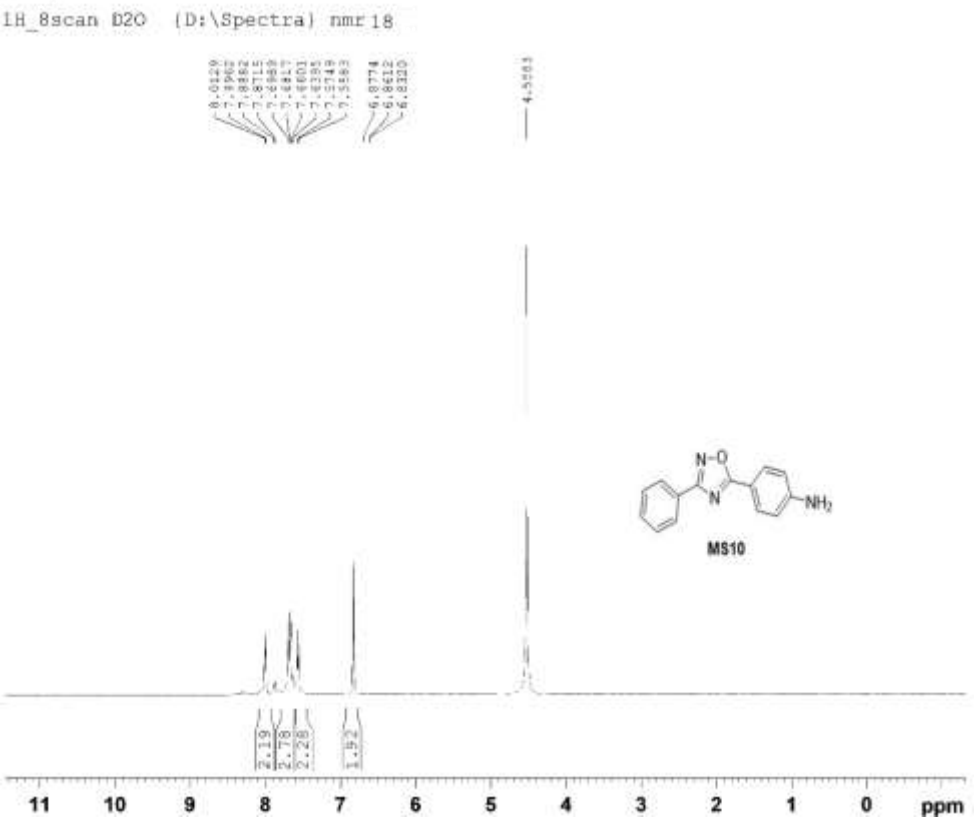
1H_8scan D2O (D:\Spectra) nmr 18
MS10
11
10
9
8
7
6
5
4
3
2
1
0
ppm

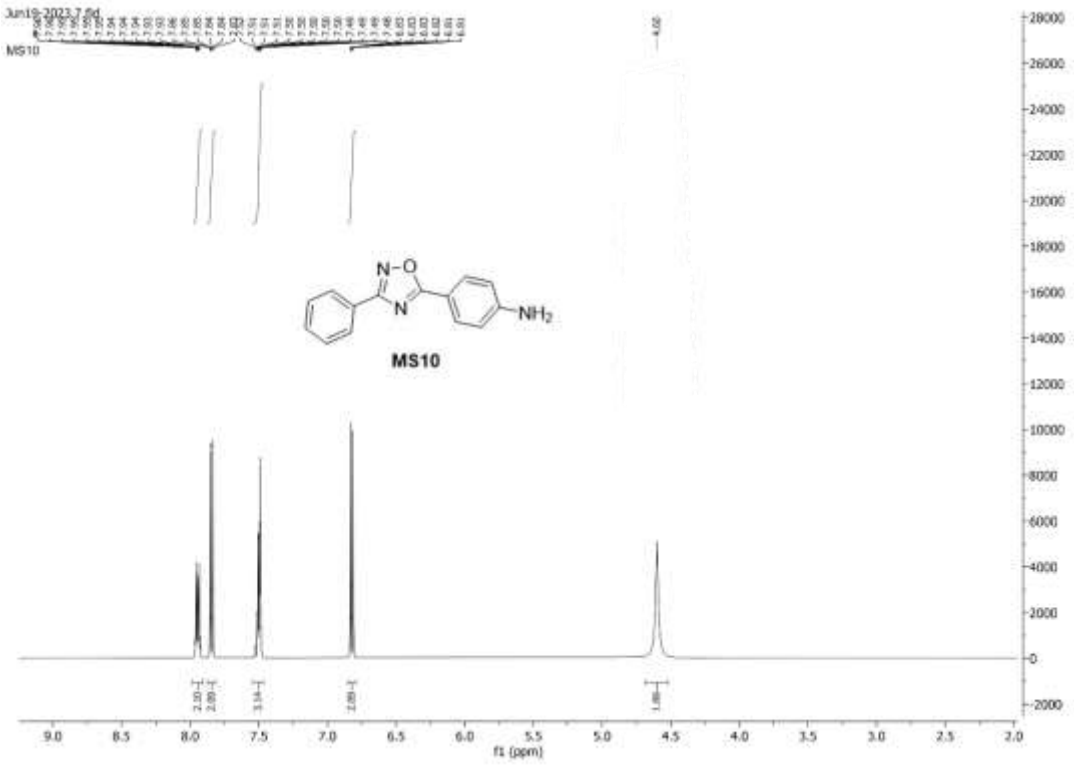
MS10
f1 (ppm)

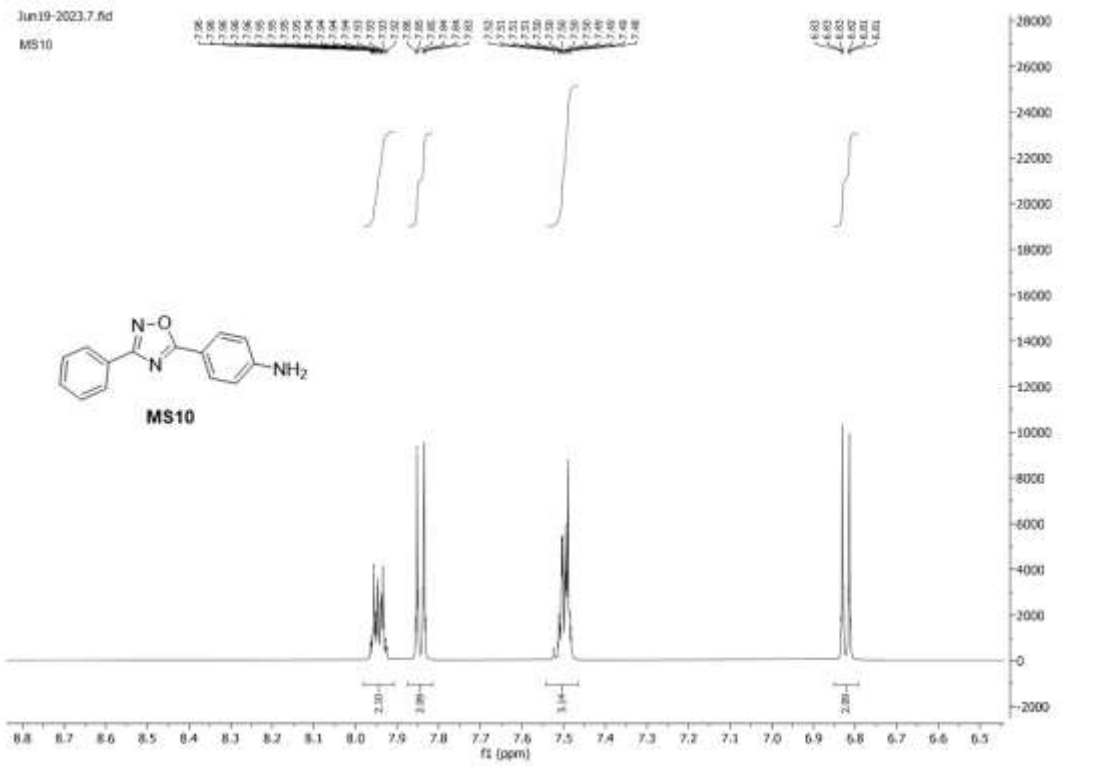
Jun19-2023.7.fid
MS10
MS10
f1 (ppm)

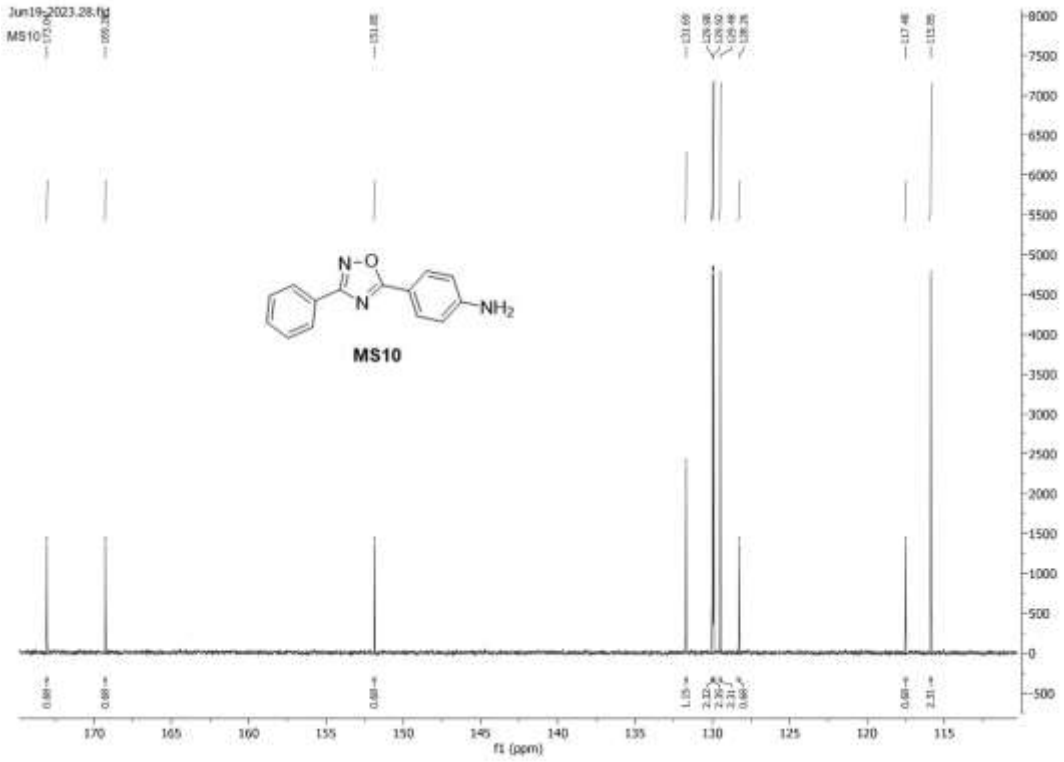
Jun19-2023.28.fid
MS10
MS10
f1 (ppm)

\

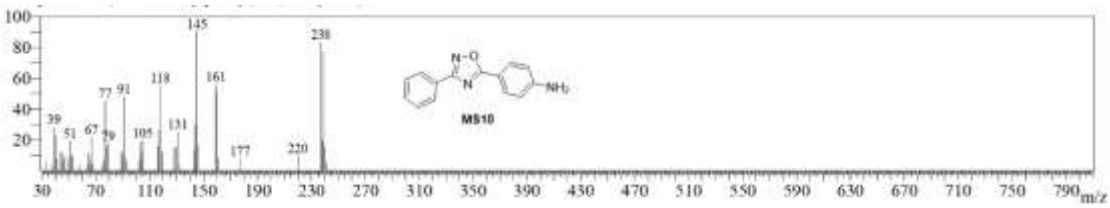
MS10
m/z

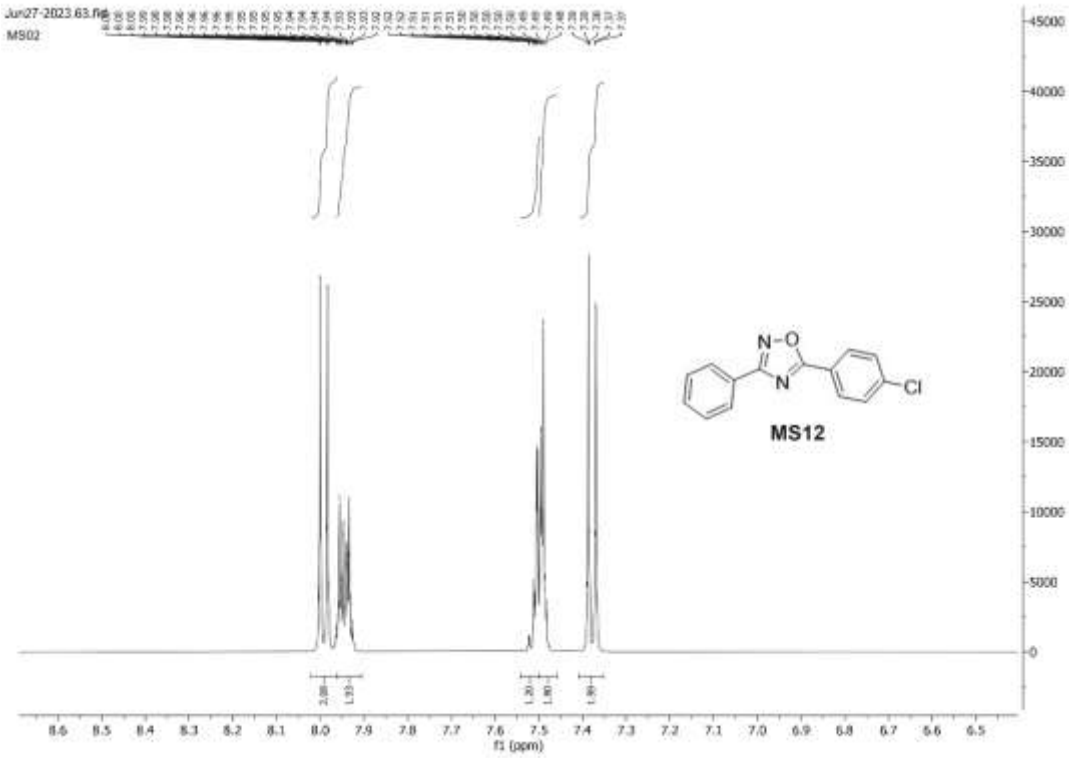
MS02
MS12
f1 (ppm)

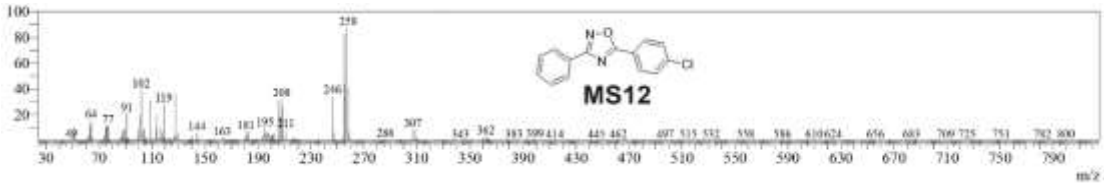
MS12
m/z

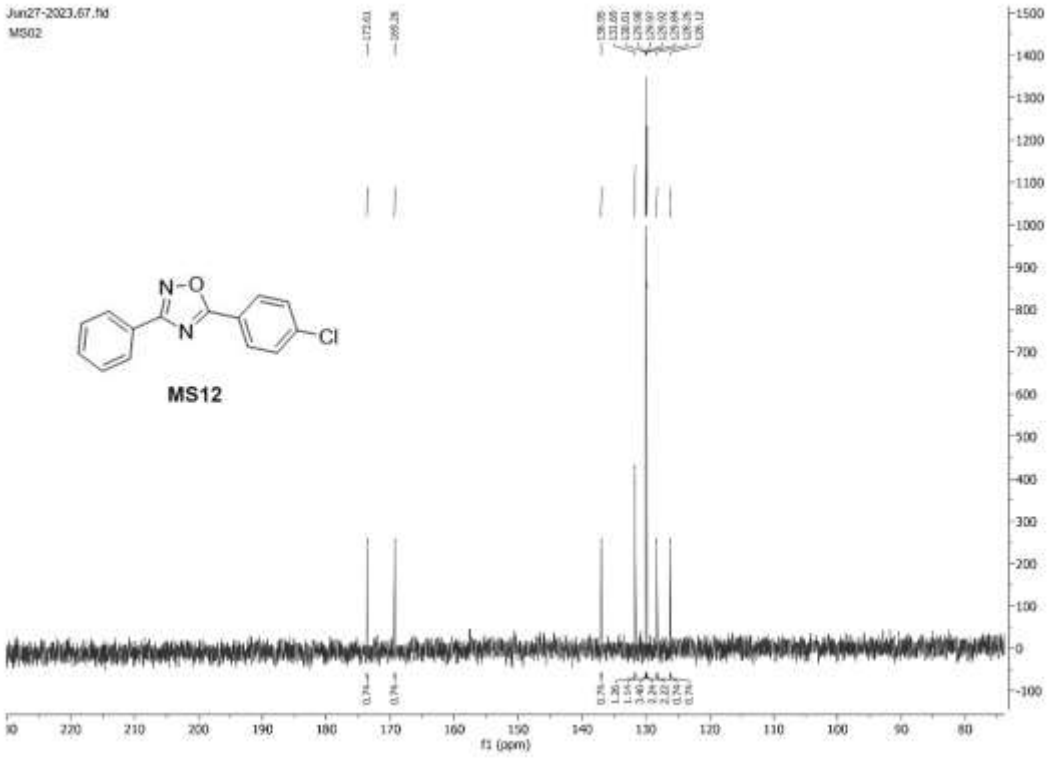
Jun27-2023,67.fid
MS02
MS12
f1 (ppm)

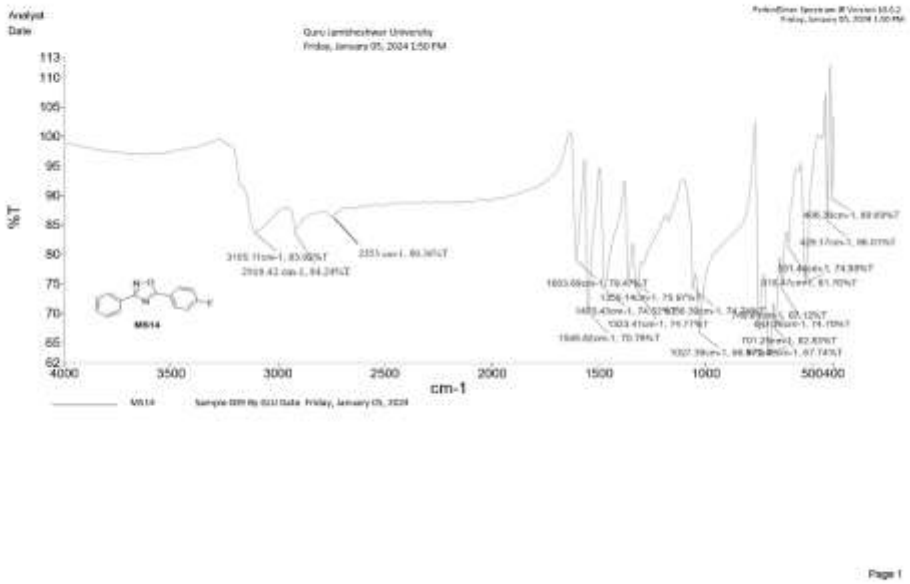
Analyst
Date
Guru Jambheshwar University
Friday, January 05, 2024 1:50 PM
%T
cm-1
MS14
Page 1

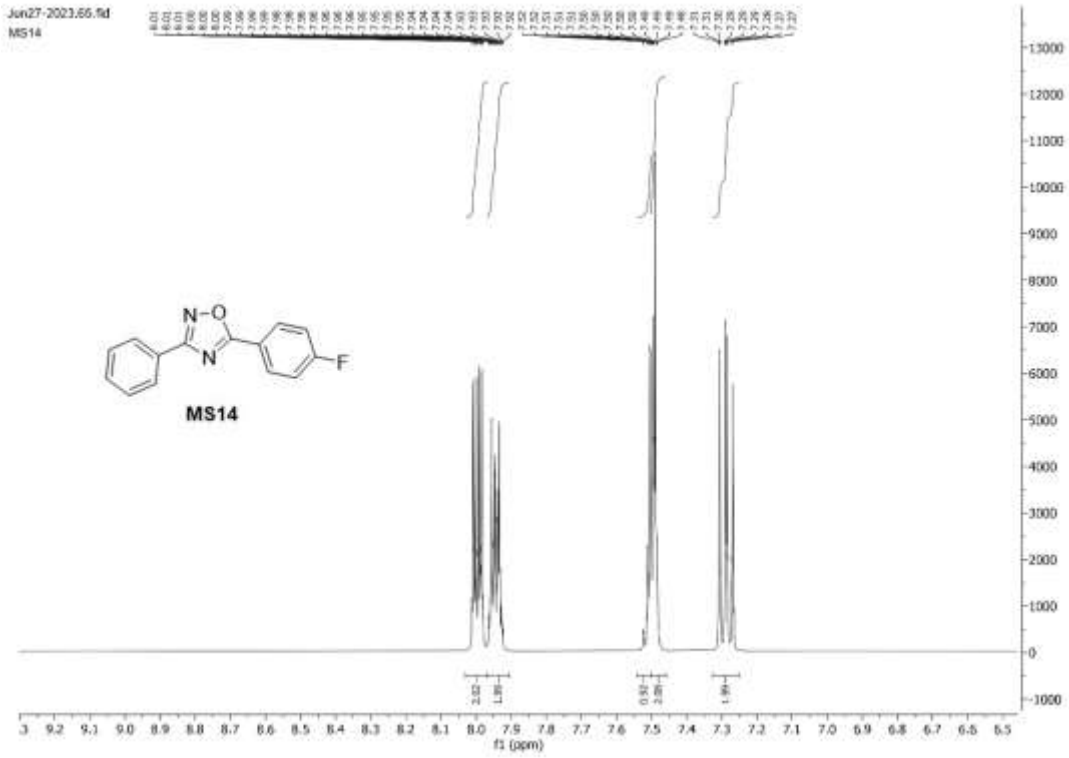
Jun27-2023.66.fid
MS14
MS14
f1 (ppm)

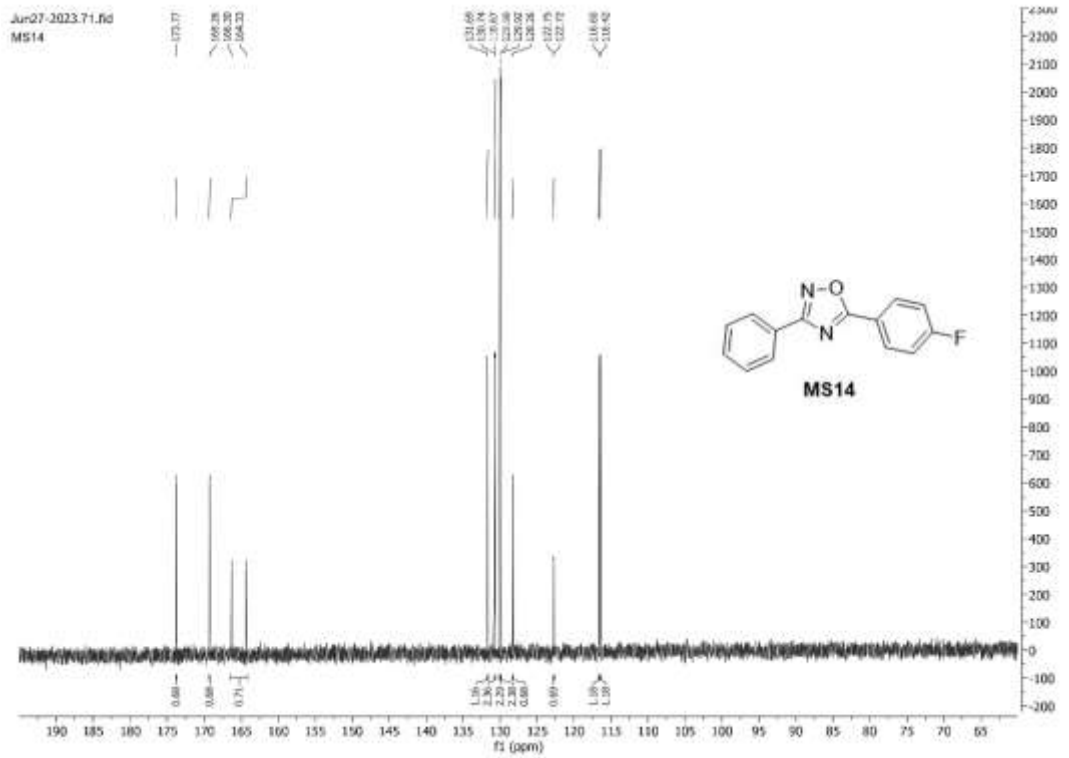
Jun27-2023.71.fid
MS14
MS14
f1 (ppm)

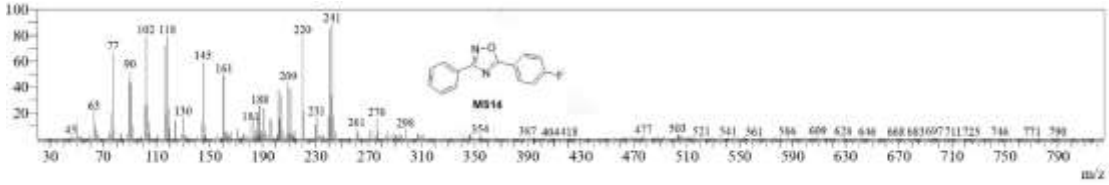
MS14
m/z

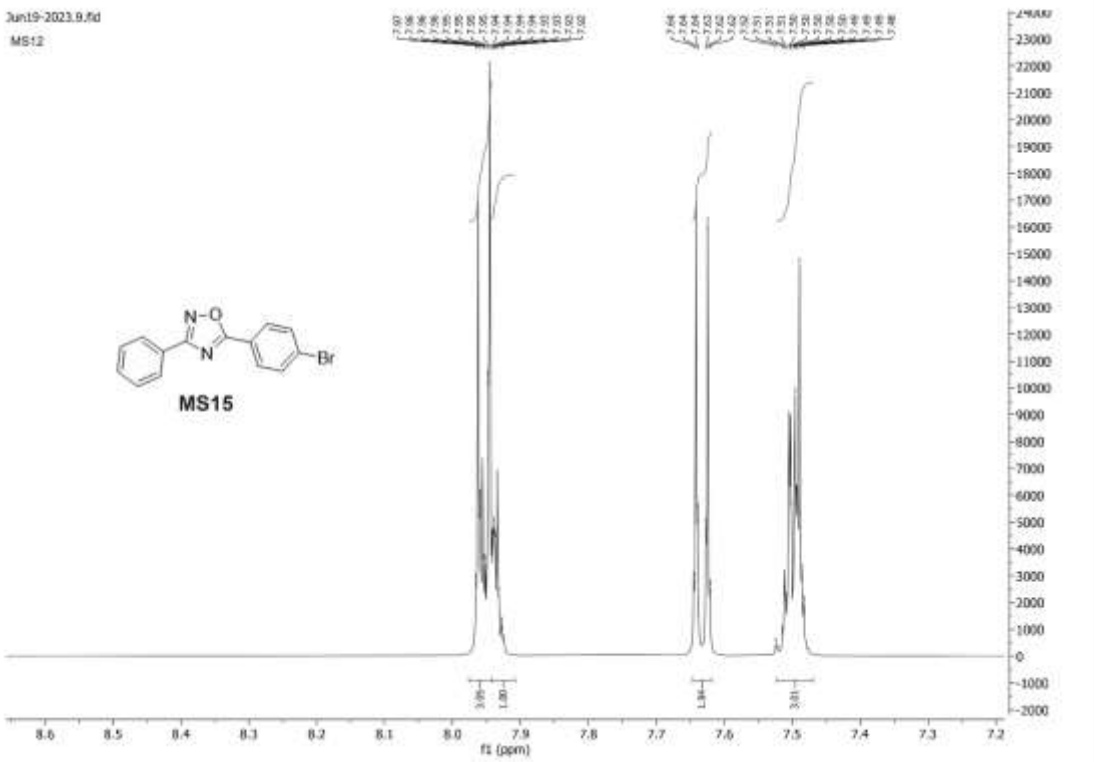
Jun19-2023.9.fid
MS12
MS15
Br
f1 (ppm)

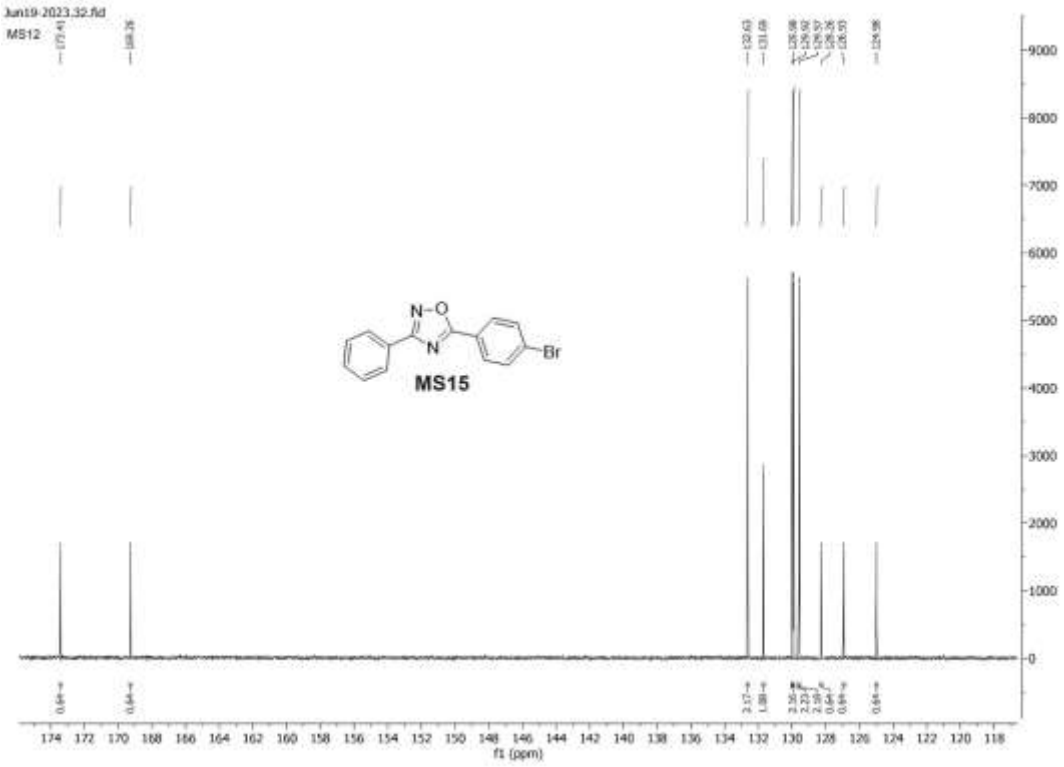
Jun19-2023.32.fid
MS12
MS15
f1 (ppm)

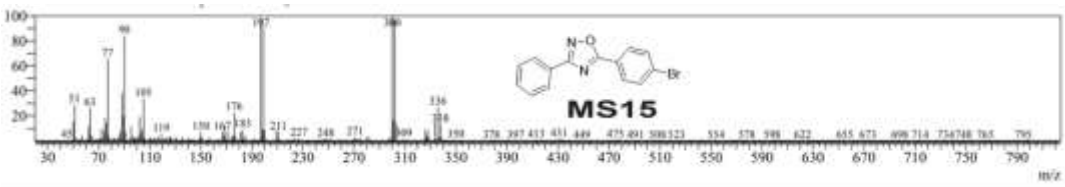
MS15
m/z

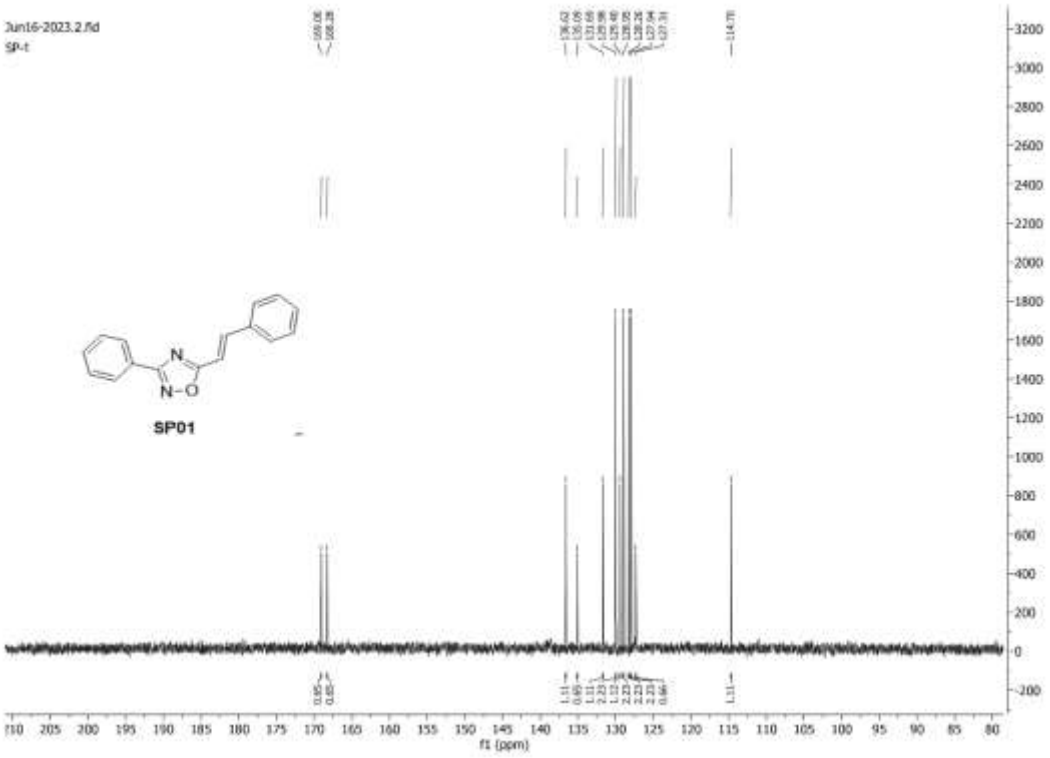
Jun16-2023.2.fid
SP-t
SP01
f1 (ppm)

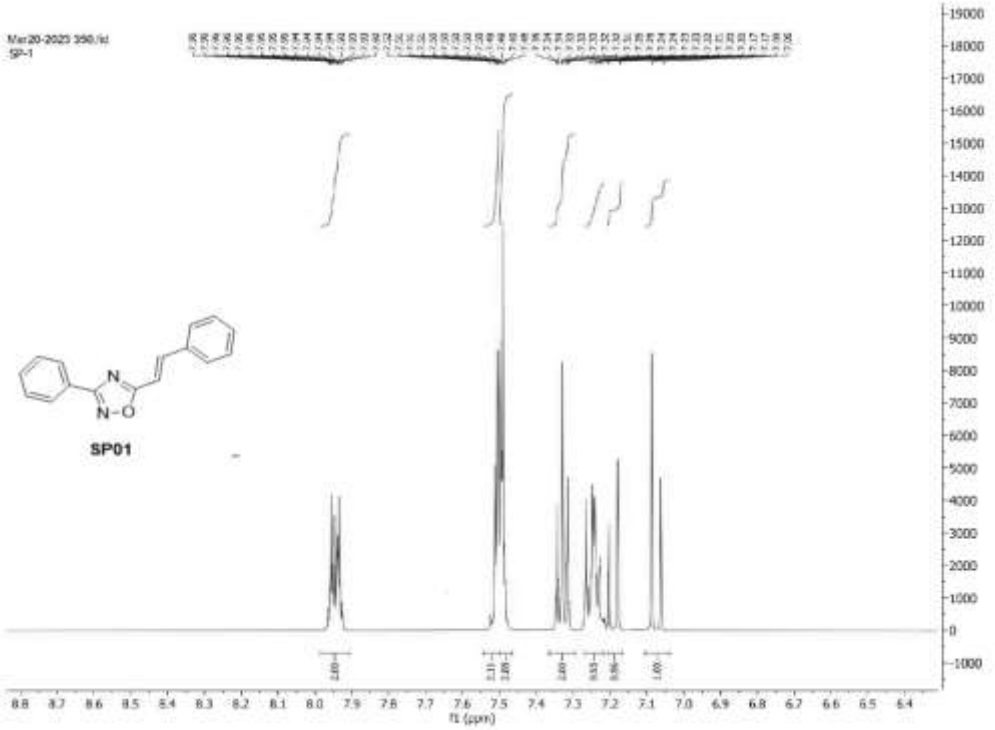
Mar20-2023 390.fid
SP-1
SP01
f1 (ppm)

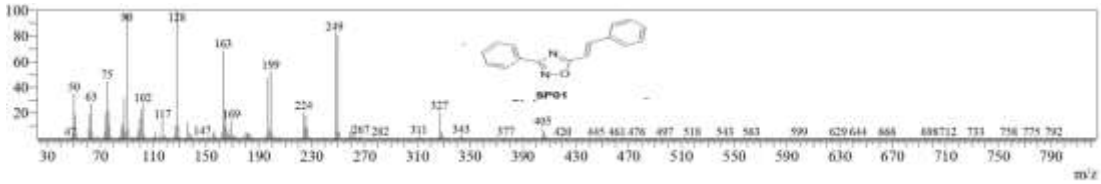
SP01
m/z

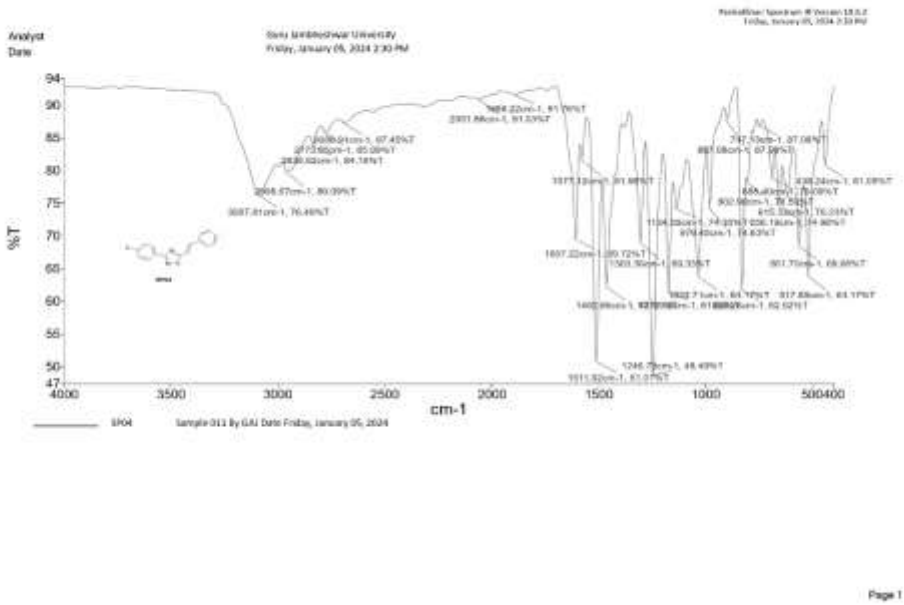
Analyst
Date
%T
cm-1
Page 1

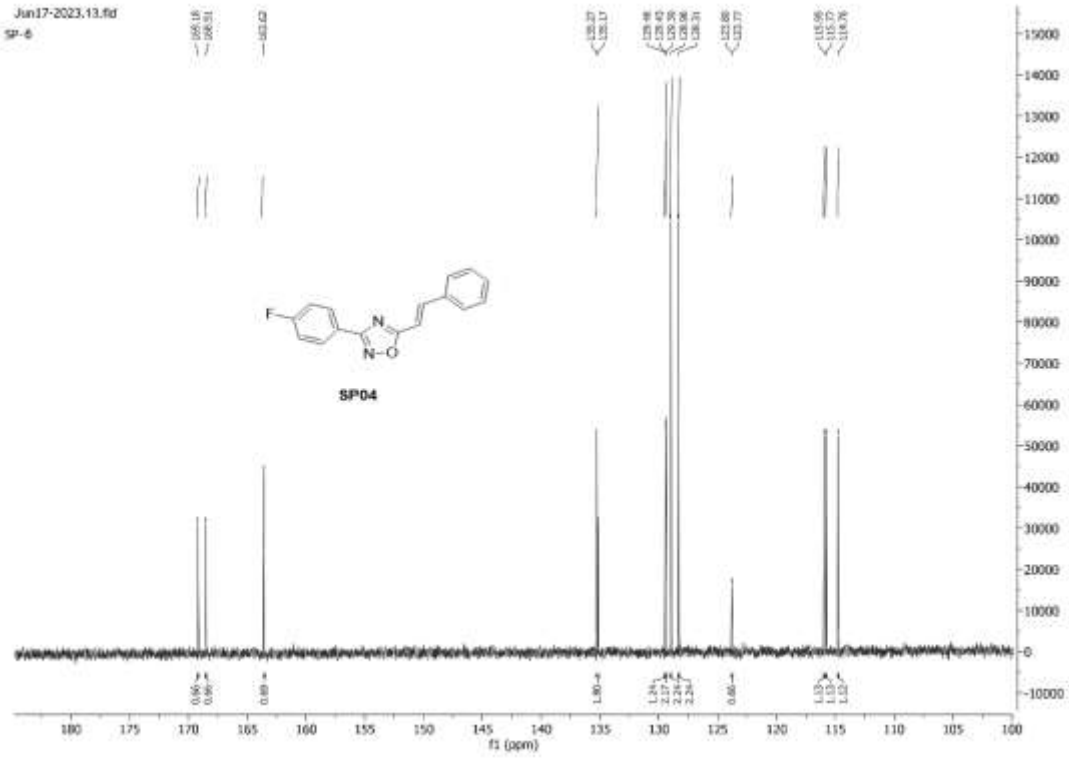
Jun17-2023.13.fid
SP-6
SP04
f1 (ppm)

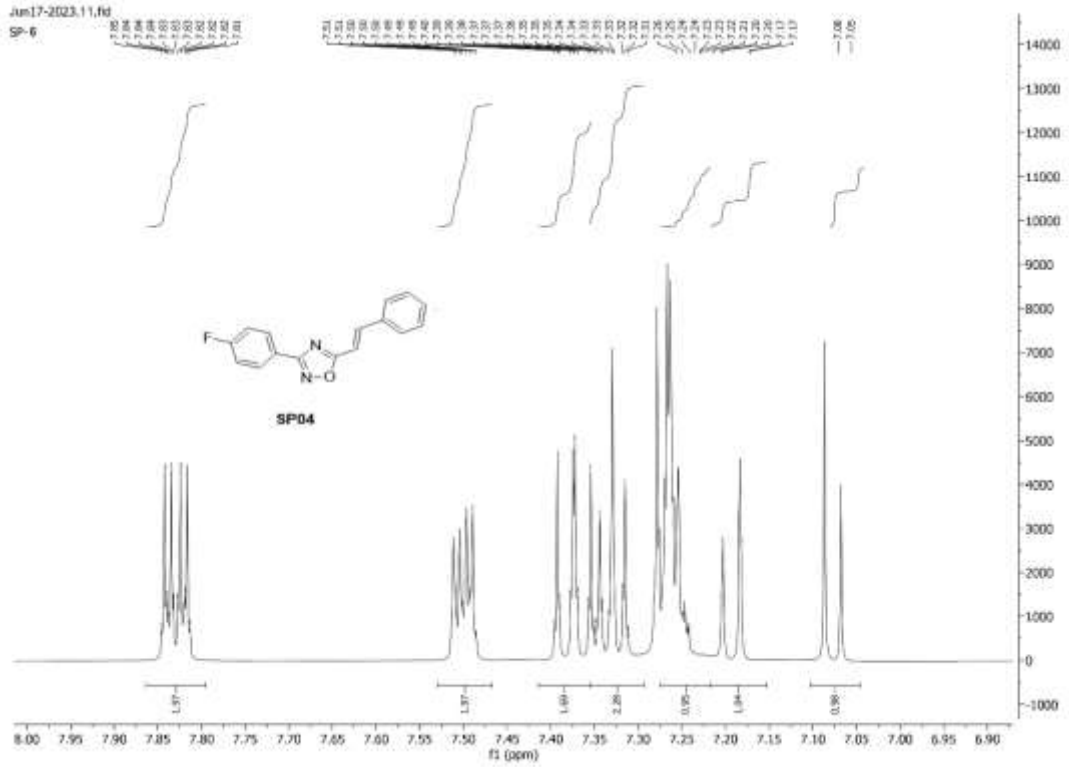
Jun17-2023.11.fid
SP-6
SP04
f1 (ppm)

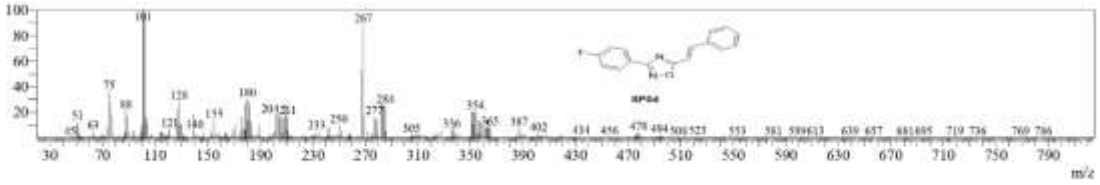
SP04
m/z

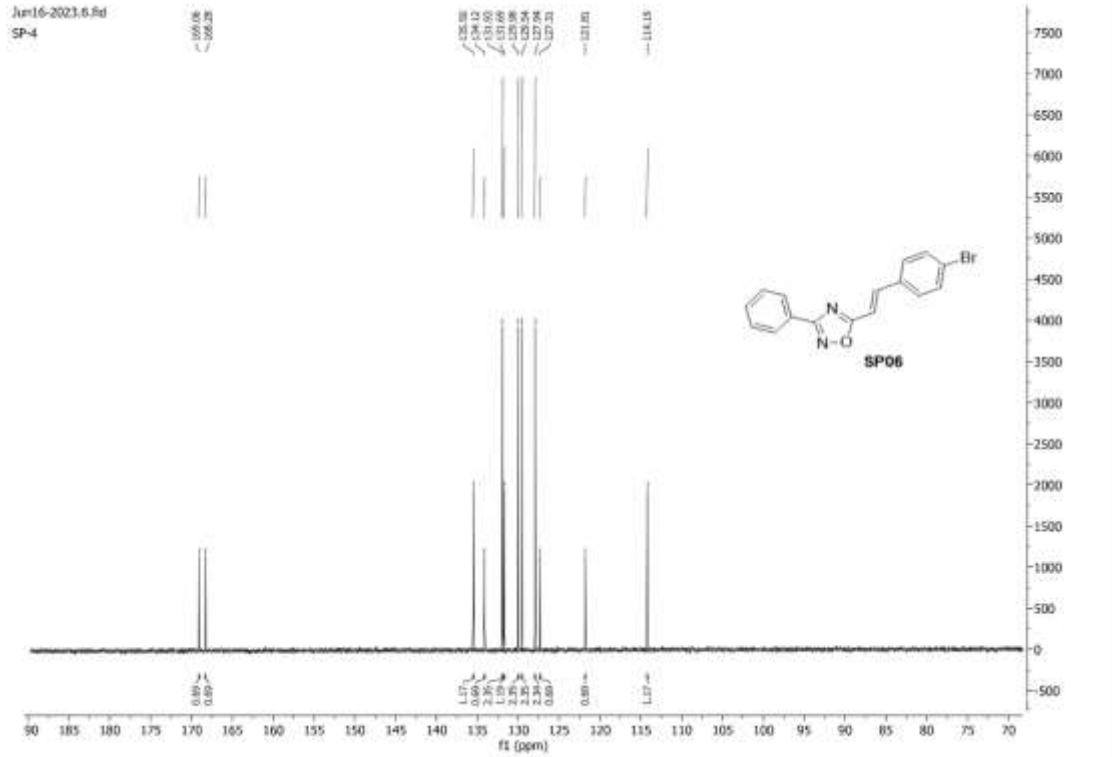
Jun16-2023.6.fid
SP-4
Br
N
N-O
SP06
f1 (ppm)

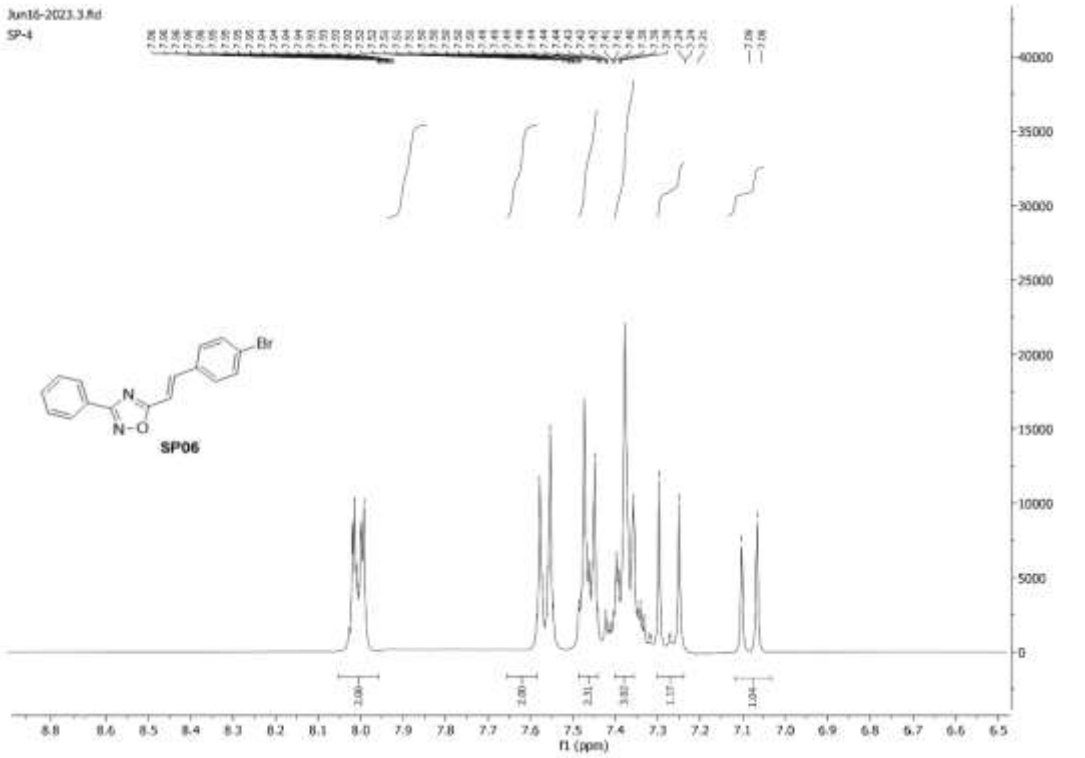
Jun16-2023.3.fid
SP-4
Br
N
N-O
SP06
f1 (ppm)

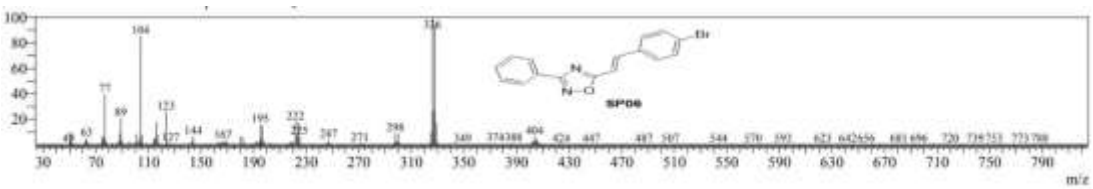
Br
N
N-O
SP06
m/z

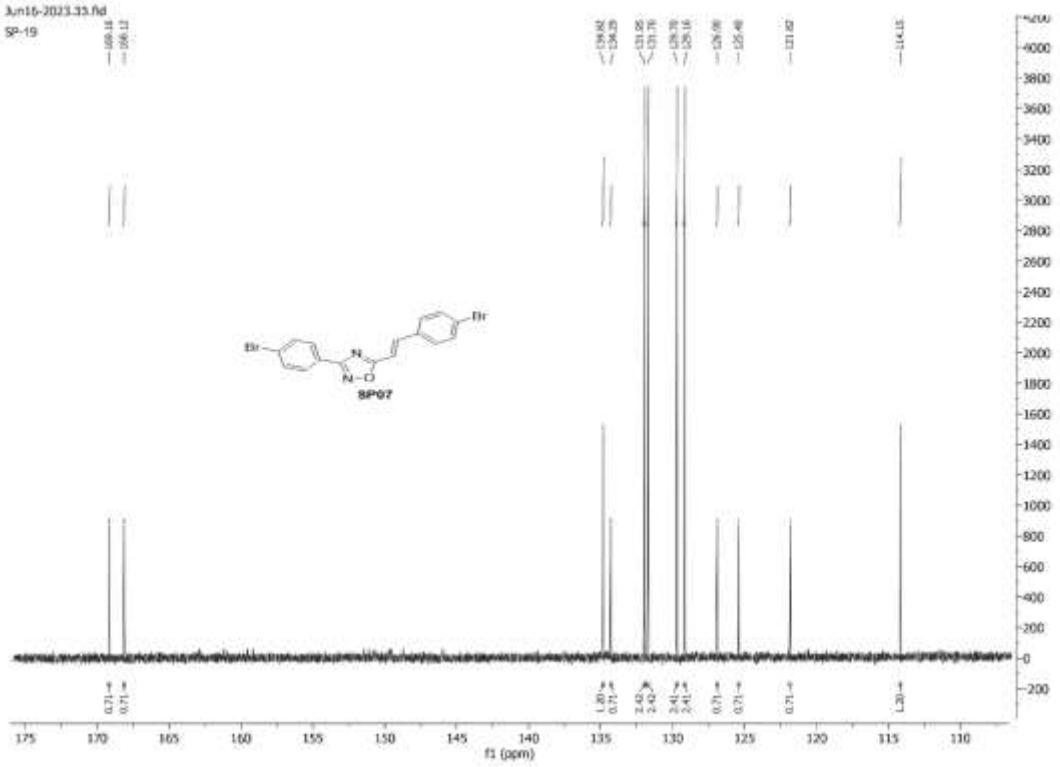
Jun16-2023.33.fid
SP-19
SP07
f1 (ppm)

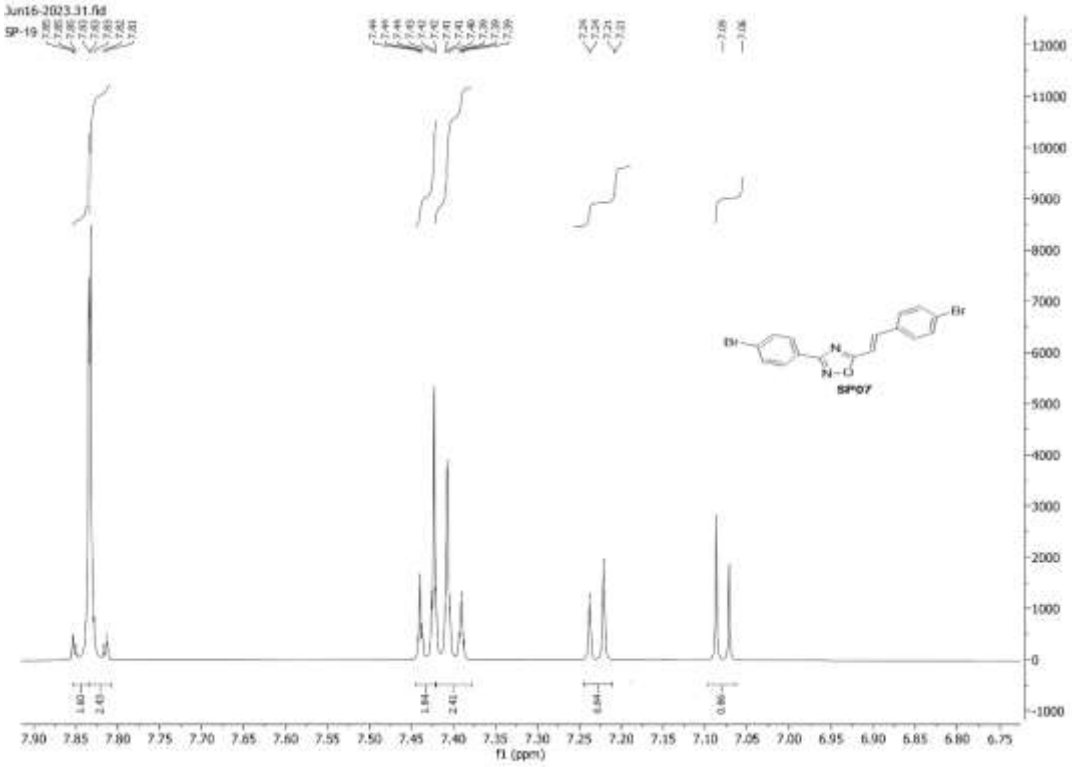
Jun16-2023.31.fid
SP-19
SP07
f1 (ppm)

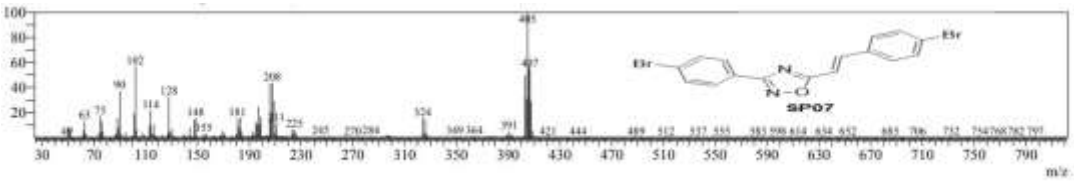
SP07
m/z

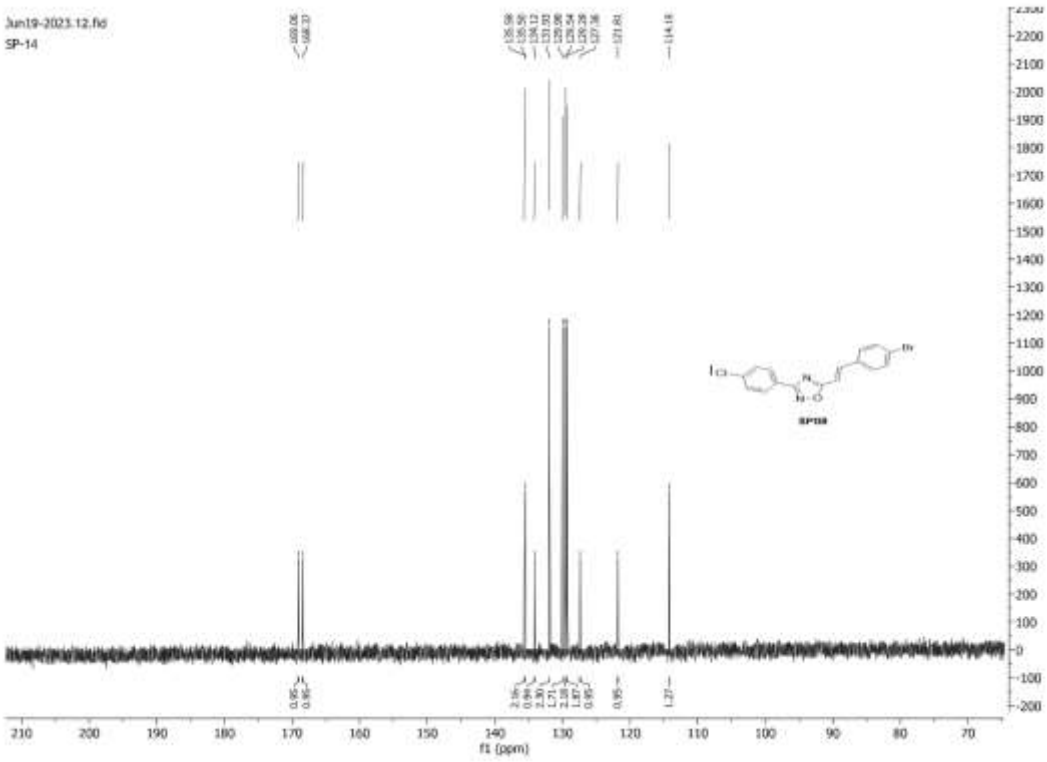
Jun19-2023.12.fid
SP-14
f1 (ppm)

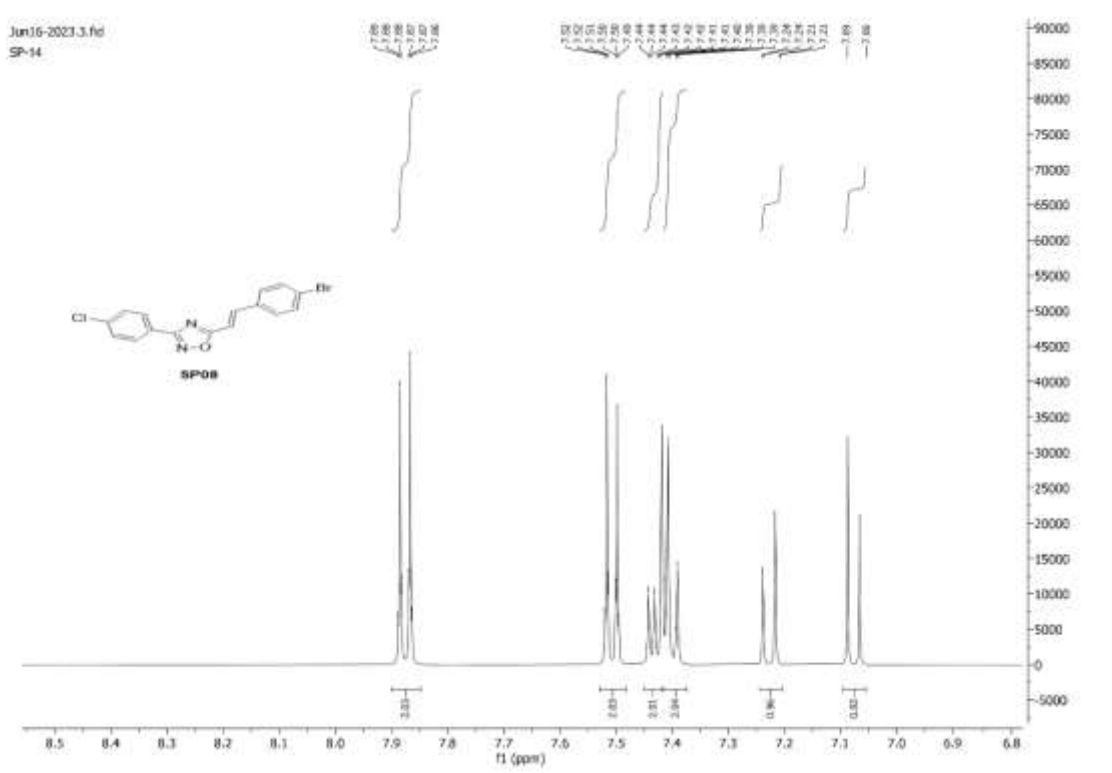
Jun16-2023.3.fid
SP-14
SP08
f1 (ppm)

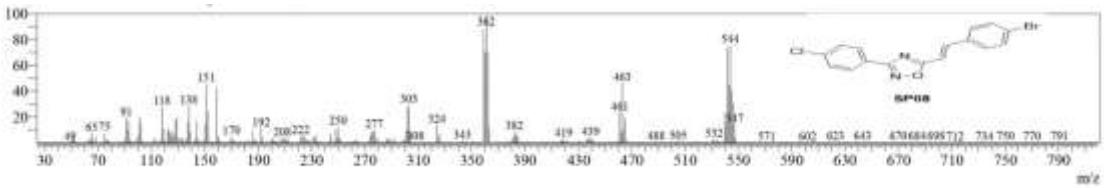
SP08
m/z

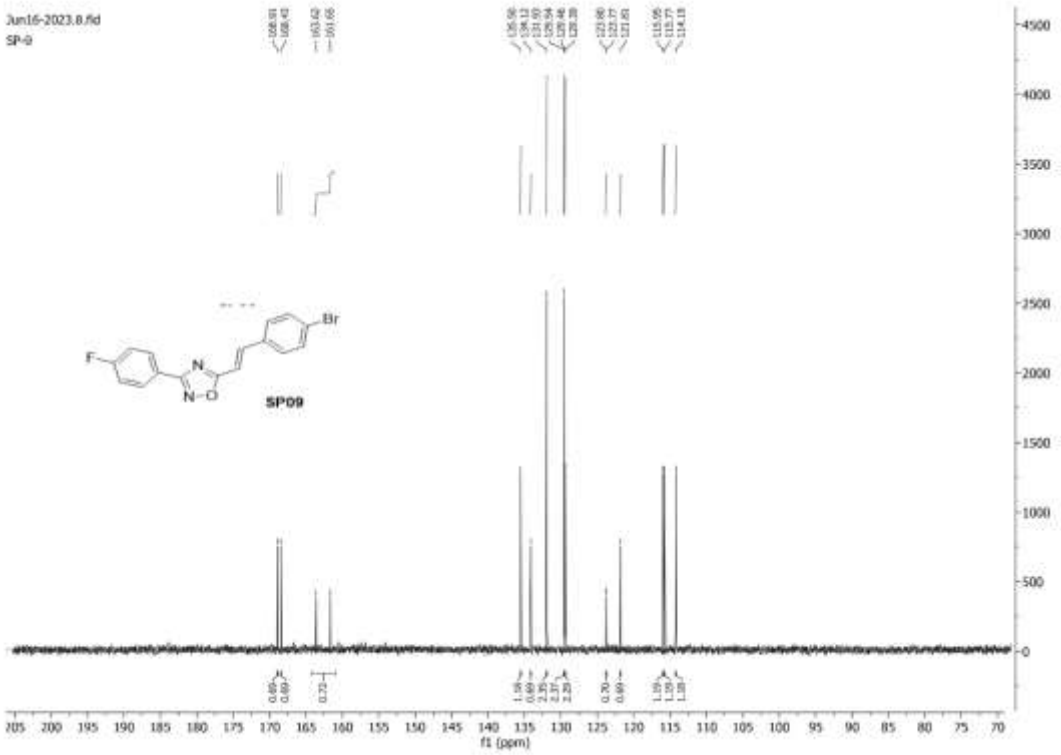
Jun16-2023.8.fid
SP-9
SP09
f1 (ppm)

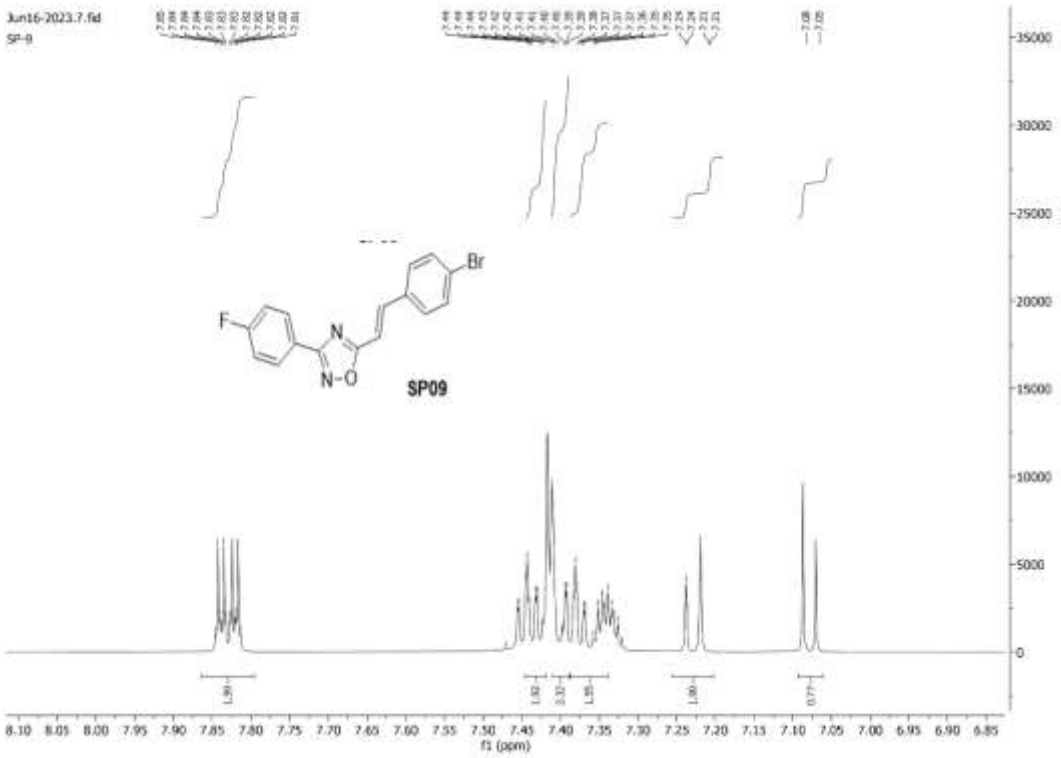
Jun16-2023.7.fid
SP-9
SP09
f1 (ppm)

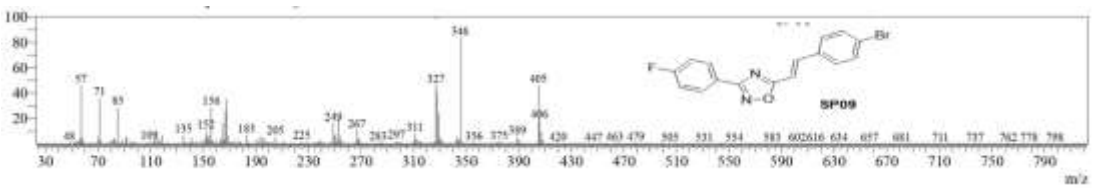
SP09
m/z

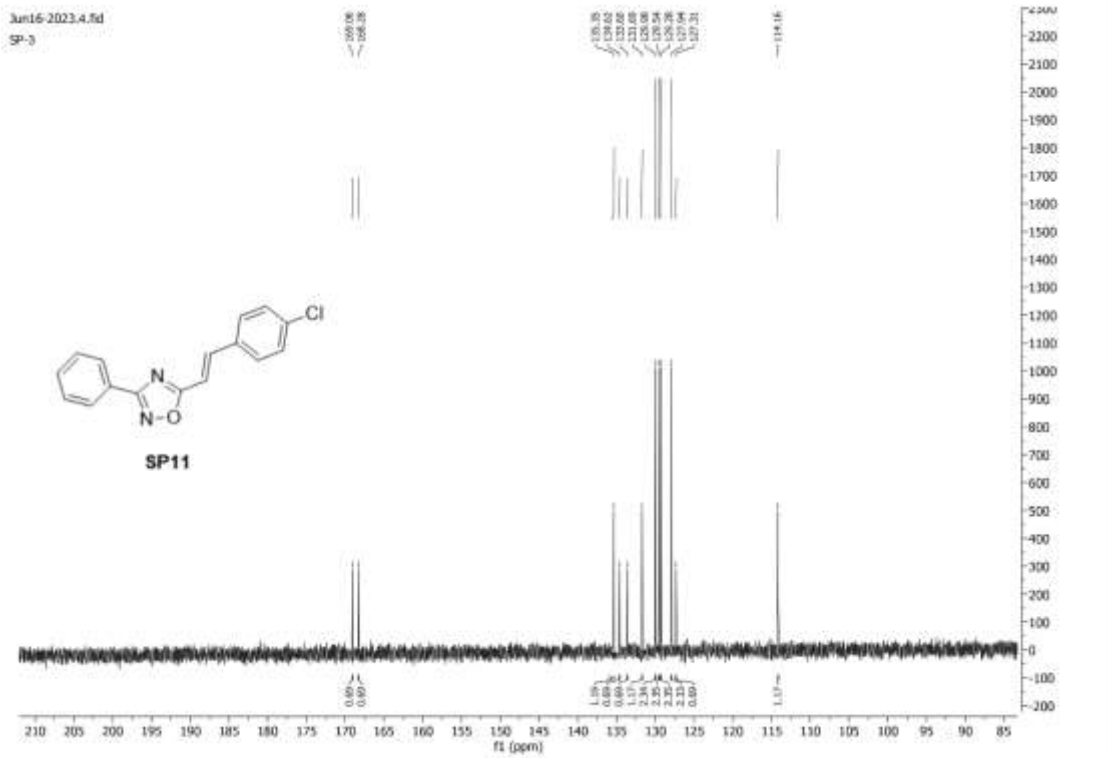
Jun16-2023.4.fid
SP-3
SP11
f1 (ppm)

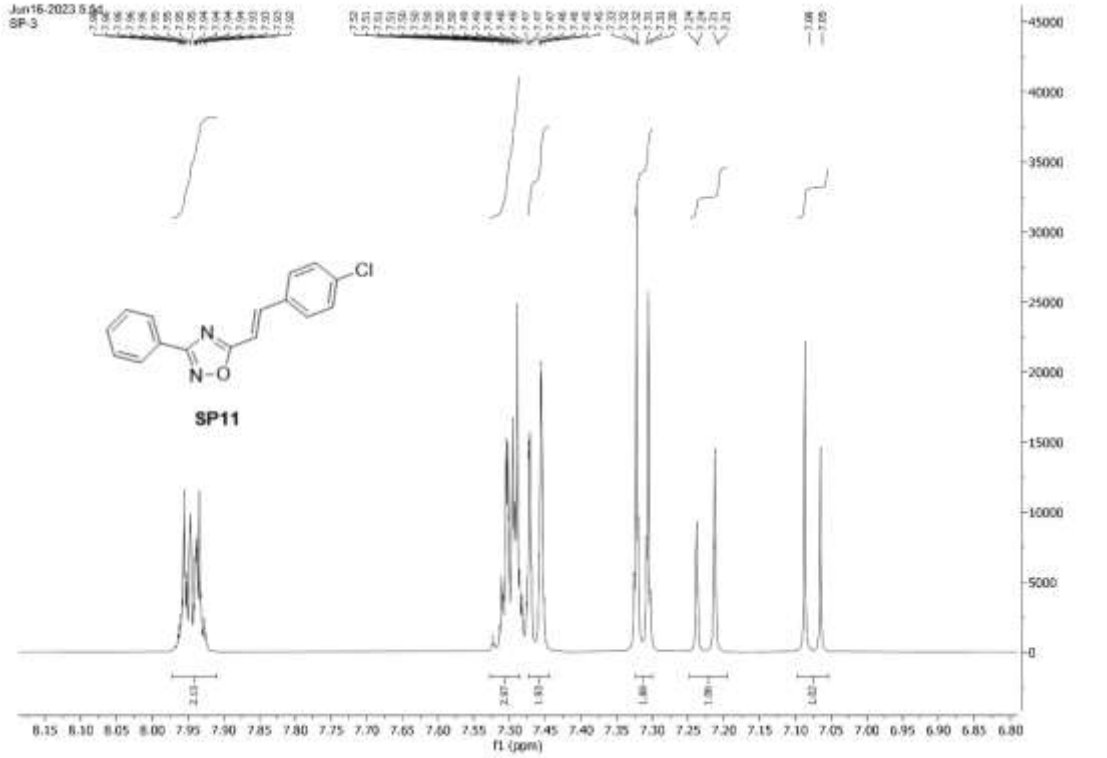
Jun16-2023 5:54
SP-3
Cl
N
N-O
SP11
f1 (ppm)

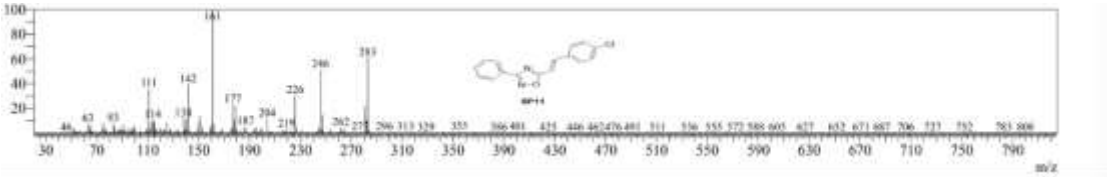
m/z

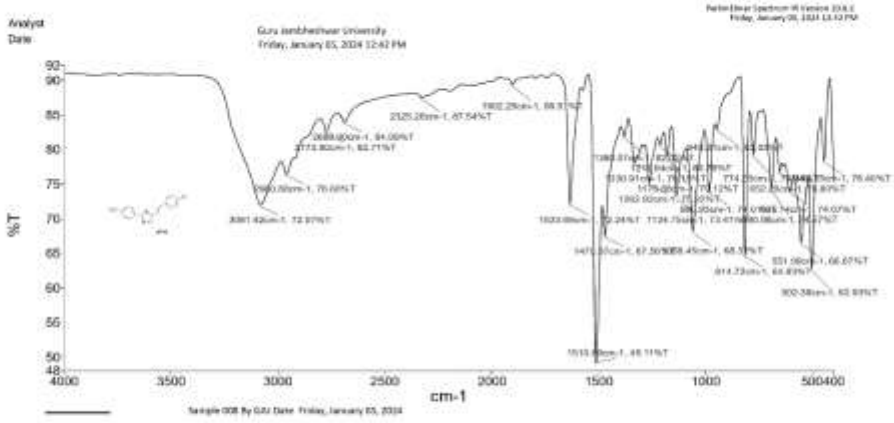
Analyst
Date
Guru Jambheshwar University
Friday, January 05, 2024 12:42 PM
%T
cm-1
4000
3500
3000
2500
2000
1500
1000
500400

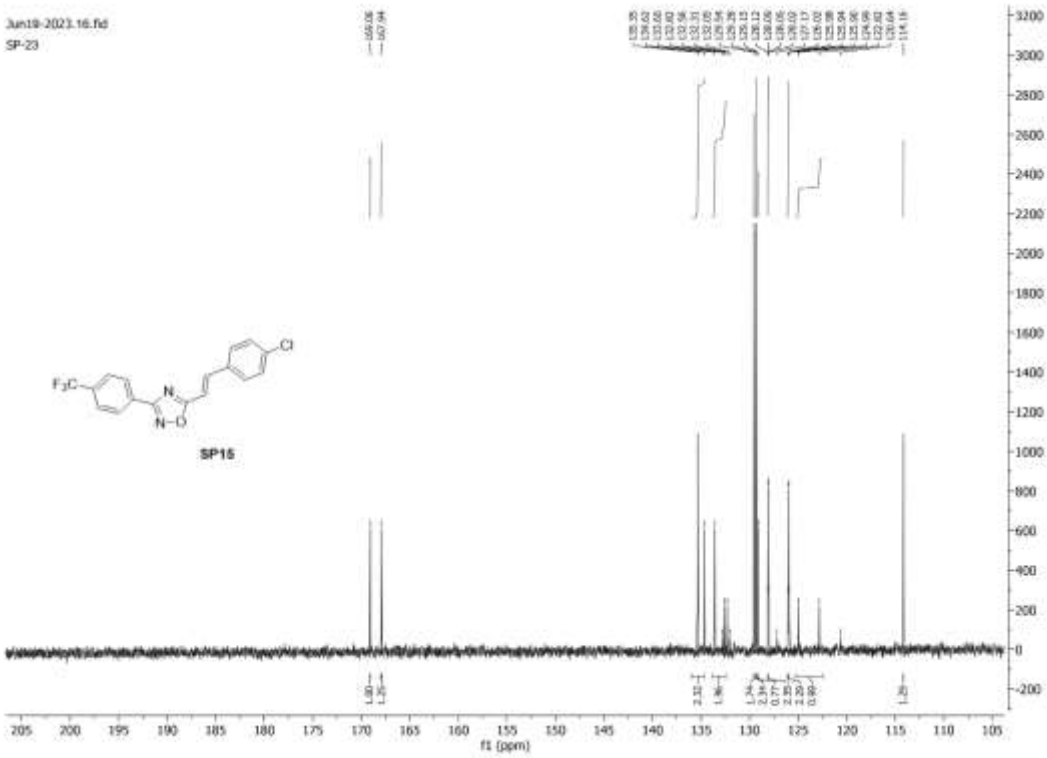
Jun19-2023.16.fid
SP-23
SP15
f1 (ppm)

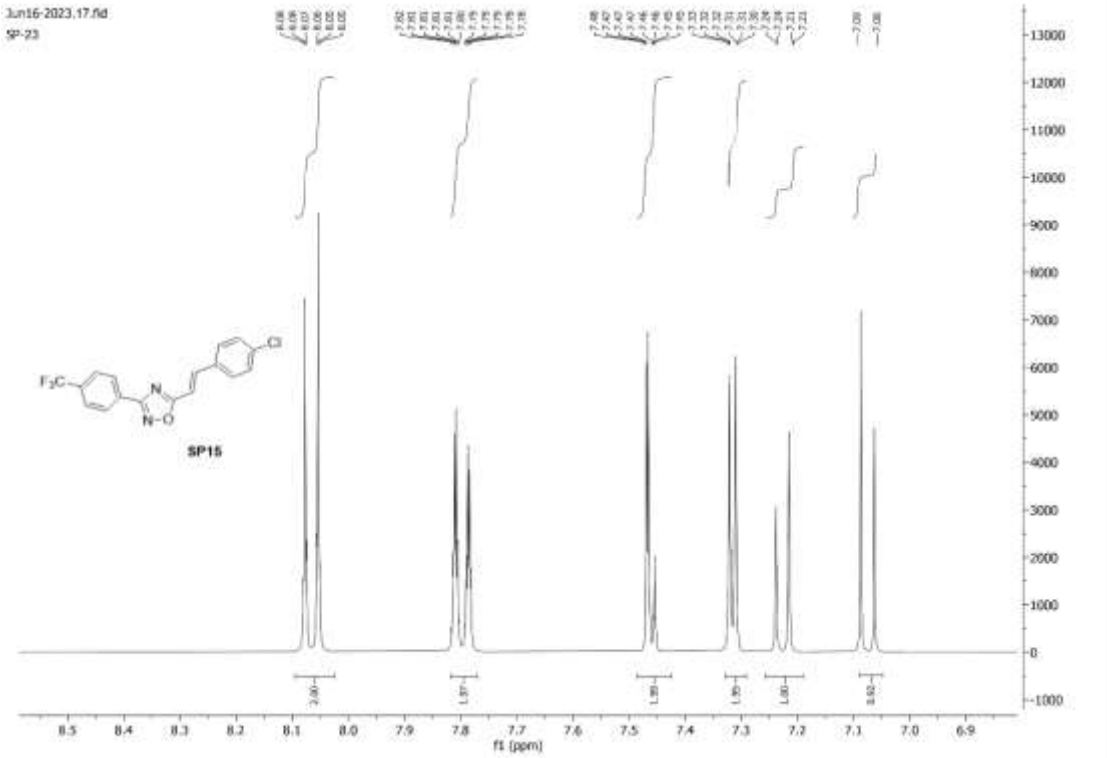
Jun16-2023.17.fid
SP-23
SP15
f1 (ppm)

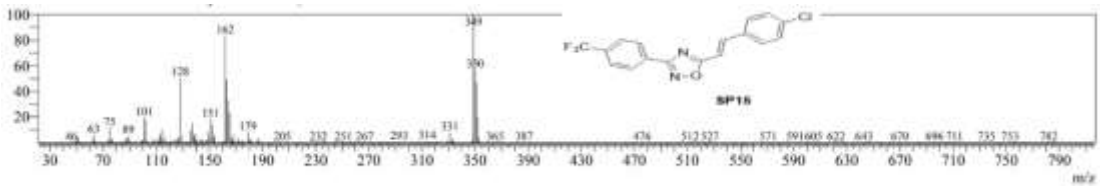
SP15
m/z

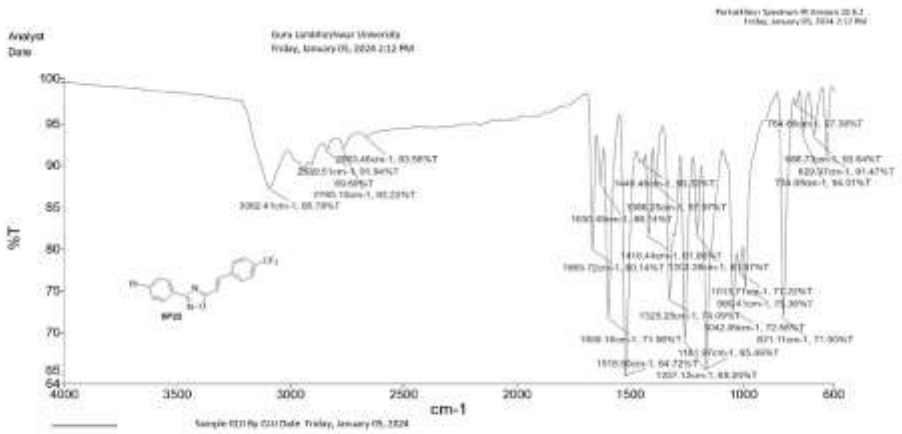
Analyst
Date
%T
cm-1
SP22

Page 1

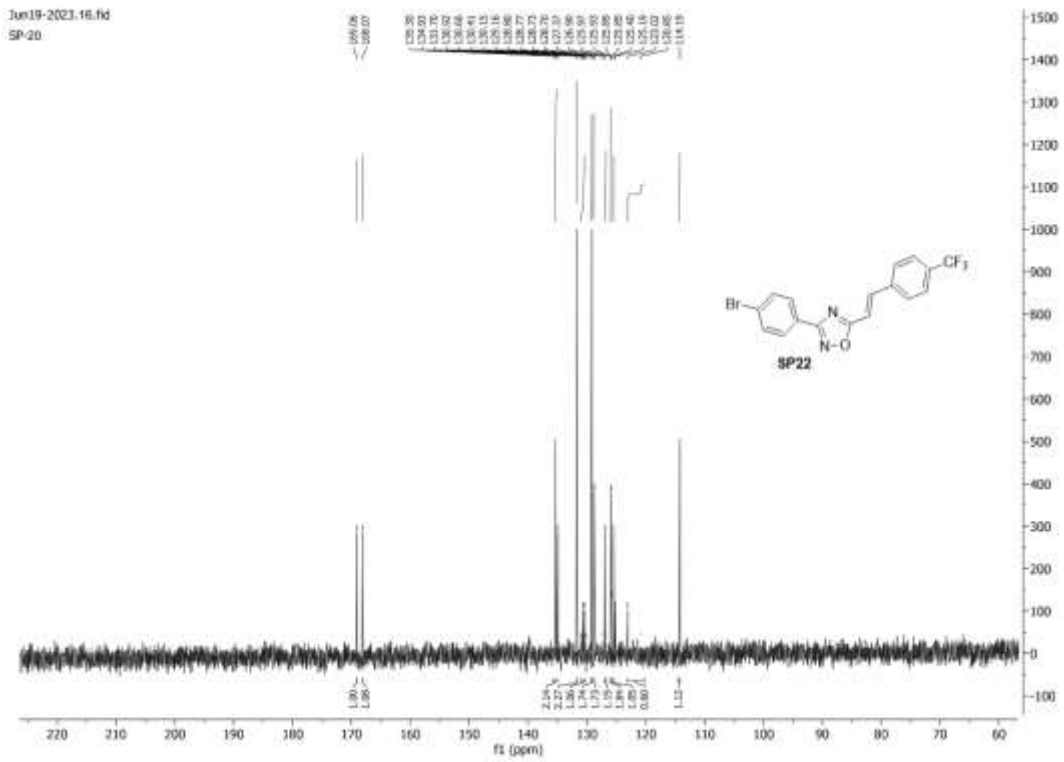
Jun19-2023.16.fid
SP-20
Br
N
N-O
CF3
SP22
f1 (ppm)

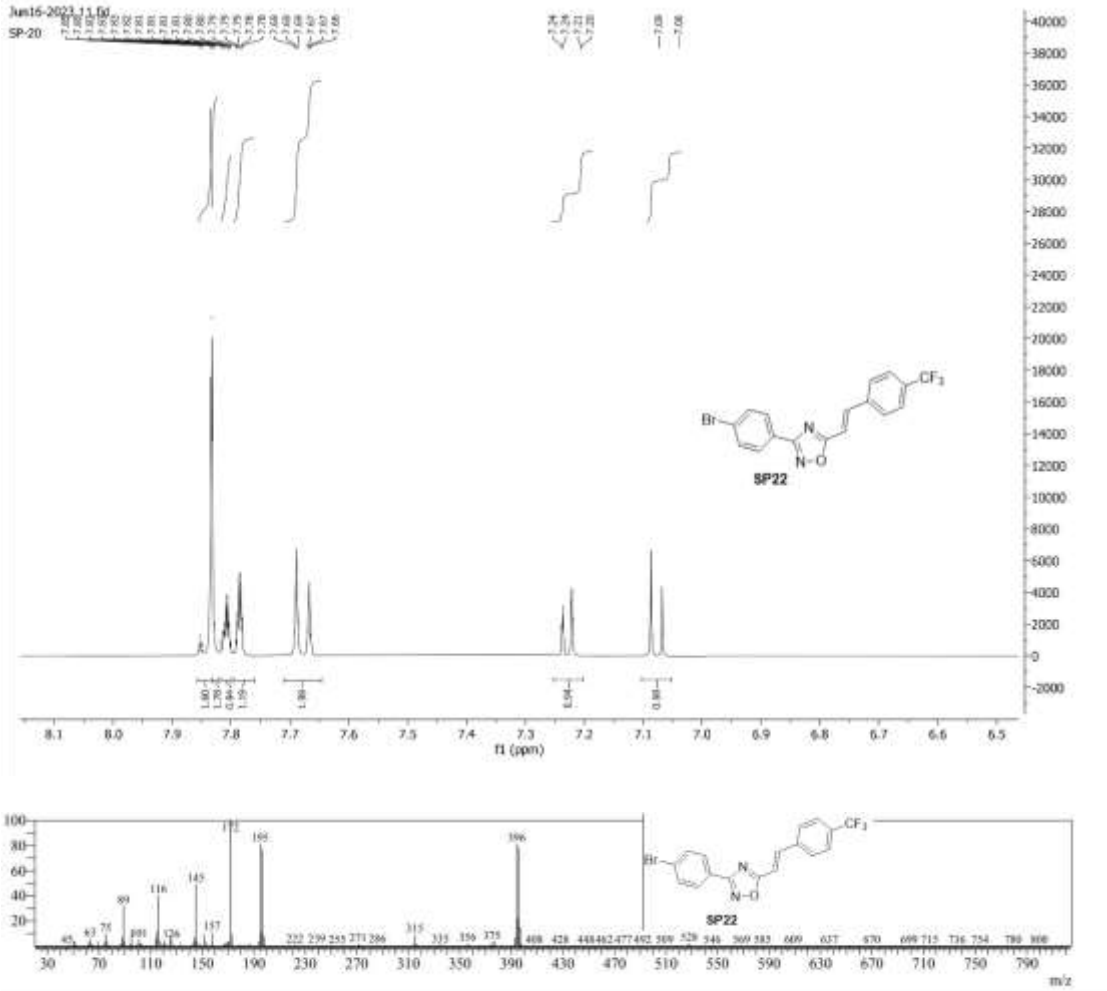
SP-20
SP22
f1 (ppm)
SP22
m/z

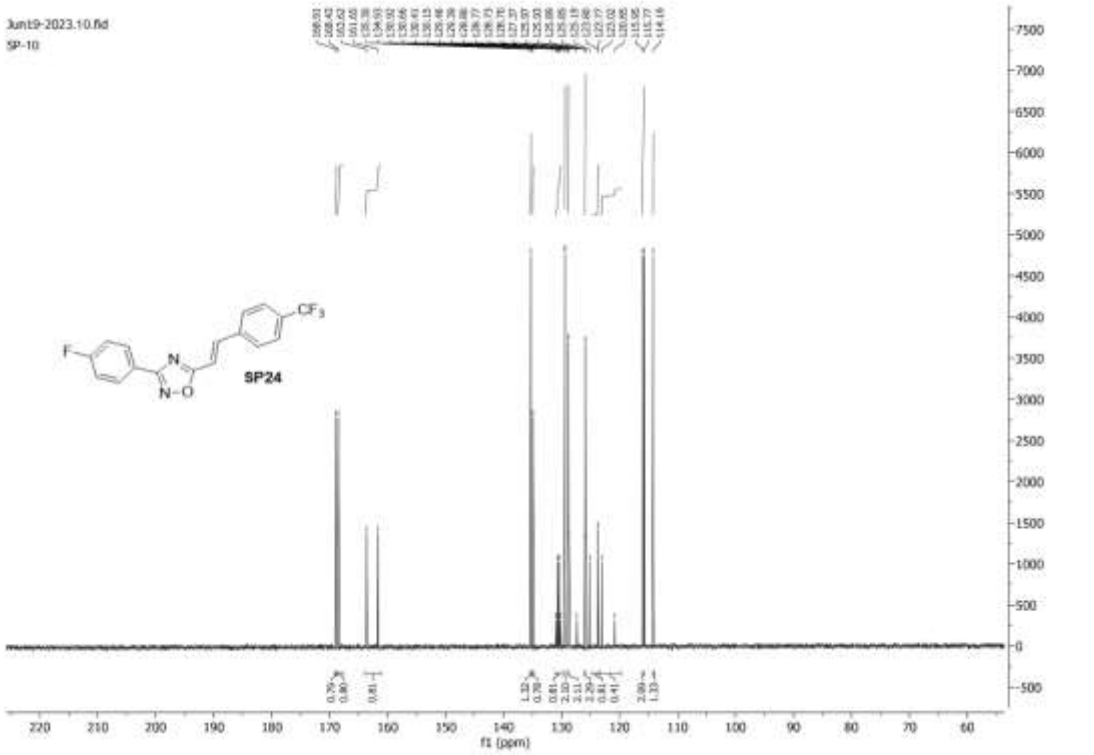
Jun19-2023.10.fid
SP-10
SP24
f1 (ppm)

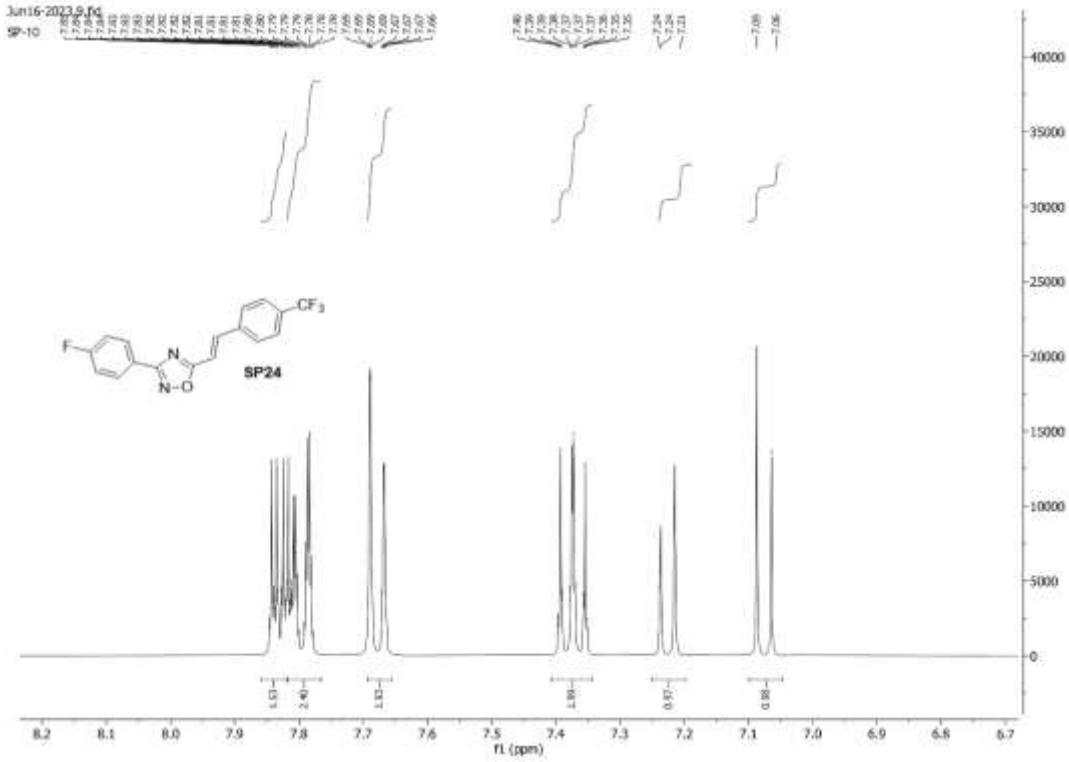
Jun16-2023.9.fid
SP-10
SP24
f1 (ppm)

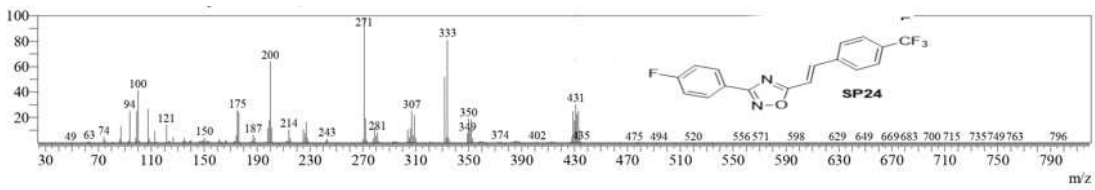
SP24
m/z

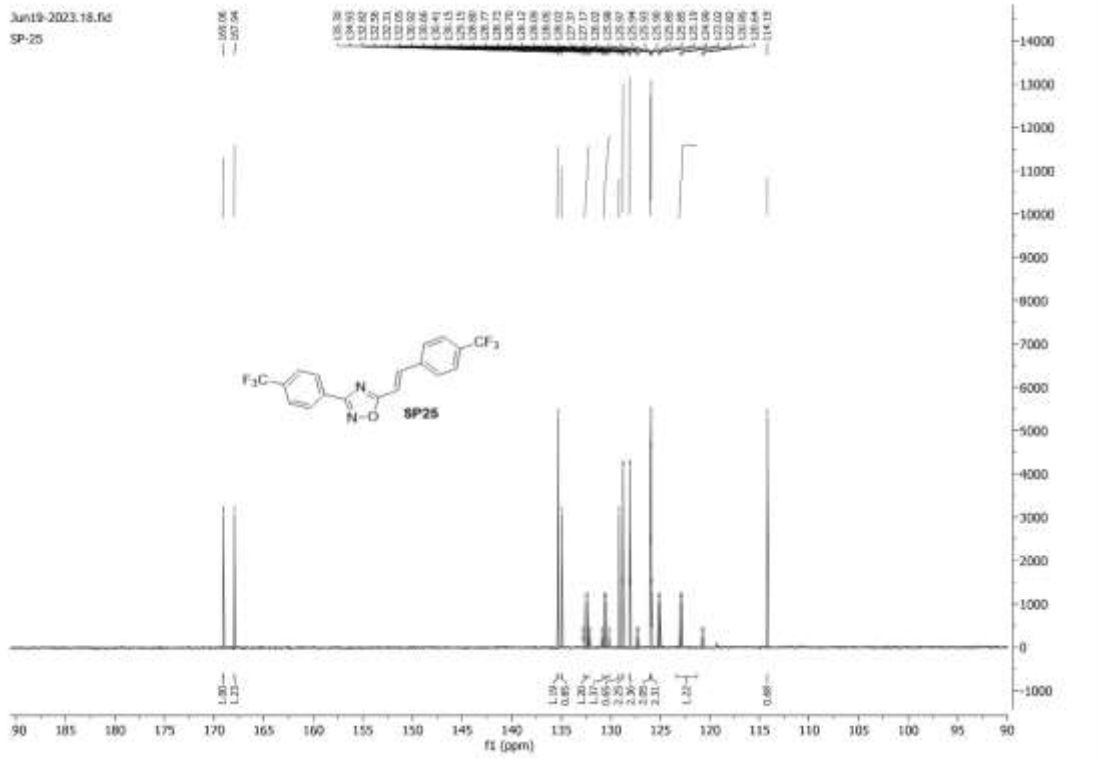
Jun19-2023.18.fid
SP-25
SP25
f1 (ppm)

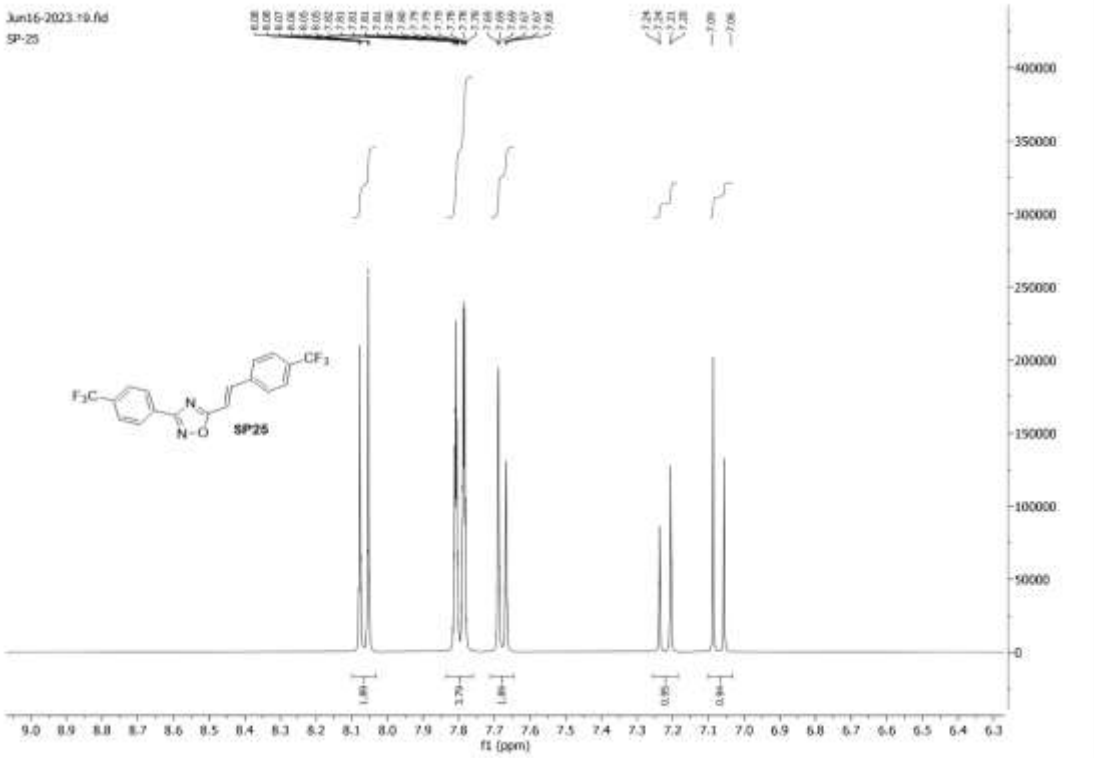
Jun16-2023:r9.fid
SP-25
SP25
f1 (ppm)

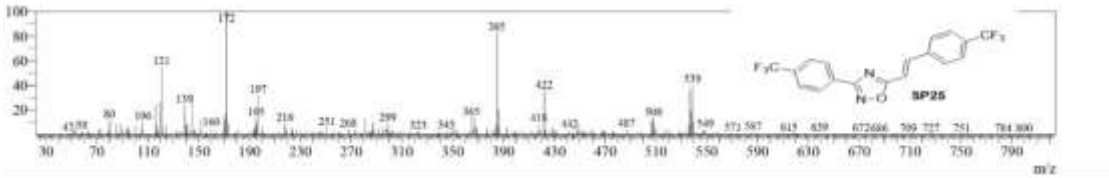
SP25
m/z

III. List of Publications

Research Article from Current Research Work

1. Shubham Kumar, Pankaj Wadhwa, Synthesis, molecular docking and biological evaluation of 1,2,4-oxadiazole based novel non-steroidal derivatives against prostate cancer, *Bioorganic Chemistry*, Volume 143, 2024, 107029, https://doi.org/10.1016/j.bioorg.2023.107029.

Bioorganic Chemistry 143 (2024) 107029

Contents lists available at ScienceDirect

Bioorganic Chemistry

journal homepage: www.elsevier.com/locate/bioorg

Synthesis, molecular docking and biological evaluation of 1,2,4-oxadiazole based novel non-steroidal derivatives against prostate cancer

Shubham Kumar, Pankaj Wadhwa *

School of Pharmaceutical Sciences, Lovely Professional University, Jalandhar Delhi G.T. Road, Phagwara, Punjab 144411, India

ARTICLE INFO

Keywords:
Androgen receptors
Non-steroidal derivatives
PC-3
ROS
Docking studies
ADMET

ABSTRACT

Prostate cancer is one of the most prevalent cancers in men leading to second most death causing cancer in men. Despite the availability of multiple treatment still the prevalence is high for prostate cancer. Steroidal antagonists associated with poor bioavailability, side effects while non-steroidal antagonists show serious side effects like gynecomastia. Therefore, there is a need of potential candidate for the treatment of prostate cancer with better bioavailability, good therapeutic effect and minimal side effects. In the same context, we have designed the series, **SP1–SP25** based 3-phenyl-5-styryl-1,2,4-oxadiazole as the core structure. We successfully synthesized all 25 molecules in this series and characterized them using ^{1}H, ^{13}C-NMR, and mass spectroscopy. Subsequently, we conducted MTT assays using PC-3 cells and observed that all the compounds exhibited a dose-dependent decrease in cell viability. Notably, compounds **SP04**, **SP16**, and **SP19** demonstrated a significant decrease in cell viability and exhibited potent activity compared to the other synthesized molecules and standard drug bicalutamide. Among them, **SP04** emerged as the one of the most potent compounds with an IC_{50} value of 238.13 nM and an 89.99 % inhibition of PC-3 cells, compared to synthesized molecules and standard drug bicalutamide.

Furthermore, we conducted ROS assays and androgen receptor inhibition assays using the potent compound **SP04** and bicalutamide. The results indicated that **SP04** increased ROS production and decreased androgen receptor expression dose-dependent manner. Additionally, we conducted a docking study to analyse the interaction patterns within the active site of the androgen receptor. ADMET analysis revealed that all the compounds exhibited favorable physicochemical properties and manageable toxicity profiles.

1. Introduction

One of the most prevalent cancers and the second leading cause of cancer-related deaths in males worldwide is prostate cancer. As per the recent reports of World Health Organization (WHO), a total of 1.41 million males are suffering from prostate cancer while approx. 3,76,000 were died due to prostate cancer [1,2]. The prostate, situated below the urinary bladder, is a part of male reproductive system and has been classified as an exocrine gland which have a size of a walnut with three lobes [3]. Prostate cancer or carcinoma of the prostate gland is generally developed at the age of 50 years in men with the symptoms like increased frequency of urination, weak flow during urination, red coloured urine/ blood in urine, persistent lower back pain, trouble with urination & incomplete emptying of urinary bladder [4]. These are the various symptoms which can classify a man with prostate cancer. Multiple treatment options are available for the prostate cancer like radiation therapy in which high powered X-Ray damaged the DNA and kill prostate cancer cells [5], cryotherapy by which cancerous cells of prostate were damaged by freezing the tissues, hormonal therapy, removal of prostate by surgery (prostactomy) & chemotherapy [6]. Chemotherapy act by antagonizing the androgen receptors which is precursor for binding of androgens [7]. Chemotherapy is further divided in to two parts: a) Steroids based antiandrogen agents and b) non-steroids based anti-androgen agents for prostate cancer treatment [8]. Few Steroidal antagonists are marketed like cyendelone [9], cyproterone, spironolactone, etc, but these agents have various limitations like poor oral bioavailability & pharmacokinetics [10], potential hepatotoxicity, lack of tissue selectivity, cross reaction with other steroid receptors [11] and structural modifications of steroidal ligands are limited because of its rigidity [12]. Further, many non-steroidal antagonists like flutamide, nilutamide, & bicalutamide, apalutamide, etc., are available in market and more favourable for clinical applications (Fig. 1) [13].

* Corresponding author.
E-mail address: pank@outlook.com (P. Wadhwa).

https://doi.org/10.1016/j.bioorg.2023.107029
Received 12 October 2023; Received in revised form 1 December 2023; Accepted 8 December 2023
Available online 10 December 2023

2. Kumar Shubham, Arora Pinky, Wadhwa Pankaj*, Kaur Paranjeet*, A Rationalized Approach to Design and Discover Novel Non-steroidal Derivatives through Computational Aid for the Treatment of Prostate Cancer, *Current Computer-Aided Drug Design* 2023; 19() . https://dx.doi.org/10.2174/1573409919666230626113346

Send Orders for Reprints to reprints@benthamscience.net

Current Computer-Aided Drug Design, XXXX, XX, 0-0 1

RESEARCH ARTICLE

A Rationalized Approach to Design and Discover Novel Non-steroidal Derivatives through Computational Aid for the Treatment of Prostate Cancer

Shubham Kumar[1], Pinky Arora[2], Pankaj Wadhwa[1,*] and Paranjeet Kaur[3,*]

[1]*Department of Pharmaceutical Chemistry, School of Pharmaceutical Sciences, Lovely Professional University, Jalandhar-Delhi G.T. Road, Phagwara, Punjab, 144411, India;* [2]*Department of Biochemistry, School of Bioengineering & Biosciences, Lovely Professional University, Jalandhar-Delhi G.T. Road, Phagwara, Punjab, 144411, India;* [3]*Chitkara College of Pharmacy, Chitkara University, Punjab, India*

Abstract: ***Background***: Prostate cancer is one of the most prevalent cancers in men, leading to the second most common cause of death in men. Despite the availability of multiple treatments, the prevalence of prostate cancer remains high. Steroidal antagonists are associated with poor bioavailability and side effects, while non-steroidal antagonists show serious side effects, such as gynecomastia. Therefore, there is a need for a potential candidate for the treatment of prostate cancer with better bioavailability, good therapeutic effects, and minimal side effects.

Objective: This current research work focused on identifying a novel non-steroidal androgen receptor antagonist through computational tools, such as docking and *in silico* ADME/T analysis.

Methods: Molecules were designed based on a literature survey, followed by molecular docking of all designed compounds and ADMET analysis of the hit compounds.

Results: A library of 600 non-steroidal derivatives (*cis* and *trans*) was designed, and molecular docking was performed in the active site of the androgen receptor (PDBID: 1Z95) using AutoDock Vina 1.5.6. Docking studies resulted in 15 potent hits, which were then subjected to ADME analysis using SwissADME. ADME analysis predicted three compounds (**SK-79**, **SK-109**, and **SK-169**) with the best ADME profile and better bioavailability. Toxicity studies using Protox-II were performed on the three best compounds (**SK-79**, **SK-109**, and **SK-169**), which predicted ideal toxicity for these lead compounds.

Conclusion: This research work will provide ample opportunities to explore medicinal and computational research areas. It will facilitate the development of novel androgen receptor antagonists in future experimental studies.

ARTICLE HISTORY

Received: December 05, 2022
Revised: March 16, 2023
Accepted: March 15, 2023

DOI:
10.2174/1573409919666230626113346

Keywords: Androgen receptors, non-steroidal derivatives, prostate cancer, docking studies, ADME, toxicity.

1. INTRODUCTION

Prostate cancer is one of the most prevalent cancers and the second leading cause of cancer-related deaths in males worldwide [1]. According to recent reports from the World Health Organization (WHO), approximately 1.41 million males are suffering from prostate cancer, with approximately 376,000 deaths attributed to the disease [2]. The prostate, located below the urinary bladder, is a part of the male reproductive system and is classified as an exocrine gland. It is roughly the size of a walnut and consists of three lobes [3]. Prostate cancer, or carcinoma of the prostate gland, generally develops in men around the age of 50 and is characterized by symptoms such as increased frequency of urination, weak flow during urination, red-colored urine/blood in urine, persistent lower back pain, trouble with urination, and incomplete emptying of the urinary bladder [4]. These various symptoms can help identify the presence of prostate cancer. Multiple treatment options are available for prostate cancer, including radiation therapy, which uses high-powered X-rays to damage DNA and kill prostate cancer cells [5] cryotherapy, which involves freezing the cancerous cells of the prostate tissue; hormonal therapy; surgical removal of the prostate (prostatectomy); and chemotherapy [6]. Chemotherapy works by antagonizing the androgen receptors, which are involved in the binding of androgens [7]. Chemotherapy can

*Address correspondence to these authors at the Department of Pharmaceutical Chemistry, School of Pharmaceutical Sciences, Lovely Professional University, Jalandhar-Delhi G.T. Road, Phagwara, Punjab, 144411, India and Chitkara College of Pharmacy, Chitkara University, Chandigarh-Patiala National Highway (NH-64), Chandigarh, Punjab, 144411, India; Tel: +91-9063754780 and +91-9041308499; E-mails: pankajwadhwa88@gmail.com and paran.pharma@gmail.com

1573-4099/XX $65.00+.00

Filed Patent From the Research Work

Office of the Controller General of Patents, Designs & Trade Marks
Department for Promotion of Industry and Internal Trade
Ministry of Commerce & Industry,
Government of India

INTELLECTUAL PROPERTY INDIA

Application Details	
APPLICATION NUMBER	202311080213
APPLICATION TYPE	ORDINARY APPLICATION
DATE OF FILING	25/11/2023
APPLICANT NAME	**LOVELY PROFESSIONAL UNIVERSITY**
TITLE OF INVENTION	DESIGN, SYNTHESIS AND BIOLOGICAL EVALUATION OF 3,5-DISUBSTITUTED-1,2,4-OXADIZOLES AS ANTI-PROSTATE CANCER AGENTS
FIELD OF INVENTION	BIOTECHNOLOGY
E-MAIL (As Per Record)	ashish.iprindia@hotmail.com
ADDITIONAL-EMAIL (As Per Record)	
E-MAIL (UPDATED Online)	
PRIORITY DATE	
REQUEST FOR EXAMINATION DATE	--
PUBLICATION DATE (U/S 11A)	29/12/2023

Application Status	
APPLICATION STATUS	Awaiting Request for Examination

View Documents

Filed → Published → RQ Filed → Under Examination → Disposed

Review Article from Project Work

Chaudhary Manish, Kumar Shubham, kaur Paranjeet*, Sahu Kumar Sanjeev and Mittal Amit, Comprehensive Review on Recent Strategies for Management of Prostate Cancer: Therapeutic Targets and SAR, *Mini-Reviews in Medicinal Chemistry* 2023; 23() . https://dx.doi.org/10.2174/1389557523666230911141339

REVIEW ARTICLE

Comprehensive Review on Recent Strategies for Management of Prostate Cancer: Therapeutic Targets and SAR

Manish Chaudhary[1], Shubham Kumar[1], Paranjeet Kaur[1,2,*], Sanjeev Kumar Sahu[1] and Amit Mittal[3]

[1]*School of Pharmaceutical Sciences, Lovely Professional University, Jalandhar-Delhi G.T. Road, Phagwara, Punjab, 144001, India;* [2]*Chitkara College of Pharmacy, Chitkara University, Punjab, India;* [3]*Faculty of Pharmaceutical Sciences, Desh Bhagat University, Amloh Road, Mandi Gobindgarh, Punjab, 147301, India*

ARTICLE HISTORY

Received: May 23, 2023
Revised: July 09, 2023
Accepted: July 18, 2023

DOI:
10.2174/1389557523666230911141339

Abstract: Prostate cancer is a disease that is affecting a large population worldwide. Androgen deprivation therapy (ADT) has become a foundation for the treatment of advanced prostate cancer, as used in most clinical settings from neo-adjuvant to metastatic stage. In spite of the success of ADT in managing the disease in the majority of men, hormonal manipulation fails eventually. New molecules are developed for patients with various hormone-refractory diseases. Advancements in molecular oncology have increased understanding of numerous cellular mechanisms which control cell death in the prostate and these insights can lead to the development of more efficacious and tolerable therapies for carcinoma of the prostate. This review is focused on numerous therapies that might be a boon for prostate therapy like signaling inhibitors, vaccines, and inhibitors of androgen receptors. Along with these, various bioactive molecules and their derivatives are highlighted, which act as potential anti-prostate cancer agents. This article also emphasized the recent advances in the field of medicinal chemistry of prostate cancer agents.

Keywords: Prostate cancer, therapeutic targets, recent advances, flavonoids, bicalutamide, arylpiperazine

1. INTRODUCTION

Health challenges cause major implications on the population's economic standards, life expectancy and mortality. These challenges have adverse effects on healthcare costs, productivity, and economic growth, with increased expenses and decreased efficiency. Additionally, high mortality rates and shorter life expectancy lead to a decline in human capital. Cancer is one of the major contributors to global pressures with epidemiological evidence of about more than 14 million new cases and a high mortality rate of approximately 8 million every year. The severity of cancer's consequences and its impact on individuals and communities highlights the pressing need for effective prevention, early detection, and advancements in treatments [1]. Cancer is the disease in which body cells begin to divide without stopping as these cells lose the contact inhibition property and may spread into surrounding tissues. Moreover, cancer cells possess the capability to invade nearby tissues and spread throughout the body, a process known as metastasis. This invasive nature of cancer contributes to its progression and presents challenges in its treatment [2, 3].

*Address correspondence to this author at the School of Pharmaceutical Sciences, Lovely Professional University, Jalandhar-Delhi G.T. Road, Phagwara, Punjab, 144001, India; Mobile no: +91-9041308499;
E-mail: paran.pharma@gmail.com

1389-5575/xx $65.00+.00

Prostate cancer is the most common with second major mortality rate among men globally (with more than 1.2 million confirmed cases and 358,000 deaths in accordance with data from the GLOBOCAN database provided by WHO). It occurs when cells of prostate gland grow uncontrollably. The prostate is male reproductive organ and produces 1/3rd part of semen. Prostate gland is present below the bladder and in front of the rectum. Just behind the prostate, seminal vesicles are present that make 1/3rd part of the semen. The urethra passes through the center of the prostate [4, 5].

Mainly prostate cancers are adenocarcinomas. This cancer occurs from the gland cells. Other types of cancer like small cell carcinomas, Transitional cell carcinomas and Sarcomas can also occur in prostate. These types of prostate cancer are generally rare. If the patient is diagnosed with prostate cancer, he is certainly having an adenocarcinoma. Some of these spread fast, however most of these, grow slowly. In fact, certain autopsy studies suggest that many older men (and some young) who died (by other disease or accident) might had cancer which did not affected their lives.

1.1. Causes of Prostate Cancer

This is generally caused DNA alterations of a normal glandular cell. DNA is essential chemical in the cells which makes up genes, responsible for controlling functions of cell [6]. DNA changes can be:

IV. Other Allied Publications

1. Handa Jasmeen, Kumari Baby, Negi Samir, Arora Pinky and **Kumar Shubham***, Utilization of computational tools for discovery of reticuline based derivatives as AChES inhibitors to treat Alzheimer's disease, Letters in Drug Design & Discovery 2023; 20() . https://dx.doi.org/10.2174/1570180820666230713112757.

2. Tiwari S, Kaur P, Gupta D, Chaudhury S, Chaudhary M, Mittal A, **Kumar S**, Sahu SK. An Insight into the Development of Potential Antidiabetic Agents along with their Therapeutic Targets. Endocr Metab Immune Disord Drug Targets. 2023 May 22. doi: 10.2174/1871530323666230522112758. Epub ahead of print. PMID: 37218182.

3. Mittal Roopal*, Sharma Shailesh, Mittal Amit, **Kumar Shubham** and Kushwah Singh Ajay, Virtual Screening, Molecular Docking, and Physiochemical Analysis of Novel 1,3-diphenyl-2-propene-1-one as Dual COX-2/5-LOX Inhibitors, Letters in Drug Design & Discovery 2022; 19() . https://dx.doi.org/10.2174/1570180819666220523093435

4. Sharma Shivani, Mittal Amit, **Kumar Shubham**, Mittal Amit. Structural Perspectives and Advancement of SGLT2 Inhibitors for the Treatment of Type 2 Diabetes. Curr Diabetes Rev. 2022;18(6):e170921196601. doi: 10.2174/1573399817666210917122745. PMID: 34538233.

5. **Kumar Shubham**, Mittal Anu, Mittal Amit. A review upon medicinal perspective and designing rationale of DPP-4 inhibitors. Bioorg Med Chem. 2021 Sep 15;46:116354. doi: 10.1016/j.bmc.2021.116354. Epub 2021 Aug 10. PMID: 34428715.

V. Conference Attended

AMITY UNIVERSITY
MADHYA PRADESH

INTERNATIONAL CONFERENCE
on
RECENT TRENDS IN CHEMICAL BIOLOGY AND DRUG DISCOVERY
8th & 9th September, 2021

Certificate of Award

This is to Certify that **Dr./Mr. Shubham Kumar,** Lovely Professional University, Delhi G.T. Road, Phagwara was awarded **THIRD Position** for his paper presentation in International conference on "Recent Trends In Chemical Biology and Drug Discovery" organized by Amity Institute of Pharmacy, Amity University Madhya Pradesh, Gwalior during 8th and 9th September, 2021.

Dr. S. Vijayaraj	Dr. V. Murugesan	Dr. S. Mohanalakshmi	Prof. (Dr.) A.N. Nagappa
(Co-Organiser)	(Organising Secretary)	(Joint Convener)	(Convener)

ICSPC

MEDICRATES

Phri

LOVELY PROFESSIONAL UNIVERSITY

Certificate of Merit

This is to certify that Prof./Dr./Mr./Ms. Shubham Kumar of Lovely Professional University has participated in **Poster Presentation/Oral Presentation** on the topic entitled Design & Discovery of Non steroidal based derivatives against Prostate Cancer and stood 3rd International Conference on Synthetic and Pharmaceutical Chemistry (ICSPC) held from 15th -16th September 2023 organized by School of Pharmaceutical Sciences, under the aegis of Lovely Professional University, Punjab.

Dr. Sanjeev Kumar Sahu (Program Chair)

Dr. Manish Vyas (General Chair)

Dr. Monica Gulati (Conference Chair)

EUSTM European Society for Translational Medicine

Certificate of Attendance & CPD

This certificate is awarded for Attending 9 th Annual Virtual Congress of the European Society for Translational Medicine on Immunotherapeutics
(EUSTM-2022) | 3-5 October 2022 (Held Virtually)

Shubham Kumar

EUSTM-2022 Full Congress Participation has been granted 26.5 CPD points Accreditation by the Faculty of Pharmaceutical Medicine, Royal Colleges of Physicians of the UK.

Attenddee can only claim 'Specific Credits Points' for the actual time spent in the activity.
EUSTM will confirm only 'Specific CPD points' for the actual time spent by the attendee in the congress.

Mag. Sandra Oberhuber

Mag. Sandra Oberhuber
Manager, EUSTM

Confirmation Email:info@eutranslationalmedicine.org
Issuing date:08/12/2022

Serial No. 31CP2022PRPP1-52

LOVELY PROFESSIONAL UNIVERSITY

Transforming Education Transforming India

IPC

Certificate of Participation

This is to certify that Prof./Dr./Mr./Ms. SHUBHAM KUMAR has successfully participated as Delegate & Presented Poster/ ~~Oral Presentation~~ on _____ in the 3rd International Conference of Pharmacy (ICP-2022) on the Theme of "Practice, Promotion & Publication of Innovation : A Way of Transforming Health" held on 09th & 10th November 2022 organized by School of Pharmaceutical Sciences in a collaboration with Indian Pharmaceutical Association (IPA) at Lovely Professional University, Punjab.

Mr. Suresh Khanna, National Hon. Gen. Secretary, IPA

Dr. Bimlesh Kumar, Organizing Secretary

Dr. T.V. Naryana, National President, IPA

Dr. Monica Gulati, LOC Chairperson

Sri Herbasia Biotech

Tishk International University, Iraq

NIPER GUWAHATI

10th National Symposium for Young Researchers On Drug Discovery to Delivery 2022

RSC LOCAL SECTION DECCAN

Organized by
National Institute of Pharmaceutical Education & Research (NIPER) Guwahati
& Royal Society of Chemistry (UK) – Local Section Deccan (RSC-LSD)

Certificate of Presentation

This is to Certify that Kumar Shubham Presented in the '10th National Symposium for Young Researcher on Drug Discovery to Delivery 2022' jointly organized by NIPER Guwahati and Royal Society of Chemistry (UK)- Local Section Deccan (RSC-LSD) through Online Mode on 4th March, 2022.

Dr. KR Radhika, Honorary Secretary, RSC-LSD

Dr. RNB Prasad, Chairman, RSC-LSD

Dr. USN Murty, Director, NIPER-Guwahati